Stress Corrosion Cracking of pipeline steels in contaminated aqueous CO_2 environments

By

Daniel Sandana

A thesis submitted in partial fulfilment
of the requirements for the degree of
Doctor of Philosophy

School of Chemical Engineering and Advanced Materials

July 2016

Abstract

This work addresses the risk of Stress Corrosion Cracking (SCC) in CO_2 transport pipelines. The susceptibility of X80 pipeline steels in aqueous CO_2 environments in the presence of nitrates and sulphites is investigated using electrochemical potentiodynamic tests and Slow Strain Rate Tests (SSRT) at 23 and 75°C.

The electrochemical measurements showed that in CO_2-free and CO_2–saturated systems, the material presents an active-passive transition in bicarbonate / carbonate solutions with nitrate and sulphite. This indicated that SCC is possible in all the test environments.

SCC occurred in bicarbonate / carbonate solutions with nitrates and sulphites at 75°C, both under CO_2-free and CO_2-saturated conditions.

SCC severity declined as the potential moved towards the free corrosion potential. Cracking was still observed at +50 mV from E_{corr}. The cracking mode in the active domain was transgranular for all the systems.

In CO_2-free systems, the severity and cracking mode in the HCO_3^--CO_3^{2-}-H_2O and $NaNO_3$-HCO_3^--CO_3^{2-}-H_2O systems was similar in the active-passive transition domain at 75°C. Crack growth was controlled by anodic dissolution and the crack mode was intergranular for both systems. At high pH (>9), the overall cracking mechanism remains dominated by the HCO_3^--CO_3^{2-}-H_2O system even in the presence of nitrates. The addition of sulphites to bicarbonate / carbonate solutions however decreased the severity of cracking and shifted the cracking mode to transgranular.

In CO_2-saturated systems, the SCC susceptibility in all test environments decreased with lower pH. Yet the highest susceptibility to cracking in the active-passive domain was identified in the nitrate-containing systems. With the drop in pH, nitrate SCC becomes the dominant mechanism when nitrates are present in the HCO_3^--CO_3^{2-}-H_2O system.

The addition of CO_2 shifted the mode of cracking to transgranular in the active-passive domain in the pure bicarbonate / carbonate solution.

Acknowledgements

I would like to express my gratitude to Dr Alasdair Charles, Dr Julia Race, and Professor Don Hardie for their supervision and support during my time spent at Newcastle University. I would like to extend my most sincere appreciation to Professor Anne Neville from Leeds University and Dr David Swailes from Newcastle University for their patience and contribution in the review and examination of this thesis.

I would like to express my most grateful thanks to MACAW Engineering to have offered me the opportunity to enter this PhD programme, and for their huge financial and logistic support without which this work would have not been possible.

My sincere thoughts go particularly to Mr Mike Dale who has been a great Mentor since I started my career in the Oil and Gas Industry 8 years ago. His timeless support and our endless discussions have been very important for me to grow personally and professionally. His immense knowledge, experience and wisdom have been a great source of inspiration, and have without doubt been essential for me to approach confidently the experimental work and to be able to reflect critically on the results.

I am also very grateful to Chris Dunn and Neville Dickman for their hard-work during the preparation of the test specimens and for their effortless technical support during the countless stressful troubleshooting times. I would like to acknowledge Pauline Carrick and Dr Isabel Arce-Garcia for their ever kind help during my long hours in the dark with the Hitachi. My deep thanks are extended to: Alhadji, Brian Poulsen, Gaurav, Khalid, Maggie, Octavio, Ramoon, Yahuk. The members of the Corrosion Research Group, of the ACMA and of the Nanotechnology Research Group have been a great source of friendships who made my time at Newcastle University very much enjoyable and the long hours in the lab bearable.

I would like to thank Dorian, Jimmy, Youssef, Joël, Anthony, Tom, Chris, Tato, Borja, Oscar, Samy who have been great friends and have helped me keeping my sanity over these years.

My final thoughts are for Margaret, my Family and God.

Margaret, because of the happiness, smiles and peace you are bringing to my heart.

My Family for their unconditional love and encouragement. My Parents who raised me and have given me the chance to become the person I am.

And God because everybody needs Light and Hope.

“Success is not final, failure is not fatal:
it is the courage to continue that counts”
(Churchill)

Table of contents

List of figures

List of Tables

Relevant nomenclature

EAC	Environmentally-Assisted Cracking
E_{corr} (OCP)	Free corrosion potential (Open Circuit Potential)
Ep	First oxidation peak potential
CCS	Carbon Capture and Storage
Ip	Current density at first oxidation peak
NO_x	Nitrogen oxides
SCC	Stress Corrosion Cracking
SO_x	Sulphur oxides
SSRT	Slow Strain Rate Test
RA	Reduction of Area

Chapter 1. Introduction

Global warming and climate change have been considered to be linked with the release of greenhouse gases e.g. carbon dioxide (CO_2), methane (CH_4) and nitrous oxides (NO_x) into the atmosphere as a result of human activities.[1] CO_2 represents a significant proportion of greenhouse gas emissions (approximately 77% vol). In recent years, the development of Carbon Capture and Storage (CCS) projects has attracted interest from governments and the industry around the world to slow down the sustained increase of global atmospheric CO_2 emissions. The main objective of CCS is to capture the CO_2 from the major source of production and to store it to prevent its release into the atmosphere.

As part of the realisation and implementation of a successful CCS chain from capture to storage, the transport of anthropogenic CO_2 by pipelines is a critical component. It is expected that the transport of anthropogenic CO_2 will be mainly completed in pipelines designed in carbon steel or low alloy steel rather than of corrosion resistant alloys (CRAs) such as stainless steel due to economical constraints over long transport distances, and the conversion of existing pipeline facilities for CCS purposes. Similarly, the transport of carbon dioxide in its dense phase is generally preferred economically; but technical challenges related to possible multi-phase flow developing in long distance transport and the risk of brittle fracture propagation in dense phase operation have meant that the transport of gaseous CO_2 has been considered as a viable option.

The development of CCS necessitates that the integrity risks related the transport of anthropogenic CO_2 pipeline are understood so that they could be effectively mitigated at design stage or during operation, and the facilities safely fulfil their entire operational life cycle. Much attention has been given to the occurrence and magnitude of general corrosion and localised corrosion (pitting) of carbon steel materials in CO_2 environments containing impurities such as nitrogen oxides (NO_x) and sulphur oxides (SO_x) in the presence of moisture or liquid water.[2,3,4,5,6,7,8,9] However the risk of Stress Corrosion Cracking (SCC) of pipeline steel materials in these environments has not been extensively investigated.

The primary objective of this thesis is the discussion of SCC occurrence for typical High-Strength Low-Alloy Steel (HSLA) pipeline materials exposed to CO_2-containing environments and in the presence of impurities.

More precisely, the objectives of this thesis are to determine the susceptibility to SCC of a X80 pipeline steel in CO_2-simulated environments in the presence of NO_x and SO_x. The experimental program investigates the following:

- The effect of nitrates (produced by NO_x) on the susceptibility to SCC of X80 pipeline steel in the CO_2-HCO_3^--CO_3^{2-} system.
- The effect of sulphites (produced by SO_x) on the susceptibility to SCC of X80 pipeline steel in the CO_2-HCO_3^--CO_3^{2-} system.
- The effect of temperature and pH on the susceptibility to SCC in nitrate- and sulphite- containing CO_2-HCO_3^--CO_3^{2-} systems.

Chapter 2. Literature review

2.1. CCS and transport of anthropogenic CO_2

2.1.1. The Concept of Carbon Capture and Storage (CCS)

Carbon Capture and Sequestration or CCS involves three distinct stages :[10]

1. Capturing CO_2 from the gas streams emitted from power plants, industrial sources or natural gas wells.
2. The CO_2 in a gaseous or dense phase is transported by pipelines to storage.
3. Storing CO_2 underground in deep saline aquifers, depleted oil and gas reservoirs, or re-injecting it into producing wells for 'Enhanced Oil Recovery' (EOR).

At present carbon dioxide can be captured from four different sources i.e. post-combustion, oxy-fuel combustion, pre-combustion and other industrial processes. The different process routes for CCS are illustrated in Figure 1[11].

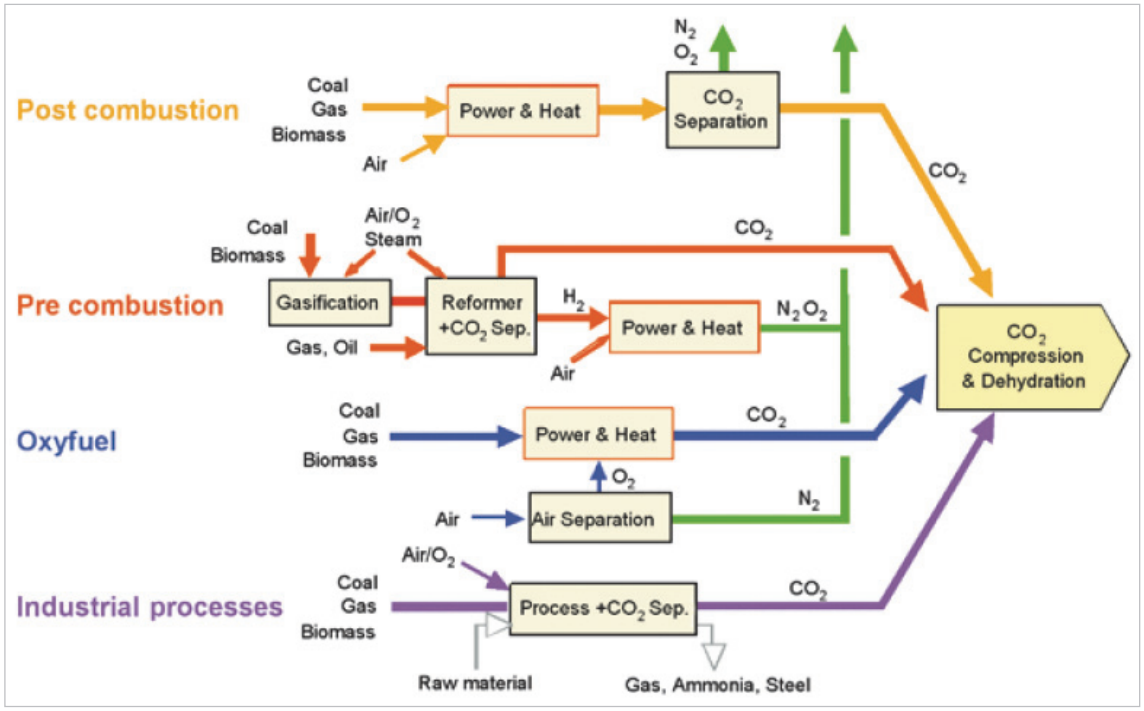

Figure 1: The different process options available for Carbon Capture[11]

2.1.2. CCS stream compositions: carbon dioxide and the presence of impurities

There are currently over 3,500 km of operational, long distance high-pressure carbon dioxide pipelines. These pipelines are mainly located in the U.S.A and are mostly transporting CO_2 from natural sources for Enhanced Oil Recovery. CO_2

from natural sources is relatively pure, and this means that defining a specification for such product is, in many respects, not a too complex problem.[12] In contrast, the capture of carbon dioxide from power plants means that different types and levels of impurities are present in the CO_2 stream, and the purity of the CO_2 becomes significantly affected. The impurity composition of such product via pipelines to its destination is dependent on many parameters, essentially:[8,12]

1. The nature and chemical composition of the fuel gas source
2. The carbon capture technology; currently there are three main options, i.e. pre- or post-combustion, or oxyfuel
3. The conditioning / treatment process e.g. sulphur- or nitrogen- scrubbing plants to limit hydrogen sulphide (H_2S), oxides of sulphur and nitrogen (SO_x and NO_x) content
4. The use and type of drying plant to restrict water content
5. The process used to separate CO_2 from the rest of the flue gases, e.g. chemical or physical absorption.
6. Local regulatory requirements and safety considerations

The types and levels of impurities as a function of the fuel source and the carbon capture technology source used are provided in various publications. Table 1 gives a comparison of published CO_2 compositions from different capture technologies.[11,12]

Table 1: CO_2 % vol. compositions from different capture technologies[11]

Impurities in dried CO_2 (%vol.)	SO_2	NOx	H_2S	H_2	CO	CH_4	N_2/Ar/ O_2	Total (%vol.)
Coal Fired plants								
Post-combustion	<0.01	<0.01	0	0	0	0	0.01	0.01
Pre-combustion	0	0	0.01-0.6	0.8-2.0	0.03-0.4	0.01	0.03-0.6	2.1-2.7
Oxy-fuel	0.5	0.01	0	0	0	0	3.7	4.2
Gas fired plant								
Post-combustion	<0.01	<0.01	0	0	0	0	0.01	0.01
Pre-combustion	0	0	<0.01	1.0	0.04	2.0	1.3	4.4
Oxy-fuel	<0.01	<0.01	0	0	0	0	4.1	4.1

The Inter-governmental Panel for Climate Change (IPCC) considers that the main impurities in flue gases generated from a post-combustion process by coal combustion will include nitrogen (N_2), oxygen and water, but also SO_x and NO_x, hydrochloric and hydrofluoric acids (HCl and HF), and mercury (Hg).[11] In comparison, flue gases from natural gas combustion processes typically contain low levels of SO_x and NO_x and higher concentrations of oxygen O_2; HF can however also be present. Desulphurisation plant is generally necessary to prevent sulphur-poisoning of the solvent in the CO_2 absorption process.

In the pre-combustion process, the captured CO_2 may contain very small levels of impurities such as N_2, O_2, hydrogen (H_2), methane (CH_4), CO and sulphur compounds like H_2S. The levels of SO_x and NO_x present in captured CO_2 from pre-combustion processes are insignificant. CO_2 from pre-combustion physical solvent scrubbing processes typically contains about 1-2% H_2 and CO, and traces of H_2S and other sulphur compounds.

In oxy-fuel process, the CO_2 rich stream commonly contains O_2, N_2, argon (Ar), sulphur (S) and NO_x.

The presence of impurities in the CO_2 stream will have a significant impact on the pipeline design and operation,[10,12,13] but also on the pipeline integrity in terms of internal corrosion risks.[7,8]

2.1.3. *CO_2 pipeline integrity and operational production scenarios during pipeline life cycle*

This thesis focuses on the transportation component of the Carbon Capture and Storage chain, i.e. the anthropogenic CO_2 transport pipeline downstream of a carbon capture plant.

The integrity management for a CO_2 transporting pipeline does not start at the pipeline inlet but needs to consider the overall upstream process from fuel source, and the modes of operation of the CCS capture and conditioning plant (Figure 2). In this document, the term of integrity is related to issues associated with the concept of corrosion as defined in section 2.4.

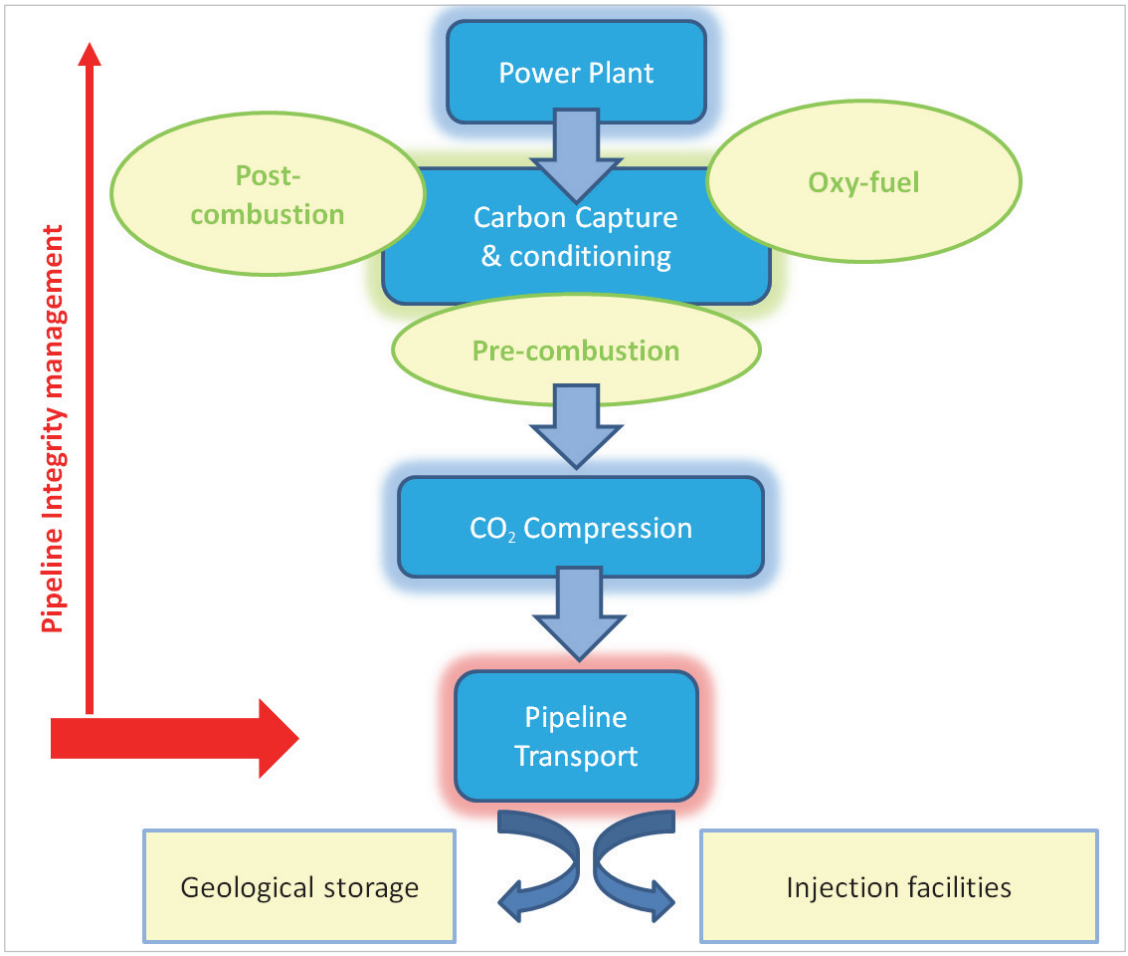

Figure 2: CCS and Pipeline Integrity Management

A. Pipeline integrity: The importance of water content specification and water solubility in CO_2

It is generally accepted as a simplified rule that if no aqueous phase condenses out from the CO_2 stream, the risk of internal corrosion in the pipeline transporting facilities will remain low.[7,8,14] The occurrence of aqueous phase condensation is dependent on the water solubility in the CO_2 fluid which is a function of the operating pressure, operating temperature and the types and levels of impurities present.[15,16]

CO_2 pipelines: Water solubility in pure CO_2 streams

In pure CO_2, the condensation of water will occur when the water content is above its solubility limit for the considered pressure and temperature. Figure 3 illustrates water solubility in pure CO_2 as a function of pressure and temperature from which it can be seen that:[17]

- A rise in temperature increases the solubility of water (H_2O) in gaseous and dense phase CO_2

- Where CO_2 is a gas, typically at low pressures, the solubility of water decreases with increasing pressure. However, during a phase transition of CO_2 from a gas to dense phase, the solubility of H_2O in CO_2 increases with pressure.

An acceptable water specification for avoiding corrosion in pipelines transporting pure CO_2, at operating temperatures above 4^0C, is generally considered to be in the range 300-500 ppm wt (0.4 kg/m^3 or 0.0003-0.0005 ppm vol).[14,17]

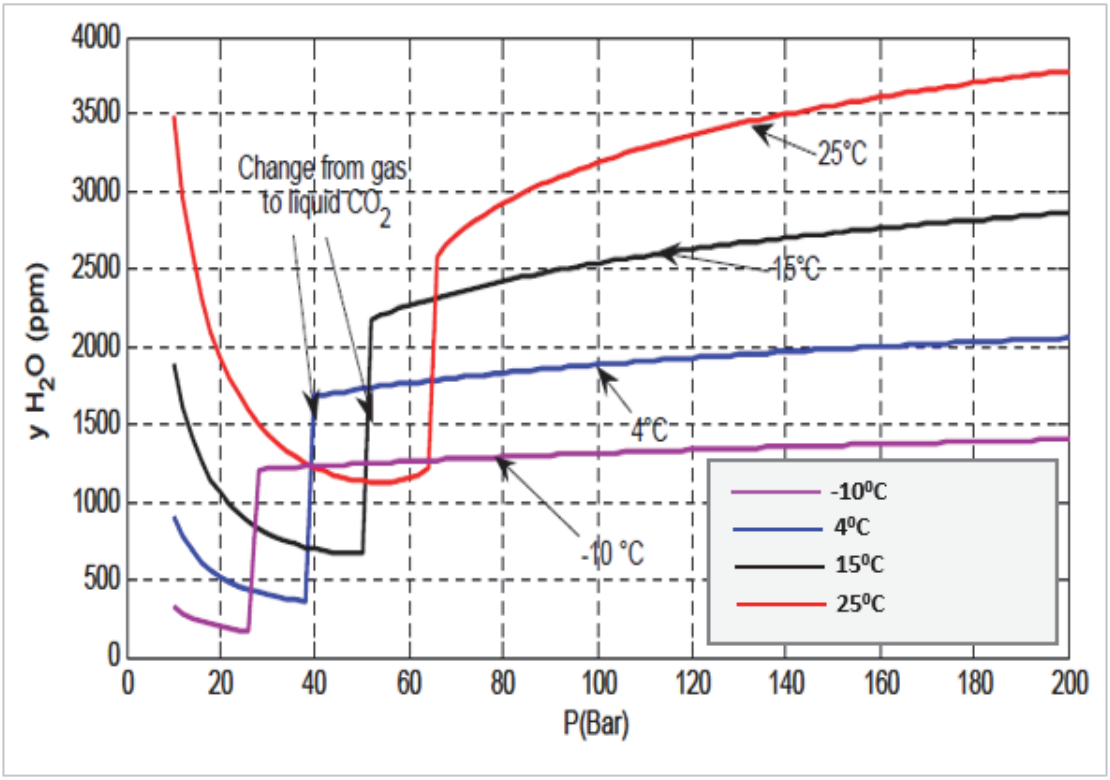

Figure 3: Solubility of water in pure CO_2 as a function of pressure and temperature[17]

CO_2 pipelines: Water solubility in CO_2 and the effect of impurities

Depending on the type and concentration of impurities, water solubility in CO_2 may decrease. For example, Austegard et al.[16] showed that CH_4 will lower the solubility of water in CO_2, and this is also potentially the case for other impurities[11], such as H_2S, O_2 and N_2.

Similarly the presence of sulphur oxides SO_x will drive the condensation of acid aqueous phases at water contents much lower than the water solubility limit in otherwise pure CO_2 streams. This is related to the formation of acids (whose nature is dependent on the type of oxide compounds) at a temperature much higher than the water dewpoint, which is commonly referred as the acid dewpoint[18]. Typically the presence of SO_2 / SO_3, even at small concentrations, will react with water vapour (or liquid) to form sulphurous or sulphuric acids

Although nitrogen oxides (e.g. NO and NO_2) can also react with water to form acids, e.g. nitrous (HNO_2) or nitric acids (HNO_3), the effect of NO_x on the dewpoint temperature is negligible in comparison with the effect of SO_2 / SO_3.[19] Hence, in the absence of SO_x, the dewpoint can be considered as being solely determined by the water content in the gases.

The variation of the acid dewpoint for gases containing different concentrations of water as a function of H_2SO_4 and SO_3 is illustrated in Figure 4[18] and Figure 5[19], respectively. As the amount of water is increased, the acid dewpoint temperature increases; this is also the case when the concentration of SO_3 in the gas is increased.

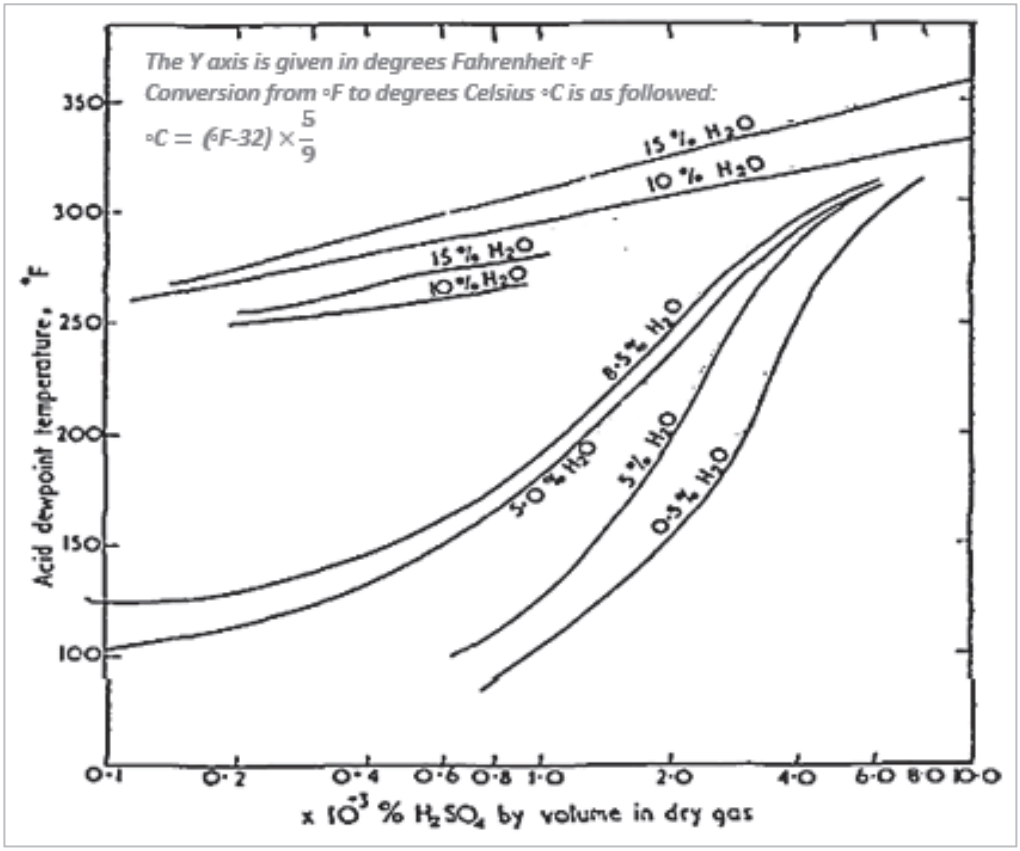

Figure 4: Variation of sulphuric acid dewpoint for gases having different water vapour contents[18]

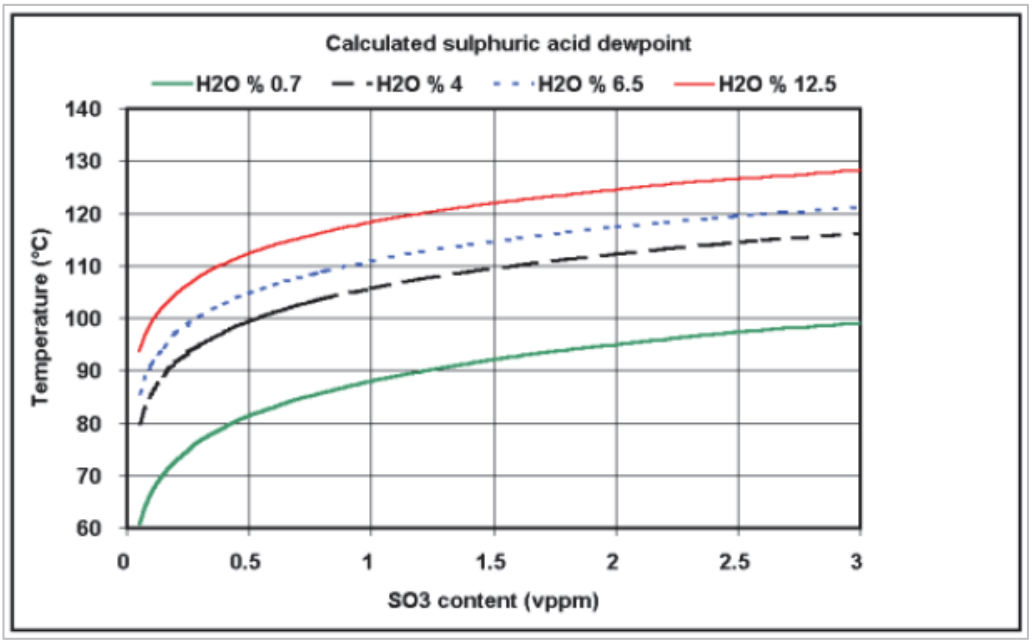

Figure 5: Variation of sulphuric acid dewpoint for gases having different water vapour contents as a function of SO_3 levels[19]

B. CO_2 pipeline integrity and operational production scenarios

Despite all the precautions taken at the process design stage to guarantee acceptable water contents in CO_2, upset conditions in the CO_2 dehydration process and water breakouts are still a possibility in complex pipeline systems, especially over decades of operating life. Hence the resulting risk of internal corrosion from such excursions should not be excluded. One may argue that if a continuous flow of dry CO_2 is present following an event of water incursion, the water may rapidly dissolve in the stream minimising any internal damage to the pipeline. However, in the case of a delay in response to process upsets or in the case of a shutdown (pipeline shut-in or total depressurisation), situations could exist where free water may be present over long time periods in the pipeline. Indeed, during long shutdowns, water removal operations will be required and experience from the oil and gas industry has indicated that this may take weeks.[5,8]

The following generic operational scenarios may be envisaged during the life cycle of an anthropogenic CO_2 pipeline:[8,20]

A. The CO_2 is dehydrated to specification and the impurity levels are identified as negligible, (according to CO_2 plant conditioning specification).
B. The CO_2 is dehydrated to specification but upsets in CO_2 stream conditioning have occurred. Impurity levels above agreed specification have entered the pipeline transportation system.
C. Upset in dehydration occurs such that a free liquid water phase is present at the bottom (6-o-clock position) of the pipeline transportation system. Levels of impurities are considered negligible.
D. Upset in dehydration occurs such that a free liquid water phase is present at the 6-o-clock position of the pipeline transportation system. Upset in the CO_2 conditioning plant has also occurred with levels of impurities above the specified levels.

This thesis considers the worst case operational scenario of liquid water being present in the pipeline as well as excessive amounts of impurities typically NO_x and SO_x. The next section considers the chemistry of water in the presence of carbon dioxide and impurities, NO_x and SO_x.

2.2. Water chemistries in CO_2 containing environments and in the presence of impurities

2.2.1. Solubility of gaseous species in water

The solubility of a gaseous species is determined by pressure, temperature, and the types and levels of other chemicals present in solution.

A. Effect of pressure

The diffusion and the dissolution of a gas *i* into liquids e.g. water is enhanced by increasing its activity a_i or fugacity f_i, which can be simplified as its partial pressure, if the gas is considered as ideal i.e. the fugacity coefficient Φ_i is equal to 1.

The gas activity a_i is associated with the fugacity f_i via:

$$a_i = \frac{f_i}{P^o} = \Phi_i . x_i . \frac{P}{P^o}$$

Where,

x_i is the molar fraction of the gas i

P is the pressure of the system

P^o is the standard pressure (1 bar)

The term $x_i . P$ is the partial pressure P_i of the gas i.

The relation between gas solubility in water and the gas partial pressure P_i is often quoted through Henry's law for ideal gases. The law states that at a constant temperature, the amount of gas dissolved in a liquid is proportional to the partial pressure of the gas in equilibrium with the liquid:

$$\mathrm{C_i} \cdot K_H^i = P_i$$

Where C_i is the concentration of the gas in the liquid, P_i is the partial pressure of the gas above the liquid and K_H^i is Henry's constant.

The above implies that with an increase in the partial pressure of the gas, its solubility in water will increase. The applicability of Henry law is, however, limited to ideal gases. At high pressures gases liquefy or form supercritical fluids (dependent upon temperature) and Henry's law becomes invalid. Calculations of

solubilities at high pressures require the use of fugacity expressions as well as the use of a suitable Equation of State (E.O.S).

B. Effect of temperature

The solubility of gases in water decreases with increasing the temperature. The reason for the decrease in solubility is very similar to the reason that kinetic energy and vapour pressure increase with temperature. The higher the kinetic energy causes more motion in molecules which break intermolecular bonds and thus gas escapes from solution.

In addition to pressure and temperature, solubility also depends on the presence of other species dissolved in water; for example the presence of dissolved salts may decrease the solubility of solutes in the water. In this specific case, this is thought to be due to the change in ionic strength of solutions in the presence of salt thereby decreasing the ability of water to solvate the solute molecules.

2.2.2. Carbon dioxide and water

In the presence of water, carbon dioxide involves the formation of carbonic acid H_2CO_3, bicarbonate ion HCO_3^- and carbonate ions CO_3^{2-} as a result of its dissolution in water. H_2CO_3 is a weak acid as it does not entirely dissociate into hydroniums and bicarbonate ions.

The steps of carbon dioxide reaction with water may be outlined as below:

$$CO_2(g) + H_2O \leftrightarrow CO_2(aq) + H_2O$$

$$CO_2(aq) + H_2O \leftrightarrow H_2CO_3(aq)$$

$$H_2CO_3(aq) + H_2O \leftrightarrow H_3O^+(aq) + HCO_3^-(aq)$$

$$HCO_3^-(aq) + H_2O \leftrightarrow H_3O^+(aq) + CO_3^{2-}(aq)$$

Studies[4] have investigated the chemistries of aqueous phase in the presence of pure CO_2 over a wide spectrum of pressure, where CO_2 could exist as a gaseous phase or as a dense phase. The levels of carbonic acid, bicarbonates and carbonates in deionised water as function of CO_2 partial pressure and temperature are identified in Figure 6, Figure 7, Figure 8.[4] The concentrations increase with increasing pressure whilst decreasing with temperature.

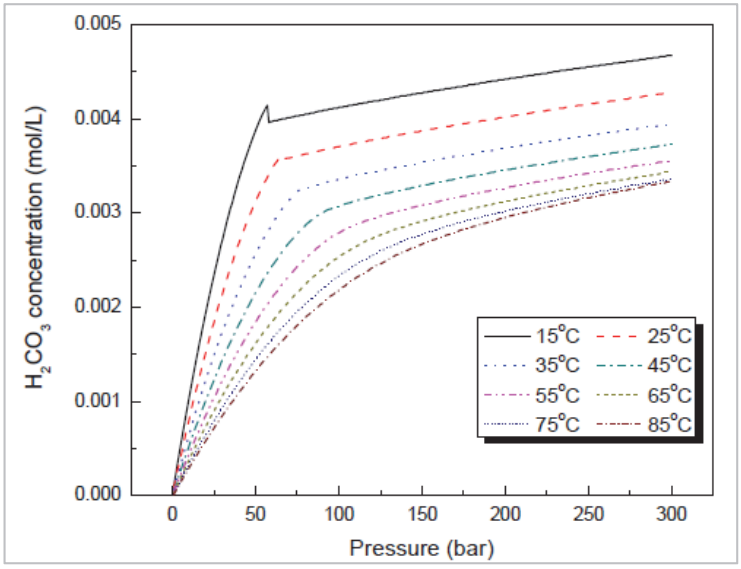

Figure 6: Predicted carbonic acid concentrations in water vs. CO_2 partial pressure at various temperatures[4]

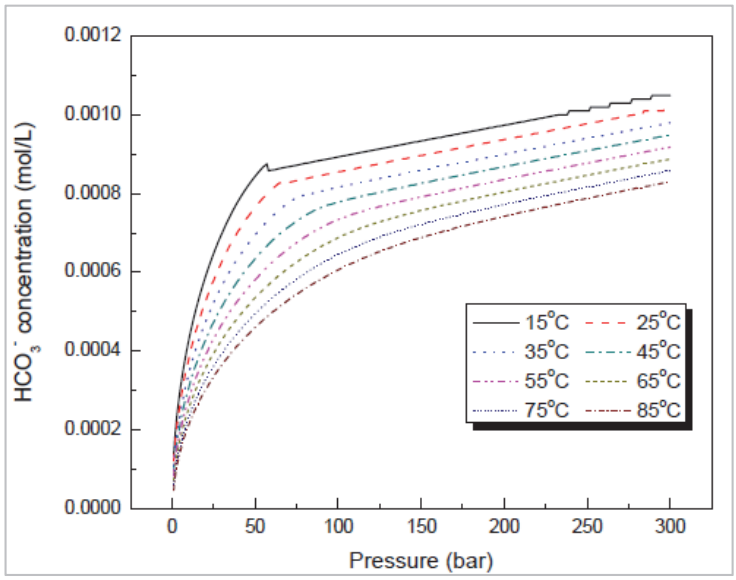

Figure 7: Predicted bicarbonate concentrations in water vs. CO_2 partial pressure at various temperatures[4]

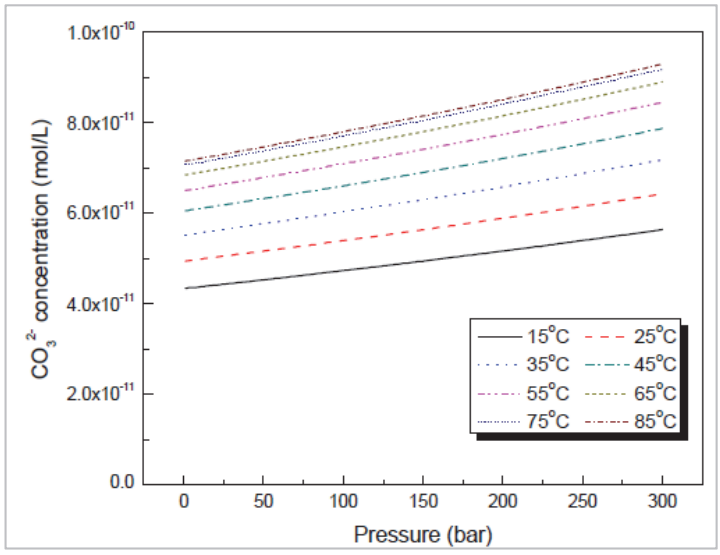

Figure 8: Predicted carbonate concentrations in water vs. CO_2 partial pressure at various temperatures[4]

The pH value also decreases with higher CO_2 pressures, and will be in the range of 3 to 3.4 above 50 bar Figure 9 [4].

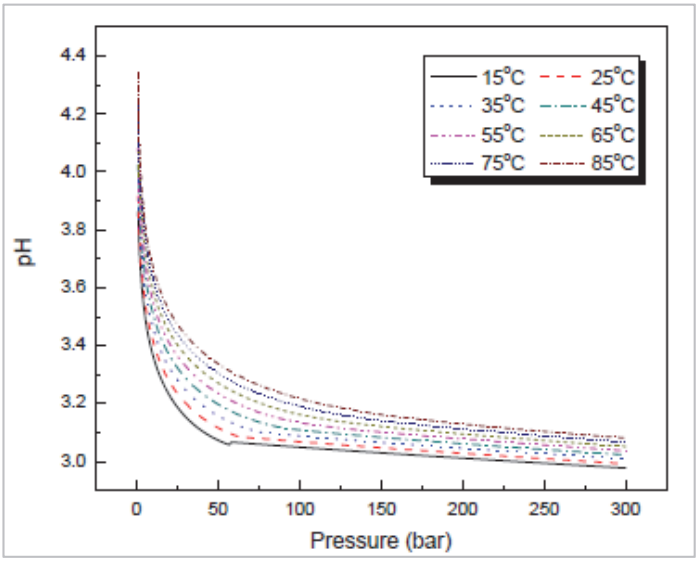

Figure 9: Predicted pH of water vs. CO_2 partial pressure at various temperatures[4]

The chemistry of the aqueous phase in rich CO_2 environments will be further modified by the presence of impurities in the CO_2 stream, and the magnitude of the change will be dependent on the type and concentration of the impurity, but also on the partitioning behaviour of these impurities between the different CO_2 and water phases.

This partitioning will be a function of the CO_2 physical state, temperature, pressure, and on the synergy effects between the different mixture compounds. The presence of impurities of SO_x and NO_x in the CO_2 stream will further decrease the pH of any aqueous phase formed due to the formation of acids such as sulphuric/sulphurous or nitric/nitrous.[8,21]

2.2.3. Nitrogen oxides and water

There are various forms of nitrogen oxides (NO_x) including nitric oxide (NO) and nitrogen dioxide (NO_2), dinitrogen trioxide (N_2O_3), and dinitrogen tetroxide (N_2O_4). NO is unstable in the presence of oxygen, and oxidises into NO_2:

$$2NO(g) + O_2(g) \rightarrow 2NO_2(g)$$

Whilst NO is non-reactive in water[22], NO_2, N_2O_3, N_2O_4 are, on the other hand, greatly reactive with water and such reaction leads to the formation of oxyacids as discussed below.

The reactivity of gases with water makes the evaluation of Henry's law constant a challenge, and has resulted in inconsistency and paucity in reported coefficient

data for NO_2, N_2O_3, N_2O_4. Based on a review of nitrogen oxides solubility in water, Schwartz et al[23] suggest the following set of Henry's law coefficients should be adopted:

Table 2: Solubility of NOx in water at ambient pressure and at 25°C[23]

Gas	Henry's constant (K_H, $M.atm^{-1}$) at 25°C
NO	1.93
N_2O_4	1.4
NO_2	1.2
N_2O_3	0.6

From Table 2, the solubilities of NO_x in water are in this order: N_2O_3> NO_2> N_2O_4> NO. This reflects in some ways the order of reactivity of these gases with water. The solubility of nitrogen oxides and the reactivity with water will be increased with the partial pressure of NO_x in the gas. The solubility will be however affected by the presence of other chemical species in solution e.g. bicarbonates and carbonates in CO_2 environments.

In the presence of liquid water or moisture, nitrogen oxides lead to the formation of nitric acid (HNO_3) and nitrous acid (HNO_2):[24]

$$3NO_2\,(aq) + H_2O\,(l) \leftrightarrow 2HNO_3\,(aq) + NO\,(g)$$

$$N_2O_3\,(aq) + H_2O\,(l) \leftrightarrow 2HNO_2\,(aq)$$

$$N_2O_4\,(aq) + H_2O\,(l) \leftrightarrow HNO_2\,(aq) + HNO_3\,(aq)$$

Nitric acid and nitrous acid are respectively strong and weak acids which subsequently ionise in aqueous solution into hydroniums cations (H_3O^+), and nitrates (NO_3^-).

$$HNO_3\,(aq) + H_2O\,(l) \rightarrow H_3O^+\,(aq) + NO_3^-\,(aq)$$

$$HNO_2\,(aq) + H_2O\,(l) \leftrightarrow H_3O^+\,(aq) + NO_2^-\,(aq)$$

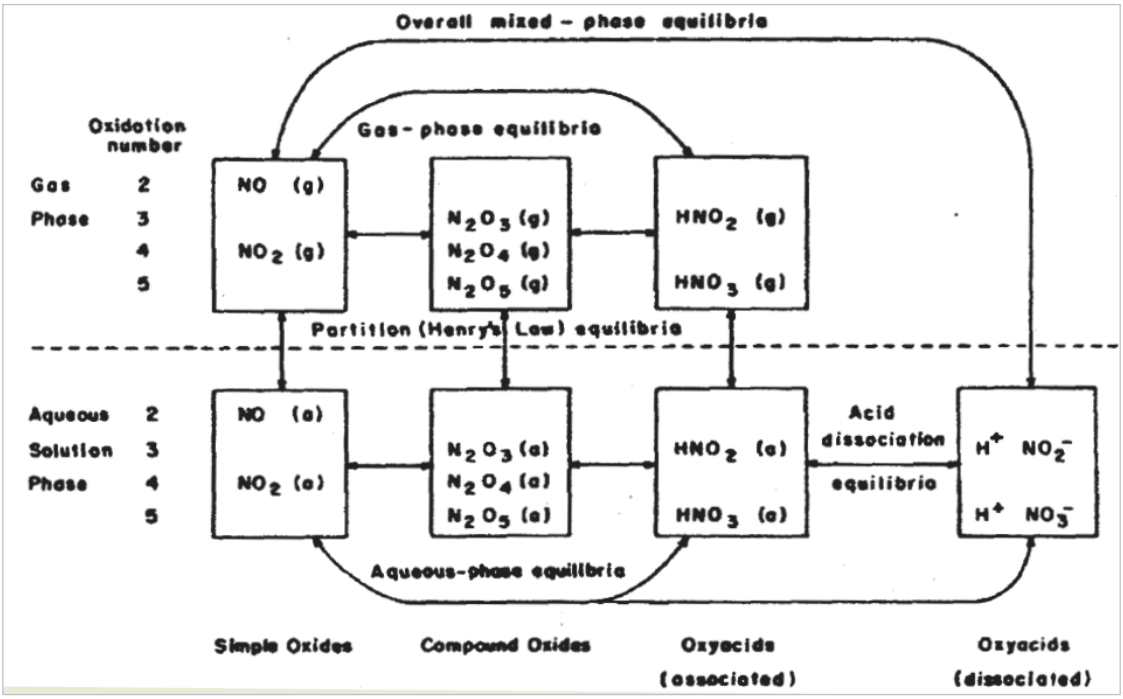

Figure 10: Equilibria relating gaseous and aqueous nitrogen oxides and oxyacids[23]

2.2.4. Sulphur oxides and water

In the presence of liquid water or moisture, gaseous sulphur dioxide (SO_2) forms sulphurous acid (H_2SO_3). Sulphurous acid is a weak acid which subsequently ionises in aqueous solution into hydroniums cations (H_3O^+), bisulphite (HSO_3^-) and sulphite anions (SO_3^{2-}). The succession of SO_2 principal reactions with pure water is described below:[25]

(1) $SO_2\,(g) \leftrightarrow SO_2\,(aq)$

(2) $SO_2\,(aq) + H_2O\,(l) \leftrightarrow H_2SO_3\,(aq)$,

(3) $H_2SO_3\,(aq) + H_2O\,(l) \leftrightarrow H_3O^+\,(aq) + HSO_3^-\,(aq)$

(4) $HSO_3^-\,(aq) + H_2O\,(l) \leftrightarrow H_3O^+\,(aq) + SO_3^{2-}\,(aq)$

It should be noted that sulphurous acid is an unstable chemical compound which readily decomposes into its original reactants, i.e. sulphur dioxide and water.

In aqueous solutions (or in the presence of moisture), sulphite species behave as reducing agents by combining with oxygen contained in the electrolyte to form a more stable compound sulphate (SO_4^{2-}). Sulphite compounds e.g. sodium sulphite (Na_2SO_3) are recognised as oxygen scavengers in the process industry.

$$SO_3^{2-}\,(aq) \; + O_{(aq)} \leftrightarrow SO_4^{2-}\,(aq)$$

Cape[25] plotted the concentrations of SO_2 (aq), HSO_3^- and SO_3^{2-} in water, and the solution pH as a function of SO_2 partial pressure in the gas phase and temperature (see Figure 11). Cape uses Maahs[26] equilibrium constants, which are discussed to possibly underestimate the species concentrations in solution by 30-40% at low partial pressures of SO_2 below 2.10^{-4} atm. Experimental equilibrium constants determined experimentally by Hales and Sutter[27] at low SO_2 levels were indeed reported larger than Maahs.[28,29,30] The relative proportion of chemical species in solution was nevertheless considered not to be significantly affected.

As illustrated in Figure 11, the concentration of SO_2 (aq) increases with the SO_2 (g) partial pressure, but decreases with temperature. The concentrations of HSO_3^- (aq), H_3O^+ (aq) increase with rise of SO_2 (aq) levels. However, it appears that the levels of SO_3^{2-} (aq) remain unaltered between 10^{-7} and 10^{-8} atm. The

solubility of SO_2 will be affected by the presence of other chemical species in solution e.g. bicarbonates, carbonates in CO_2 environments.

The increased presence of aqueous SO_2 in solution increases the acidity of the solution due to greater production of sulphurous acid. Cape[25] indicates that the concentrations of HSO_3^- (aq) and SO_3^{2-} (aq) will increase with initial solution pH, whilst the concentration of SO_2 (aq) is not dependent on the latter. Hence, the overall concentration of sulphur (S^{IV}) decreases with pH, whilst the proportion of SO_2 increases.

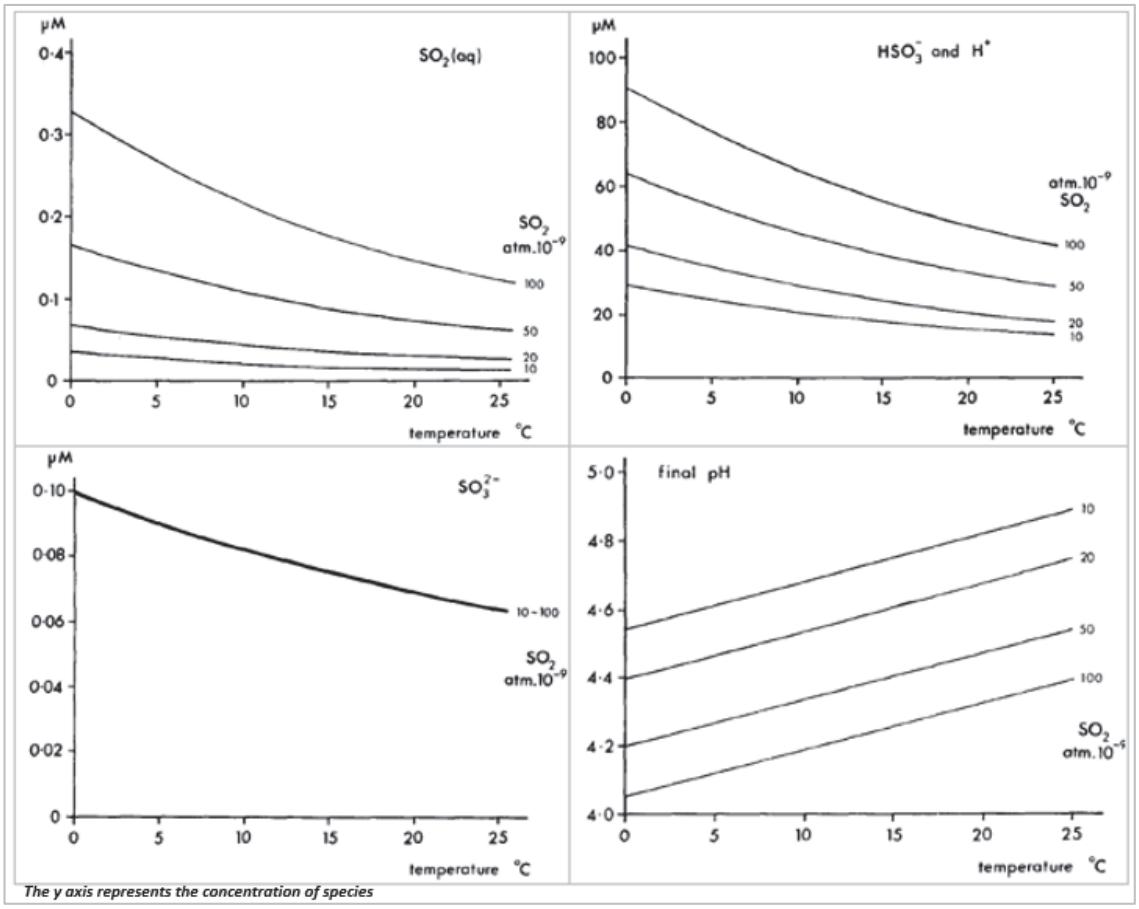

Figure 11: Chemistry of water in equilibrium with gaseous SO_2 as a function of pressure and temperature[25]

Ayello et al.[3] simulated the change of pH of an aqueous phase in equilibrium with dense CO_2 at 75.8 bar following the addition of small amounts of sulphur dioxide (100 ppm vol) (Figure 12). The simulated pH shifted approximately one pH unit down to become more acidic with the presence of SO_2.

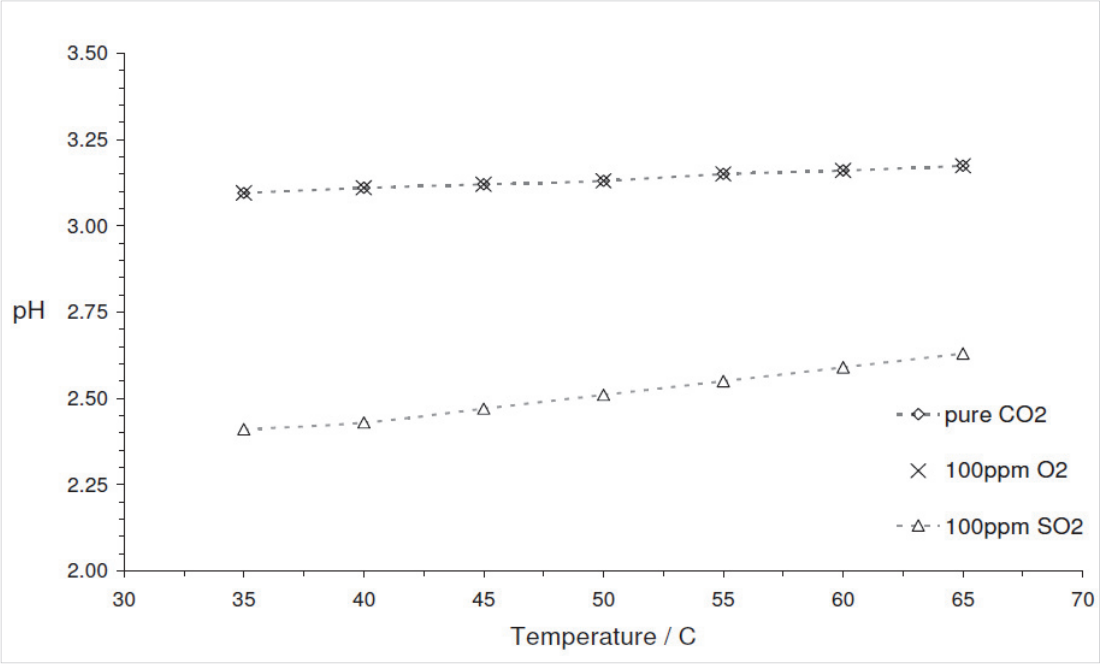

Figure 12: Evolution of the aqueous phase's pH in supercritical CO_2 as a function of impurities added to supercritical CO_2 at 75.8 bar (OLI software)[3]

2.3. Pipeline steel making evolution: Towards High-Strength Low-Alloy Steels (HSLAs)

The transport of carbon dioxide to a storage site via pipelines is the most practical option since CO_2 can be effectively transported in large volumes. In the Oil and Gas industry, pipelines are recognised as the most economical and the safest option for transcontinental transportation of energy.[10]

Due to the cost of corrosion resistant alloys (typically stainless steels), long distance CO_2 pipelines are likely to be designed in carbon steel materials; new infrastructures will include newer grades of High-Strength Low-Alloy Steels. Additionally transportation of CO_2 could also be realised in existing carbon steel pipeline networks, and therefore old pipeline steel grades should also be considered.

2.3.1. Semi-killed and fully-killed normalised steels

Until the 1960s, the conventional grade of steel for High pressure (HP) pipelines was API 5L X52. X52 was manufactured from semi-killed ingot cast steel, which means that the oxygen was not entirely removed from the molten steel bath. At such time, no specific requirements on toughness were defined on purchase of steel. Steel plates were produced from the semi-killed steel ingot by hot rolling above 1000°C; the linepipe materials produced from such a steel-making process were characterised as low strength and with an inherent poor toughness.[31,32]

The toughness requirement was eventually introduced when long running brittle fractures of operational pipelines were experienced in the United States of America (U.S.A.). The Batelle Drop Weight Tear Test (DWTT)[33] was developed to provide assistance in conforming to the new toughness criteria requirements and to prevent brittle fracture. To produce steels with greater or suitable resistance to brittle fracture, it was found necessary to remove all the oxygen from the steel melting bath i.e. to “fully kill” the steel. Such treatment was achieved with the addition of aluminium to the bath. However in opposition to semi-killed steels which maximised the ingot yield, fully-killed steels generated a loss of ingot yield of about 40%.

The introduction of concasting or continuous casting in the early 1960s, in opposition to the original “ingot casting” marked a significant evolution in the steel-making process, and meant that a yield of 100% could be eventually

achieved; the steel producers could finally take advantage of the fully-killed steel making process without any incurred cost penalty.[31,32]

In the 1960s to early 1970s, the steels were fully-killed with Al and Si. After hot rolling the fully-killed steel plates were then normalised at 900°C to produce microstructures with finer grain sizes and thus with improved toughness. However, higher strength in linepipe materials could only be reached by alloying, which was detrimental to the materials weldability due to high carbon equivalent. [31,32]

2.3.2. Hot rolling and controlled rolling

As discussed above, prior to the 1970s, the fully-killed linepipe steels (i.e. API5L X52 to X60) were conventionally manufactured from steel plates that were initially hot rolled (cold rolling was practically and economically not feasible as it would have involved in impossibly high rolling loads), and normalised i.e. slow cooling in air.

In the hot rolling process, whose primary objective is to optimise productivity, the rough and the finish rolling all occur at the highest possible temperature i.e. above the austenite recrystallization temperature. This means that the grain growth of recrystallized austenite is very likely during hot rolling, but also after rolling as the plate slowly cools. The result of this is the production of coarse steel microstructures which are detrimental to the essential mechanical properties of the steel i.e. strength and toughness.

It was demonstrated that the steel mechanical properties, i.e. strength and toughness, are significantly enhanced with a reduction of the microstructure grain size. This is defined via the Irvine equations:[34]

Strength: $YS = 69.5 + 32.4\%Mn + 83.4\%Si + 335.2\left(\%N_f^{\frac{1}{2}}\right) + 17.5d^{-\frac{1}{2}} + \Delta$

Toughness: $T_c = -19 + 44\%Si + 700\left(\%N_f^{\frac{1}{2}}\right) - 11.5d^{-\frac{1}{2}} + 2.2(\%pearlite) + 0.26\Delta$

Where:

$YS = Yield\ Strength\ (N/mm2)$

$T_c = Charpy\ toughness\ transition\ temperature\ (^\circ C)$

$\%Mn\ and\ \%Si = \ manganese\ and\ silicon\ weight\ contents\ of\ steel$

$\%N_f = free\ nitrogen\ weight\ content\ in\ steel$

$d = ferrite\ grain\ size\ (mm)$

$\%pearlite = pearlite\ weight\ content$

$\Delta = precipitation\ hardening\ factor\ (N/mm^2)$

From the mid-1970s, the offshore industry initiated demand for pipeline steels capable of operating at higher operating pressures, which would not be withstood by conventional X60 grades. This meant that thicker linepipes, or higher pipeline grades were required.

The introduction of "Controlled Rolling" in place of the conventional rolling method in the 1970s constituted a significant development in the steel-making industry, which marked the real onset of the High-Strength Low-Alloy Steel (HSLA) linepipe production. "Controlled rolling" made the production of X65, X70, X80, X100 steel grades possible.[35]

2.3.3. Development of HSLAs: Change in pipeline chemistry and thermo-mechanical processing

As discussed above, the development of HSLAs, i.e. the production of steels with greater yield strength and toughness (brittle fracture resistance) relies principally on the generation of microstructures with finer grains. This grain refinement has been achieved in practice by the following fundamental changes in the steel making process: [35,36,37]

- Treatment with aluminium and silicon to fully-kill the steel, and microalloying with elements such as niobium (Nb), titanium (Ti), vanadium (V). Al, Nb, Ti, V produce nitride and carbide precipitates that restrict austenite grain growth, typically AlN, NbC, VN. It is noted that the formation of precipitates such as VC could hinder the motion of dislocations, and hence enhance yield stress. This process is referred to precipitation-hardening. Precipitation hardening could however be detrimental for the resistance to brittle fracture propagation.
- The introduction of Controlled Rolling in place of conventional hot rolling.

A. Controlled rolling and thermo-mechanical processing

The most essential objective of Controlled Rolling (CR) is to refine the microstructure of steels to produce materials with enhanced strength and toughness. In contrast to conventional hot rolling, CR involves the careful control of austenite conditioning during the temperature cycles by application of loading.

For Controlled Rolling, loading is applied over the cooling cycle of the steel from the region of austenite recrystallisation temperatures (typically above 950◦C) and involves deformation in the domains of (i) austenite recrystallization, (ii) austenite non-recrystallisation, (iii) austenite-ferrite co-existence.

The application of loading over the cooling cycle during Controlled Rolling and the its impact on steel microstructure is illustrated in Figure 13: [35,38]

- Above the temperature of austenite recrystallization $T_{recr\text{-}\gamma}$, the steel is within the austenite recrystallization domain (Region 1 in Figure 13). Deformation within this domain is referred as static recrystallization, and this leads to the refinement of austenite grains. Small austenite grains generated at this stage will produce finer ferrite grains.
- As the temperature drops below $T_{recr\text{-}\gamma}$, the steels enters the austenite non-recrystallisation domain (Region 2 in Figure 13). Deformation in this domain substantially increases the nucleation rate of ferrite at austenite grain boundaries and within the austenite grains due to the presence of heavily deformed band structures and sub-structures. The intragranular nucleation of ferrite within austenite grains is one of the most crucial characteristics of controlled rolling (dynamic recrystallization). It is noted that microalloying such as Nb, V and Ti can increase the temperature of austenite recrystallisation which is beneficial to enhance further the phenomenon of dynamic recrystallization.
- As the temperature drops below Ar_3, the steel enters the austenite/ferrite co-existence domain (Region 3 in Figure 13). Deformation in this domain produces substructures within ferrite grains and enhance microstructure hardening.

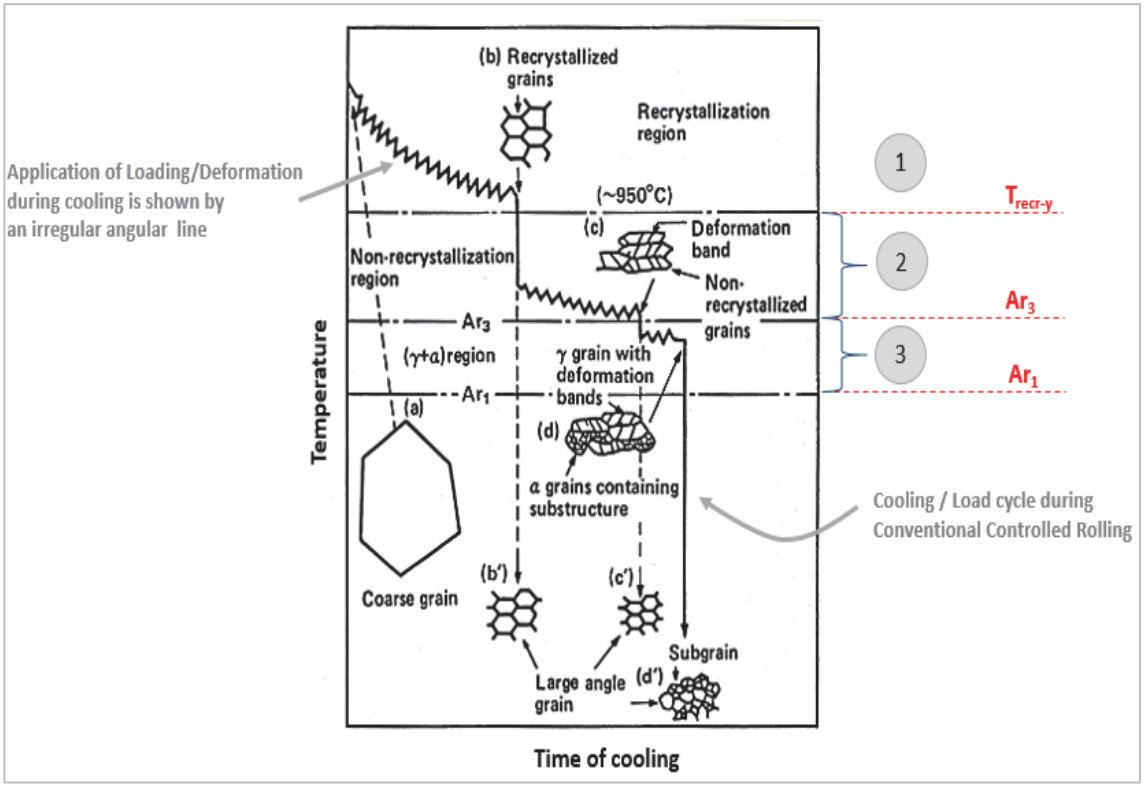

Figure 13: Controlled rolling: rolling in the austenite recrystallization and non-recrystallization regions and microstructural changes over time of cooling[38]

The development of CR has allowed the production of steels up to X70 grades. CR is part of the wider family of thermo-mechanical controlled processes (TMCP). Other processes belonging to the TMCP family only differ from conventional CR by the heat treatment following hot rolling. Instead of the slow cooling conducted after hot rolling in CR, accelerated cooling was used from 1990s onwards to produce microstructures with even higher strength, and thus linepipes of grades above X70, e.g. X80, X100 could be developed (Figure 14 and Figure 15).[39,40]

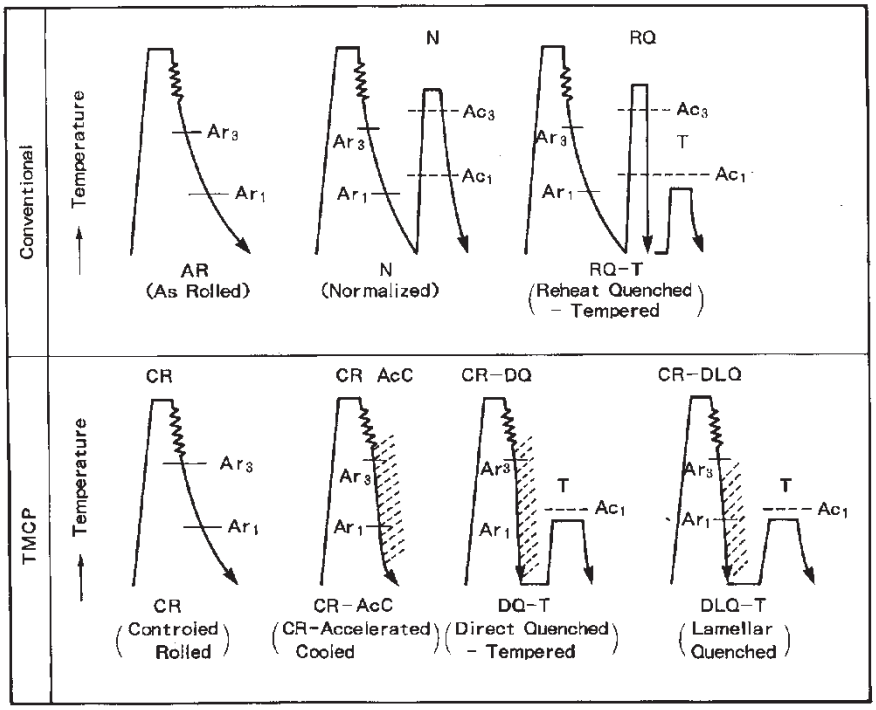

Figure 14: Thermomechanical controlled processes vs. Conventional rolling[39]

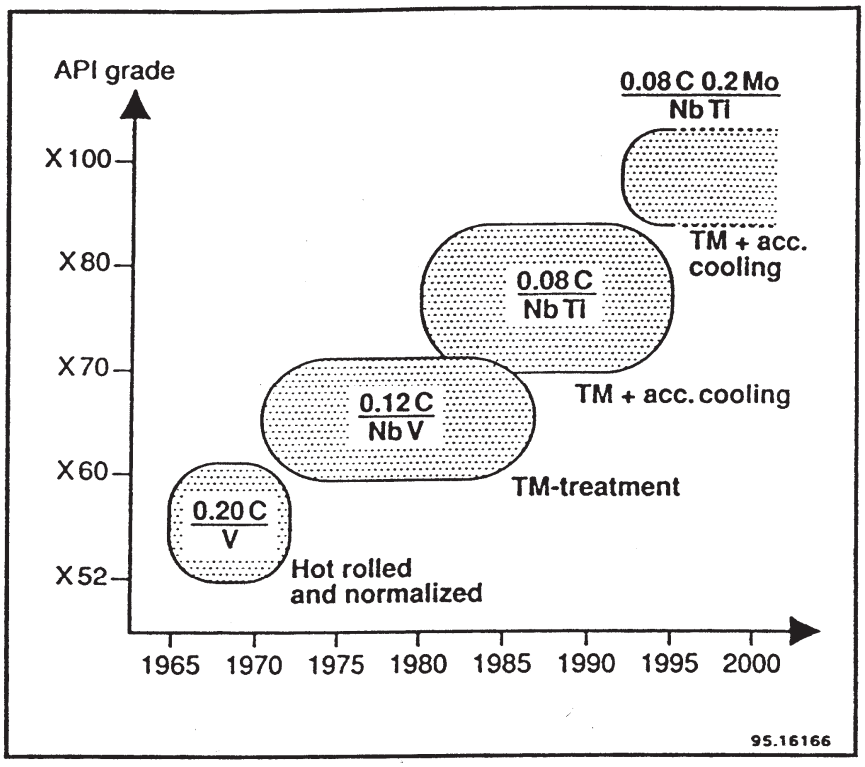

Figure 15: Evolution of linepipe steel grade with TMCP and steel chemistry[40]

B. The Onset of X80 steel in pipeline application

The use of grade X70 steel was introduced in Germany in the early 1970s for the development of gas transmission pipelines. Following satisfactory experiences with X70 steel applications, X80 pipeline grade steels was developed for trial in

1985. X80 steel was first introduced for field application by Ruhrgas AG for the construction of a 250 km pipeline in Germany in 1992-1993.[41]

X80 steel pipes spread worldwide (Table 3) and became a standard and reliable solution for high pressure gas transportation. Most of the operational X80 pipelines for field application are located in the United Kingdom and in North America.[42]

In the UK, offshore structures have been traditionally built with moderate strength steels, typically with yield strengths up to 350MPa (e.g. X52 steel grade). However, there has been a significant growth in the use of high-strength steels in the offshore industry in recent decades. Alongside X65, X80 has become a prominent steel grade for the manufacturing of subsea pipelines in the UK.[43]

In 2001-2002, 158 km of X80 steel pipeline were manufactured in the UK for the development of the TRANSCO pipeline gas network.[44] In Canada, the TransCanada pipeline system has more than 400 km of operational X80 steel pipelines (as per 2013).[45]

Table 3: Example of projects executed with X80 steel line pipes[46]

Project	Dimensions	Quantity	Realization
Megal II, Germany	1118 × 13.6 mm	3.2 km	1985
Fourth Transit gas pipeline, Czechoslovakia	1420 × 15.5 mm	1.5 km	1985
Werne–Schlüchtern pipeline, Ruhrgas, Germany	48 in. × 18.4 and 19.3 mm	250 km	1992–1993
Nova pipeline; Matzhiwn project, Alberta, Canada	48 in. × 12.1 mm	54 km	1994
TransCanada pipeline,	48 in. × 12.0 and 16.0 mm	118 km	1997
Transco, UK	48 in. × 15.1 and 21.8 mm	42 km	2001
Canadian Natural Resources, Canada	24 in. × 25.4 mm	18 km	2001

It is likely that the anthropogenic CO_2 will be transported in existing or newly-developed high pressure gas pipeline networks, which will consist in part of X80 grade steel pipelines (especially in the UK and in North America). This thesis will specifically look at X80 pipeline steel materials.

2.4. The phenomenon of corrosion: thermodynamics and kinetics

2.4.1. Definition

The term "*corrosion*" is often associated with a deleterious deterioration of a material, which is detrimental to the application for which it was designed. Such definition suits the interests of engineers, who aim at designing structures and equipment which could fulfil their operational life cycle with little maintenance and inspection costs. Initially, the concept of corrosion was mainly intended for metals or alloys,[47,48] but has been since extended[49] to non-metallic materials such as ceramics, concretes, and plastics.

All material/environment reactions are however not detrimental to the materials e.g. surface film passivation, and one has to decide in which limits and boundaries a materials transformation as a result of exposure to environment could be classed as positive or negative. A reaction that is considered at first glance harmful for the materials in consideration could be so slow that the damage and/or deterioration will never be realised during operational life. Scientifically, corrosion covers all interactions between alloys and the environment.

Ultimately, two definitions[49] for *corrosion* could be formulated depending on which philosophy is embraced:

1. Corrosion science: "*the reaction of solids with their environment*"
2. Corrosion engineering: "*the reaction of an engineering constructional metal (material) with its environment with a consequent deterioration in the properties of the metal"*

The term of environment encompasses reactions in aqueous solutions, non-aqueous electrolytes, and dry media i.e. with gases. This thesis only focuses on the scientific principles associated with *aqueous corrosion (see section 2.4.2 and 2.4.3);* the reactions of solids in non-electrolytic solutions (e.g. *liquid embrittlement*), and with gases in dry atmospheres (e.g. *high temperature corrosion*) are not considered.

Aqueous corrosion could cause various types of attack for example:

- Uniform (general) corrosion

- Pitting
- Crevice
- Intergranular corrosion
- Cracking

and the causes of attack are multiple and various. These include for example:

- Redox reactions
- Concentration cells
- Galvanic corrosion
- Stress Corrosion Cracking
- Embrittlement
- Erosion

This thesis concentrates on the aspect of Stress Corrosion Cracking of alloys; this is discussed in section 2.5.

2.4.2. Corrosion thermodynamics: Is a reaction possible?

A. Redox reactions

The nature of corrosion in an aqueous electrolyte is associated with the realisation of redox reactions and to the concept of electron transfer between oxidising and reducing agents.

An oxidiser, *Ox,* is always associated to a reducing species, *Red,* via the half electronic reaction $Ox + n.e- \leftrightarrow \mathrm{Re}\,d$. Together, the oxidiser and the reducer form a redox couple defined as *Ox/Red*.

A redox reaction always involves two redox couples, since the electrons produced during oxidation of a reducer should be accepted or captured by an oxidiser. When the oxidiser Ox_1 of the redox couple Ox_1 / Red_1 is made in the presence of the reducer *Red 2* of the couple Ox_2/Red_2, the following reaction may take place:

$$\mathrm{Re}\,d_2 \leftrightarrow Ox_2 + n_2.e- \quad (\textit{Oxidation of } Red_2)$$
$$Ox_1 + n_1.e- \leftrightarrow \mathrm{Re}\,d_1 \quad (\textit{Reduction of } Ox_1)$$
$$\text{---}$$
$$n_2.Ox_1 + n_1.\mathrm{Re}\,d_2 \leftrightarrow n_2.\mathrm{Re}\,d_1 + n_1.Ox_2 \quad \textit{(Redox reaction)}$$

The prediction of this reaction is dependent on electrode potentials, as defined by the Nernst equation.[50]

B. Electrode potentials

An electrode is the 2-phase system interface constituted by a conductive solid phase (e.g. metal) and a liquid phase (i.e. electrolyte).

When a conductive material, e.g. a metal M, is exposed to an electrolytic solution, the equilibrium $M \leftrightarrow M^{n+} + n.e-$ is realised across the surface of the metal. The metal cations M^{n+} have a natural tendency to go into solution, since their chemical potential in the solution tends to the negative infinite, leaving electrons behind in the metal. This phenomenon creates a double interface layer constituted of metal cations and electrons, which behave as a condenser. This layer is referred as the *Helmholtz layer*. In reality, the metal cations tend to move away from the metal surface due to thermal agitation, and this extends the Helmholtz layer to a new region associated with the diffused layer of Gouy-Chapman (see Figure 16).

The imbalance of positive and negative charges across the surface of the metal generates the establishment of a voltage, referred as the absolute electrode voltage or as the absolute electrode potential, V_{abs} (see Figure 16):

$$V_{abs} = V_M - V_{sol},$$

Where,

V_M is the metal potential and V_{Sol} is the electrolyte potential

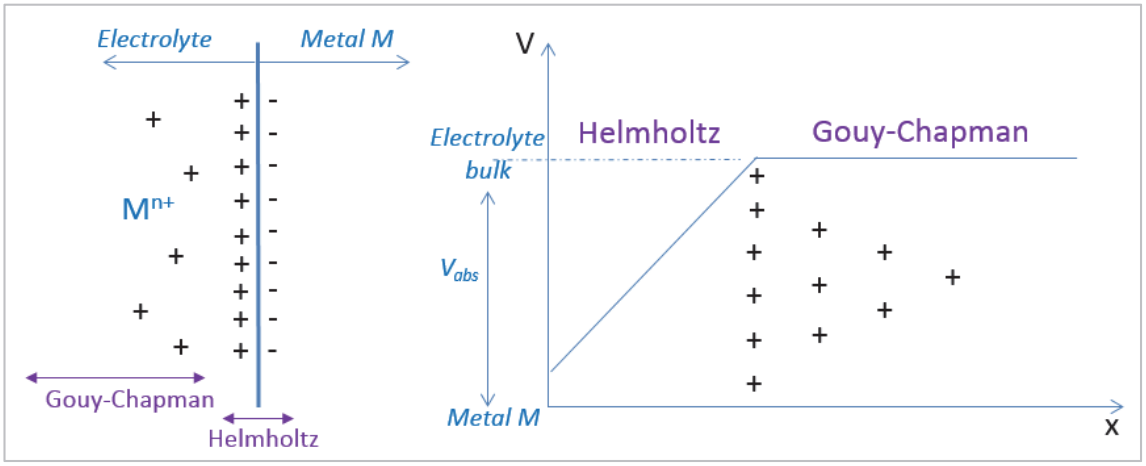

Figure 16: Concept of Helmholtz and Gouy-Chapman Layers on an immersed conductive electrode

In any electrochemical studies, V_{abs} is the measurement of interest that we want to measure or control. However, V_{abs} cannot be measured practically since it is established between two phases of different nature i.e. solid and liquid. Consequently, only the difference of absolute potentials between two electrodes

is accessible by measurement (with a voltmeter). If one of these electrodes is defined as the reference, the difference of potentials measured between the two electrodes with a voltmeter (Figure 17), is defined as the relative potential or as the electrode potential, $E_{electrode/ref}$:

$$E_{electrode/ref} = V_{abs,\ electrode} - V_{abs,\ reference}$$

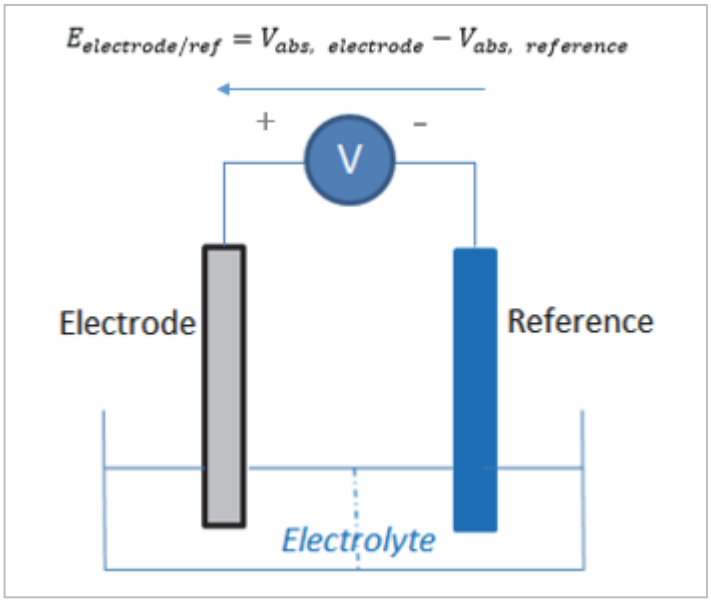

Figure 17:Practical measurement of the electrode potential with a reference electrode

In Figure 18, the electrochemical cell is illustrated as a simplified network of electronic components. As discussed above, the physical dimension of interest that we want to measure, control and study in any electrochemical experiments is the absolute electrode potential which is established across the interface of the metal/electrolyte (i.e. between points C and D). However, the voltmeter does only a good work at measuring the voltage between A and B. Figure 18 shows the concept of the indirect measurement of the absolute electrode potential with a voltmeter using a reference electrode. The voltage measured across the voltmeter is directly related to the difference between the absolute potential of the electrode and that of the reference electrode, as mathematically demonstrated below:

1. $V_{measured} = V_A - V_B$
2. *If* $R_{w\ is}$ *negligible,* $V_A = V_C$
   and, $V_B = V_F$
3. *if* R_S *is negligible (e.g. Electrolyte with high conductivity),* $V_D = V_E$
4. By definition, $V_F - V_E = Reference\ Electrode\ (RE) Absolute\ Potential$

5. $V_{measured} = V_C - V_F$

   $= V_C - RE\ Abs.Potential - V_E$

   $= V_C - V_D - RE\ Abs.Porential$

6. By definition, $V_C - V_D = Electrode\ Absolute\ Potential$

   Then, $V_{measured} = Electrode\ Absolute\ Potential - RE\ Absolute\ Potential$

   and $V_{measured} = Electrode\ Potential$

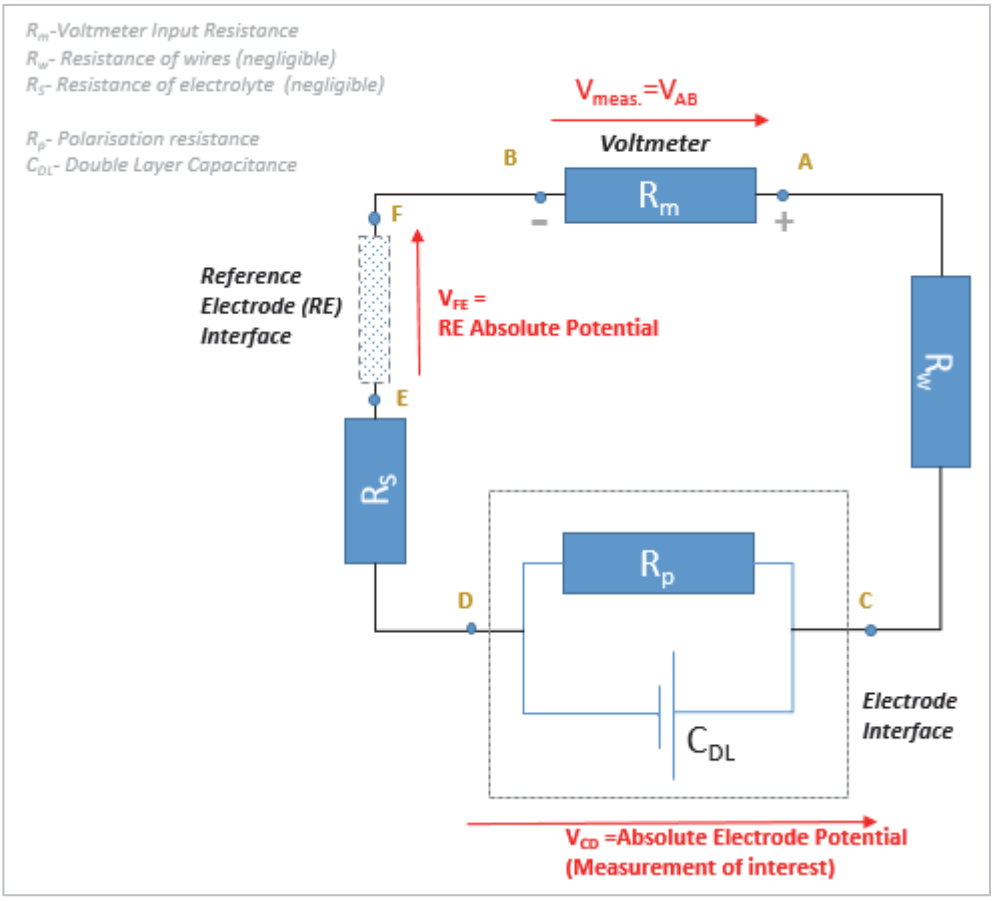

Figure 18:Concept of electrode potential measurement with a reference electrode

The passage of metallic ions to the solution via the reaction $M \leftrightarrow M^{n+} + n.e-$ theoretically occurs for all metals for thermodynamic reasons (see below), but the magnitude of the phenomenon depends on the nobility of the metal. Electronegative or noble materials such as platinum Pt do not particularly favour the formation of electrons and are practically considered as inert, in contrast to electroactive metals such as magnesium (Mg) which favour the generation of electrons.

A potential may be seen as a measurement of the distribution of negative and potential charges in a localised region of the space. The electrode potential is shifted to low or negative values as the oxidation of metal becomes substantial and the presence or concentration of negative charges (electrons) at the interface

is greater than that of the positive charges. Electronegative (noble) metals have a higher electrode potential than that of electroactive (less noble) metals.

C. Redox potential and Nernst equation

When only one redox couple Ox/red is present at the electrode surface, and the electronic transfer between Ox and Red across the electrode interface is such that the system is at equilibrium i.e. $Ox + n.e- \leftrightarrow \mathrm{Re}d$, the electrode potential is associated with the potential of the redox couple, which is determined by the *Nernst Equation*, i.e.:

$$E_{electrode/ref} = E_{Ox/red}$$

For example, this is realised in the following cases (Figure 19):

- A metal is exposed to an electrolyte in which its cations M^{n+} are present at electrode interface
- An inert metal (e.g. Pt) is exposed to a solution in which an oxidiser Ox (e.g. O_2) and its associated reducer Red (e.g. H_2O) are present at the electrode interface

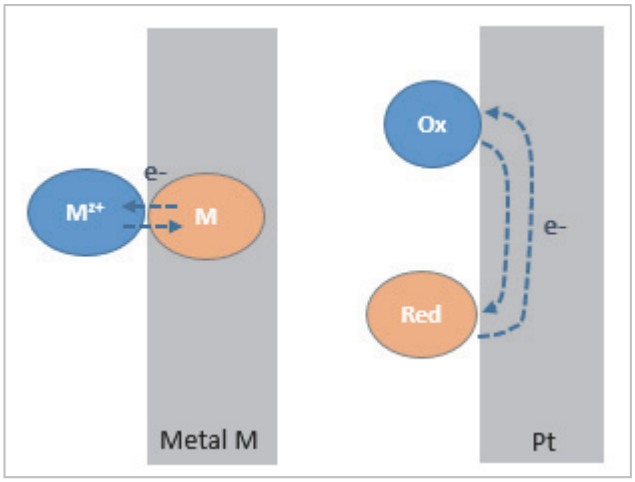

Figure 19: Cases in which the electrode potential is defined by the Nernst Equation

Therefore, if a redox reaction $vOx + n.e- \leftrightarrow x\,\mathrm{Re}d$ is considered at the electrode, and the electronic transfer across the interface is such that the overall reaction is in equilibrium, then the associated electrode potential could be defined as per the Nernst Equation as follows:

- The total variation of free energy of the above electrochemical reaction ΔG_R is the sum of the variation of chemical free enthalpy ΔG and the electrical work We:

$$\widetilde{\Delta G_R} = \Delta G + We$$

- If the electrochemical reaction is in equilibrium so that neither the oxidation or the reduction is privileged, then:

$$\widetilde{\Delta G_R} = 0 \text{ and } \Delta G = -We$$

- $If\ \Delta G\ and\ We\ are\ defined\ as\ followed$:

$$\Delta G = \Delta G^0 + \frac{R.T}{n.F}.\ln(\frac{a_{red}^x}{a_{ox}^v})$$

$$We = n.F.E_{ox/red}$$

Then, the Nernst Equation can be written:

$$E_{ox/red} = E_{ox/red}^0 + \frac{R.T}{n.F}.\ln(\frac{a_{ox}^v}{a_{red}^x}),$$

Where,

$E_{ox/red}^0$ *is the potential of the redox couple at standard conditions*

T is the temperature in Kelvin

R is the universal gas constant (8.314 J.K^{-1}.mol^{-1})

F is the Faraday constant (96, 485 C.mol^{-1})

a is the chemical activity of the species considered

If other species than the oxidiser and the reducer intervene in the redox equilibrium (e.g. hydroniums, hydroxyls, water), then the most general definition of the Nernst equation is given by:

$$E_{ox/red} = E_{ox/red}^0 + \frac{R.T}{n.F}.\ln(\prod a_i^{v_i}),$$

where *v*<0 if the species is a reactant and >0 if it is a product

D. Reaction prediction

The realisation or prediction of a redox reaction may be determined using the electrode potentials associated with the couples *Ox_1 / Red_1 and Ox_2 / Red_2* as determined by the Nernst equation.

If the following redox reaction is considered:

$$Red_2 \leftrightarrow Ox_2 + n_2.e - (\times n_1) \text{ (1)} \quad \textit{(Oxidation of } Red_2\textit{)}$$

$$Ox_1 + n_1.e - \leftrightarrow Red_1 \ (\times n_2.) \text{ (2)} \quad \textit{(Reduction of } Ox_1\textit{)}$$

$$n_2.Ox_1 + n_1.Red_2 \leftrightarrow n_2.Red_1 + n_1.Ox_2 \text{ (3)} \quad \textit{(Redox reaction)}$$

The total variation of the free energy of the redox reaction (3) is the sum of the variation of free energies of reaction (1) and (2):

$$\widetilde{\Delta G_3} = \widetilde{\Delta G_1} + \widetilde{\Delta G_2}$$

With:

$$\widetilde{\Delta G_1} = \Delta G_1 + We_1$$

$$\widetilde{\Delta G_2} = \Delta G_2 + We_2$$

If the reactions (1) and (2) are both at equilibrium then, as defined above:

$$\Delta G_1 = n_2.F.E_{ox_2/red_2}$$

$$\Delta G_2 = -n_1.F.E_{ox_1/red_1}$$

And, $\widetilde{\Delta G_3} = n_1.n_2.F.(E_{ox_2/red_2} - E_{ox_1/red_1}) + We_1 + We_2$

As the electrical work provided by the electrochemical reaction (1) is that received by reaction (2), then:

$$We_1 = -We_2$$

Then:

$$\widetilde{\Delta G_3} = n_1.n_2.F.(E_{ox_2/red_2} - E_{ox_1/red_1})$$

When $E_{ox_1/red_1} > E_{ox_2/red_2}$, $\widetilde{\Delta G_3}$<0 and the redox reaction (3) from left to right is readily favoured. The most oxidising species react with the most reducing

species; this is usually referred as the Gamma law. The reaction is at the equilibrium when ΔG =0 and $E_{ox_1/red_1} = E_{ox_2/red_2}$

$\widetilde{\Delta G_3}$is therefore solely a function of the variation of free chemical enthalpy of reaction (1), ΔG_1 and reaction (2), ΔG_2:

$$\Delta G_1 = \Delta G_1^0 + R.T.\ln(\frac{a_{ox2}^{n1}.}{a_{red2}^{n1}.})$$

$$\Delta G_2 = \Delta G_2^0 + R.T.\ln(\frac{a_{red1}^{n2}}{a_{ox1}^{n2}})$$

$$\widetilde{\Delta G_3} = \Delta G^0 + R.T.\ln(\frac{a_{red1}^{n2}.a_{ox2}^{n1}.}{a_{ox1}^{n2}.a_{red2}^{n1}.})$$

When the reaction (3) is favoured from left to right then$\Delta G = \Delta G_1 + \Delta G_2 < 0$, otherwise the reaction is not thermodynamically favoured. When Red_1 or Ox_2 are initially absent, $\ln x \overset{0}{\rightarrow} -\infty$, and $\widetilde{\Delta G_3} < 0$. Therefore a redox reaction always starts. But the question is to determine how far it continues.

2.4.3. Corrosion kinetics: how fast is the reaction?

A. Polarisation curves: Current Density-Potential curves

If the following reduction reaction is considered at an electrode:

$$a.Ox + n.e- \rightarrow b.Red$$

The associated kinetics are defined as:

$$v = v_{red} = -\frac{1}{a}\frac{dn_{ox}}{dt} = \frac{1}{b}\frac{dn_{red}}{dt}$$

Where,

dn_{ox} *is the variation of the number of moles of Ox by unity of electrode surface during a time period of t; the variation is negative since the oxidant is consumed.*

dn_{red} *is the variation of the number of moles of Red by unity of electrode surface during a time period of t; the variation is positive since the reducer is produced.*

If an oxidation reaction is considered:

$$b.Red \rightarrow a.Ox + n.e-$$

Then,

$$v = v_{ox} = -\frac{1}{b}\frac{dn_{red}}{dt} = \frac{1}{b}\frac{dn_{ox}}{dt}$$

The kinetics of oxidation and reduction could be associated with a current density, which corresponds to the number of electrons arriving (reduction) or leaving (oxidation) the reaction site at the electrode surface. By convention the current density associated with reduction, J_{red}, is taken as negative, and that associated with the oxidation, J_{ox}, is taken as positive.

$$v_{red} = -\frac{J_{red}}{n.F}$$

$$v_{ox} = \frac{J_{ox}}{n.F}$$

If the oxidation and the reduction reactions simultaneously occur on the electrode surface:

$$a.Ox + n.e- \leftrightarrow b.Red,$$

Then,

$$J_{tot} = J_{ox} + J_{red} = n.F.(v_{ox} - v_{red})$$

If the reaction is at equilibrium:

$$J_{tot} = 0;\ v_{ox} = v_{red}$$

When looking at the Nernst equation,

$$E_{ox/red} = E^0_{ox/red} + \frac{R.T}{n.F}.\ln(\frac{a^v_{ox}}{a^x_{red}})$$

it may be seen that by shifting the electrode potential around, the activities of the Ox and Red species, or their respective concentrations (in ideal conditions), are also displaced:

- By imposing an electrode potential $E > E_{ox/red}$; the oxidation of Red is favoured, $v_{ox} > v_{red}$

- By imposing an electrode potential $E < E_{ox/red}$; the reduction of Ox is favoured, $v_{ox} < v_{red}$
- At the equilibrium, $E = E_{ox/red}$, and $v_{ox} = v_{red}$

Thus, by studying the influence of electrode potential on the current density traversing the electrode surface where the electrochemical reaction takes place, the influence of the electrode potential on the reaction kinetics at the electrode interface may be determined. Such study is commonly visually illustrated by the plotting of *polarisation curves* or *Current density- Potential Curves J-E* (Figure 20).

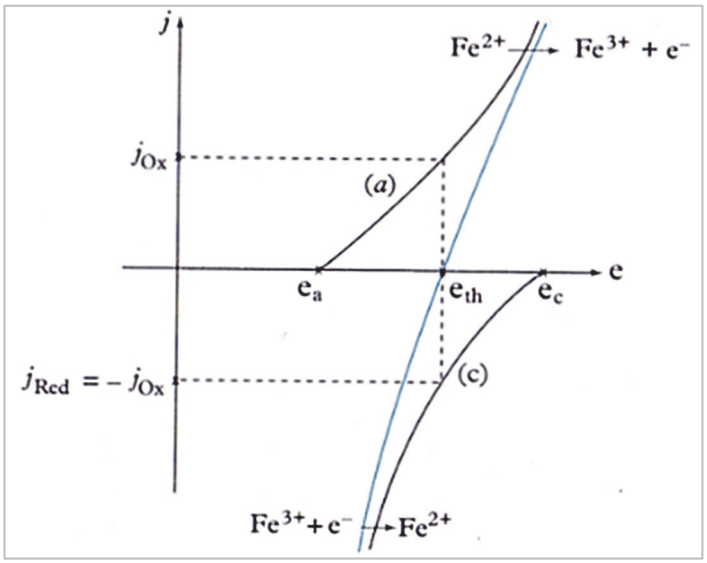

Figure 20: Typical Curve J-E with illustration of oxidation and reduction for a couple Ox/Red[51]

The plotting of such curves is discussed further in section 3.3.3.

In the next section, the specific case where two redox couples are simultaneously involved on the surface of an electrode, typically during a redox reaction or during a corrosion reaction, is discussed.

B. Mixed polarisation curve and Butler-Volmer equation

It is considered that two redox couples Ox_1 / Red_1 and Ox_2 / Red_2 are involved in a redox reaction on the surface of an electrode, and the electrode potential (provided by the Nernst Equation) related to Ox_1 / Red_1 is higher than that of Ox_2 / Red_2, i.e. $E_{eq,\ ox_1/red_1} > E_{eq,\ ox_2/red_2}$.

The associated redox reaction is as followed:

$$Red_2 \leftrightarrow Ox_2 + n_2.e - (\times n_1) \text{ (1)}$$

$$Ox_1 + n_1.e - \leftrightarrow Red_1 \ (\times n_2) \text{ (2)}$$

$$n_2.Ox_1 + n_1.Red_2 \leftrightarrow n_2.Red_1 + n_1.Ox_2 \text{ (3)}$$

Under these conditions, if the electrode is left in its free condition, i.e. no potential is imposed to the electrode from an external source, the electrode goes to equilibrium and takes an electrode potential defined as the Open Circuit Potential (OCP), which is equivalent to a mixed potential E_M. The mixed potential lies between $E_{eq,\ ox_1/red_1}$ and $E_{eq,\ ox_2/red_2}$.

The exact position of the OCP between $E_{eq,\ ox_1/red_1}$ and $E_{eq,\ ox_2/red_2}$ will be dependent on the relative sizes of the anode and the cathode (where the oxidation and the reduction reaction take place respectively), the location of the reference electrode in regards to the anode and cathode and the cell resistance to current flow. For example, if the reference electrode is moved closer to the anode site then the OCP will move towards $E_{eq,\ ox_2/red_2}$. Similarly, if it is closer to the cathode site, then the OCP will move towards $E_{eq,\ ox_1/red_1}$.

A diagram of Evans is illustrated in Figure 21 to show the evolution of the electrode potential to the OCP as a polarisation between the couples *Ox_1 / Red_1* and *Ox_2 / Red_2* is established across the electrode surface, and the redox reaction $n_2.Ox_1 + n_1.Red_2 \leftrightarrow n_2.Red_1 + n_1.Ox_2$ is produced. If no polarisation can be established between the sites where the respective *Ox_1 / Red_1* and *Ox_2 / Red_2* equilibriums *are* established (e.g. due to solution resistance), then the local electrode potentials would remain specific to that of the respective Nernst potentials associated with *Ox_1 / Red_1* and *Ox_2 / Red_2, i.e.* $E_{eq,\ ox_1/red_1}$ and $E_{eq,\ ox_2/red_2}$ respectively.

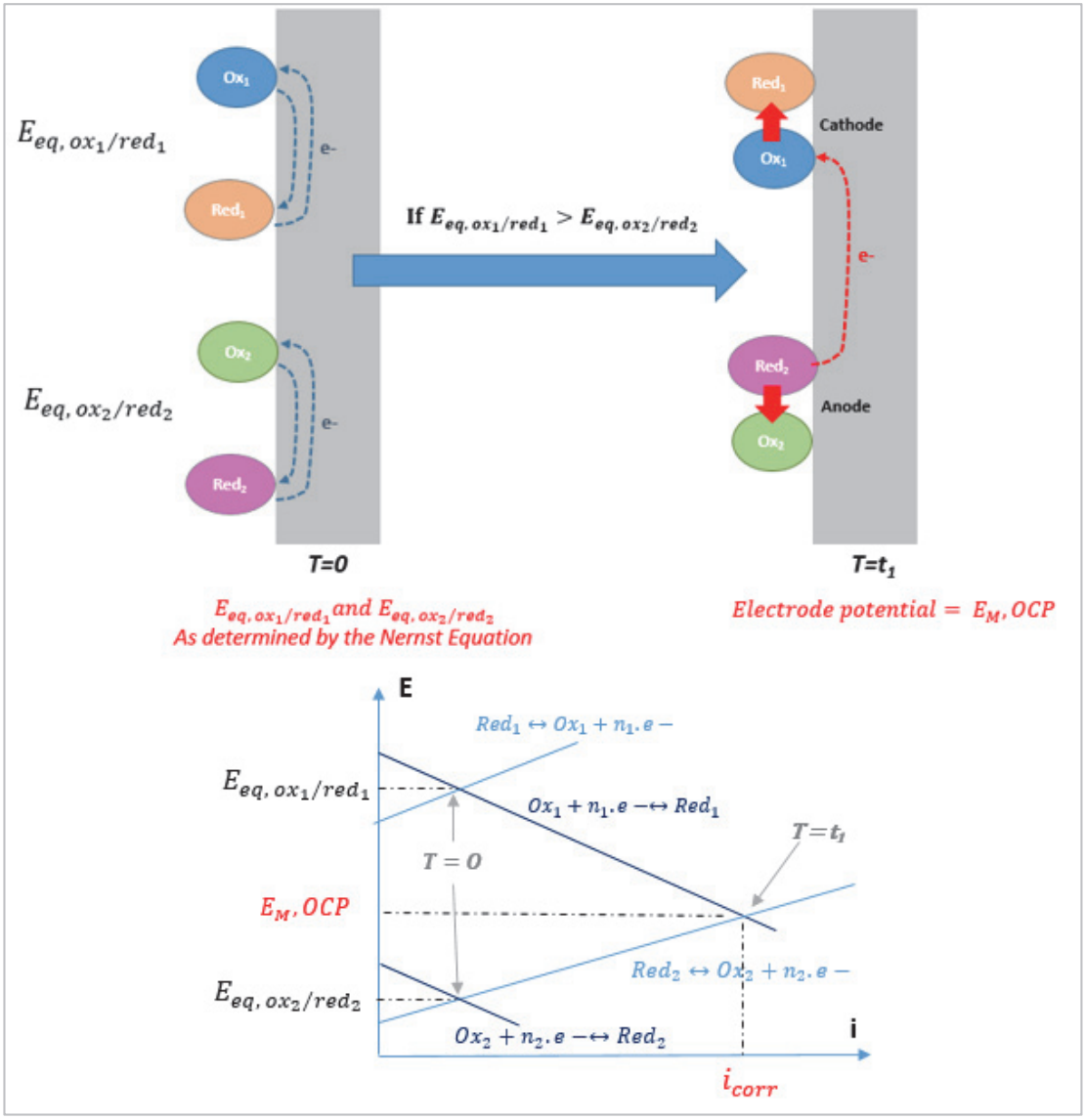

Figure 21: Concept of the Open Circuit Potential as defined by Evan diagram

At E_M, the respective current densities related to the half reactions (1) and (2) that compose the redox reaction (3), J_1 and $J_2$are equivalent and the overall current density of (3) is nil: $J = J_1 + J_2$=0.

When a potential is imposed on the electrode, and the electrode potential is shifted to a value E away from that of the electrode under equilibrium conditions (i.e. E_M), the electrode is said to be polarised; the difference $\theta = E - E_M$, is called the electrode polarisation. One of the half-reactions (1) or (2) becomes privileged to the other.

We could then define three domains:

- $E < E_{eq,\ ox_2/red_2}$, the reduction of *Ox₁* and *Ox₂* are simultaneous, but that of *Ox₁* is faster than *Ox₂*, and the total current density J is dominated by J_2

- $E > E_{eq,\ ox_1/red_1}$, the oxidation of *Red₁* and *Red₂* are simultaneous, but that of *Red₂* is faster than *Red₁* and the total current density J is dominated by J_1
- $E_{eq,\ ox_2/red_2} < E < E_{eq,\ ox_1/red_1}$, the reduction of *Ox₁* and the oxidation of *Red₂* are occurring at the same time; however the kinetics of reaction are different. In this interval,:
    - If $E = E_M$, then $J_1 = |J_2|$.
    - If $E < E_M$, then $J_1 < |J_2|$
    - If $E > E_M$, then $J_1 > |J_2|$

The curve Current Density-Electrode potential for a redox reaction (3) at an electrode surface is illustrated in Figure 22; the mixed polarisation curve for the redox reaction (3) could be seen as the sum of the polarisation curves established for each redox couple:

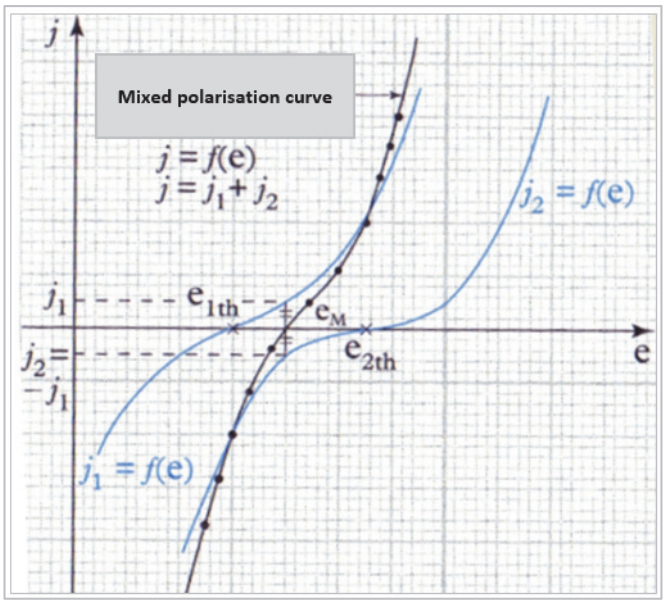

Figure 22: Typical mixed polarisation curve for two redox couples involved in a redox reaction at the electrode surface[51]

The relation between the electrode potential E and the current density J of a redox reaction (3) occurring at an electrode surface is given by the *Butler-Volmer Equation. T*his relation assumes that the electrode reaction rate is controlled by electron transfer:

$$J = J_0.\left(\exp\left(\frac{\alpha.n.F}{RT}.(E - E_M)\right) - \exp\left(-\frac{\beta.n.F}{R.T}.(E - E_M)\right)\right)$$

where,

J_0 is the exchange current density, A/m²

α, β are respectively the anodic and cathodic charge transfer coefficient (dimensionless)

The term $J_0 . \exp\left(\frac{\alpha.n.F}{RT} . (E - E_M)\right)$ is related to the current density associated with the oxidation of *Red_2 (reaction (1))*, whilst the term $-J_0 . \exp\left(-\frac{\beta.n.F}{R.T} . (E - E_M)\right)$ is related to the current density associated with the reduction of *Ox_1 (reaction (2)).* One term is dominated by the other depending upon where the electrode potential E lies in relation to E_M as discussed above.

C. Passivation of alloys

In general and as defined by the *Butler-Volmer* Equation, the rate of anodic dissolution should increase as the potential E is increased to positive values. However, certain systems "metals or alloys / electrolyte solutions" feature passivity when the potential is increased above a threshold potential in the anodic potential domain. The passivity of a metal or alloy is associated with the formation of a surface protective film which "isolates" the materials from the environment. The oxidation (or corrosion) of the metallic materials becomes hindered, and low anodic current densities are monitored in the region of anodic potentials where the alloy is passive. Above a certain anodic potential, the film becomes degraded and active anodic dissolution or corrosion is allowed to take place again; the metal (or alloy) is said to be in its transpassive state.

A typical polarisation curve I-E of a metallic material featuring passive and transpassive behaviour in the anodic region is illustrated in Figure 23.

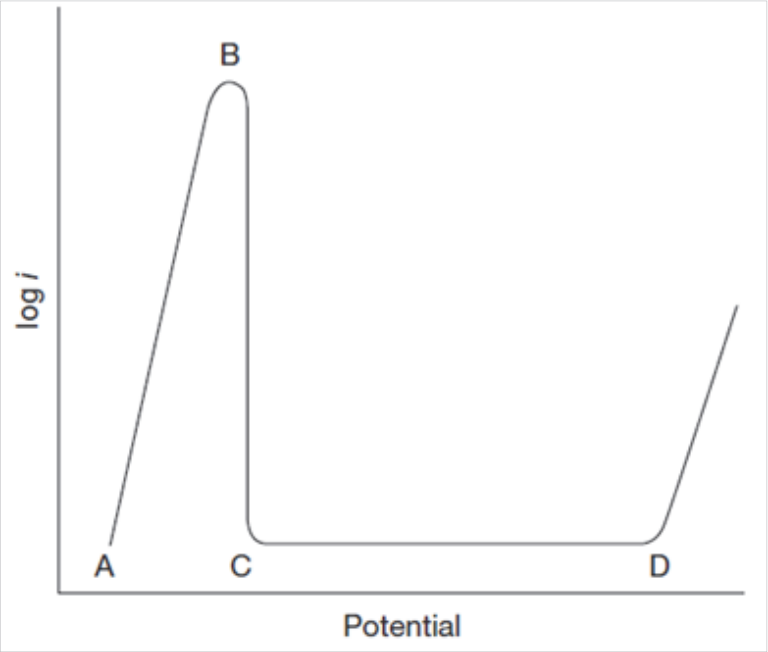

Figure 23: Typical polarisation curve I-E of a metallic material featuring passive (B-D)and transpassive behaviour (D onwards) in the anodic region[52]

The establishment of a protective film is dependent both on the nature of the materials and the environment. The concept of metal/alloy passivation is key for Stress Corrosion Cracking to be realised; this will be discussed further in section 2.5

2.4.4. Examples of possible anodic dissolution processes in anthropogenic CO_2 pipelines

A. Effect of carbon dioxide on steel corrosion

In the presence of liquid water, CO_2 can cause significant corrosion of carbon steel materials used in pipeline design due to the formation of carbonic acid (see section 2.2.2) – this is usually referred to as CO_2 corrosion or sweet corrosion. Aqueous CO_2 corrosion of carbon steel is an electrochemical process involving the anodic dissolution of iron and the cathodic evolution of hydrogen.

The key parameters influencing the sweet corrosion rate are CO_2 partial pressure, temperature, pH, and iron carbonate supersaturation which could drive the formation of protective iron carbonate (see section 2.7.1).

This subject has been widely discussed in the literature.[7,8,53,54,55] In summary, it has been discussed that, H_3O^+ and H_2CO_3 serve as the main oxidising agent at low pH, whilst HCO_3^- will dominate at high pH (pH>5).[54]

<u>pH<5</u> $$Fe + 2H_2CO_3 \leftrightarrow Fe^{2+} + 2HCO_3^- + H_2$$

<u>pH>5</u> $$Fe + 2HCO_3^- \leftrightarrow Fe^{2+} + 2CO_3^{2-} + H_2$$

B. Effect of sulphur dioxide on steel corrosion

Sulphur dioxide is known to generate significant external corrosion of carbon steel materials exposed to industrial atmospheres.[18,56] The increased susceptibility to corrosion in polluted SO_2 environments could be initially related to the formation of acids in the presence of moisture, which provide an additional source of hydronium cations for cathodic reduction and produce lower pH in solution: The weak sulphurous acid is formed from the reaction of SO_2 with water as discussed previously. In the presence of metals or metallic oxides catalysts, SO_2 can be oxidised in sulphur trioxide (SO_3). [50]

Early work conducted by Rozenfeld (1962)[57] at relatively high levels of SO_2 (0.5%vol.) suggests that the increased dissolution rates in the presence of SO_2 is associated with the great solubility of SO_2 in water (about 1300 times more soluble than oxygen). As a result of its high solubility, it was suggested that SO_2 could be a more effective cathode reactant than O_2 (aq). Rozenfeld[57] also indicated that SO_2 can play the role of cathodic depolariser, which thus would enhance dissolution rates. Other studies[58] have suggested that the reduction of SO_2 into SO_4^{2-} (supported by oxidation of iron metal) is the first step of iron corrosion in these environments:

$$SO_2 + O_2 + 2e- \leftrightarrow SO_4^{2-}$$

$$Fe \leftrightarrow Fe^{2+} + 2e-$$

However in a later study, Cox and Lyon (1993)[59] stipulate that it is rather the drop in pH and the increase in solution conductivity that lead to higher degradation rates in the presence of SO_2. The presence of sulphur compounds and low pH will further hinder the precipitation and establishment of protective scales such as iron carbonate in CO_2 containing environments.[60] This is discussed in section 2.7.2.

Effect of sulphur dioxide on steel corrosion in CO_2 environments

Xiang et al.[61] (Figure 24) investigated corrosion of X70 steels exposed in CO_2 saturated-water phase in the presence of different levels of SO_2 at 100 bar and 50°C under flowing conditions; weight loss coupons were exposed for 12 days. The study confirms that the additional presence of SO_2 increases the corrosion

rates in a CO_2 saturated-water phase. This was also confirmed by Choi et al. and Farelas et al..[62,63]

The mechanism of dissolution in the presence of SO_2 in wet CO_2 environments needs to be investigated further, but it is likely that the formation of sulphurous acids and the associated drop of aqueous phase pH will be significant contributors to the corrosion processes due to their role in anodic dissolution and prevention of passivating conditions.

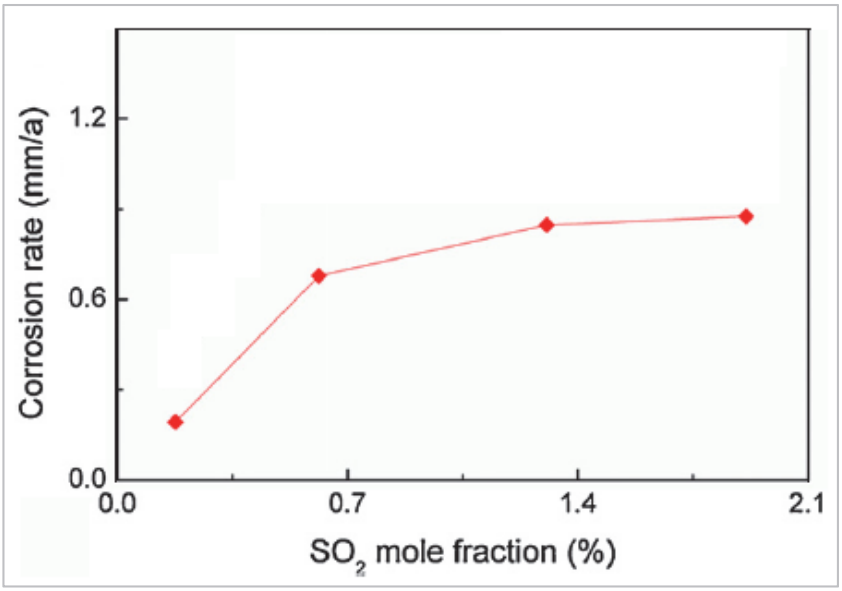

Figure 24: Effect of sulphur dioxide on the corrosion rates of Carbon Steel in CO_2 saturated-water phase (1000 ppm O_2) (100 bar, 50°C) for 12 days[61]

C. Effect of nitrogen oxides on steel corrosion

Nitrogen oxides (especially NO_2) also lead to corrosion of carbon steel in polluted atmospheres although the magnitude has not been found to be as severe as in the presence of sulphur dioxide (see Figure 25) in atmospheric conditions.[64]

Similarly to sulphur dioxide, as discussed in section 2.2, these impurities produce acids which in turn provide an additional source for hydroniums which will directly result in anodic dissolution (acid corrosion). Furthermore, the establishment of low pH values will hinder the formation of protective films.

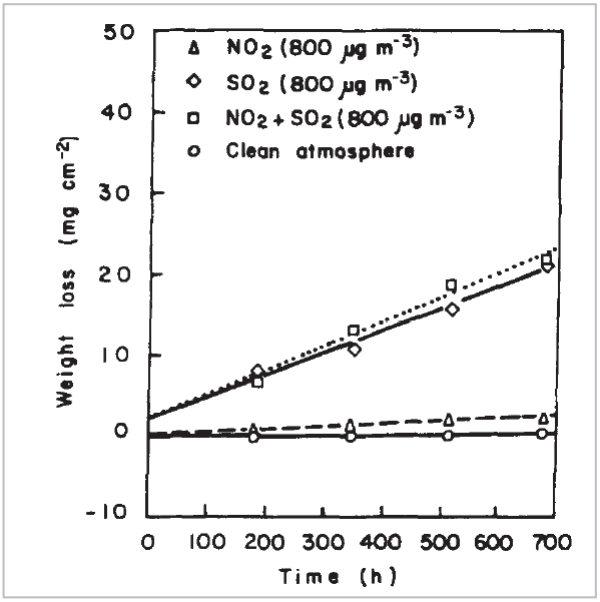

Figure 25: Evolution of weight loss with exposure time to NO_2 and SO_2 in atmospheric conditions[64]

Effect of nitrogen oxides on steel corrosion in CO_2 environments

Data on the effect of NOx on steel corrosion in CO_2 environments is sparse. Dugstad suggests that the presence of NOx is more aggressive than SO_x in CO_2 environments.[21]

The mechanism of dissolution in the presence of NO_x in wet CO_2 environments needs to be investigated further, but it is likely that the formation of nitric and nitrous acids and the associated drop of aqueous phase pH will be significant contributors to the corrosion processes due to their role in anodic dissolution and prevention of passivating conditions.

2.5. The phenomenon of Stress Corrosion Cracking

2.5.1. Overview

A. Environmentally-assisted cracking (EAC)

As part of the most generic concept of corrosion, which encompasses all interactions between materials and environments that are deleterious to the material properties to be preserved[49], metals and alloys could fail in a catastrophic manner by various cracking mechanisms.

These cracking mechanisms, which are produced by the combined effect of a corrosive environment and mechanical stresses, have been collected within the common terminology of Environmentally-assisted cracking (EAC); EAC can be described by five forms of cracking:[65]

- Corrosion fatigue; the fatigue of metal or alloy due to cyclic mechanical stress is aggravated by the co-joint action of a corrosive environment
- Stress-assisted localised corrosion, in which narrow corrosion paths which have been drawn by localised corrosion mechanisms, especially intergranular attack, are opened by tensile stress aggravating the localised corrosion process
- Stress Corrosion Cracking (SCC), in which the simultaneous action of a static tensile stress and a corrosive environment is required to promote the formation of cracks more or less perpendicular to the mechanical stress.
- Hydrogen cracking, which could be the result of:
    - Hydrogen embrittlement: atomic hydrogen diffuses into the solid solution causing crystal embrittlement, and causes cracking under tensile stress
    - Hydrogen induced cracking (HIC): atomic hydrogen recollects into molecular hydrogen at microstructure irregularities such as inclusions, causing localised pressure build-up and eventually blistering
- Liquid metal embrittlement, in which cracking occurs due to the exposure of a metal / alloy to liquid metal

This Thesis focuses on the occurrence of Stress Corrosion Cracking (SCC) of carbon steel and low-alloy steel materials.

B. Stress Corrosion Cracking (SCC)

Definition of SCC

The generic definition and description of Stress Corrosion Cracking could be a challenge whilst not mentioning a specific mechanism. The most adequate definition for SCC is probably to describe SCC as the fracture of a metallic material, essentially by cracking, which requires the synergistic action of a residual or applied tensile stress, and an environment capable of causing the corrosion of this material. The balance between the active (dissolution) and passive behaviour of a material in an environment is generally crucial in generating SCC, and this will be discussed further in the following sections.

Should the material or the environment or the tensile loading characteristics be altered, even so slightly, SCC may be or may not be realised. Stress Corrosion Cracks could either develop in an intergranular (i.g.) or in a transgranular (t.g.) mode. Intergranular SCC is defined as the crack pattern follows the grain boundary paths, in opposition to transgranular cracking for which the crack readily pierces and crosses through grains. In certain situations, mixed i.g. and t.g cracks have been reported from the same fracture surface.

SCC initiation and propagation

The phenomenon of SCC is usually described as a sequential process which involves three main stages, i.e.:

1. Crack initiation or incubation
2. Steady crack-propagation
3. Final failure (due to overload)

The realisation of SCC, i.e. its initiation and propagation, can be materialised with little physical outside evidence of corrosion which means that a catastrophic failure as a result of stress corrosion cracks could occur with little or no warning, especially if specific non-destructive inspection techniques (e.g. radiography, ultrasonics) are not used.

The cracks generally initiate at:

- Surface discontinuities or defects, which could have been generated mechanically at the manufacturing stage or during operational life. Typical mechanically-produced surface flaws are grooves, blurs and laps. During service, these sites could act as crevices where the gradient of aqueous species concentrations could favour localised pitting which in turn may develop as a crack (see below). The local high density of stresses at these defects could support the initiation of cracks.
- Corrosion pits. By their nature, corrosion processes are chaotic i.e. not homogeneous due to spatial heterogeneity of the environment (e.g. gradient of species concentration, aeration, temperature) across materials surface and local differences in material surface chemistries and microstructure (e.g. grain boundaries, inclusions, various phases and constituents). Pits could be produced as a result of localised corrosion processes, which may then eventually transform into cracks.
- Grain boundaries or material slip planes. Localised corrosion could occur where surface protective films are weaker. Grain boundaries are typical culprits since the associated chemistries are usually different from that of the materials bulk, and this will lead to preferential active corrosion around grains or intergranular corrosion. In low-stacking fault materials, the emergence of slip planes at the surface could disrupt a film resulting in localised corrosion.

The transition from crack initiation to crack propagation remains unclear, as the challenge stands in defining at which point a pit actually acts as a crack, and intergranular corrosion becomes i.g. stress corrosion cracks. It has been discussed that the ratio between the depth and the width of a pit must be greater than 10 before a pit behaves as a crack initiation site. A depth to width ratio of approximately 1000 has generally been observed for a growing stress-corrosion crack.[66]

Whether a pit or a localised corrosion feature will act as an initiating site for cracking propagation is dependent on the environment (and electrochemistry), the material metallurgy at the pit base or at the localised corrosion penetration tip, and to the corrosion feature associated mechanical parameters (e.g. morphology / geometry, stresses). The associated environmental and metallurgical

parameters for sustained crack growth are not necessarily those that generated pitting or localised corrosion in the first instance, and are precisely primarily related to the micro-system at the crack tip.

Section 2.5.2 will discuss the metallurgical and environmental parameters controlling the realisation of SCC.

2.5.2. SCC controlling parameters

A. Environment-control parameters, and rate-determining step

SCC: Alloy and Environment systems

As part of the definition of SCC, SCC is specific to the intimate couple of a metallic alloy and a suitable corrosive environment. The requirement of a corrosion component for the occurrence of SCC means that exposure to an aqueous environment has generally been necessary to cause SCC. Aqueous environment encompasses bulk solutions and condensed moisture surface films. High temperature corrosion processes which involve reactions between gases and metals are not considered in this thesis.

A list of a few common alloys / aqueous environments systems where SCC has been identified is indicated in Table 4.

Table 4: Typical Alloy-Environment SCC systems[67]

Materials	Environment
Carbon steel	Hydroxides
	Nitrates
	Bicarbonate/Carbonate
	Liquid ammonia
	$CO_2/CO/H_2O$
	H_2S
Stainless steel	Chlorides
	Thiosulphate or polythionate
Titanium	Methanol
Copper alloy	Ammoniacal solutions

Crack growth and rate-determining step

The interaction of the material and its environment will lead to the cascade of a series of physical and chemical events at the surface metal, which sequential order will drive or not the initiation and propagation of stress corrosion cracks. As part of this sequence of events, and once it is considered the crack is within the propagation regime, it is necessary to bring forward the rate-determining (or

limiting) step, which speed, precisely the slowest, will drive the steady crack propagation kinetics, or crack growth rate (SCC stage 2) until the materials fails from mechanical fracture due to overload (SCC stage 3).

The characteristics of the rate-determining step i.e. the nature of the reaction and its kinetics are closely related to the environmental parameters within the crack domain which could be pictured as a micro-system. This domain essentially consists of the crack-tip but could be easily extended to the crack walls up to the metal surface surrounding the crack. The environmental parameters which could affect the crack growth within this domain include:

- Nature of the chemical species
- Concentration and activity of the chemical species
- Temperature
- Pressure
- pH
- Electrochemical potential

Should any of these conditions be modified, this may result in a change in the rate-determining step nature or kinetics, which in turn could either accelerate, decelerate or arrest the crack growth. Whichever environmental parameter(s) becomes predominant on the crack propagation is hence dependent on the nature of the rate-determining step, and ultimately to the Stress Corrosion Cracking mechanism; SCC mechanisms will be discussed in section 2.5.3.

SCC: thermodynamics and kinetics

Irrespective of the SCC mechanism, the realisation of SCC relies on two major scientific concepts:

1. Thermodynamics: is the chemical / physical reaction feasible?
2. Kinetics: if the reaction is feasible, at what speed will it happen?

For example, anodically-assisted SCC, in which the crack growth essentially relies on the active dissolution (corrosion) of the crack-tip, will require that the two following reactions are thermodynamically possible:

- Oxidation of the metal (via a Redox reaction)

- Formation of a stable protective film along crack walls and at the metal surface surrounding the crack

In anodically-assisted SCC, the balance between active and passive behaviour between the crack-tip and the crack walls is particularly sensitive to the realisation of SCC, since it is the preferential localised corrosion at the crack tip that is required, rather than an overall general corrosion behaviour.[68] Domains of electrochemical potentials and pH in which SCC may be hypothetically generated could be determined using the Pourbaix stability E-pH diagrams, in which regions of metal oxidation and passivation are identified.

In contrast to dissolution-controlled SCC, hydrogen-assisted-crack growth (or hydrogen embrittlement) will rely on the feasibility of hydrogen reduction, and its adsorption and diffusion within the metal bulk ahead of the crack-tip.

However, even though these reactions could be determined as theoretically possible via thermodynamics, it is still not sufficient for SCC to be physically materialised. If the kinetics of reactions and the rate-determining step are indeed too low then a component may be considered as suitable for service, despite SCC remaining a hypothetical threat.

B. Effect of steel chemistry and microstructure on SCC susceptibility: Intergranular SCC vs Transgranular SCC

The relationship between SCC and the environment only represents one aspect of the SCC phenomenon. The environmental criteria are essential but not sufficient for the realisation of SCC. The complexity of SCC is augmented by its relationship with the materials. When the influence of metallurgy on SCC is being investigated, one has to look to the materials chemistry and microstructure. These essentially include:

- General material alloying composition
- Chemistry at grain boundaries
- Nature of phases and distribution in space
- Crystal structure
- Grain morphology and texture, and grain sizes
- Inclusion chemistry and inclusion density
- Dislocation type and density

One way to discuss the role of chemistry and microstructure in SCC is through their influence on the occurrence of intergranular and transgranular SCC, although many of the parameters intrinsic to materials could contribute to both i.g. and t.g. cracking.

Intergranular SCC

Intergranular cracking generally relies on an active dissolution path at, or adjacent to, the grain boundaries or intergranular corrosion, whilst the overall material bulk is mainly within a passive state or sees much lower dissolution rates in comparison with the grain boundaries. The conditions for this are usually ideal when the alloy bulk chemistry is favourable to the formation of a stable and protective surface film whilst the grain boundaries remain locally exposed to the corrosive environment.

The preferential activity at the grain boundaries is generally maintained by the segregation of impurities such as sulphur or phosphorus at the grain boundaries which contribute to the precipitation of weaker or more unstable films which are generally not sufficiently protective. The precipitation of secondary metallic phases at the grain boundary, whose electrochemical potentials are different from that of the grain matrix, could contribute to the formation of a local galvanic cell generating preferential corrosion along the grain boundaries.

The activation of slip planes at grain boundaries as a result of high plastic straining, could also disrupt the presence of a protective film, and therefore promote intergranular SCC.[49,69] This effect is captured in the slip-dissolution model.

Due to the nature of intergranular Stress Corrosion Cracking, the understanding of the alloy grain texture as a result of manufacturing rolling-direction is critical as this will affect the SCC susceptibility, depending on which direction the tensile stress is applied. This is illustrated in Figure 26.[49] When the grain matrix is stressed in the short transverse direction (a) which is perpendicular to the rolling direction, it is easy for the cracks to propagate through the grain boundary paths. However, if this same materials is stressed in the long transverse or longitudinal direction, the intergranular crack encounters resistance to growth due to the complexity of the path.

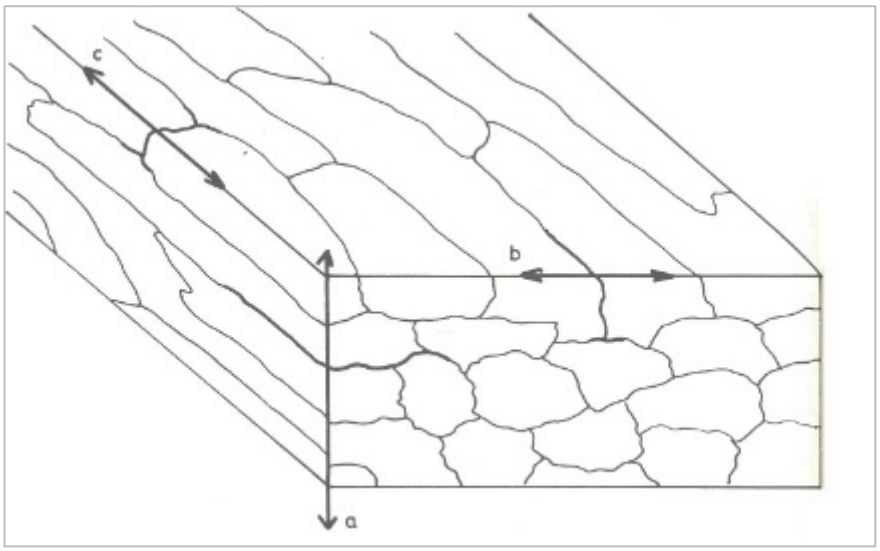

Figure 26: Effect of microstructure and stress direction on SCC susceptibility[49]

Transgranular SCC

By definition, t.g. SCC is associated with cracks propagating through grains. The main parameters for the occurrence of transgranular SCC are thus related to the intrinsic material properties that could offer preferential conditions for localised corrosion activation within grain bulk (for anodically assisted SCC), and easy passage (or resistance) to the crack growth across grains, e.g.:

- Phase chemical composition and crystal structure
- Grain morphology and size
- Phase mechanical properties (yield strength, hardness)
- Dislocation types and density
- Crystal stacking-fault energy
- Crystal anisotropy

As part of these parameters, the overall capacity of the materials to generate the incidence of planar slip has been mentioned as a common metallurgical factor (for anodically assisted SCC) in producing transgranular SCC.[66,70,71,72] The emergence of slip planes at grain surfaces could indeed result in local film breakdown which would result in preferential localised corrosion along the active slip plane; the condition here is that the slip offset should be greater than the thickness of the passive film. Large planar slip offsets are generally identified in alloys with a low crystal stacking-fault energy, ordered phases, or alloys with short or long-range ordering. Parkins[73] confirmed there was some correlation between the occurrence of transgranular cracking and low stacking-fault-energy alloys. The concept of planar-slip-localised corrosion for transgranular crack growth[70]

has been recognised in several SCC models such as the slip- dissolution and corrosion-tunnel model. In the slip- dissolution model, the crack advances in intermittent steps driven by the cycle of film rupture along a slip plane, dissolution at the crack tip, re-passivation as illustrated in Figure 27[74]. This model has been used to explain transgranular cracking of carbon steel within CO_2-CO-H_2O (see section 2.6.2).

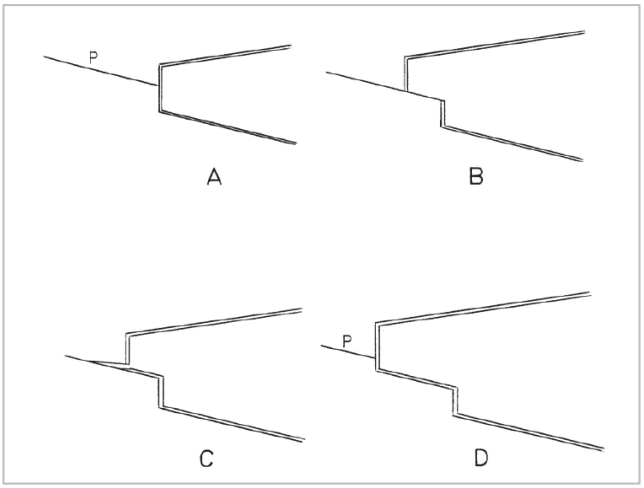

(A) The tip of the crack. The surface is protected by a film. P is the slip plane (B). Plastic flow at the slip plane disrupts the film and exposes bare metal surface to the environment (C). Metal dissolution proceeds on the exposed metal surface allowing crack growth (D). Repassivation occurs and then the whole process is repeated

Figure 27: Schematic diagram of the sequence of events occurring at the tip of a propagating stress-corrosion crack[74]

The presence of alloying elements or impurities on the slip plane could also generate the establishment of a galvanic cell with the surrounding matrix, promoting transgranular stress corrosion cracking.[66,72]

It is however emphasised that, in recent times, the question of the morphology of cracking resulting from planar slips, i.e. whether the crack will be transgranular or intergranular, appears to be controversial[66,69,75]. Although the nature of transgranular SCC suggests it will be facilitated by planar slip offsets, the current tendency[69] goes towards associating slip dissolution-models with i.g. cracking rather than t.g. cracking. The challenge for explaining transgranular SCC via plane slips also stands in the nature of the transgranular SCC fracture surface, whose features are cleavage-like, and has not been found on the slip planes.

2.5.3. SCC mechanisms and the Stress Corrosion Spectrum

The complexity of the SCC phenomenon as a result of its sensitivity to the triangle Environment-Materials-Stress is symptomatic of the challenge of rationalising all

the parameters and processes within a singular model, and thus to the existence of a multitude of Stress Corrosion Cracking mechanisms. Some of the key chemical and physical processes that could influence SCC have been summarised by Staehle[76] in a diagram illustrated in Figure 28. As has been already discussed, the existence of a balance between the general passivity (or relative inactivity) at the crack walls and the activity at the crack tip is critical so that SCC could develop instead of general corrosion or pitting.

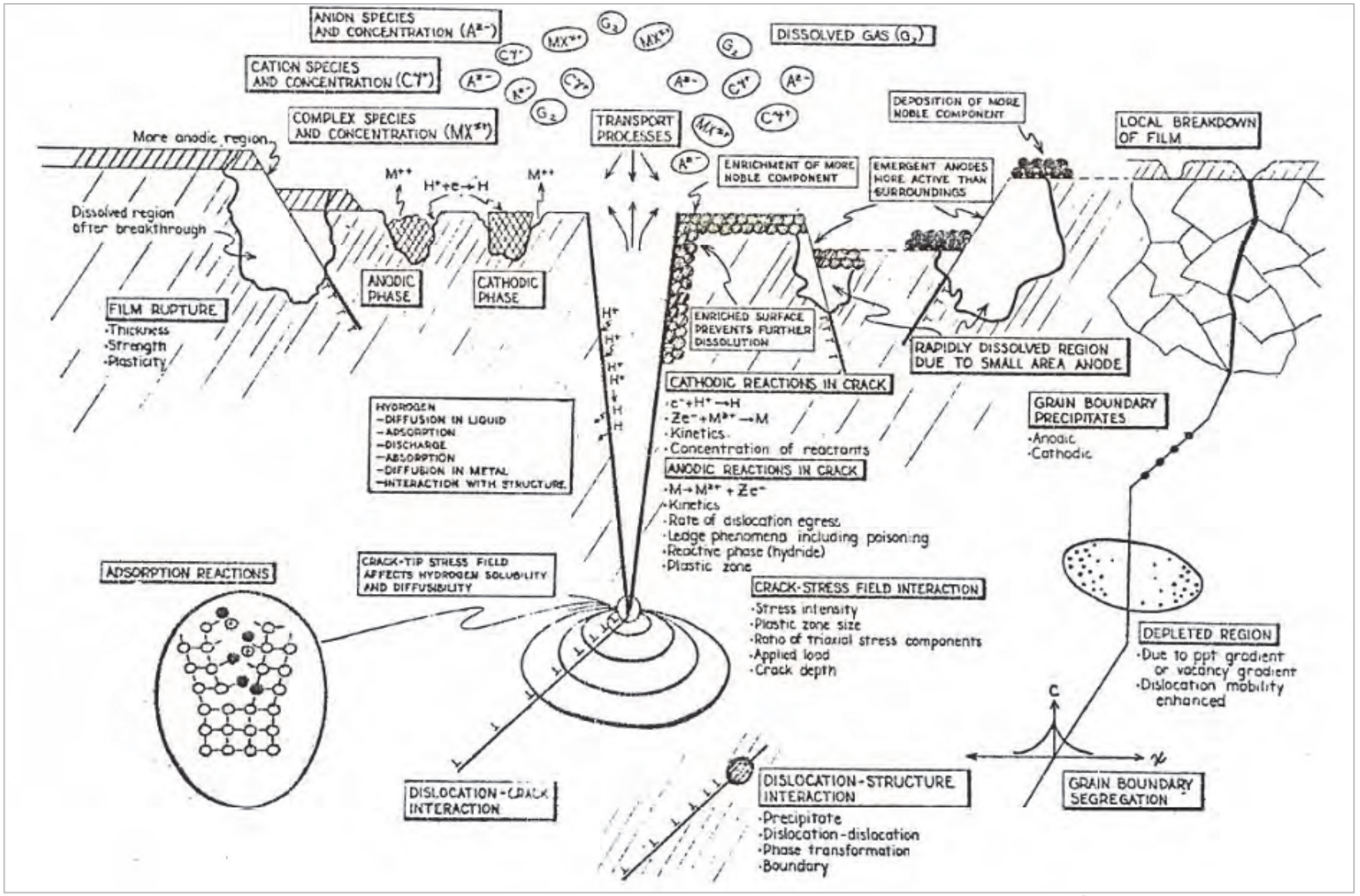

Figure 28: Schematic diagram of the possible processes affecting SCC by Staehle[76]

Parkins[77] discussed that stress corrosion cracking mechanisms could be rationalised in a Spectrum (commonly referred as the *Parkins SCC spectrum*), in which the emphasis swings from active corrosion playing the driving role over stress, to mechanical stress being the important factor with marginal assistance from corrosion. As the spectrum (Figure 29[77]) is traversed from left (i.e. corrosion driven SCC) to right (i.e. stress driven SCC), three main SCC zones could be visualised; examples of materials/environment systems known to produce SCC have been located on the spectrum:

- *Pre-existing active path*; when active dissolution paths are naturally present upon unstressed specimens due to the nature of the environment and the materials, and their interaction. Such a mechanism is especially pronounced for structurally-sensitive attacks such as intergranular corrosion. The reason for preferential activity at the grain boundary has been discussed in section 2.5.2-B).
- *Strain-generated active path*; the surface of the alloy is maintained within a general passive state due to the presence of a protective film, usually an oxide. Plastic flow in the structure as a result of straining could result in film disruption (see section2.5.2-B), exposing the bare metal locally to the corrosive environment until repassivation occurs (followed by further disruption).
- *Specific adsorption at sub-critically stressed sites;* this mechanism mainly refers to embrittlement of metal at the crack tip region, as a result of adsorption/absorption of species from the environment and their diffusion at the crack tip where stress and strain densities could favour the nucleation of cracks. In this case, hydrogen is usually regarded as the usual suspect due to its generation as part of the corrosion processes (reduction reaction) required for SCC and its relatively high diffusion rates which could sustain crack growth.

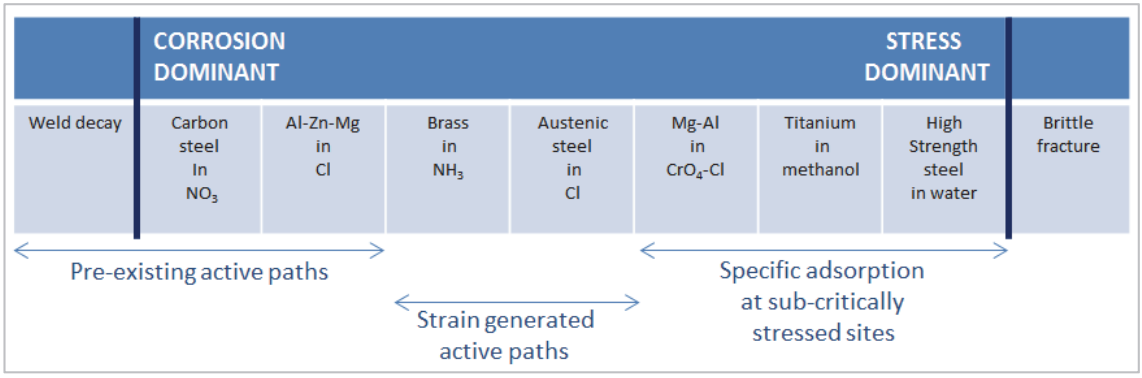

Figure 29: Parkins SCC Spectrum[77]

Parkins[77] explained that the borders between each mechanistic region are not absolute and strict, and emphasised more the *continuous* nature of the spectrum, in which the SCC mechanistic characteristics will gradually change when moving across the spectrum.

The Parkins SCC spectrum has successfully travelled the times, and remains a valid representation or description of the SCC mechanism.[78] Recent reviews have proposed some modifications to the original "*1980s spectrum".* An alternative modern representation of the Parkins SCC spectrum has been proposed by Newman[78], in which the dissolution (anodic) -assisted SCC mechanisms are separated from those involving (cathodic) hydrogen influence. In Newman's representation[78], the accent is put on three generic mechanisms, which have been considered by Newman to cover most of the identified SCC systems for alloys: slip-dissolution model, film-induced cleavage model and hydrogen embrittlement.

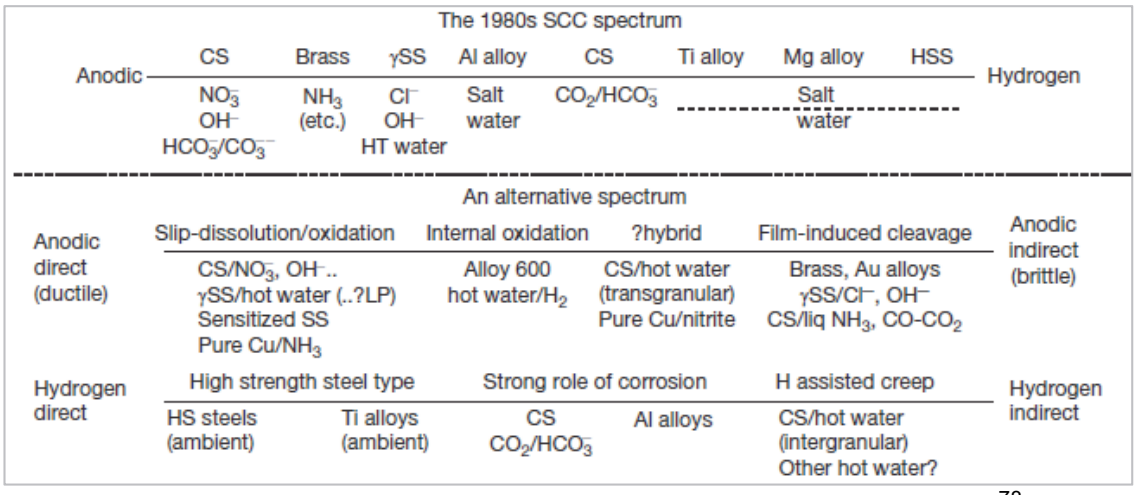

Figure 30: An alternative modern representation of the SCC Spectrum[78]

2.6. Stress Corrosion Cracking mechanisms in anthropogenic CO_2 steel pipelines

2.6.1. Why SCC should be considered?

It is generally considered that the presence of CO_2 alone (in the presence or not of free water) is not sufficient to drive initiation and propagation of Stress Corrosion Cracks. Hudgins et al.[79] nevertheless indicate that cracking may be generated in high-strength carbon steel exposed to high pressure CO_2 environments under extreme stress conditions at relatively long exposure times. At 20 bar CO_2, failures were produced within exposures as low as 22 hours on steel materials with hardness of 34Rc and deformation levels of 115%. The production of cracks was associated with the potential leaching of sulphur from the steel materials. Scenarios under which such high stresses may arise e.g. from geological ground motion or at localised corrosion features should be considered.

The additional presence of other impurities in the CCS stream could further increase the likelihood of SCC in CO_2-H_2O environments. This is discussed in the following sections.[80]

2.6.2. CO_2-CO-H_2O SCC

Carbon monoxide is a significant impurity in CO_2 captured from pre-combustion processes.[1] In the 1970s, cracking of carbon steels was observed in environments constituted of wet mixtures of carbon dioxide and carbon monoxide gases, such as those present in chemical-processing plants for coal, and town-gas manufacture, transport and storage systems.

Microscopic examination of the failures indicated fine transgranular cracks initiated from the internal surface of the vessel containing the gas mixture. The investigations also showed that cracking initiated at sites subject to tensile stress typically generated from the high pressure of the contained gas. The occurrence of such cracking in practical engineering situations worldwide, particularly in town-gas high pressure pipelines, meant that great interest was generated and various research studies were conducted mainly by Brown et al.[81] and Kowaka and Nagata[82]. The current understanding for the occurrence of CO_2-CO-H_2O SCC is summarised:

- The presence of water is critical for the incidence of cracking.

- The presence of CO in CO_2-H_2O systems is critical for the occurrence of transgranular cracking in carbon steels.
- An increase in the CO activity in CO_2-H_2O systems increases the susceptibility to cracking (see Figure 31[81]), i.e. the crack growth rate is greater, and the minimum initial stress to be applied for SCC occurrence is lower. At high CO activity, fine branched cracks are formed during crack propagation, whilst at low CO activities voids are created below the metal surface. It is possible to generate cracking under freely corroding conditions at high CO partial pressures.
- The additional presence of oxygen will increase the susceptibility to SCC in this system.
- Crack growth rates of 10^{-6} mm/s were reported.
- The mechanism of SCC for the CO_2-CO-H_2O system can be classed under the ‘strain-generated active path’ model. This is the result of the formation of a mono-molecular CO film on the surface of the carbon steel and its rupture under stress.
- Most of the experimental data are limited to low partial pressures of CO_2 (<20 bar (<2 MPa)).

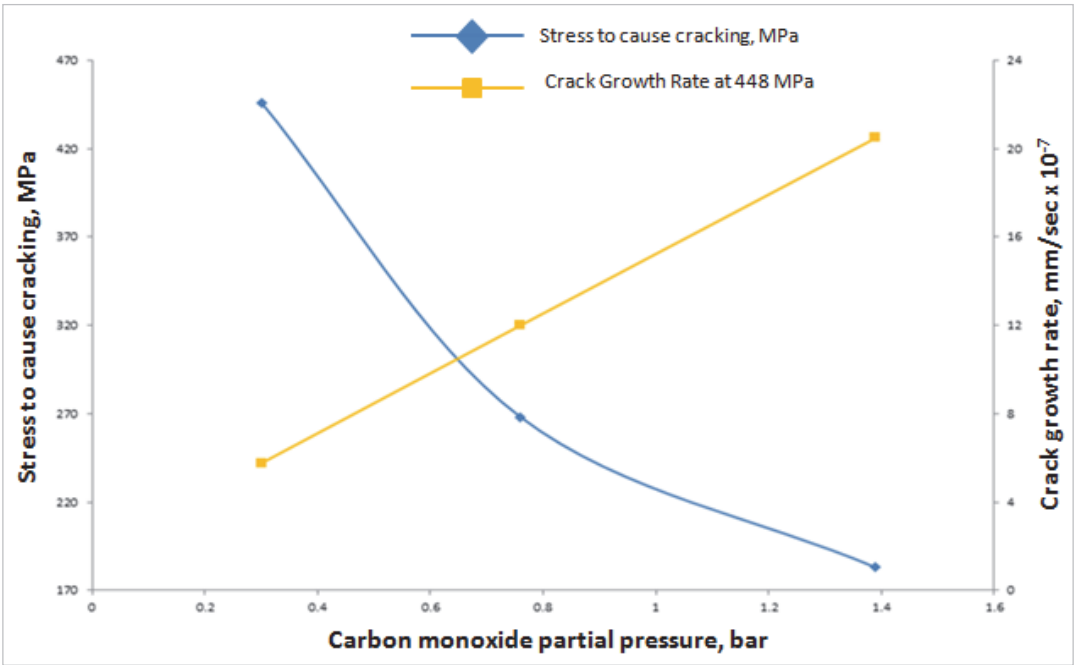

Figure 31: Effect of carbon monoxide partial pressure on minimum stress to initiate cracking and on crack growth rate (Total pressure-7.9 bar (0.79 MPa), +100 mV from F.C.P.) [81]

Under upset dehydration conditions, there is a potential risk of CO_2-CO-H_2O SCC in pipelines transporting CO_2 from pre-combustion capture processes.

2.6.3. H_2S-H_2O SCC

Hydrogen sulphide is a significant impurity in CO_2 captured from pre-combustion processes, but can also be present in streams generated from post-combustion and oxy-fuel technologies.

The presence of H_2S can lead to different types of sour cracking, mainly Sulphide Stress Corrosion Cracking (SSCC) and Hydrogen Induced Cracking (HIC): Hydrogen is produced on the surface of the steel as part of corrosion processes (cathodic reduction). The presence of H_2S enhances the formation of atomic hydrogen in contrast to molecular hydrogen. The atomic H is absorbed in the materials bulk and diffuses into the microstructure of the steel. In the case of HIC, the hydrogen atoms collect at irregularities such as MnS inclusions, and recombine to form molecular H_2 which, by local build-up of pressure, creates blisters. In the case of SSCC, the atomic H diffuses into solid solution which causes crystal distortion and associated embrittlement, which by application of residual /applied stresses lead to cracking.

These threats and their respective mitigation requirements have been documented in the Oil and Gas Industry. The standard NACE

MR0175/ISO15156[83] has been used to mitigate the risk of sour cracking. This standard is based on Oil and Gas industry experience and testing for hydrocarbon systems (i.e. CO_2 is present as an impurity). This document is a starting point to potentially decrease the susceptibility of sour cracking in CO_2 pipelines.

If a CO_2 pipeline is expected to see significant levels of H_2S during service, sour resistant steels will need to be considered to prevent catastrophic failure of the pipeline which could occur within days, or hours under the most severe conditions. Compliance to maximum hardness will have to be specified for the parent and weld materials.

2.6.4. CO_2 and HCO_3^-/CO_3^{2-} SCC

The excessive presence of water in rich CO_2 environments will drive the formation of an acid aqueous phase in which dissolved CO_2, bicarbonates and carbonates will be in equilibrium. The concentrations of these species as a function of the partial pressure are illustrated in Figure 6, Figure 7 and Figure 8.[4]

Aqueous concentrated carbonate-bicarbonate solution environments are known to result in intergranular SCC of pipeline low-alloy steel materials. This mechanism is generally referred to as high-pH SCC since it readily occurs in solutions with a pH of 9-10, conditions under which iron carbonate films will precipitate on steel. The occurrence of such cracking has only occurred on operational pipelines as an external mechanism due to the importance of potential polarisation to generate SCC initiation and growth. The critical potential for SCC is related to the steel surface active-passive transition as a result of iron carbonate formation. This potential is dependent on the actual pH environment and temperature of the pipe.

This mechanism has been extensively studied:

- The critical potential for SCC is in the range of -650 to -750 mV (CSE). This potential can be present on operating pipelines where the 100 mV shift criteria is used, where the CP is monitored by ON potentials, or where there is some degree of CP shielding, for example in areas of disbonded coating or from a porous coating.

- In the bicarbonate-carbonate system, the susceptibility to cracking decreases with decreasing concentration of bicarbonate. This is illustrated in Figure 32.[84]
- The susceptibility to cracking is maximum at temperatures of 75-80ºC, and diminishes with decreasing temperature. The risk of cracking is usually considered to be low at temperatures below 40 ºC, but it is still possible at ambient temperatures as illustrated in Figure 33.[84]

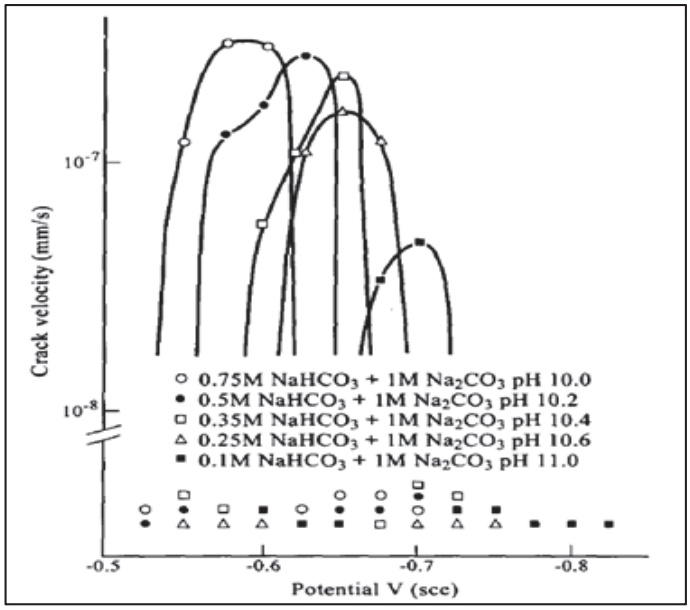

Figure 32: Effect of bicarbonate levels on the average crack velocity for low-carbon steel in 1 M Na_2CO_3 solution[84]

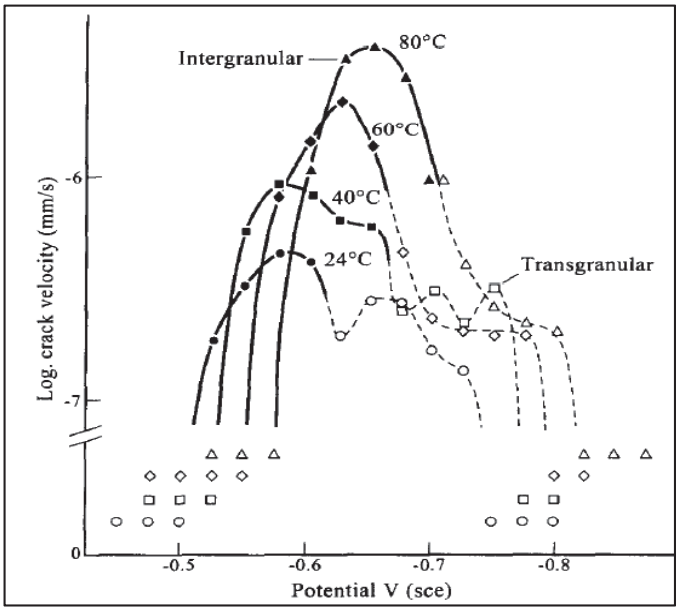

Figure 33 : Effect of temperature on the average crack velocity for low-carbon steel in 1 M $NaHCO_3$ + 0.75 M Na_2CO_3 solution[84]

The risk of bicarbonate / carbonate SCC in CO_2 pipelines in presence of free liquid water may in the first instance be discarded due to:

- Non-existence of surface electrochemical polarisation to drive internal pipeline surface steel potential in the critical range for SCC initiation.
- A low pH (<4) which will mitigate the formation of protective iron carbonate
- Relatively low concentrations of bicarbonates (<0.001M for CO_2 partial pressures < 100 bar (<10 MPa) –see Figure 7) and carbonates in free water

However, other operational considerations should be given to the impact of events/conditions in generating a SCC mechanism in CO_2 pipelines, whose characteristics can be similar to bicarbonate/carbonate SCC:

- Following significant dehydration upsets, impact of water evaporation due to re-establishment of dry gas operations in concentrating the levels of bicarbonates/carbonates, and impurities, such as nitrates and sulphates in existing water pools.
- The solution has initially a low pH due to the presence of acids; over time as the solution becomes saturated with bicarbonates/carbonates and corrosion products, the pH of the solution may increase to become alkaline.
- Impact of chemicals (e.g. amine, sulphite) and by-products (e.g. ammonia) carry-over from the capture / conditioning process into the pipeline to generate more alkaline conditions in aqueous phases present in CO_2 pipeline.
- Impact of impurities such as nitrates and sulphates to shift the free corrosion potential into the critical range for SCC and increase the susceptibility to SCC under freely corroding conditions.
- The presence of scales such as iron sulphide may shift the potential into the critical range of potentials for SCC.

2.6.5. Nitrate SCC

As described in section 2.2.3, the reaction of nitrogen oxides and moisture could lead to the formation of nitrate solutions. Aqueous nitrate solutions have been known to promote intergranular Stress Corrosion Cracking of mild steels.[85] SCC was for example reported in flue gas and waste heat recovery systems where NO_x is generated as part of the combustion process.[19,86]

A summary of key points are listed:

- The susceptibility to cracking is increased with the associated cation series $NH_4^+ > Ca^{2+} > Li^+ > K^+ > Na^+$, and also with the concentration of nitrates. In addition to decreasing the resistance to SCC, the cation series is also associated with an acidification of the environment as a result of cation hydrolysis; this leads the open circuit potential of the steel to move to more anodic values.[87]

- The susceptibility to cracking is increased with the temperature and becomes significant at temperatures above 75°C. The higher susceptibility to SCC at higher temperature could be associated with the nature of the corrosion product formed. As in many SCC systems, it was indicated that passivation was critical to produce SCC of steels in nitrate solutions[88] (see section 2.7.3).

  Although most of the work is conducted at boiling temperature, nitrate SCC is indicated to occur over a wide range of temperatures. The crack growth rate is nevertheless small at ambient temperatures.[89]

- Lower pH increases the susceptibility to SCC.[85,90] Mohammed[91] suggested that the critical range for cracking is between pH 3.0 and pH 7.5, but indicated that cracking can still be produced in alkaline environments e.g. at pH 9.6 but over much longer periods due to slow SCC incubation.

2.7. Passivation of steel in CO_2 environments and effect of impurities

The presence of conditions that promote surface passivation is generally essential for Stress Corrosion Cracking to be realised, as has been discussed earlier. In CO_2 environments, steel could become passive due to the formation of iron carbonate film on its surface. The presence of impurities could however promote the formation of other types of layer with various levels of protectiveness. Impurities such as sulphur compounds could interfere with steel passive behaviour.

The nature of the films and their properties are likely to be dependent on the type of impurity present, the inter-partial pressure ratios between the CO_2 and the different impurities, the temperature and the aqueous phase pH.

2.7.1. Iron carbonate film

A. Supersaturation and precipitation of iron carbonate

In CO_2 corrosion when the concentrations of Fe^{2+} and CO_3^{2-} ions exceed the solubility limit, precipitation of iron carbonate can occur according to:

$$Fe^{2+} + CO_3^{2-} \Leftrightarrow FeCO_3$$

When solid iron carbonate film is formed, the corrosion process is slowed down but this essentially depends on the protectiveness of the scale. The protectiveness of this film will depend on its thickness, porosity and morphology, which depends on the balance between corrosion and iron carbonate precipitation.

The formation of protective iron carbonate films can be seen as a competition between precipitation of iron carbonate and corrosion of the steel surface where the precipitation can occur.[92] When the corrosion rate is much larger than the precipitation rate, the steel will corrode away beneath the precipitating iron carbonate, resulting in a porous and loosely adherent film with poor protective corrosion properties. When the precipitation rate is comparable to the corrosion rate, the corrosion film will be more continuous and less porous, offering better corrosion protection.

The corrosion product film formation is strongly dependent on the solubility of iron carbonate, which again is influenced by temperature, pH, and the flow velocity.

The effect of solubility and precipitation of iron carbonate has been investigated.[60,93]

The driving force for iron carbonate precipitation is the supersaturation of $FeCO_3$. Supersaturation (SS) for the iron carbonate considering the iron carbonate precipitation reaction is given by:

$$SS = \frac{\log_{10}[Fe^{2+}][{CO_3}^{2-}]}{K_{Sp}}$$

Where K_{sp} is the solubility constant for iron carbonate precipitation

The precipitation of $FeCO_3$ is generally a slow temperature dependent process. The direct consequence of this is that a high degree of supersaturation can be actually maintained in a corroding system. In other words, ferrous carbonate precipitation frequently occurs in the aqueous solution at concentrations much higher than that predicted by the equilibrium solubility constant K_{sp} ($FeCO_3$).[93] Therefore a key point to remember is that although thermodynamics predicts the formation of solid iron carbonate, whether it actually deposits or not depends amongst other factors on the kinetics of precipitation and how it is anchored to the surface.

There are two steps involved in the precipitation processes, i.e. nucleation and particle growth.

The precipitation of $FeCO_3$ is facilitated by increased pH, increased temperature (Figure 34) and measures that reduce the transport of reactant and corrosion products to and from the steel surface. The effect of temperature and pH will be discussed in the following sections.

At high CO_2 pressures, the pH values in aqueous phases are so low that the formation of a surface protective film may become difficult (i.e. scale-free CO_2 corrosion) due to the high solubility of iron carbonate under these conditions. However, the expected increased dissolution of iron due to higher carbonic acid concentration and lower pH with pressure may provide an increased source of ferrous ions which might lead over time to iron carbonate precipitation even at low pH although probably not as a protective layer.

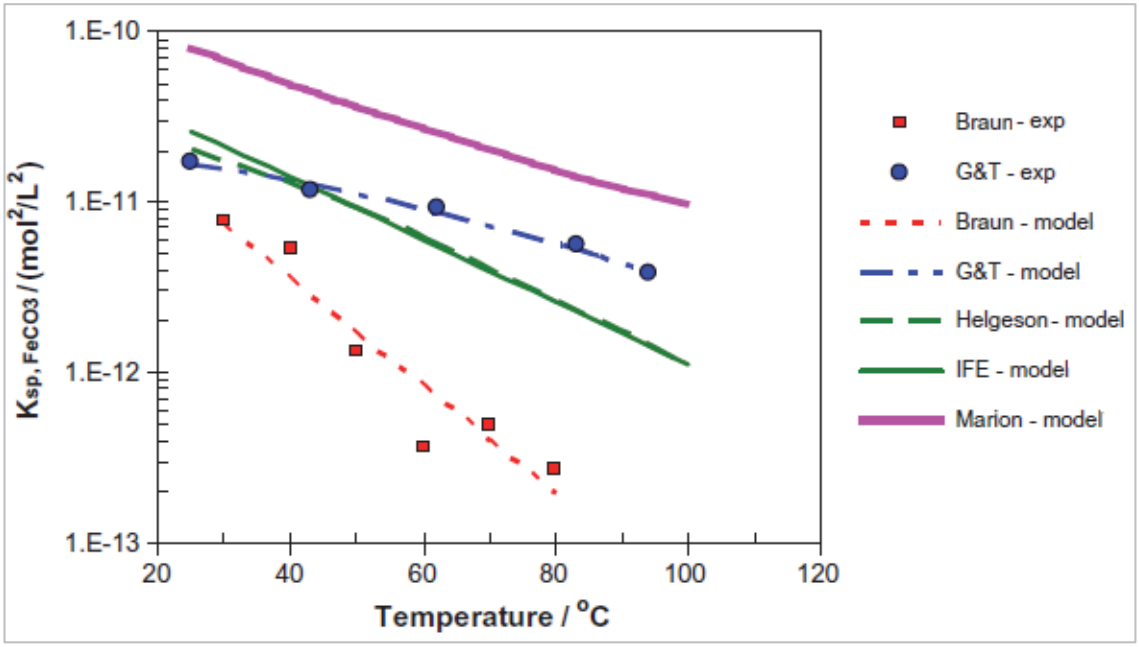

Figure 34 : Experimental and calculated values of solubility data of iron carbonate as a function of temperature[60]

B. Role of iron carbide on the formation of protective iron carbonate

The formation of iron carbide Fe_3C layer has also been discussed to create favourable conditions at the steel surface for protective iron carbonate to form, which was otherwise not possible with respect to the bulk water chemistry.

Fe_3C has often been identified aside iron carbonate in the corrosion products formed as a result of CO_2 corrosion of mild and low-alloy steels. Cementite Fe_3C is present in the steel microstructure and is harder to dissolve than the ferrite phase (α-Fe). This means that cementite is often left over the steel surface as a result of corrosion.[94] In addition, it has been alleged that since Fe_3C is conductive and more noble to ferrite, a galvanic couple is formed resulting in the acceleration of the dissolution of α-Fe.[95] Despite this, it has been discussed that under certain environmental conditions, (i.e. high temperature, alkaline pH, elevated partial pressures of CO_2 and Fe^{2+} concentrations, and low flow rate), the iron carbide films may provide anchorage for the formation of $FeCO_3$ layers.[96] Farelas[97] has recently indicated that $FeCO_3$ was identified to form within the pores of the Fe3C layer, regardless of the bulk $FeCO_3$ saturation value, and this was associated with a drop in corrosion rates.

2.7.2. Effect of sulphur-containing compounds on the formation of iron carbonate films

The presence of sulphur-containing compounds will affect the formation of surface protective films such as iron carbonate on low alloy and carbon steel materials. The corrosivity will be associated with the nature of the compound, typically Elemental Sulphur> Sulphides (XS)>Sulphates (XSO_4). The cation present in the compound is also likely to influence its reactivity.

A. Elemental sulphur effect

Elemental sulphur is known to cause severe corrosion of steel materials. In addition to increasing anodic dissolution kinetics as a result of adsorption of sulphur which may play the role of electroactive specie or oxidation catalyst, elemental sulphur could produce passive film breakdown of the existing surface layer or simply poison formation of protective surface films.[98]

- Increase in the anodic dissolution kinetics as a result of sulphur adsorption; it is indicated that this could occur by direct oxidation of sulphur, or by sulphur acting only as a catalyst.
- The adsorption of sulphur S on the surface of the material induces breakdown of the existing surface passive layer
- Adsorbed sulphur S poisons the formation of protective passive film on the surface.

B. Sulphide effect

In a production oil and gas environment where CO_2 and sulphide compounds such as H_2S could be present, the competition between the formation of iron carbonate and sulphide scale has been considered.[99,100] Whist iron carbonate (siderite) is the only scale formed in a pure CO_2 environment, various amorphous and crystalline scales could form in the presence of H_2S. This may include for example mackinawite, pirrhotite, pyrite, troilite, among which mackinawite is the most likely to precipitate first, and is the precursor of other sulphide formation. Whilst the precipitation of iron carbonate on a steel surface is significantly driven by the iron carbonate supersaturation parameter, which is a function of temperature and pH[60,93], and thus by the concentration of Fe^{2+} present in solution, iron sulphide films could form under conditions well below the respective saturation level. It was thus assumed that iron sulphide is essentially formed by direct ‘solid state’ reaction between H_2S and iron present on steel surface,

although precipitation of iron sulphide could still be produced in supersaturated systems over long exposures.[101] The heterogeneous character of the chemical reaction was discussed as a plausible reason for the high reactivity of sulphide species with iron to explain the formation of mackinawite in a few seconds, in contrast to longer precipitation process kinetics. Sulphide-containing environments will poison the formation of iron carbonate, which may only form in association with sulphide films at high levels of iron carbonate supersaturation.[99,101,102]

A continuous film of iron sulphide isolates (protects) the steel bulk from the environment. However where iron sulphide film has been ruptured and the steel surface is exposed to the environment, severe pitting of the underlying steel will occur as a result of galvanic corrosion between the steel and the iron sulphide (iron sulphide is semi-conductive, and cathodic to carbon steel).

C. Sulphate effect

Studies on the topic of reinforced concrete steel corrosion have looked at the impact of sulphates in causing corrosion of passive steels

Under normal conditions, steels embedded in concrete are exposed to a high alkaline pH (9-13) aqueous medium. At such pH and as indicated by the Pourbaix Potential-pH Diagram of Iron[103], the steel surface is protected by compact iron oxide / hydroxides films (e.g. $Fe(OH)_2$) following oxygen corrosion. The steel will thus remain in its passive state unless it is disrupted by mechanical or chemical action. In such environments chlorides are usually the most prevalent in causing localised film attack and in generating severe corrosion in reinforcing concrete steels. This phenomenon is further amplified when carbonation in concrete (due to CO_2) results in a drop of pH solution leading to film instability.[104]

The impact of sulphate anions on corrosion of steel rebars in these alkaline environments has also been mentioned. Khan et Al-Tayyib[105] (1992) indicates that sulphate-containing environments containing (5%wt magnesium sulphate ($MgSO_4$) or 4%wt SO_4^{2-}) were corrosive to reinforced concrete steels, although the aggressivity was less than chloride-containing environments (5%wt NaCl or 3%wt Cl^-). In contrast to the direct nature of attack of chlorides on passive films, it was discussed that sulphates indirectly affect the stability of the film by decreasing solution alkalinity. The work conducted by Aziz and Mansour[106] (1983)

was quoted as they reported a drop in pH from 13.1 to 9.6 by addition of 5%wt $MgSO_4$ to a saturated solution of calcium hydroxide ($Ca(OH)_2$). Haleem et al.[107] (2013) indicate that sulphates could lead to instability of steel passivation in alkaline environments above a typical threshold concentration of 10^{-5}M. The establishment of a porous and non-passivating film condition mechanism in the presence of sulphates was associated with a negative shift of the free corrosion potential to lower potentials with time.

Premlall et al.[108] (2011) confirm that the sole presence of sulphate anions in alkaline solution (pH 9-12) can induce noticeable attack of mild steels. At pH 12, pitting corrosion was observed in opposition to uniform corrosion at pH 9.

2.7.3. Effect of nitrate compounds

As discussed in section 2.6.5, nitrate solutions could lead to intergranular stress corrosion cracking of carbon steel materials. It is accepted[87,90,109] that cracking in such environments is promoted by the presence of protective oxide films on the corroding surface: hematite α-Fe_2O_3 and magnetite Fe_3O_4. Although cracking was produced in the presence of hematite and magnetite, it was discussed[109] that the susceptibility to SCC is significantly increased when α-Fe_2O_3 is formed.

When the protectiveness of these oxides was affected by depassivating agents such as chlorides, the mode of degradation shifted from SCC to general or pitting corrosion, which highlights the role of the oxides in producing SCC in nitrate environments.[90,110,111]

The susceptibility to SCC in nitrate solutions is most significant at temperatures above 70°C, although SCC could also be produced at lower temperatures. Mohammed[91] suggests that low temperatures enhance the formation of more protective passive film; however the passive state takes longer to be achieved than at high temperatures. Pushpalatha et al.[112] reported that magnetite is always formed at the proximity of the metal surface where oxygen supply is limited. Low pH conditions are catalytic to the formation of Fe_3O_4 in detriment to green rust which could be formed at high pH under quasi-anaerobic conditions. The kinetics of magnetite formation are augmented with temperature. Pushpalatha et al[112] also determined that at temperatures above 80°, α-Fe_2O_3 is the predominant surface product, which confirms the relationship between nitrate SCC at high temperatures and the role of α-Fe_2O_3 presence.

The presence of nitrates may enhance the formation of iron oxides in detriment to iron carbonate precipitation in CO_2 environments.

Chapter 3. Experimental Methodology

3.1. Research project objectives

The objective of the experimental protocol is to assess the impact of impurities such as nitrates and sulphur compounds (produced by NO_x and SO_x respectively) on the realisation of SCC of pipeline steel materials in simulated CO_2 environments in the presence of water.

More precisely, the experimental program investigates the following:

- The effect of nitrates on the susceptibility to SCC of X80 pipeline steel in the CO_2-HCO_3^--CO_3^{2-} system.
- The effect of sulphites on the susceptibility to SCC of X80 pipeline steel in the CO_2-HCO_3^--CO_3^{2-} system.
- The effect of temperature and pH on the susceptibility to SCC in nitrate- and sulphite- containing CO_2-HCO_3^--CO_3^{2-} systems.

The following assumptions are considered in establishing the experimental protocol:

I. Upset in CO_2 dehydration has occurred before CO_2 transportation, and excessive liquid water volumes are present in the pipeline. This forms an aqueous solution containing bicarbonates, carbonates, and other chemical products from impurities present in the stream.

II. As dry CO_2 operations are re-established, water evaporation occurs which leads to increasing concentrations of bicarbonate, carbonate and impurity levels in the pipeline. Saturation of solution species will eventually be reached in the aqueous phase.

III. Prior to pipeline transportation, the carbon dioxide stream is typically cooled to 40°C following compression. Further cooling (due to pipeline direct exposure to external soil or seawater environments) will occur during transport to the storage site. Higher inlet temperatures than 40°C could be present if cooling anomalies occur during operations.

High pressure gas facilities are not available at Newcastle University to reproduce the environment present in an operational CO_2 pipeline. Only CO_2 at atmospheric pressure (1 bar) has been used in the experimental programme. The impact of

increasing CO_2 partial pressure on generated results will be discussed further in Chapters 4 to 6.

The generic aqueous environments considered in the experimental program are detailed in Table 5.

Table 5: Experimental test environments

Aqueous Environments	Carbon dioxide partial Pressure	Temperature
Bicarbonates and carbonates	CO_2-free systems* and 1 bar**	23, 40 and 75°C
Bicarbonates and carbonates, with nitrates		
Bicarbonates and carbonates, with sulphites		
Bicarbonates and carbonates, with sulphates		

**The terminology "CO_2-free" is used throughout the experimental work to describe environments for which gaseous CO_2 was not deliberately bubbled in the aqueous solution. It is however acknowledged that aqueous solutions exposed to atmosphere will have a negligible amount of dissolved carbon dioxide associated with the CO_2 partial pressure in the atmosphere.*

***The pressure should be given in MPa in the International System of Units. However, it has been traditional to use pressures in bar within the oil and gas industry. The pressures are arbitrarily indicated in bar throughout the experimental work. For reference, 1 bar is equivalent to 0.1 MPa.*

More details on the environments used are given in section 3.3.3.

The following tests on pipeline steel materials were conducted:

I. Electrochemical tests
   1. Determine if the system is potentially susceptible to SCC i.e. if materials show passivation at anodic potentials.
   2. Define range of electrode potentials within which SCC can be produced. The critical region of potentials for SCC can be determined from any significant difference in current flow between anodic potentiodynamic polarisation curves plotted at a slow and a fast sweep rate; this is discussed in more detail in section 3.3.

II. Slow Strain Rate Tests were conducted to assess if SCC of pipeline steel can occur within the potential region determined during the potentiodynamic testing, and to assess susceptibility to cracking.

3.2. Material description

The test samples were sourced from a gas pipeline designed in steel of grade API 5L X80. For terminology purposes, Figure 35 defines the three orientations possible in a pipeline:[113]

- Longitudinal direction (L)
- Long transverse direction (LT)
- Short transverse direction (ST)

The pipeline section has been stored in a dry environment to prevent general corrosion.

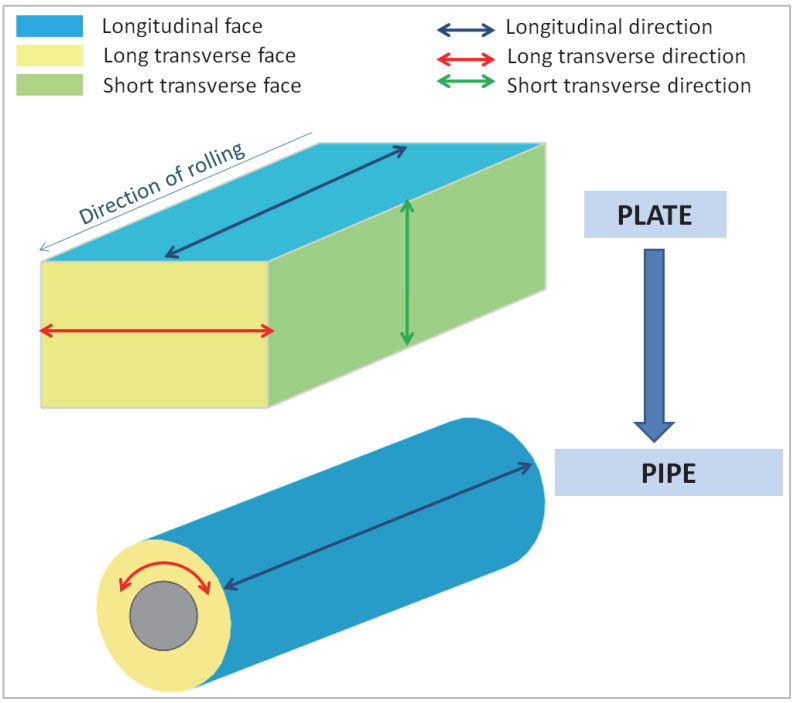

Figure 35: Terminology of spatial directions related to pipeline materials

3.2.1. Material chemistry

The chemical composition of the X80 material, including carbon content and alloying element composition, was obtained by Optical Emission Spectroscopy (OES).

An X80 steel specimen of cubic dimensions 30 mm by 30 mm was sampled from the pipe section, by water-cooled band saw, for analysis. The characterisation was conducted on the sample face which corresponds to the pipeline longitudinal direction.

The material composition of the steel grade is indicated in Table 6:

Table 6: Test material chemical composition

Elements	C	Si	Mn	P	S	Cr	Mo	Ni	Al	Cu	Nb+Ti+V
%wt	0.064	0.309	1.96	0.010	<0.003	0.217	<0.001	0.005	0.029	0.009	0.132

The API 5L specification on chemical composition for X80 steel grades is as follows:

Table 7: X80 chemical composition as per API 5L standard[114]

Elements	C	Si	Mn	P	S	Cr	Mo	Ni	Si	Cu	Nb+V+Ti
Max (%wt)	0.12	0.45	1.85	0.025	0.015	0.50	0.50	1.00	0.45	0.50	0.15

The chemical composition of the steel specimens generally fullfills the requirements of the API 5L standard[114]. Only the manganese content is slightly out of specification.

3.2.2. Material microstructure

Three X80 steel specimens of cubic dimensions roughly 10 mm by 10 mm were sampled by band saw from the pipe section. Each specimen was characterised in one specific direction i.e. in the longitudinal, long transverse or short transverse direction.

The steel specimens were hot mounted into a Bakelite resin. After mounting, the surface of the resin was ground using a ceramic discoplan to reveal the surface of the specimens; the grinding was conducted under cooling water. The specimen surfaces were then polished successively using 80, 220, 500, 800, and 1200 grit silicon carbide under cold water and then washed under running water between intermediate polishing stages.

Final polishing was conducted to 6 micron and then to 1 micron diamond paste to obtain a ‘clean’ mirror finish. The sample surface was washed under running cold water, cleaned in methanol in an ultrasonic bath for five minutes, and swept with clean dry cotton wool before and after each stage of fine polishing. Etching of the polished specimens was then conducted in Nital (2%v Nitric acid, 98%v Methanol) to reveal the steel microstructure i.e. grains, ferrite, and pearlite.

The microstructure of the X80 materials in each direction was analysed by optical microscopy, and is illustrated in Figure 36 and Figure 37 for magnifications under the microscope of x100 and x500, respectively.

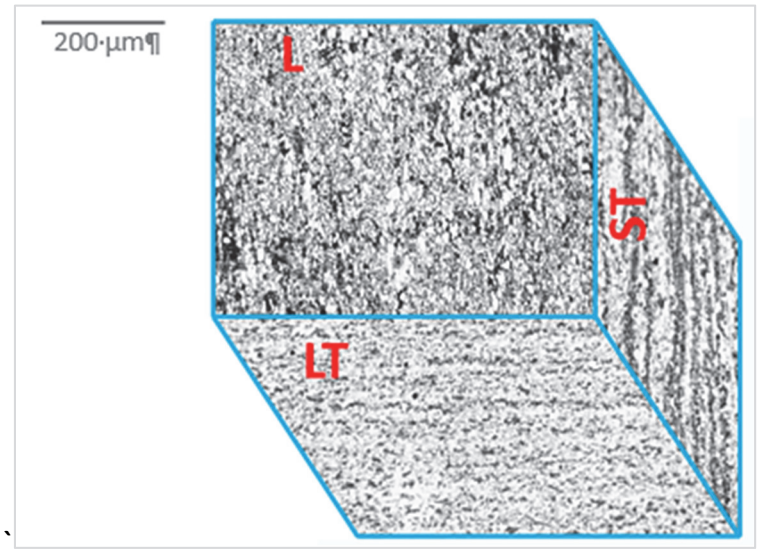

Figure 36: Etched Microstructure of the X80 steel (X100)

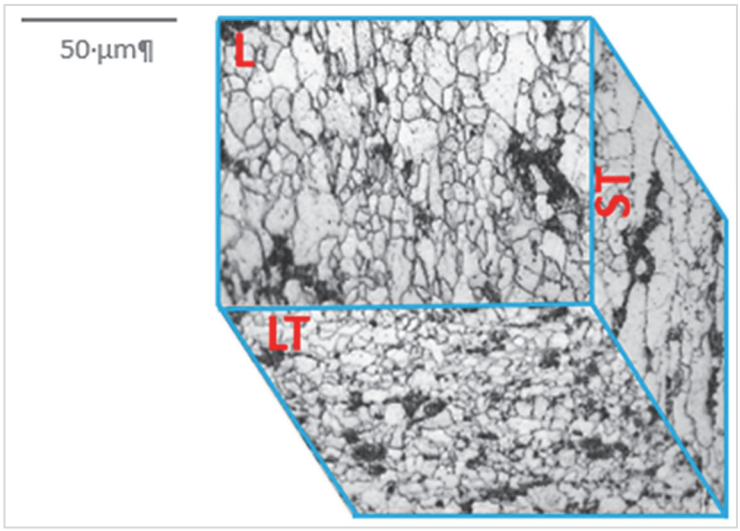

Figure 37: Etched Microstructure of the X80 steel (X500)

The microstructures of the X80 specimens show the presence of ferrite (white areas), and pearlite (dark areas) which is consistent with the low carbon content of the steel:[115]

- In the longitudinal direction, the microstructure is of lightly elongated and lightly banded pearlite in an equiaxed ferrite matrix.
- In the long transverse direction, the microstructure is of partially elongated, banded pearlite in an equiaxed lightly banded ferrite matrix.
- In the short transverse direction, the microstructure is of elongated and banded pearlite in an elongated and lightly banded ferrite matrix.

The difference in texture (grain orientation) that is observed from the different directions is the result of the pipeline manufacturing. The banded microstructure in the long and short transverse directions is the result of hot rolling of the pipeline plate over the longitudinal direction.

In the case of intergranular cracking, it is easier for cracks to propagate for specimens stressed in the short transverse direction. Considering the grain orientation, it is also likely that it is more difficult for cracks to propagate in specimens stressed in the longitudinal direction than in specimens stressed in the long transverse direction. This is discussed in section 2.5.2.B.

3.3. Electrochemistry testing: Is SCC possible?

3.3.1. SCC and Potentiodynamic E-I curves

Parkins[68] and Newman[69] have discussed the use of potentiodynamic methods to identify electrochemical potential regions in which SCC could be realised. As indicated in section 2.5, one of the key criteria for the realisation of SCC is the existence of passivating conditions at the crack walls whilst corrosion activity at the crack tip is being maintained.

Potentiodynamic polarisation E-I curves (refer to section 2.4.3) allow the identification of potential zones where the critical passive-active behaviour could be produced. A typical anodic polarisation curve E vs. I of a metal showing passivation, in relation to possible SCC zones[69], is illustrated in Figure 38.

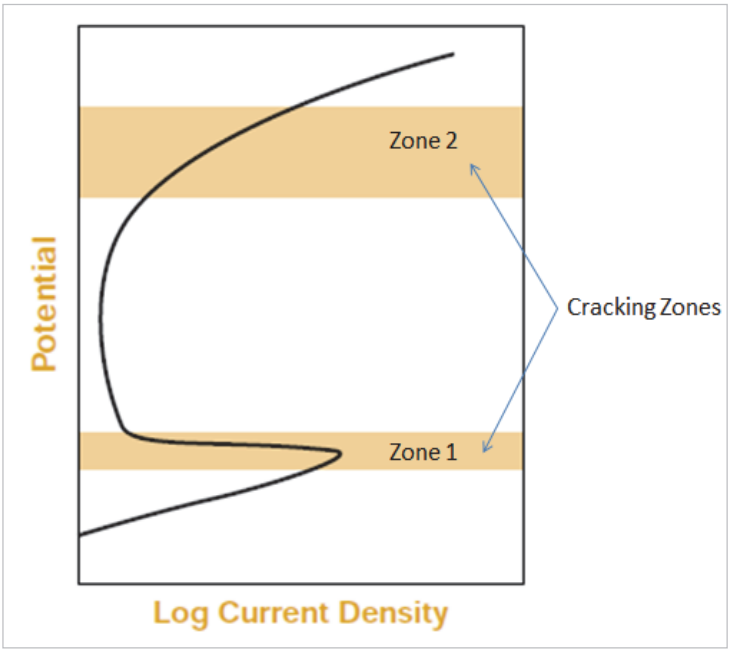

Figure 38: Typical polarisation curve showing metal active, passive and transpassive states and potential SCC regions[116]

Jones[66] suggested that transgranular cracking is most likely at potentials within Zone 1 and Zone 2, whilst intergranular cracking could be realised from Zone 1 to Zone 2 as a result of the nature of the mechanism that leads to t.g. or i.g. cracking. The nature of the morphology and its relation to electrochemical potentials is however dependent on the nature of the SCC mechanism, which is a function of the system metal and environment.

In bicarbonate/carbonate systems, Parkins and Zhou[117] indicated that low alloy steels would suffer SCC at electrochemical potentials associated with Zone 1. The crack morphology in these systems was reported to be predominantly transgranular when the potentials are associated with the anodic dissolution region, whilst it becomes intergranular when the potentials are within the active-passive transition region; this is illustrated in Figure 39.[118]

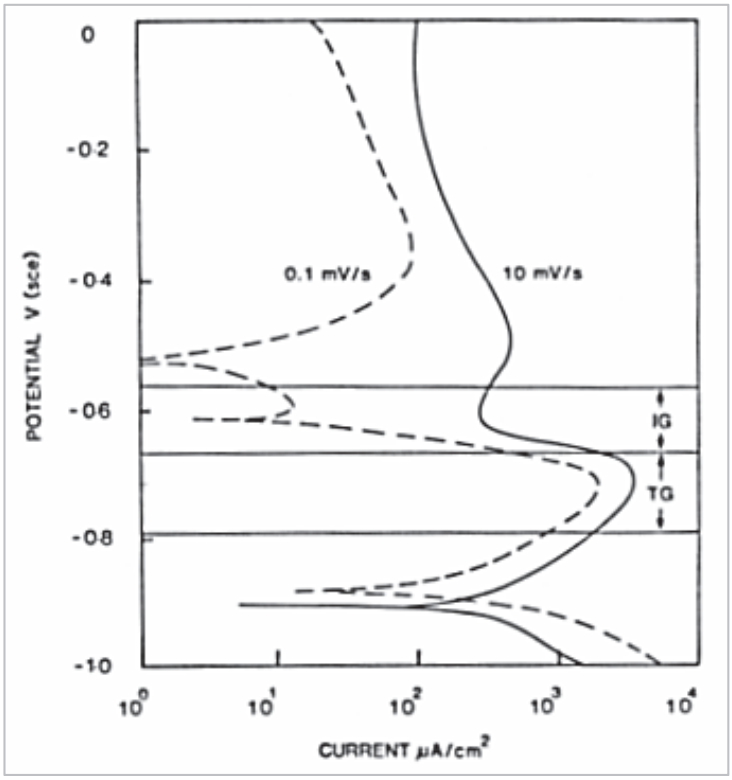

Figure 39 Potentiodynamic polarisation curves for carbon steel in 1M $NaHCO_3$+0.75M Na_2CO_3 solution at 60°C[118]

3.3.2. *Effect of sweep rate: film-rupture kinetics and SCC predictability*

As part of the use of potentiodynamic polarisation technique for the investigation of SCC, the effect of sweep rates[68,75,119] could give further indication on the SCC predictability. Slow sweep rates will promote the establishment of passivating conditions whilst high sweeps will maintain free-film conditions and thus high anodic activity.

The use of low and high sweep rates provides an indirect simulation of reaction kinetics occurring in the case of film-rupture in the micro-system “crack-tip/crack-walls”: If the currents occurring at the crack tip are higher than those at the crack walls then SCC could be generated. Therefore, a major difference between the currents obtained at low and high sweep rates will provide further validation of potential regions at which SCC is likely. An example of this is illustrated in Figure 40.

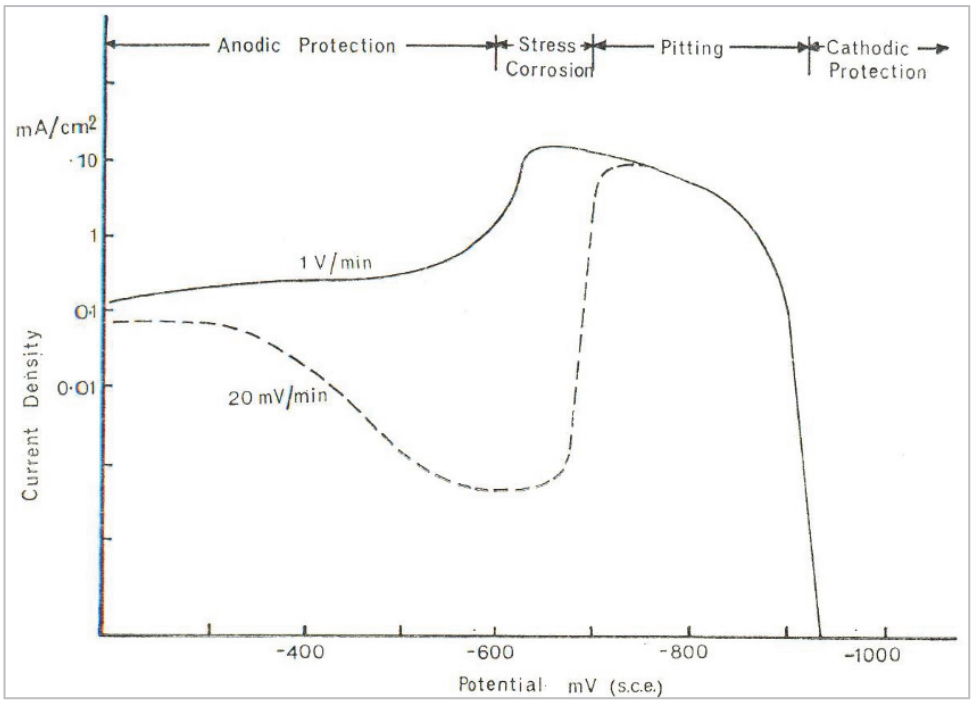

Figure 40: Potentiodynamic polarisation curves for C-Mn steel in 1 M Na_2CO_3+1M $NaHCO_3$ at 90°C showing domains of behaviour predicted from curves[68]

3.3.3. *Electrochemistry tests and test environments*

A. Electrochemistry test cell configuration

The electrochemical measurements were conducted via a three-electrode cell using an automated Solartron 1286 potentiostat. The test cell consisted of a Working electrode (WE), a Reference Electrode (RE), and a Counter Electrode (CE) (see Figure 41).

- The WE was a cylindrical stub of approximately 2 cm^2 surface area in X80 carbon steel. The external surface of the stub was polished to a 1200-grit surface finish to remove any machining defects and the presence of pits. After polishing the surface of the stub was cleaned with methanol, swept with cotton wool, and air dried. The length of the stub and its diameter were then measured under optical microscope to determine the WE exposed surface area. The WE stub was screwed into a steel holder; the holder was contained within a glass tube to prevent exposure of the stainless steel material to the test environment and hence signal interference.
- The RE was a saturated calomel electrode (SCE). This was placed into a saturated potassium chloride KCl solution; a salt bridge filled with the test solution was used to link the WE and the RE without salt contamination.
- The CE was designed in square platinum sheet; the total surface area of the CE was larger than that of the WE (roughly double). In the cell, the current flows between the WE and the CE. The electrode potential of the WE was thus adjusted by controlling the voltage applied via the potentiostat between the WE and the CE.

The working electrode potential E was measured between WE and RE, whilst the current flow (intensity), I, was measured between WE and CE. The current flow was translated into a current density using the WE exposed surface area.

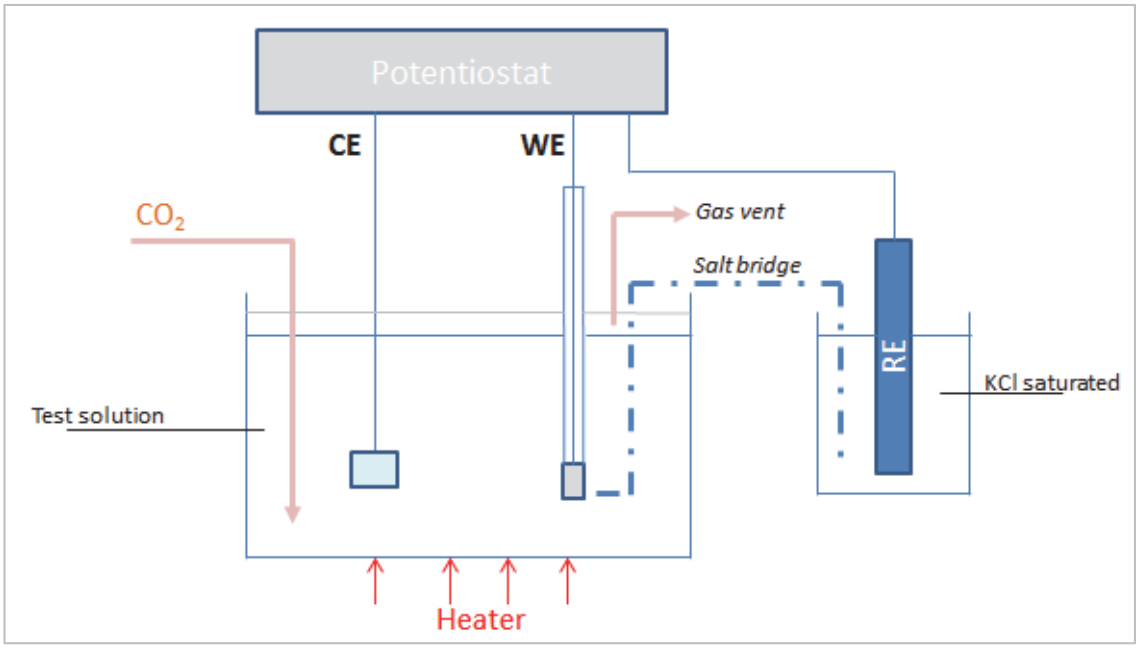

Figure 41: Schematic of three-electrode test cell used in experimental programme

B. Electrochemistry tests

Two types of electrochemical measurement were conducted:

- Open Circuit Potential (OCP) measurements
- Potentiodynamic testing

OCP measurements

No polarisation was applied to the WE from an external source. The WE was allowed to freely corrode in the environment and attained a stable electrode potential defined as the Open Circuit Potential (OCP) or the free corrosion potential (E_{corr}). In this thesis, the term of E_{corr} will be used to define the potential taken by the materials under unpolarised conditions.

Potentiodynamic testing

Potentiodynamic testing of X80 steel was carried out to identify:

1. If this system is potentially susceptible to SCC i.e. if materials shows passivation at anodic potentials.
2. The range of electrode potentials within which SCC can be produced. The critical region of potentials for SCC can be determined from any significant difference in current flow between anodic potentiodynamic polarisation curves plotted at a slow and a fast sweep rate

The WE was polarised by an external source (potentiostat). The WE potential E was swept at a constant rate (sweep rate), and the associated current flowing through the WE was measured. The electrode surface area was used to translate the current flow (intensity) I into a current density J. The polarisation curve E-J was plotted.

Potentiodynamic testing was carried out at slow and fast potential sweep rates: 0.2 $mV.s^{-1}$ and 10 $mV.s^{-1}$.

From the E-J polarisation curve produced by slow sweep rate (i.e. 0.2 mV/s), two measurements were determined (see Figure 42):

- The free corrosion potential, E_{corr}; E_{corr} is equivalent to the OCP as discussed above. However as a result of the sweep rate, the equilibrium is never reached, and a difference exists between the “true” value of E_{corr} as generated by OCP measurements and that obtained by dynamic measurements.

- The first oxidation peak potential, E_p is the WE potential associated with the start of the active-passive transition region. At E_p the current density associated with anodic dissolution is maximum before it is lowered by the formation of a surface film at the WE.

From the E-J polarisation curve obtained by fast sweep rate (i.e. 10 mV/s), the current density associated with the first oxidation peak, I_p, is determined (see Figure 42). I_p is the maximum current density associated with anodic dissolution before the current flow is decreased due to electrode surface passivation.

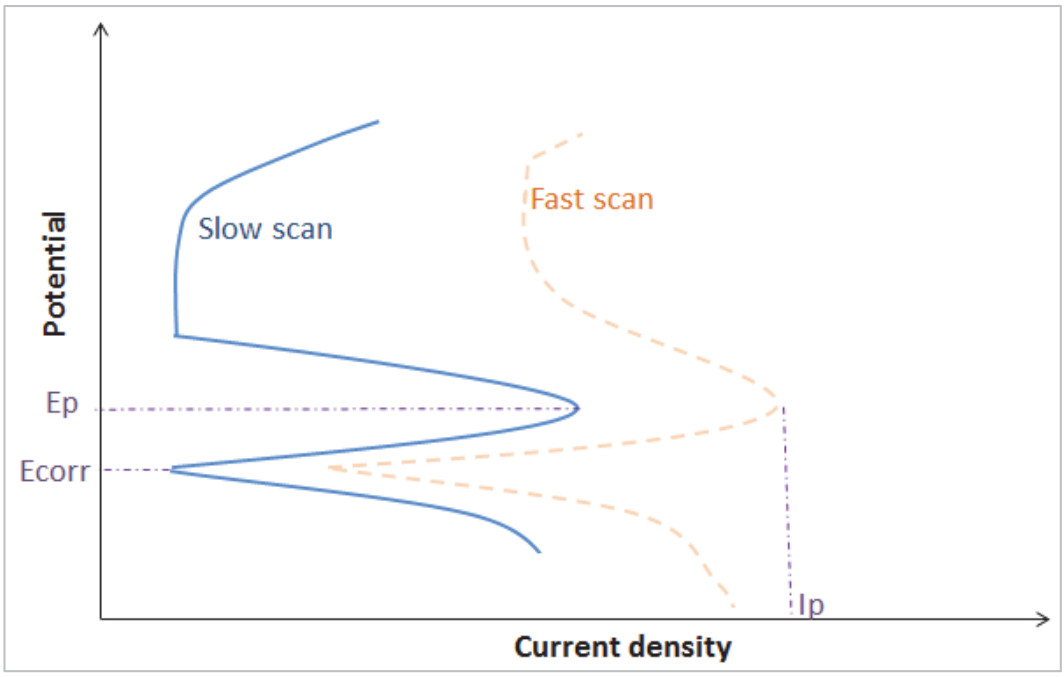

Figure 42: Potentiodynamic curves- legend terminology

C. Test environments

The test solutions for the electrochemical tests are summarised in Table 8 to Table 11.

Table 8: Electrochemistry tests-pure bicarbonate-carbonate systems

System	Temperature (°C)
CO_2-free	
1.5M $NaHCO_3$+0.75M Na_2CO_3	23, 40, 75
1.2M $NaHCO_3$+0.6M Na_2CO_3	
1M $NaHCO_3$+0.5M Na_2CO_3	
0.7M $NaHCO_3$+0.35M Na_2CO_3	
0.5M $NaHCO_3$+0.25M Na_2CO_3	
0.25M $NaHCO_3$+0.125M Na_2CO_3	
CO_2-saturated	
0.7M $NaHCO_3$+0.35M Na_2CO_3	23, 75
0.25M $NaHCO_3$+0.125M Na_2CO_3	

Table 9: Electrochemistry tests-effect of nitrates

System	Sodium nitrate (%wt)	Temperature (°C)
CO_2-free		
Pure Distilled water	10	23, 75
1.5M $NaHCO_3$+0.75M Na_2CO_3	2.5, 10	23, 40, 75
1.2M $NaHCO_3$+0.75M Na_2CO_3	10	
1M $NaHCO_3$+0.5M Na_2CO_3	2.5, 7, 10, 20	
0.7M $NaHCO_3$+0.35M Na_2CO_3		
0.5M $NaHCO_3$+0.25M Na_2CO_3		
0.25M $NaHCO_3$+0.125M Na_2CO_3		
CO_2-saturated		
Pure Distilled water	10	23, 75
0.7M $NaHCO_3$+0.35M Na_2CO_3		
0.25M $NaHCO_3$+0.125M Na_2CO_3		

Table 10: Electrochemistry tests-Effect of sulphites

System	Sodium sulphite (%wt)	Temperature (°C)
CO_2-free		
Pure Distilled water	10	23, 75
1M $NaHCO_3$+0.5M Na_2CO_3	10	23, 40, 75
0.7M $NaHCO_3$+0.35M Na_2CO_3		
0.5M $NaHCO_3$+0.25M Na_2CO_3		
0.25M $NaHCO_3$+0.125M Na_2CO_3		
CO_2-saturated		
Pure Distilled water	10	23, 75
0.7M $NaHCO_3$+0.35M Na_2CO_3		
0.25M $NaHCO_3$+0.125M Na_2CO_3		

Table 11: Electrochemistry tests-Effect of sulphates

System	Sodium sulphate (%wt)	Temperature(°C)
CO_2-free		
1.5M $NaHCO_3$+0.75M Na_2CO_3	10	23, 40, 75
1M $NaHCO_3$+0.5M Na_2CO_3		
0.7M $NaHCO_3$+0.35M Na_2CO_3		
0.5M $NaHCO_3$+0.25M Na_2CO_3		
0.25M $NaHCO_3$+0.125M Na_2CO_3		

Each test was conducted in a fresh test solution of approximately 600 mL. Additions of sodium nitrate ($NaNO_3$), sodium sulphite (Na_2SO_3) and sodium sulphate (Na_2SO_4) to the carbonate / bicarbonate solutions were made to assess the effect of impurity in bicarbonate / carbonate solutions with and without gaseous CO_2 at atmospheric pressure. The initial molar concentration ratio of sodium bicarbonate to sodium carbonate in solution was arbitrarily maintained constant at 2.

Testing was conducted at different temperatures i.e. 23, 40 and 75°C. (±2°C). The pH of the test solutions at 23 and 75°C was taken using a pH electrode meter.

In tests involving carbon dioxide, the solutions were bubbled with CO_2 once a stable solution test temperature (±2°C) was achieved. The solution was diffused with carbon dioxide for 1 to 4 hours (depending on test solution) to allow pre-saturation of solution with CO_2 before electrochemical measurements were effectively started.

The measurement of pH with time (see Figure 43 and Figure 44) was used to determine the period required for pre-saturation of solution with CO_2 before a test was started; the saturation of the solution with carbon dioxide was considered to

be achieved when the pH became stable with time. For relatively concentrated systems (typically 0.7M $NaHCO_3$+0.35M Na_2CO_3), a pre-saturation time of 4 hours was used, whilst for lower concentration systems (typically 0.25M $NaHCO_3$+0.125M Na_2CO_3), 1 h pre-saturation time was considered. The different pre-saturation periods of solutions with CO_2 are listed in Table 12. In concentrated systems (typically 0.7M $NaHCCO_3$+0.35M Na_2CO_3), the diffuser micro-pores got blocked with white products (probably carbonates). An open tube was therefore used instead of a conventional gas diffuser to saturate solution with CO_2 for such systems (see Table 12).

During the solution temperature stabilisation and CO_2 pre-saturation stages, the working electrode was maintained under suitable cathodic protection to prevent anodic dissolution before the test was started.

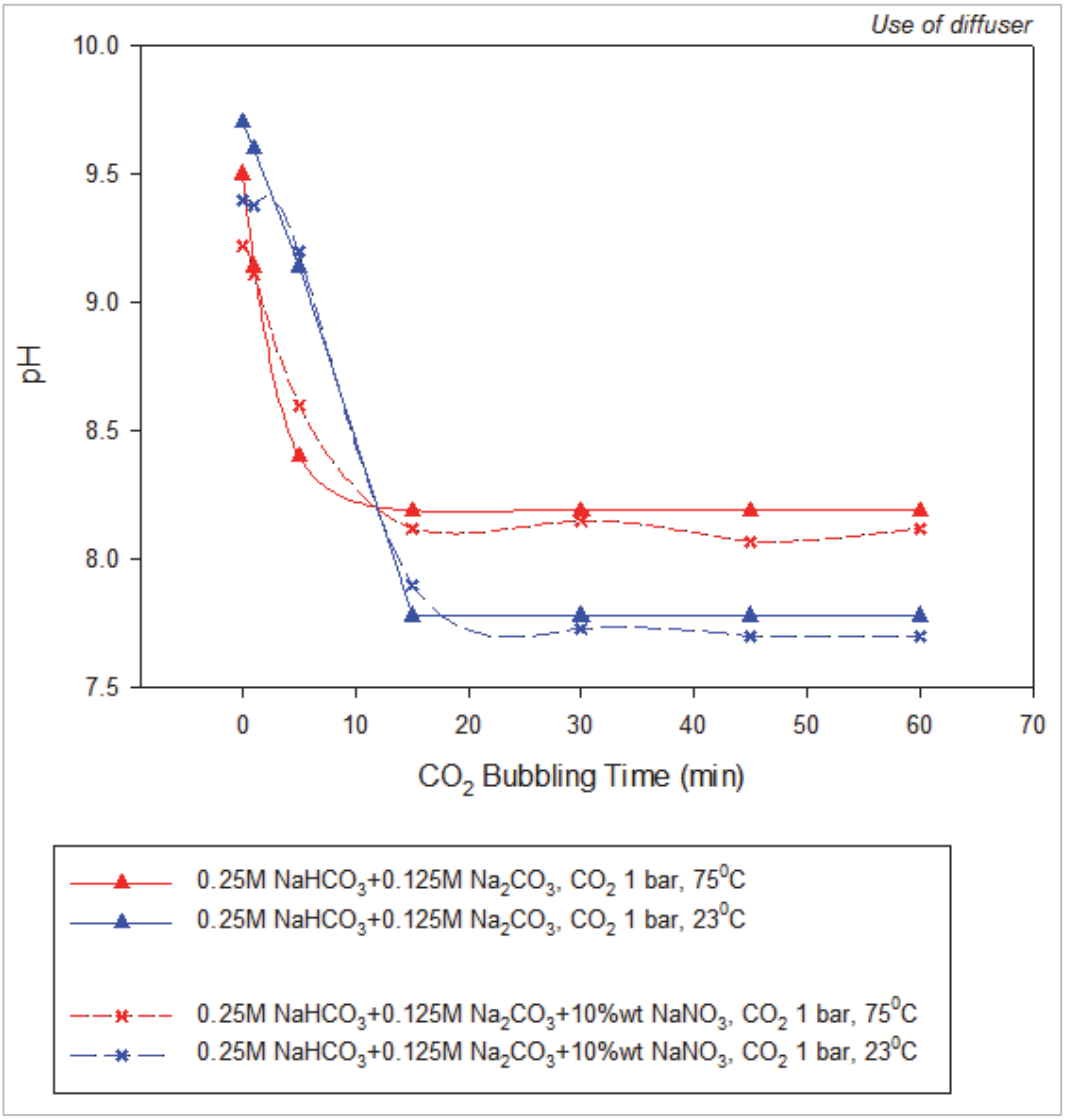

Figure 43: pH vs CO_2 bubbling time, 0.25M $NaHCO_3$+0.125M Na_2CO_3 and 0.25M $NaHCO_3$+0.125M Na_2CO_3+10%wt $NaNO_3$ systems

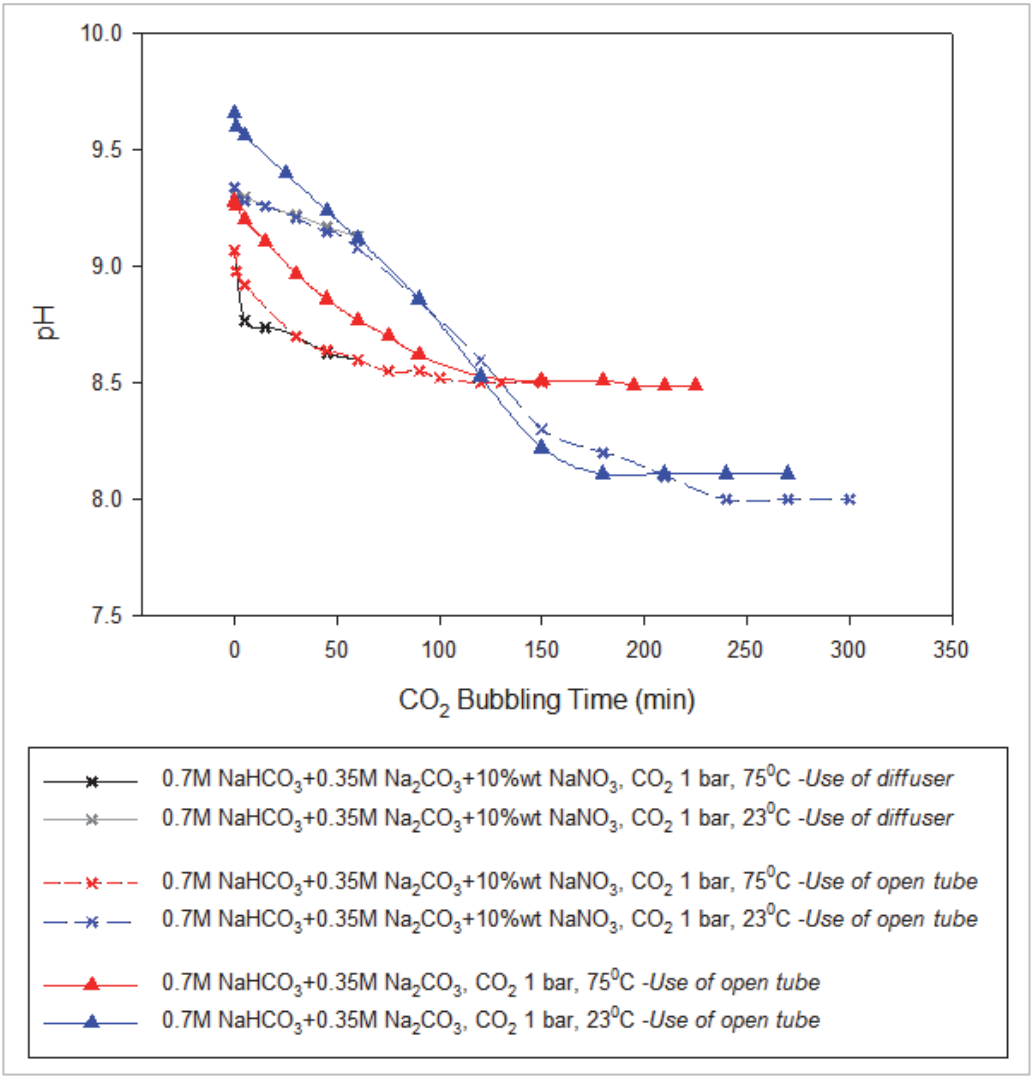

Figure 44: pH vs CO_2 bubbling time, 0.70M $NaHCO_3$+0.35M Na_2CO_3 and 0.70M $NaHCO_3$+0.35M Na_2CO_3+10%wt $NaNO_3$ systems

Table 12: Pre-saturation periods of solutions with CO_2 prior to electrochemical test start

System	Pre-saturation time with CO_2	Method for CO_2 bubbling
0.7M $NaHCO_3$+0.35M Na_2CO_3	4 hours	Open tube
0.7M $NaHCO_3$+0.35M Na_2CO_3+10%wt $NaNO_3$		
0.7M $NaHCO_3$+0.35M Na_2CO_3+10%wt Na_2SO_3		
0.25M $NaHCO_3$+0.125M Na_2CO_3	1 hour	Gas diffuser
0.25M $NaHCO_3$+0.125M Na_2CO_3+10%wt $NaNO_3$		
0.25M $NaHCO_3$+0.125M Na_2CO_3+10%wt Na_2SO_3		

3.4. Evaluation of SCC susceptibility by Slow Strain Rate test

3.4.1. Introduction to SCC mechanical test and Slow Strain Rate Test

A. SCC mechanical test

Once it is demonstrated that the steel may be prone to SCC under a certain set of environmental conditions, including electrode potential, mechanical testing is required to identify whether SCC can be truly produced. The assessment of the susceptibility of a particular system (i.e. alloy and environment) to SCC can be achieved by immersing a stressed specimen in a corrosive environment.[113]

The testing requires:[113]

- A test alloy specimen designed in the material for which the susceptibility to SCC is investigated.
- A corrosive environment which is adequately defined e.g. species concentration, pH, temperature and pressure. In addition, electrode potential control of the specimen is also required.
- Mechanical tensile stress, which can be static or dynamic

Testing to assess SCC susceptibility can be categorised as a function of the mode of stressing

- Slow Strain Rate Test (SSRT); slow dynamic straining is applied to the specimen
- Constant-load test
- Constant-strain test

The SSRT technique was used in this thesis to assess the susceptibility to SCC as a function of variation in environmental conditions.

B. Accelerating test

It is generally necessary to obtain data on SCC susceptibility in reasonably short times. All SCC mechanisms are generally constituted of two essential stages i.e. crack initiation and crack propagation as discussed[66,75] in section 2.5. It has been stated that the initiation stage takes 90% of the overall SCC mechanism and therefore this is the stage that researchers have attempted to minimize.[120] This has usually been achieved by increasing the test severity e.g.:

- Increase in the corrosivity of the environment e.g. by modifying composition or by increasing the temperature.
- Electrode potential control is another means of increasing the kinetics of dissolution and hence the corrosion crack growth.
- Increase in strain rate or load

The use of Slow Strain rate Testing enters the category of accelerating testing.

C. SSRT test method

The technique was developed in the early 1960's at Newcastle University.[121,122]

SSRT is also referred to as constant-extension rate test or straining-electrode test. In contrast to conventional SCC techniques which use static stress conditions, SSRT is conducted under dynamic stress to strain the specimen.

The increase in the load is such that the specimen, which is exposed to the appropriate environmental conditions, is subject to a slow and constant strain rate; the test ends when fracture has occurred. The generation of SCC is promoted both by the test duration which allows for the corrosion processes to take place, and the continuous straining of the specimen which assists with film rupture.[72,123] As mentioned previously, the balance between corrosion and mechanical processes is essential for the realisation of SCC, which emphasises the criticality of defining a suitable range of strain-rates: a too low strain-rate could indeed lead to a specimen failing by dissolution, whilst a too high strain rate could favour fracture of the specimen due to mechanical overload.[123]

The configuration of the SSRT is illustrated in Figure 45.[113]

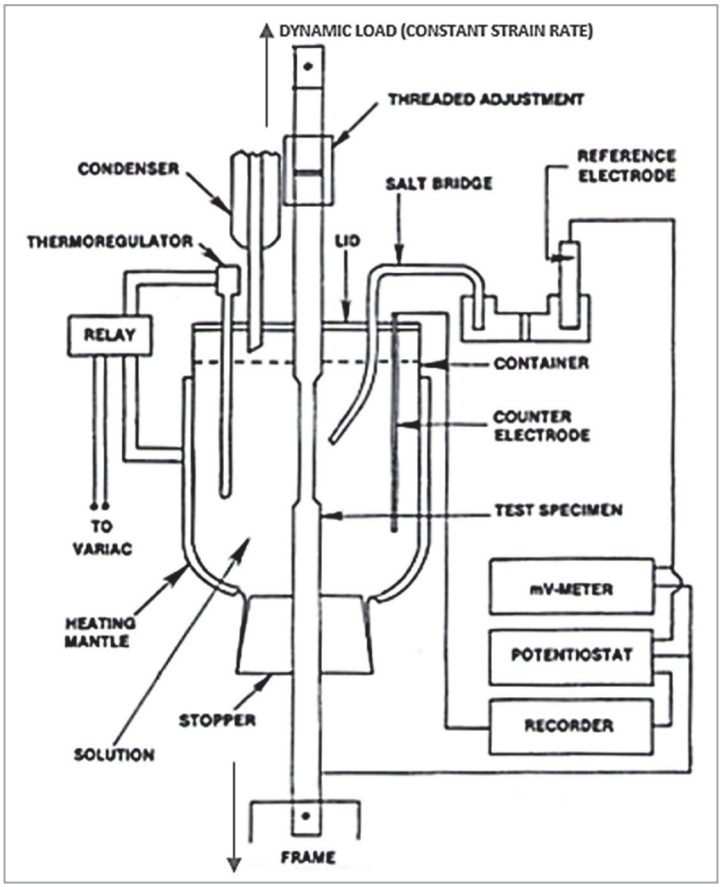

Figure 45: Schematic of Slow Strain Rate Testing at ambient pressure; solution temperature and electrode potential are under control[113]

The main advantages of SSRT are:

- SSRT produces fracture in relatively short times in opposition to constant-load or constant-strain tests
- Testing is always positive in the sense that it will invariably produce fracture either by SCC or mechanical fracture or both.
- The test stops when fracture of the specimen has been realised i.e. the test is not arbitrarily stopped because fracture takes too long to occur e.g. in the case of constant load tests.
- Constant stress (load) / strain tests usually involve a higher spread (scatter) in SCC susceptibility data than SSRT.[123]

Despite, the fact that SSRT can be used as an initial “go-no-go” test, a major drawback is that the direct application of the data for the prediction of an actual system operational life is difficult or far too conservative.[66]

3.4.2. SSRT tests and test environments

A. Test specimens

X80 tensile test specimens were produced from the pipe section. A typical schematic of tensile specimen used for the SSRT is illustrated in Figure 46. The gauge length G of the specimens was approximately 12.7 mm.[113]

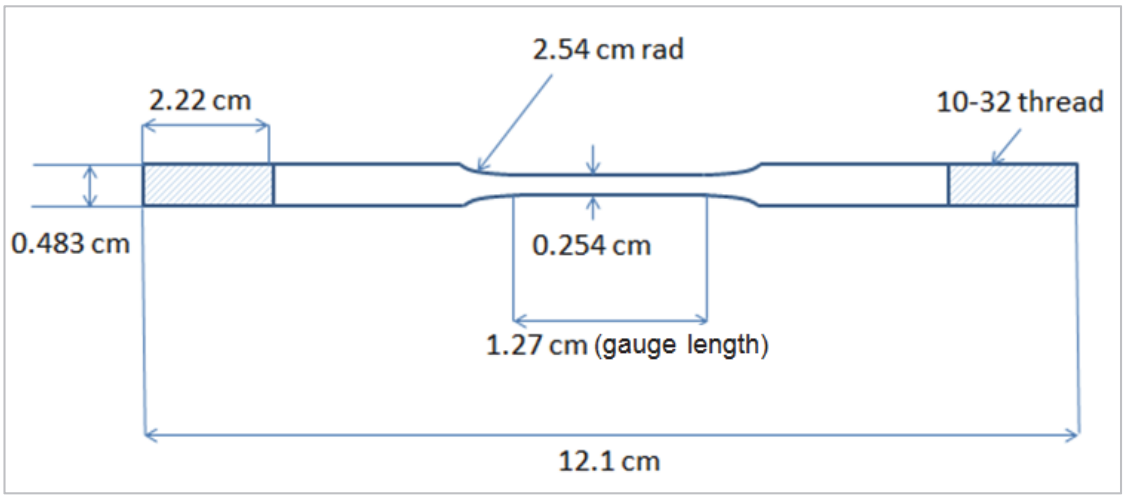

Figure 46: Schematic of a typical Slow Strain Rate Specimen[113]

As per Figure 35, the hoop stress related to the pipeline internal pressure exerted by the environment is a tensile stress parallel to the long transverse direction of the pipe. The specimens were cut from the pipe section to simulate the hoop stress: the length of the SSRT specimen gauge was cut parallel to the long transverse direction (with the gauge cross-section being parallel to the plane of the pipeline steel wall thickness in the short transverse direction); the tensile stress applied to the specimen gauge was thus parallel to the hoop stress direction.

The specimens were polished over their gauge length to a 1200 grit-finish. When the surface condition was judged satisfactory for SSRT testing, the diameter of the gauge D over gauge length was then measured. After polishing, the specimens were cleaned with methanol and air dried.

Before SSRT testing, the specimen grip sections were mechanically dented with a dot so that the total elongation at fracture could be easily determined after fracture.

B. SSRT tests and environments

The configuration of the cell used during SSRT is illustrated in Figure 47.

A potentiostat was used to apply the test potential to the specimen and this was measured against a SCE reference electrode to ensure the correct potential was achieved. A salt bridge was used to allow circuit continuity between the test cell and the SCE electrode, and a platinum wire was used as counter electrode.

A thermostat was used to achieve the correct temperature. During the heating of the solution and until a stable temperature was achieved, a cathodic potential was applied to the specimen to prevent surface anodic reactions until the SSRT test was effectively started. This was adjusted according to the environment so that neither anodic reactions nor hydrogen evolution occurred at the specimen surface.

When gaseous CO_2 at atmospheric pressure was used in the SSRT test, the carbon dioxide was only introduced into the solution once the test temperature was achieved and was stable. The SSRT test was only started once carbon dioxide had been diffused into the solution for 4 hours to allow for pre-saturation. During this time, the test specimen was also maintained under suitable cathodic protection.

The strain rate during testing was approximately 1.4×10^{-6} sec^{-1}, which is of the order of magnitude of strain rates for which SCC has been identified in low alloy steels.[75,123] The test ended when fracture of the specimen occurred.

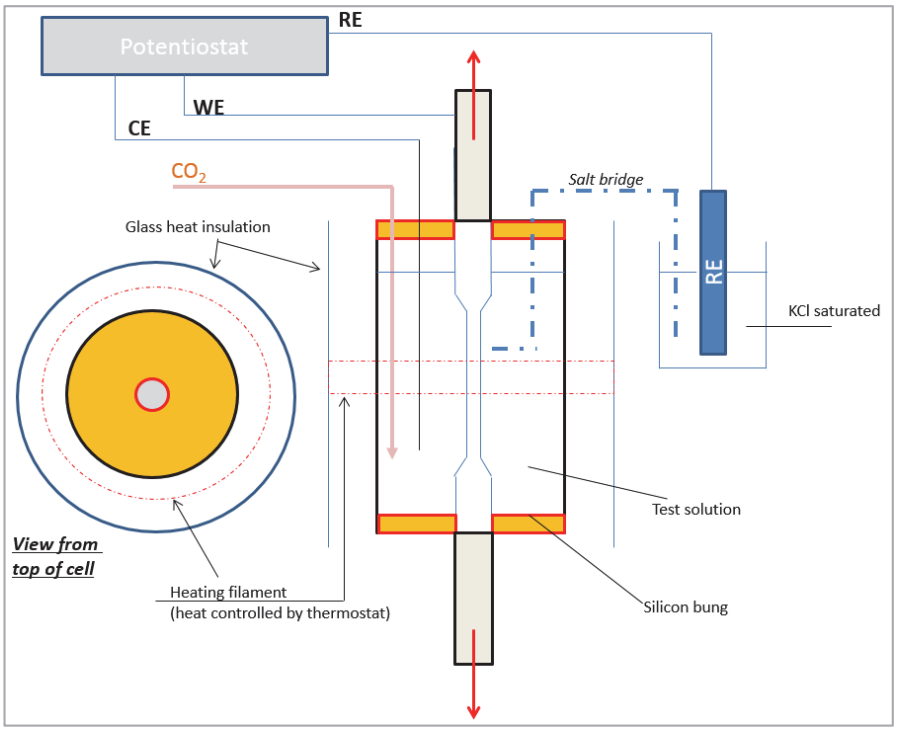

Figure 47: SSRT test cell used

The following environmental conditions have been tested for X80 materials:

Table 13: Environmental conditions tested with SSRT

	CO_2 partial pressure (bar)	Temperature (°C)	Electrode Potential (mV SCE)
Silicon oil (inert environment)	N/A	23	N/A
		75	
0.7M $NaHCO_3$ + 0.35M Na_2CO_3	N/A	23	-610, -600, -590
		75	-820, -770, -710, -685, -675, -655, -625
	1	23	OCP
	1	75	OCP, -830, -800, -730, -710, -690, -670
0.25M $NaHCO_3$ + 0.125M Na_2CO_3	N/A	23	-625, -605, -585
		75	-755, -740, -725, -710, -695
0.7M $NaHCO_3$ + 0.35M Na_2CO_3+10%wt $NaNO_3$	N/A	23	-600
		75	-790, -740, -700, -670, -650, -630, -590
	1	23	OCP
	1	75	OCP,-800, -780, -710, -680, -660, -640, -620
0.25M $NaHCO_3$ + 0.125M Na_2CO_3+10%wt $NaNO_3$	N/A	23	-600, -590, -580
		75	-720, -710, -690, -650

	CO_2 partial pressure (bar)	Temperature (°C)	Electrode Potential (mV SCE)
0.7M $NaHCO_3$ + 0.35M Na_2CO_3+10%wt Na_2SO_3	N/A	23	-690, -670, -660, -650
		75	805, -790,-730, -720, -710, -690, -650
	1	23	OCP
	1	75	OCP,-780, -750, -715, -695, -680, --665
0.25M $NaHCO_3$ + 0.125M Na_2CO_3+10%wt N a_2SO_3	N/A	23	-720, -690, -670, -650, -630
		75	-820, -790, -770, -750, -730

3.5. Characterisation of cracking and corrosion features following SSRT tests

3.5.1. Evidence of SCC: Use of imaging techniques

As mentioned previously, fracture during SSRT can be the result of either SCC, or mechanical overload, or a combination of the two. It is hence fundamental to first identify whether SCC has occurred or not.

Such a question was resolved by the use of fractographic examination of the specimen using Scanning Electron Microscopy (SEM). Further confirmation of SCC occurrence was made by metallographic examination of the specimen cross-section with an optical microscope.

A. The SEM technique

In SEM, the surface of the specimen is scanned by a focused electron beam. The beam is generated under vacuum via a heated tungsten filament located on the top of a column, referred to as the "*microscope column*". In the column, a series of lenses are present to focus the electron beam into a spot on the surface of the specimen to be examined. The sample is positioned at the bottom of the microscope column. A traditional arrangement is illustrated in Figure 48 although nowadays a frame grabber allows integration of images rather than the use of a camera

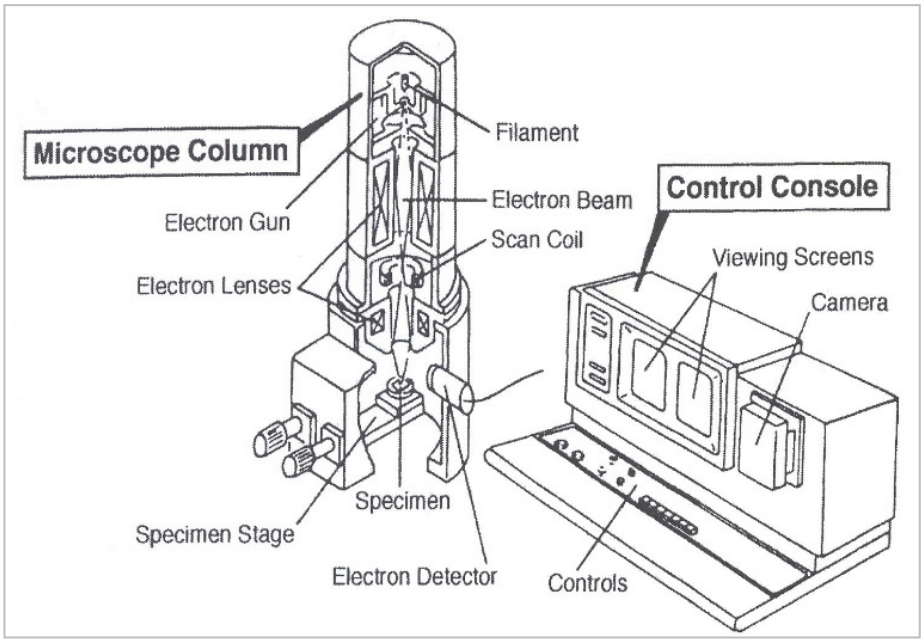

Figure 48: SEM traditional arrangement[124]

During the interaction between the electron beam and the sample surface, several physical signals are generated. As illustrated in Figure 49, the interaction

between the target beam and the specimen occurs at different depths below the specimen surface. Two key signals are collected and processed for the imaging process: the backscattered electrons (BSE), and the secondary electrons.

Backscattered electrons are primary electrons from the beam which have been deflected following interaction with the specimen atoms; the BSE eventually leave the solid specimen bulk after further elastic scattering events. The BSE provide insights of the surface topography as well as the chemical composition. The level of interaction is indeed a function of the atom nucleus size and thus of the atomic number.

Secondary electrons are low energy electrons located on the outer-shelves of the specimen atoms. These electrons have been expelled from atoms as a result of collision or inelastic scattering of beam primary electrons. Due to their low energy, only secondary electrons produced close to the surface could leave the specimen and be detected. This means that secondary electrons provide substantially more insights on topography details than BSE, such as the presence of cracking and pitting.

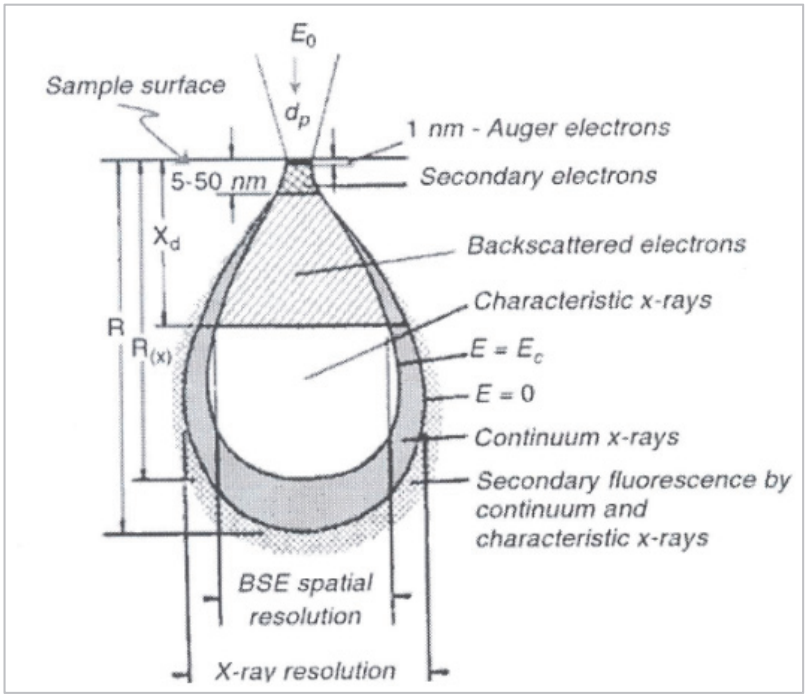

Figure 49: Interaction between SEM electron beam and metal surface for imaging purposes[125]

B. Optical microscopy

Optical or light microscope is the oldest type of microscope. It uses the visible light reflection from the specimen surface to examine surface morphology and

features. A system of lenses is provided to allow specimen magnification so that discrimination of small features can be made.

C. Imaging and evidence of SCC

SCC was evidenced by:[119,120]

- Secondary cracks located along the specimen gauge length and propagating perpendicularly to the direction of applied stress. For steels, the secondary cracks are generally identified close to the main surface of fracture.
- Significant loss of ductility: when SCC has not occurred, the fracture surface has characteristics of a ductile behaviour i.e. dimples and microvoid coalescence are observed, and the fracture has a distinctive cup-and-cone shape. In the presence of SCC, the decrease of the specimen ductility is significant and crack propagation takes place in a brittle mode; the fracture surface reveals cleavage or quasi-cleavage.

Characteristics of crack propagation e.g. whether the cracking is transgranular or intergranular was also be revealed by metallographic examination of SSRT specimen cross-section via optical microscopy, and by examination of the fracture surface via SEM. The classic morphology of the fracture surface for intergranular, transgranular is illustrated in Figure 50 and Figure 51.

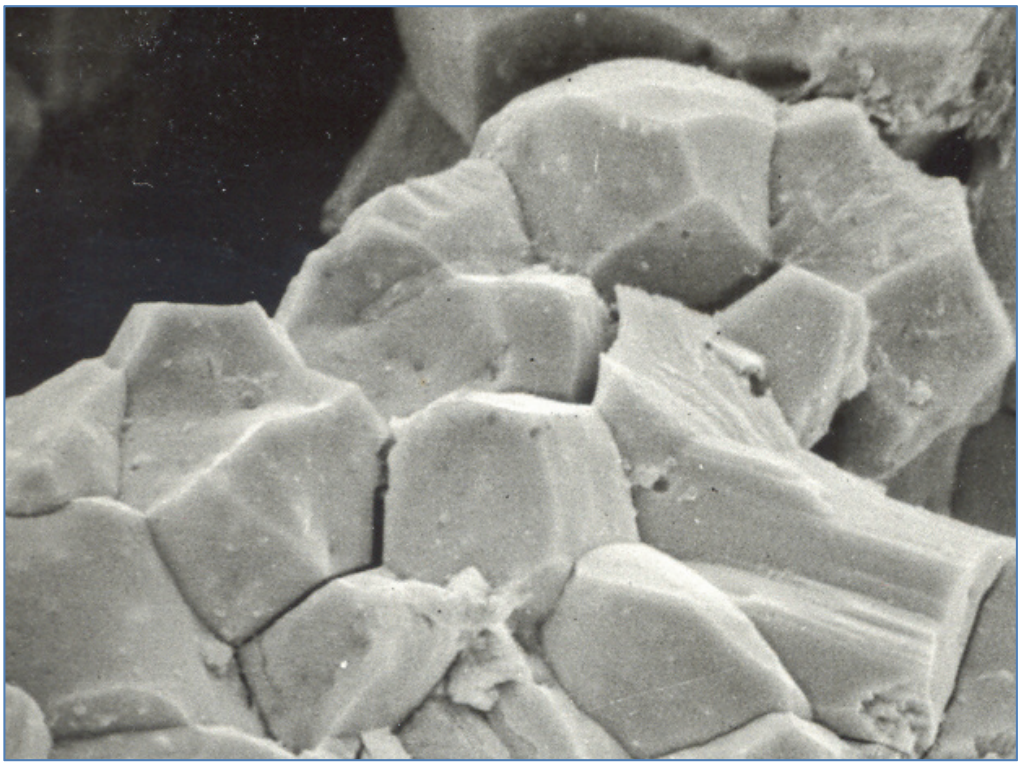

Figure 50: Classic fracture face-Intergranular cracking[126]

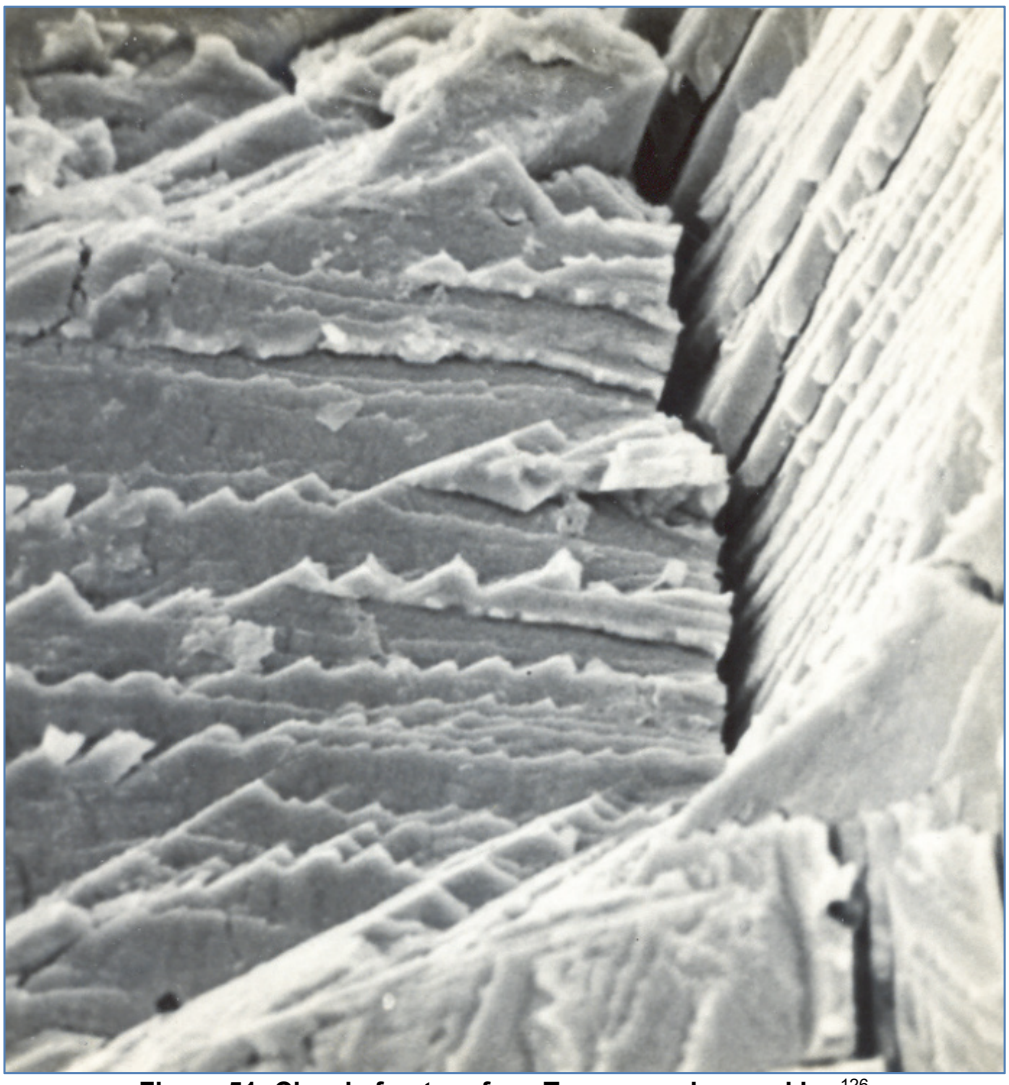

Figure 51: Classic fracture face-Transgranular cracking[126]

It is however emphasised that determining whether a system is susceptible or not to SCC is not always easy; as discussed in section 2.5 it is sometimes challenging to define at which stage a pit (initiation stage) will start behaving or acting as a crack (propagation). Payer et al.[119] have gathered various micrographs of un-etched carbon steel cross-sections following SSRT in CO_2-CO-H_2O solutions at ambient temperature and for various partial pressures of CO_2 and CO. The micrograph montage is illustrated in Figure 52[119]; it shows clear SCC pattern from the bottom to lack of SCC behaviour at the top.

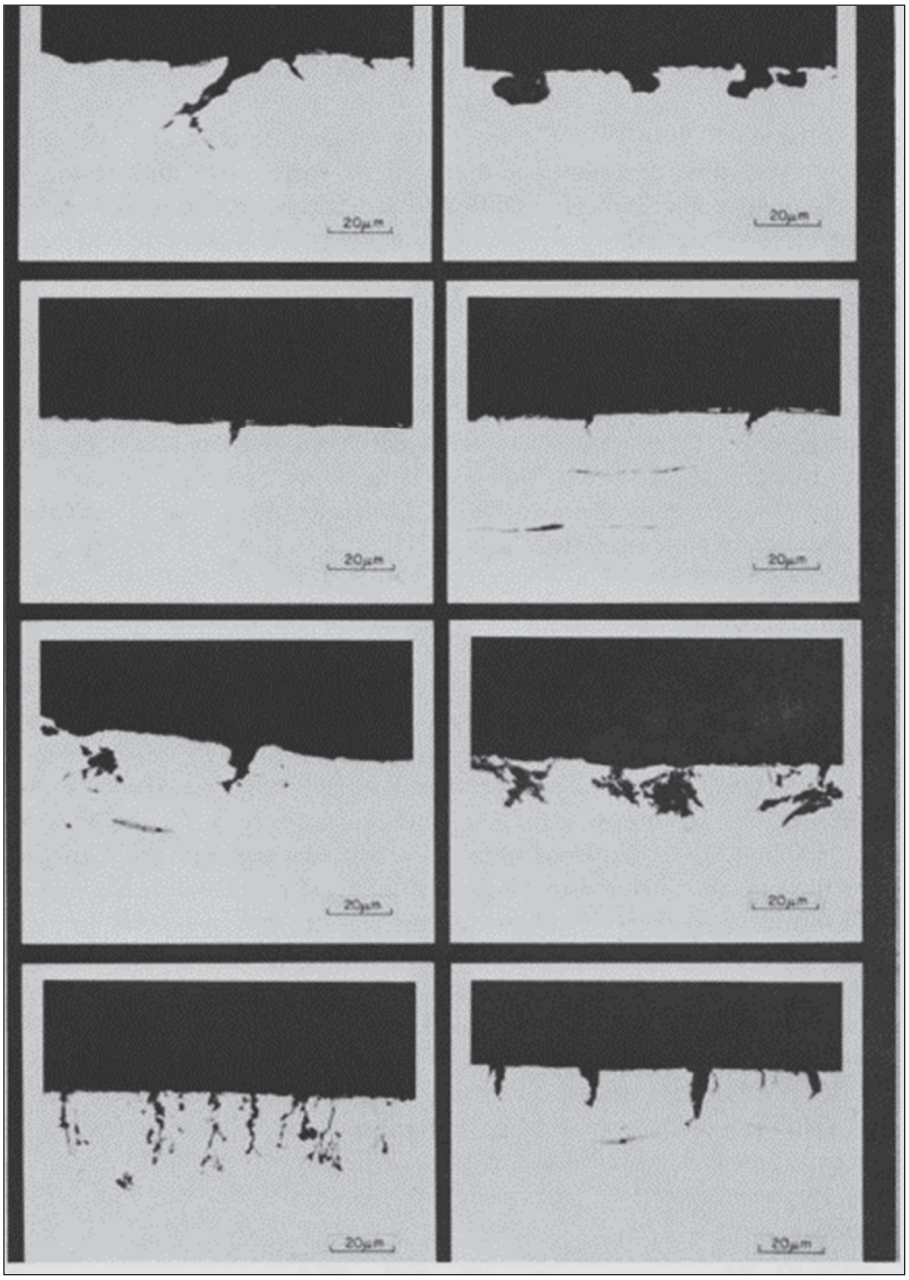

Figure 52: Susceptibility to SCC of mild steel in CO_2-CO-H_2O environments[119]

3.5.2. Ductility measurements and measurement of SCC severity

Once the susceptibility has been confirmed, it is often desired to quantify the susceptibility of the system to SCC, e.g. to investigate the effect of environmental parameters (e.g. aqueous species concentration, temperature, electrode potential) on SCC occurrence.

Several parameters have been listed to quantify the severity of SCC after SSRT; these include: [113,119]

- Time to failure
- Measures of ductility e.g. reduction in cross-sectional area and strain at rupture
- Crack growth rate calculated from the length of the secondary cracks and the time to fracture
- Secondary crack frequency over the gauge length

A. Mechanical data

After SSRT, the following parameters were determined:

- Time to failure t_f; it is defined as the interval between the start of the SSRT test and the time at which fracture of the specimen occurs
- Reduction in cross-section area RA (%): $RA = \frac{S_0 - S_f}{S_0} \times 100$, where:

  S_o is the initial cross-section area of the gauge and S_f is the cross-section area of the gauge after fracture.

  S_o is obtained by using the initial diameter of the polished gauge prior to SSRT testing.

  S_f is obtained by using the average diameter of the specimen neck in the fracture region.

Measurements of the strain at rupture or elongation ε (%): $\varepsilon = \frac{l_f - l_0}{l_0} \times 100$, where l_0 is the initial gauge length (12.7 mm) and l_f is the gauge length after fracture, were also conducted. However the elongation measurements did not provide a

suitable correlation in regards to the occurrence of SCC and the susceptibility to SCC. The measurements of RA were therefore privileged over the measurements of ε to evaluate the susceptibility to SCC in this thesis.

Due to the duration of SSRT experiments, all the tensile mechanical tests could not be repeated during the length of the research program. For each environment at 75°C, SSRT was nevertheless repeated three times at the electrochemical potential for which the system was found to be the most susceptible to SCC. The RA indicated at the potential of the "SCC susceptibility peak" is an average of the RAs measured during these three experiments.

B. Specimen preparation for fractographic analysis by SEM

The fractured specimen tip was dipped in Clarke's solution for 2 seconds to clean the surface films, and then rinsed with deionised water and washed in methanol under ultrasound. If the presence of films was still noticeable in the tip region, this process was repeated until the surface condition was judged satisfactory for visualisation.

Examination of the fracture surface and the specimen gauge for primary and secondary crack features were made using a Hitachi S2400 SEM.

C. Cross-section preparation and crack growth rate

A cross-section of the specimen tip was produced in the direction of the gauge axis. The cross-section plane was produced at 90° of the specimen orientation for which cracks appeared to be deepest and numerous under an optical microscope. The preparation of the cross-section is described in Figure 53.

The cross-section was hot mounted in Bakelite and polished to 1 micron diamond paste to obtain a 'clean' mirror finish. The maximum crack depths C_D were determined under optical microscope.

The maximum crack velocity C_v was calculated as followed:

$$C_v = \frac{C_D}{t_f}$$

The selection and the preparation of the cross section plane for the measurement of crack velocity is somewhat arbitrary and has some major limitations associated with the destructive nature of the test, and more importantly with the fact that the

propagation of the stress corrosion cracks in a 3-D network is actually resumed to a 2-D plane. This means that:

- The longest crack could actually be missed from the cut plane
- The measurements of the crack velocity are not representative of that actually present in-situ and could be under-estimated.

To overcome these limitations and to provide a more appropriate comparison of the SCC susceptibility between the different systems, it is necessary to repeat the SSRT tests and the crack velocity measurements. However, as indicated above for the RA measurements, due to the duration of SSRT experiments, all the tensile mechanical tests could not be repeated during the length of the research programme. For each environment at 75°C, SSRT was nevertheless repeated three times at the electrochemical potential for which the system was found to be the most susceptible to SCC. The crack velocity indicated at the potential of the “SCC susceptibility peak” is an average of the crack velocities measured during these three experiments; an error bar associated with the standard deviation of the data sample is provided to indicate the spreadability on the maximum crack velocity measurements (refer to section 5.2, Figure 157). The experimental data show there is a strong correlation between the reduction of area and the crack velocity measurements (refer to section 5.2, Figure 160). This provides further confidence in these measurements for the assessment of the susceptibility to SCC.

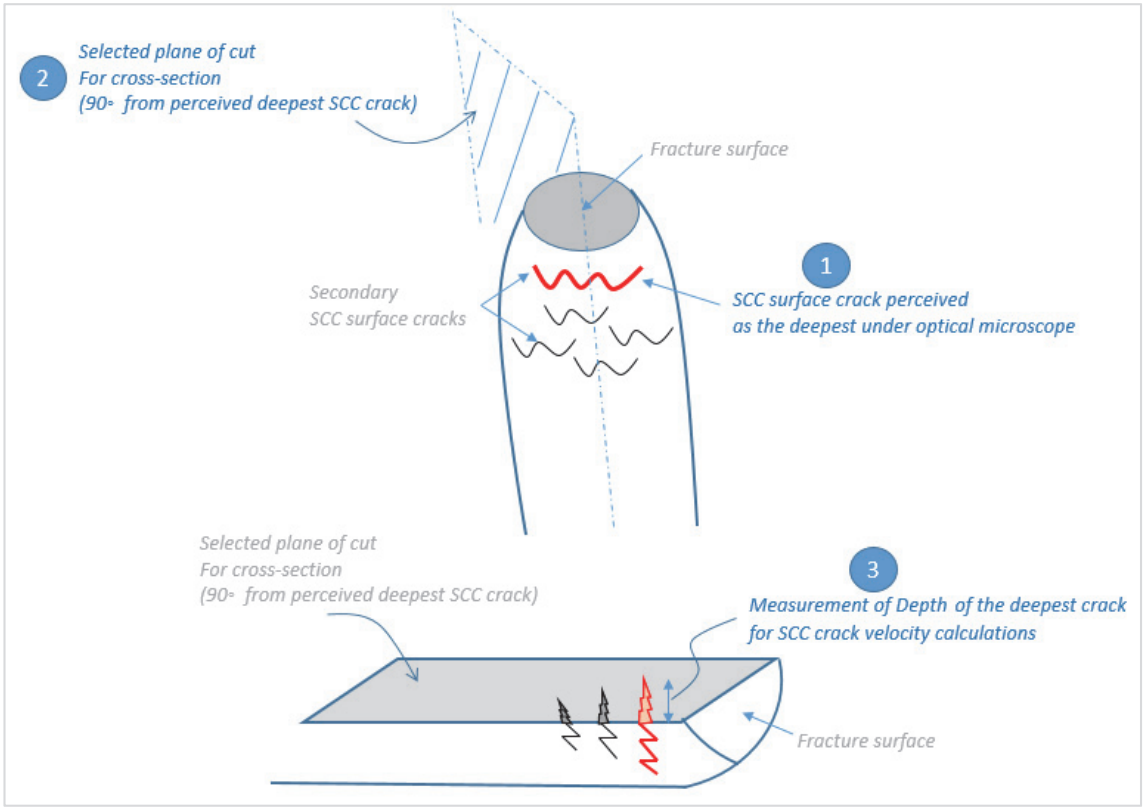

Figure 53: Production of a cross-section of SSRT specimen tip for SCC Crack Velocity measurements

Chapter 4. Results from Electrochemistry Investigation

4.1. Solution pH

4.1.1. Addition of nitrates and sulphites to bicarbonate / carbonate systems

A. Pure bicarbonate and carbonate systems

The pH of pure bicarbonate and carbonate solutions in the presence of nitrates and sulphites (CO_2-free) at 23 and 75°C is illustrated in Figure 54.

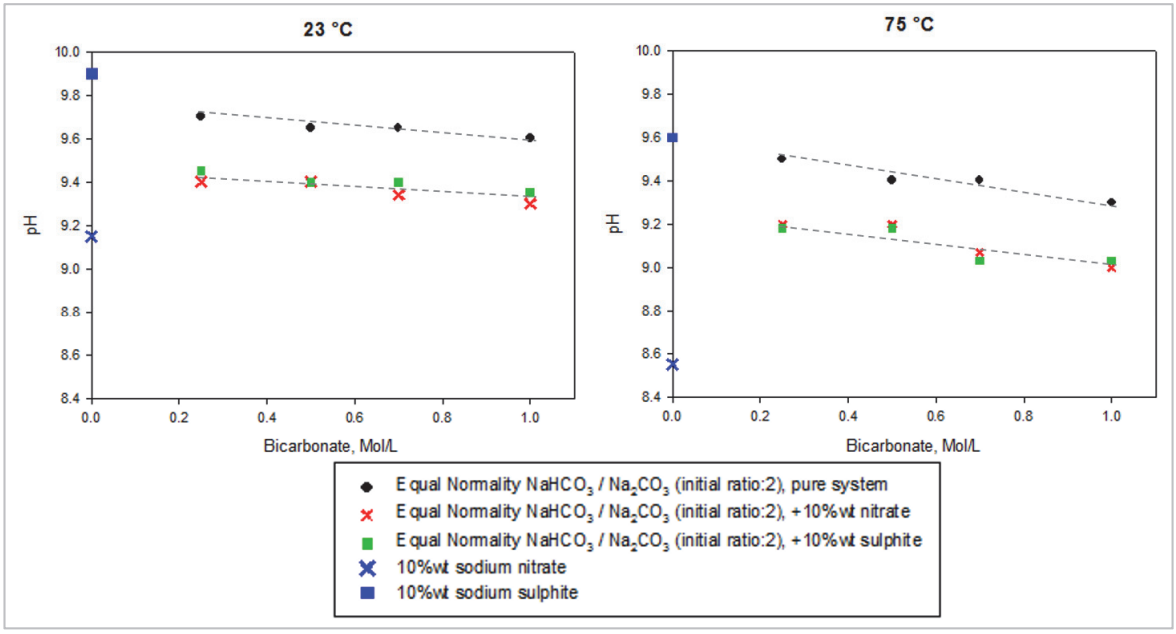

Figure 54: pH of pure carbonate and carbonate solutions in the presence of nitrates and sulphites at 23 and 75°C (CO_2-free)

Effect of bicarbonate and carbonate concentrations

The increase in bicarbonate and carbonate concentration decreases the pH slightly, despite the ratio of bicarbonate to carbonate molarity being constant. The pH of the bicarbonate and carbonate solution is the result of a complex equilibrium of carbon dioxide, carbonic acid, bicarbonate and carbonates in the overall system CO_2-H_2CO_3-HCO_3^--CO_3^2 and the distribution of these species in this system. The distribution of bicarbonates and carbonates in the H_2CO_3-HCO_3^--CO_3^{2-} system as a function of pH is illustrated in Figure 55.[127] Over the range of pH 6 to 10, the bicarbonate species are predominant over the carbonates and this balance is shifted at more alkaline pHs. As the pH goes towards a more acidic region, carbonic acid and carbon dioxide become the most predominant species. Although the ratio of bicarbonates and carbonates is maintained constant during

the solution preparation, it is considered that the increase in the respective HCO_3^- and CO_3^{2-} concentrations result in either:

- The following equilibriums being shifted to the left

$$H_2CO_3(aq) + H_2O \leftrightarrow H_3O^+(aq) + HCO_3^-(aq)$$
$$HCO_3^-(aq) + H_2O \leftrightarrow H_3O^+(aq) + CO_3^{2-}(aq)$$

- More carbon dioxide being pulled from the atmosphere into the solution,

$$CO_2(g) + H_2O \leftrightarrow CO_2(aq) + H_2O$$
$$CO_2(aq) + H_2O \leftrightarrow H_2CO_3(aq)$$

such that the overall system equilibrium is restored and maintained as per Le Châtelier equilibrium laws. With an increase in bicarbonate and carbonate concentrations, the following equilibrium $H_2CO_3(aq) \leftrightarrow HCO_3^-(aq) \leftrightarrow CO_3^{2-}(aq)$ becomes critical. Bicarbonates being at the "crossroads" remain as the predominant species which move the pH of the solution to a slightly more acidic value than that for less concentrated solutions.

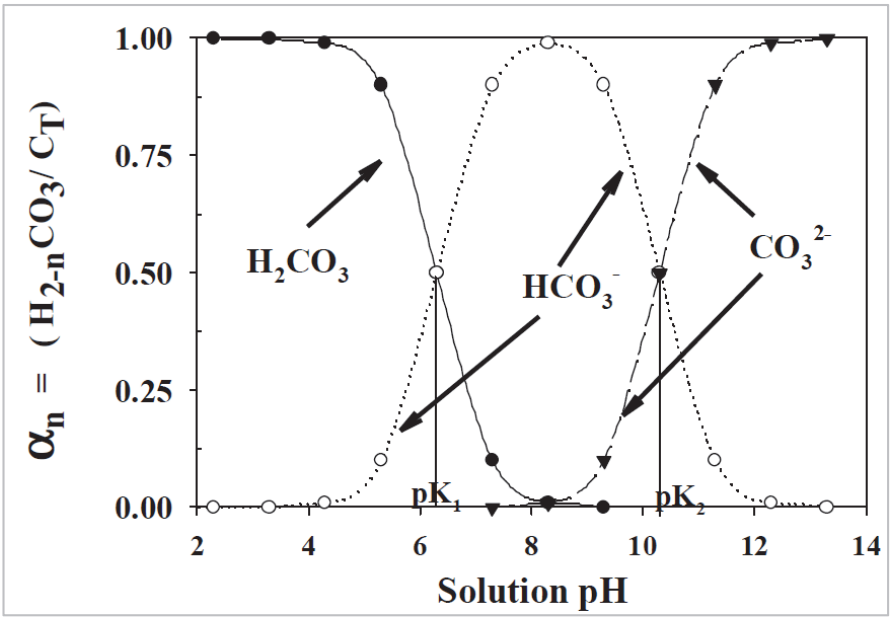

Figure 55: Distribution and activity of carbonate species as a function of pH in the H_2CO_3-HCO_3^--CO_3^{2-} system[127]

Effect of temperature

The pure bicarbonate / carbonate solutions have a pH of 9.6-9.7 at 23°C. The increase in temperature to 75°C slightly decreases the levels to 9.3-9.5. The same behaviour of pH against temperature is reported for pure bicarbonate solutions as illustrated in Figure 56.[128]

The increase in acidity in bicarbonate and carbonate systems with raising the temperature is considered to be related to the instability of bicarbonate which reverts to carbon dioxide at relatively high temperatures. This is illustrated in Figure 57, which shows the ionisation constant of carbonic acid decreasing at temperatures above approximately 50°C.[129]

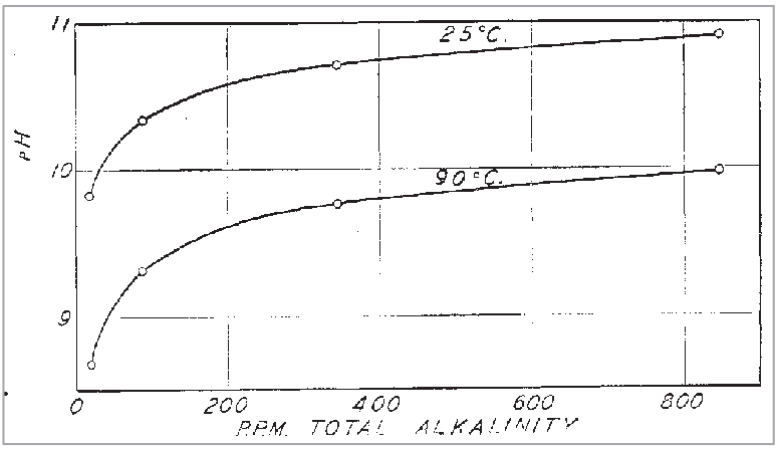

Figure 56: pH measurement in various bicarbonate solutions at various temperatures[128]

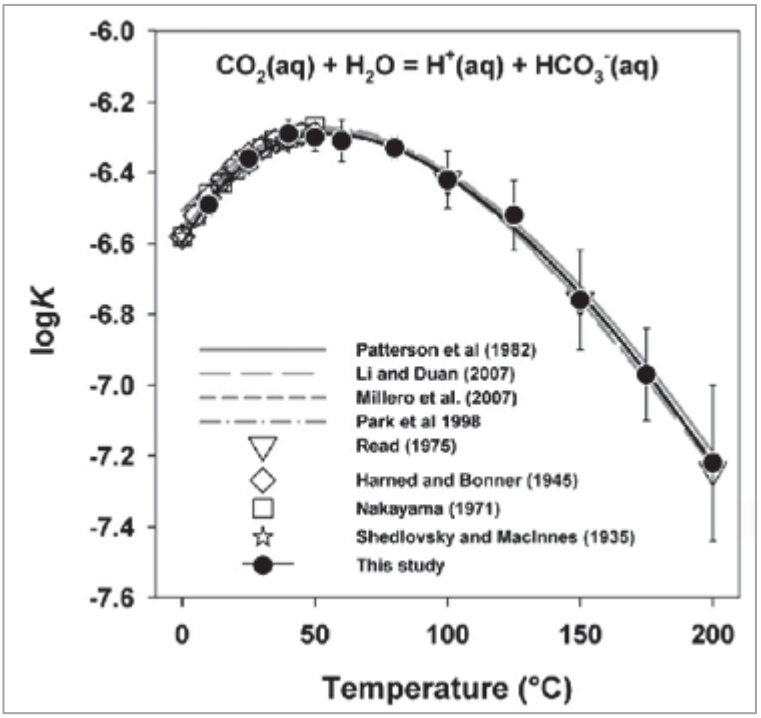

Figure 57: Ionisation constant of carbonic acid as a function of temperature[129]

B. Addition of nitrates and sulphites to bicarbonate and carbonate systems

The addition of nitrate or sulphites to bicarbonate and carbonate systems slightly decreases the solution pH by approximately 0.3-0.4 units. The fact that the shift is similar in the case of nitrate and sulphite additions suggests that the drop in pH

is not strictly influenced in this case by the nature of the compound added, i.e. whether it is sodium nitrate or sodium sulphite.

The addition of nitrates and sulphites probably affects the solubility of bicarbonates and carbonates in the solution. Bicarbonates are less soluble than carbonates, and it will be expected that these reach saturation and 'salts-out' before carbonates. The displacement of the equilibrium $HCO_3^-(aq) + H_2O \leftrightarrow H_3O^+(aq) + CO_3^{2-}(aq)$ to the left could be preferred to restore the system equilibrium and this will shift the pH to lower values as per Figure 55.

4.1.2. Effect of carbon dioxide

As illustrated in Figure 58, the solution pH dropped following solution saturation with CO_2.

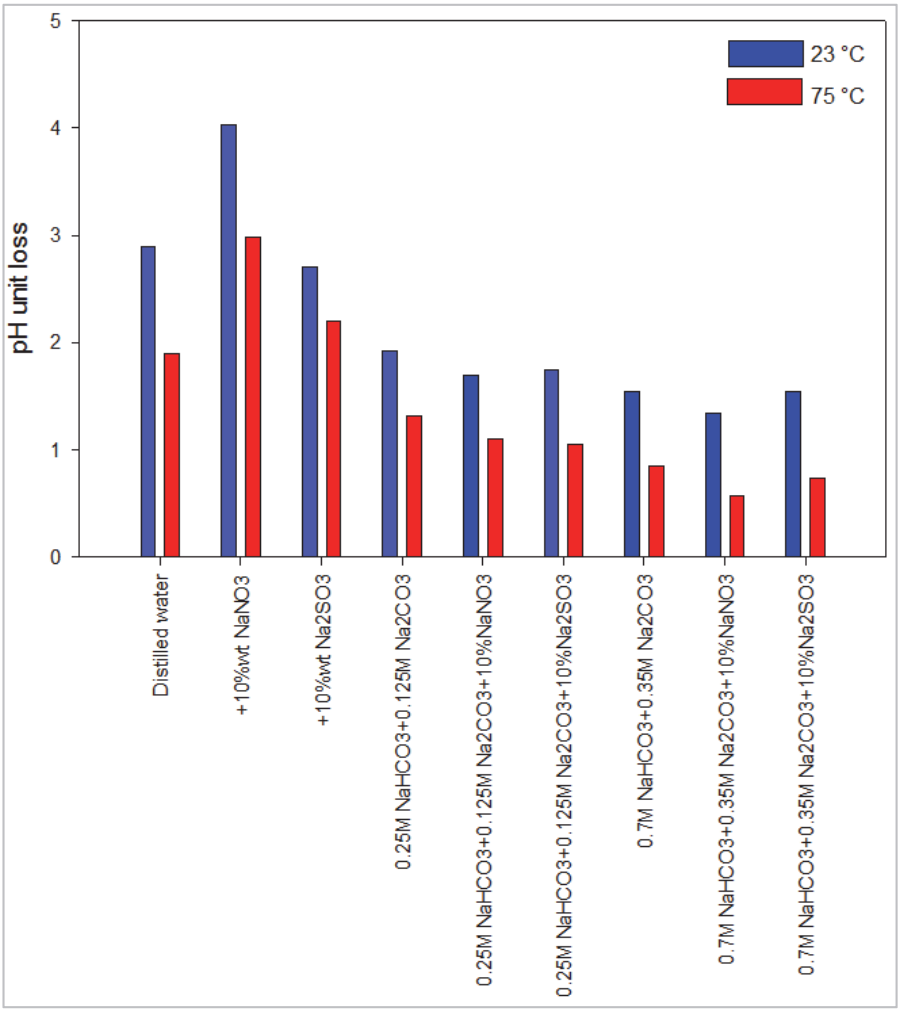

Figure 58: pH change in different test solutions following CO_2 saturation at 1 bar at 23 and 75°C

This is related to the solubility of CO_2 in water and the subsequent formation of carbonic acid as per the equilibrium reactions:

$$CO_2(g) + H_2O \leftrightarrow CO_2(aq) + H_2O$$

$$CO_2(aq) + H_2O \leftrightarrow H_2CO_3(aq)$$

The drop in pH due to the ionisation of carbon dioxide is less at 75°C than at 23°C. This is associated with the solubility of gases in liquids decreasing as the temperature is increased (see section 2.2.1).

In systems that contain bicarbonates, the drop in pH is noticeable but less significant than in bicarbonate-free systems (e.g. distilled water and sodium nitrate solutions). Bicarbonate species are solution buffers, which have the property due to their chemical nature to maintain the pH in the alkaline region when acids are introduced. For the test systems containing bicarbonates, the pH establishes itself between 7.5 and 8.5 after CO_2 saturation (see Figure 59), whilst it is above 9 when the system is CO_2-free (irrespectively of the temperature).

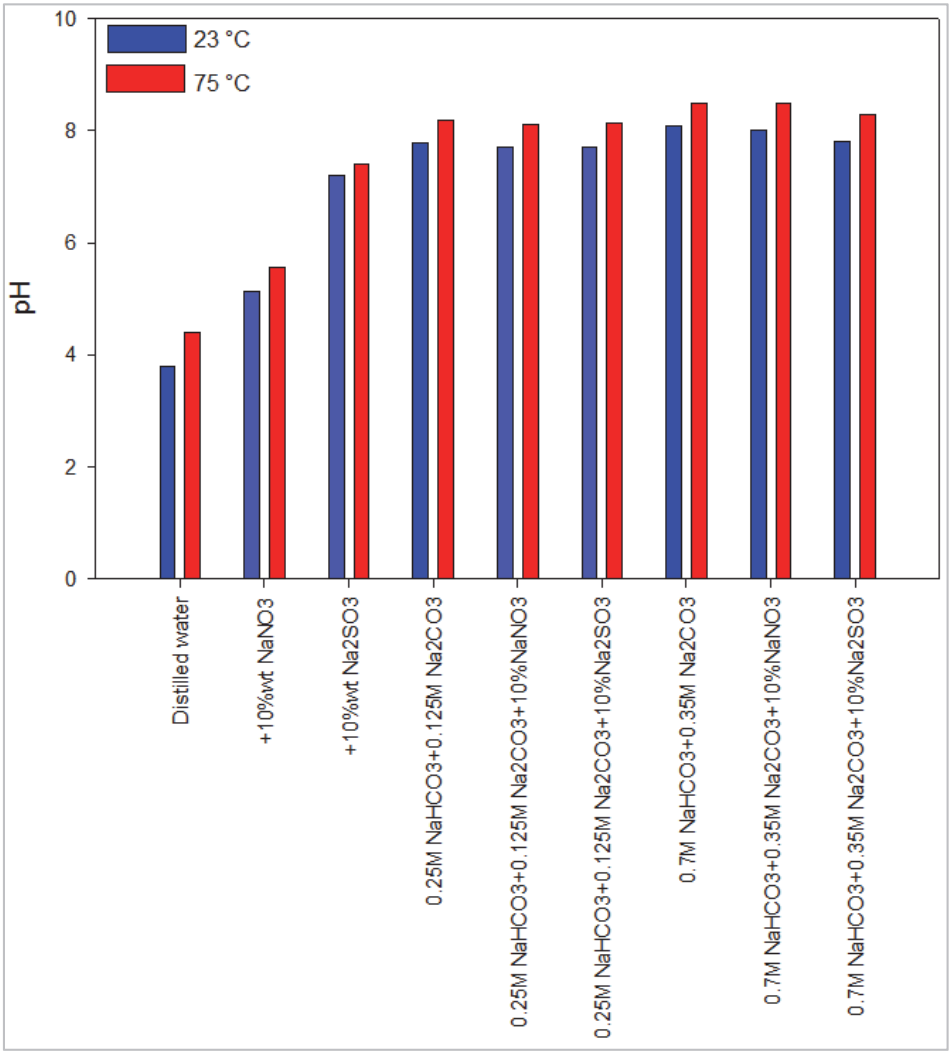

Figure 59: pH in different test solutions following CO_2 saturation at 1 bar at 23 and 75°C

Sodium nitrate and sulphite are not buffers and the introduction of CO_2 to distilled water containing these compounds induces a substantial drop in pH, although the final equilibrium pH remains above that of pure water saturated with carbon dioxide (see Figure 59). The drop in pH is more significant in sodium nitrate solutions than in sodium sulphite solutions; this possibly suggests that the solubility of carbon dioxide is greater in sodium nitrate solutions than in sodium sulphite solutions. However this effect is cancelled or at least mitigated in the presence of bicarbonates.

For all these test solutions, lower pH in solution can be achieved by increasing the partial pressure of CO_2, i.e. by increasing the system pressure above atmospheric pressure.

4.2. Electrochemistry results

4.2.1. Potentiodynamic curves: Is SCC possible?

A. CO_2-free systems

As discussed in section 2.5, the presence of a surface passive film is an essential condition for the materials to be susceptible to SCC.

In the pure bicarbonate-carbonate systems (CO_2-free), the alloys display a sharp active-passive transition at anodic potentials at both 23 and 75°C (Figure 60).

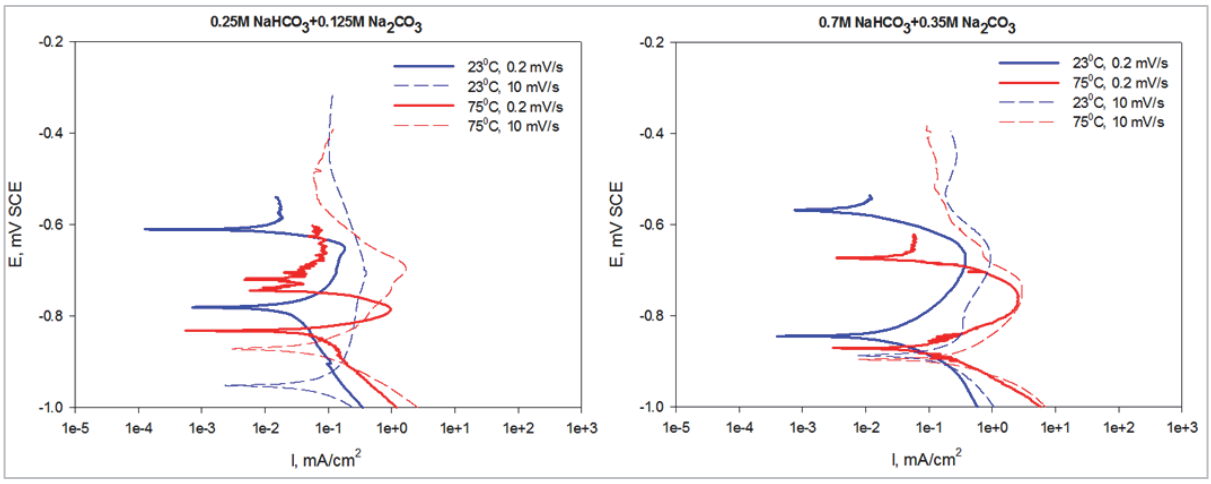

Figure 60: Potentiodynamic curves, X80 steel in $NaHCO_3$ / Na_2CO_3 (CO_2-free) at 23 and 75°C

In such environments, the material passivity is associated with the precipitation of iron carbonate $FeCO_3$.[130] Although iron carbonate formation is possible at 23°C, it is expected that its thickness and protectiveness will be less than at 75°C, which will affect the SCC susceptibility at low temperatures. Similarly, the electrochemistry measurements indicate that passivation is possible at lower carbonate / bicarbonate concentrations (0.25M $NaHCO_3$+0.125M Na_2CO_3) at 23 and 75°C. It is however expected that the supersaturation for iron carbonate precipitation will be less than at higher concentrations, which will eventually diminish the iron carbonate protectiveness and hence the susceptibility of the material to SCC.

A distinctive active-passive transition is still present when nitrates (Figure 61) or sulphites (Figure 62) are added to the various bicarbonate-carbonate systems at 23 and 75°C, suggesting that SCC is still possible in these environments.

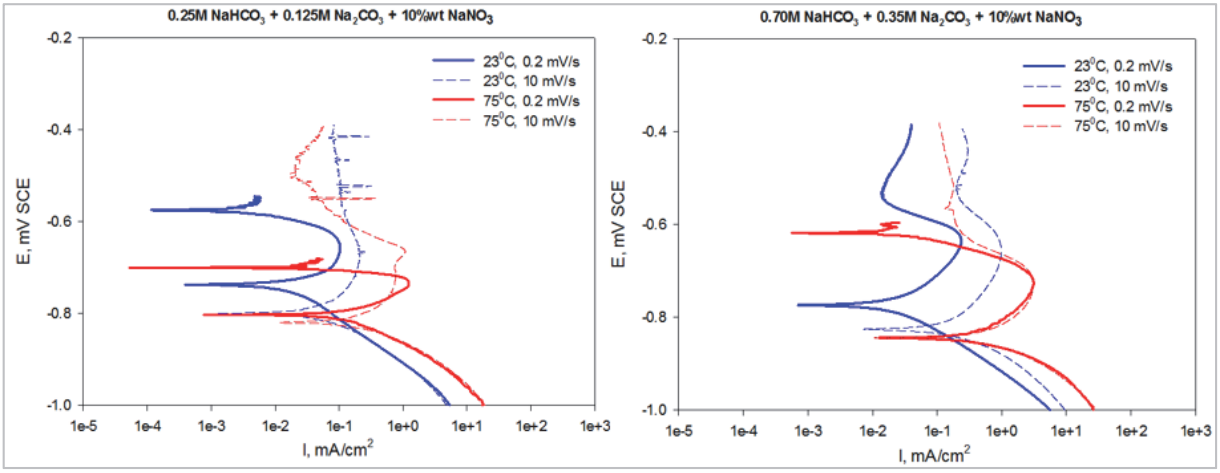

Figure 61: Potentiodynamic curves, X80 steel in $NaHCO_3$ / Na_2CO_3 / $NaNO_3$ (CO_2-free) at 23 and 75°C

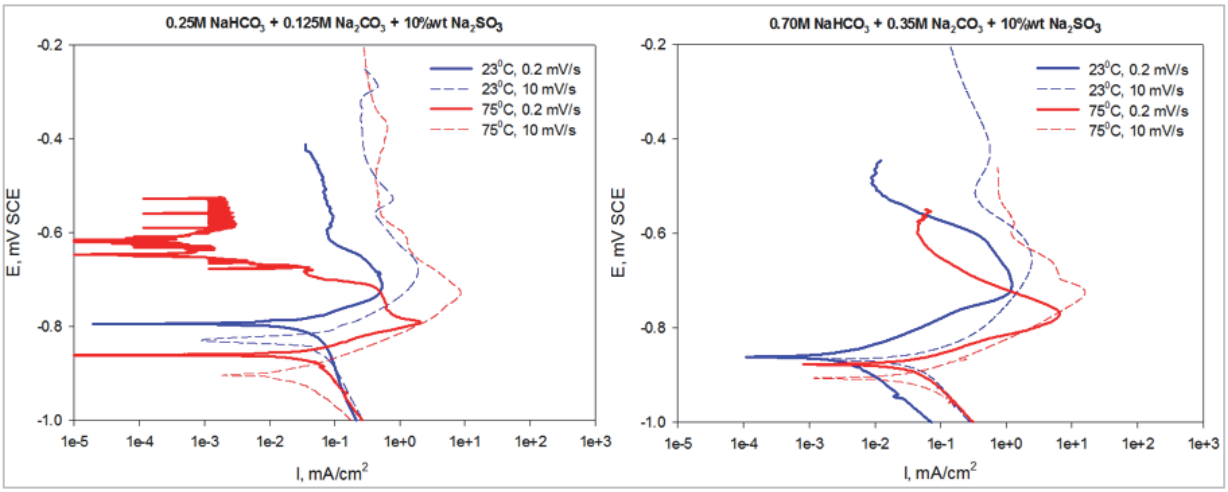

Figure 62: Potentiodynamic curves, X80 steel in $NaHCO_3$ / Na_2CO_3 / Na_2SO_3 (CO_2-free) at 23 and 75°C

Whether the additional presence of nitrate or sulphite interferes with the surface film protectiveness in a beneficial or a detrimental way will dictate the steel susceptibility to SCC.

The susceptibility of the pipeline steel to SCC in these environments have been mechanically tested and this is discussed in Chapter 5.

B. CO_2-saturated systems

With the presence of carbon dioxide (1 bar), the active-passive transition in the pure bicarbonate/carbonate system becomes less sharp at 23°C. The current densities remain significant once the pseudo- first oxidation peak is passed (10^{-1} to 10^{1} $mA.cm^{-2}$) indicating that the establishment of a protective film is compromised by the presence of CO_2 at 23°C (see Figure 63). In many cases, the passivity of steels is favoured at higher pH, i.e. in alkaline conditions. Acidic conditions tend indeed to dissolve films and scales. As discussed previously, the

addition of carbon dioxide promotes the formation of carbonic acid which results in a pH drop, and this will ultimately hinder the formation of protective layers and thus the SCC susceptibility.

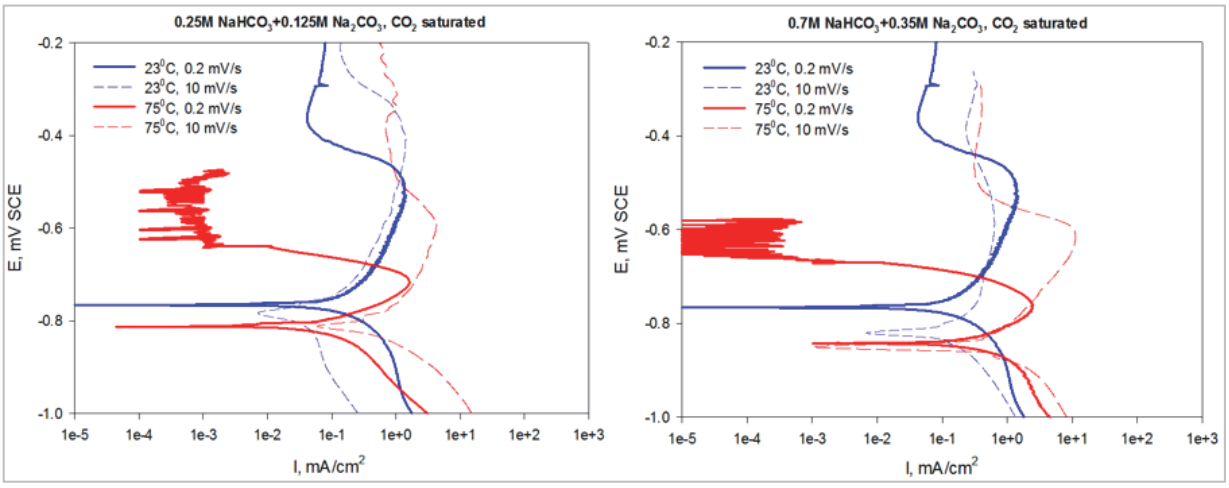

Figure 63: Potentiodynamic curves, X80 steel in $NaHCO_3$ / Na_2CO_3 (CO_2-saturated, 1 bar) at 23 and 75°C

The formation of iron carbonate films is typically driven by pH, temperature, and by concentrations of carbonate and iron species. These films easily form at high pH and high temperatures. If it is assumed that the films in the different test environments are predominantly iron carbonate based, then the combination of low temperature and more acidic pH explains the high activity (dissolution) of the materials at increased anodic potentials in the pure bicarbonate/carbonate system at 23°C.

In contrast, a sharp active-passive transition can still be observed at 75°C in the presence of CO_2, especially in bicarbonate / carbonate environments (see Figure 63). Two reasons can be postulated to explain the presence of protective film at 75°C rather than at 23°C:

- The precipitation of iron carbonate is more likely at elevated temperatures
- The solubility of the carbon dioxide is less at 75°C than at 23°C (at constant pressure). This means that the acidification of the solution at 75°C is less than at 23°C, which augments the chances of passivation.

When nitrates are added to the CO_2 saturated-bicarbonate / carbonate system, the material still manifests a sharp active-passive transition at 75°C (see Figure 64). The active-passive transition appears to be significant at the higher and lower concentrations of $NaHCO_3/Na_2CO_3$, which suggests the possibility of producing SCC in both systems (i.e. 0.7M $NaHCO_3$+0.35M Na_2CO_3+10%wt

$NaNO_3$ and 0.25M $NaHCO_3$+0.125M Na_2CO_3+10%wt $NaNO_3$) in the presence of CO_2. At 23°C, passivation becomes more difficult, especially at low levels of bicarbonates / carbonates for which the materials mainly suffer from anodic dissolution.

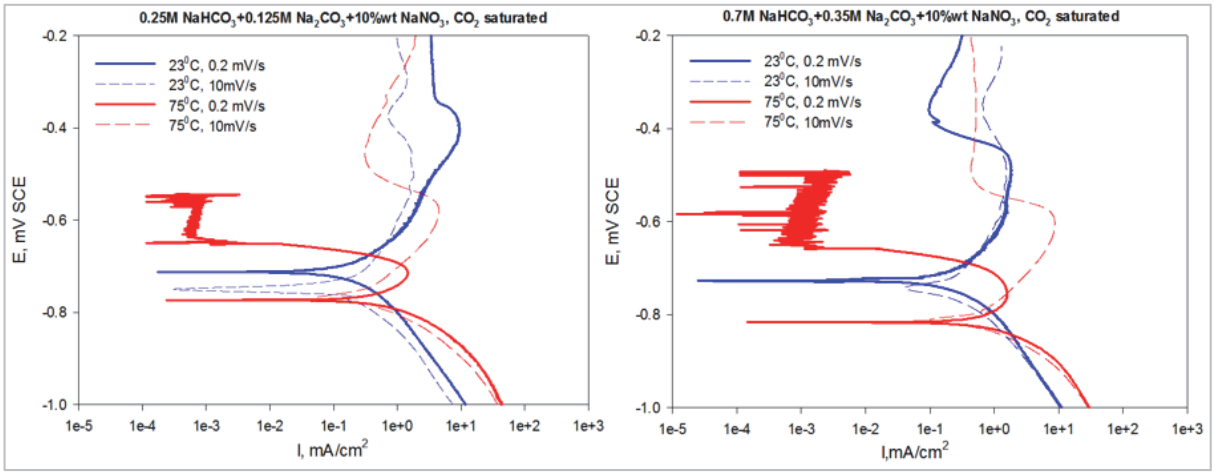

Figure 64: Potentiodynamic curves, X80 steel in $NaHCO_3$ / Na_2CO_3 / $NaNO_3$ (CO_2-saturated, 1 bar) at 23 and 75°C

In the presence of sulphites (Figure 65), an active-passive transition is also present in the CO_2 saturated- bicarbonate/carbonate system at 75°C. However, the transition is not as sharp, especially at the lower concentrations of bicarbonate/carbonate, which suggests that the passivation of the material is to some extent compromised. In addition to the increased acidity of the solution with the presence of CO_2, the oxygen-scavenging property of the sulphite could hinder further the establishment of passive oxide films on the steel surface.

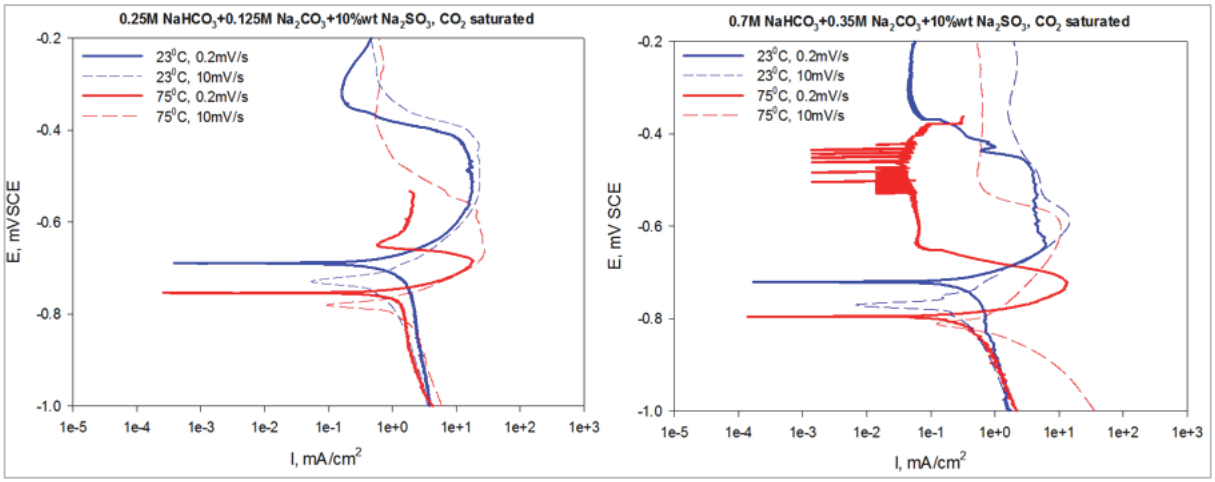

Figure 65: Potentiodynamic curves, X80 steel in $NaHCO_3$ / Na_2CO_3 / Na_2SO_3 (CO_2-saturated, 1 bar) at 23 and 75°C

4.2.2. *Free corrosion potential, E_{Corr}*

The difference between the free corrosion potential as obtained from static measurement (i.e. OCP) and dynamic measurements (at a sweep rate of 0.2 $mV.s^{-1}$) is illustrated in Figure 66. As discussed in section 3.3.3, the equilibrium is never reached during potentiodynamic measurements, and a deviation exists between the "true" value of E_{corr} as generated by OCP measurements (i.e. for a system in complete equilibrium), and that obtained by dynamic measurements.

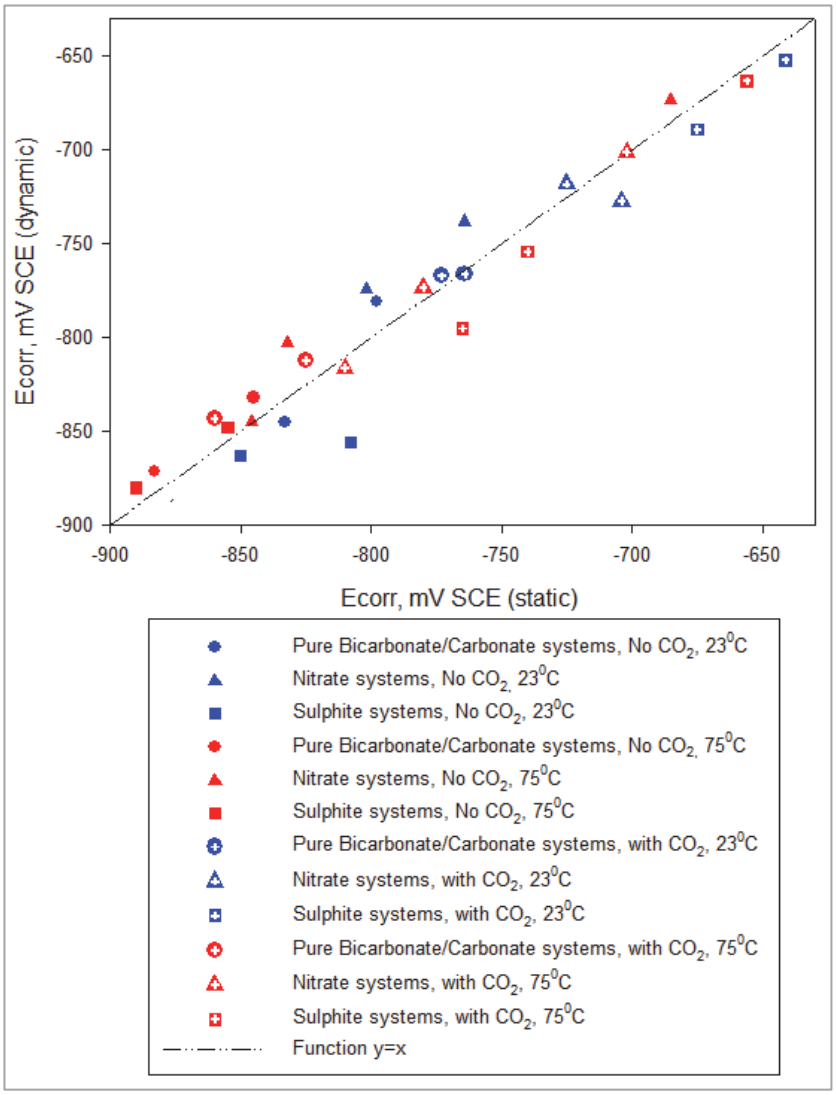

Figure 66: Free corrosion potential: dynamic vs. static measurements for various test environments

The deviation between the E_{corr} value generated by static and dynamic measurements grows as the sweep rate increases. At low sweep rates, the system is at quasi- or near- equilibrium. For the rest of Chapter 4, the E_{corr} as reported from dynamic measurements at slow sweep rates (i.e. 0.2 $m.s^{-1}$) will be used arbitrarily to discuss the effect of environmental parameters.

The free corrosion potentials for various test environments are listed in Table 14.

Table 14: Free corrosion potentials for various test environments

	Temperature °C	E_{corr} (CO_2-free)	E_{corr} (CO_2-saturated, 1 bar)
0.25M $NaHCO_3$+0.125M Na_2CO_3	23	-781	-767
	75	-832	-812
0.25M $NaHCO_3$+0.125M Na_2CO3+10%wt $NaNO_3$	23	-738	-718
	75	-803	-773
0.25M $NaHCO_3$+0.125M Na_2CO_3+10%wt Na_2SO_3	23	-795	-689
	75	-861	-754
0.7M $NaHCO_3$+0.35M Na_2CO_3	23	-845	-766
	75	-871	-843
0.7M $NaHCO_3$+0.35M Na_2CO_3+10%wt $NaNO_3$	23	-774	-727
	75	-845	-816
0.7M $NaHCO_3$+0.35M Na_2CO_3+10%wt Na_2SO_3	23	-863	-720
	75	-878	-795

A. Effect of temperature

As the temperature increases the likelihood of protective surface films forming will also increase, especially in the pure bicarbonate/carbonate and nitrate-containing systems, where protective iron carbonate and iron oxide films could be produced on steel. As the surface becomes passive (and less active), a shift of the free corrosion potential to more positive values would also be expected.

However, as illustrated in Figure 67, the free corrosion potential has been found to decrease as the temperature increases. This trend has been identified for all the test systems i.e. pure bicarbonate/carbonate, nitrate- and sulphite- containing systems. This suggests that another process is responsible for the drop of E_{corr} with the rising temperature.

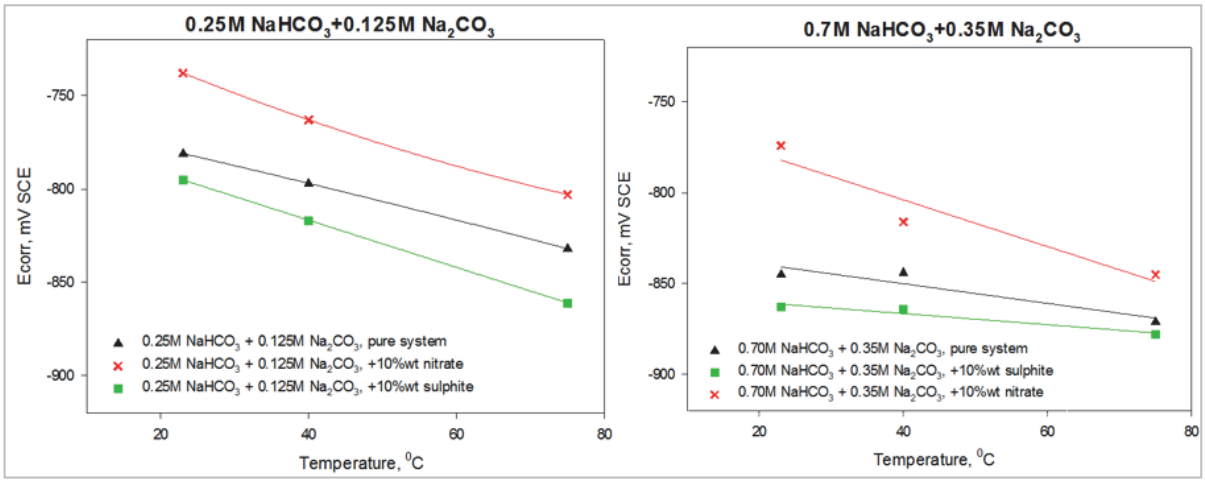

Figure 67: Effect of temperature on E_{corr}, CO_2-free environments

It is considered that the shift of the free corrosion potential to more cathodic potentials with the rise in temperature, as illustrated in Figure 67, is related to the decreasing concentration of oxygen in the aqueous solution with the temperature: The solubility of oxygen in aqueous solution is a function of the solution chemistry, e.g. composition and pH, but also of temperature and system pressure. At constant pressure, the content of oxygen in solution will decrease with increase in temperature.

The increase in oxygen content in aqueous solution has been widely discussed as promoting a rise in the free corrosion potential E_{corr} for steel materials.[49] The increase in E_{corr} of carbon steel as a function of dissolved oxygen, as reported by Indig et al. is illustrated in Figure 68.[131,132]

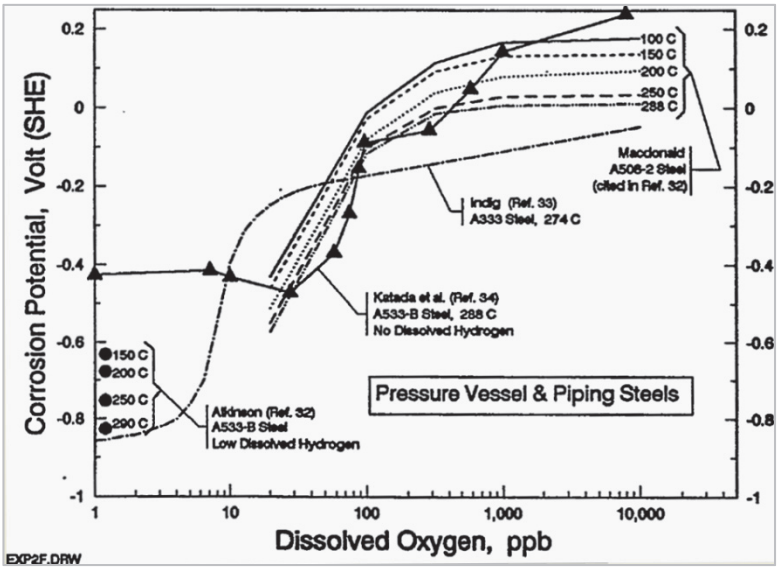

Figure 68: Free corrosion potential of different low alloy and carbon steel materials versus dissolved oxygen concentration[113]

This trend is associated with the high electroactivity of the redox couple O_2/H_2O ($E^0{}_{O_2/H_2O} = +1.23\,V$), which means that oxygen is a strong oxidant or in other words a very powerful acceptor of electrons in comparison with other oxidants such as H_3O^+cations ($E^0{}_{H_3O^+/H_2} = +0.00\,V$).

The redox potential for the couple O_2/H_2O, E_{O_2/H_2O}, is given by the Nernst equation:

$$O_2 + 4H_3O^+ + 4e- \rightarrow 6H_2O\,,\; E_{O_2/H_2O} = E^0{}_{O_2/H_2O} + R \cdot T \cdot \ln\left(a_{O_2(aq)} \cdot a^4{}_{H_3O^+(aq)}\right)$$

If the activity $a_{O_2(aq)}$ is represented for simplification by the oxygen concentration in solution [O_2 (aq)], then it could be visualised that by increasing the oxygen content the redox potential is also increased.

During a redox or corrosion reaction between oxygen (oxidant) and iron (reductor), ($E^0{}_{Fe^{2+}/Fe} = -0.41V$), the iron will take a mixed potential or free corrosion potential E_{corr} at which the system is in equilibrium, i.e. the anodic and cathodic current are equal. E_{corr} will be located between the Nernst potential of the O_2/H_2O and Fe^{2+}/Fe couples, E_{O_2/H_2O} and $E_{Fe^{2+}/Fe}$. If the E_{O_2/H_2O} is increased as a result of oxygen concentration, it is then likely that E_{corr} will follow the same direction.

B. Effect of bicarbonates / carbonates

As the bicarbonate/carbonate levels are increased, the environmental conditions would be expected to become more favourable for protective iron carbonate to precipitate on the steel surface, especially at 75°C. As the surface of the steel becomes passive, a shift of the free corrosion potential to more anodic values should be anticipated. This would suggest that E_{corr} should increase as the bicarbonate/carbonate levels are increased.

However, as indicated by Figure 69, the free corrosion potential decreases with increasing concentration of bicarbonates.

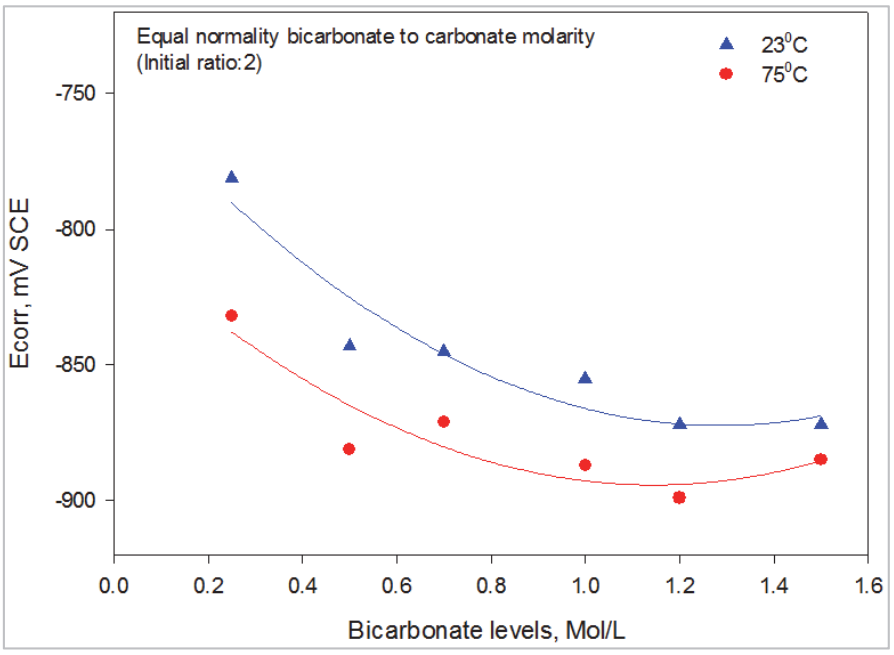

Figure 69: Effect of bicarbonate / carbonate concentrations on E_{corr}, CO_2-free environments

The drop of E_{corr} with the increasing level of bicarbonate/carbonate could be eventually explained by:

- Despite the fact that higher levels of bicarbonates should promote passivation, it has also been reported[133] that increased concentrations enhance iron anodic dissolution in the steel active domain i.e. under film free- surface conditions. The levels of anodic currents in the material active domain have also been identified to increase with the bicarbonate concentrations within this thesis (see section 4.2.4-B). It is therefore likely that until surface passivation is achieved, higher levels of anodic dissolution could occur in solutions with higher concentrations of bicarbonates, which would explain the decrease in E_{corr}.
- The solubility of oxygen is a function of the nature and concentration of salts dissolved in the solution. The presence of salts or other chemicals in solution will affect the solubility of oxygen; this is illustrated in Figure 70 in the case of sodium chloride NaCl.[134] It is considered that similarly to the effect of temperature, the shift of the free corrosion potential to lower values with increasing bicarbonate/carbonate concentrations is influenced to some extent by the solubility of oxygen in solution decreasing as the system becomes more concentrated in salts.

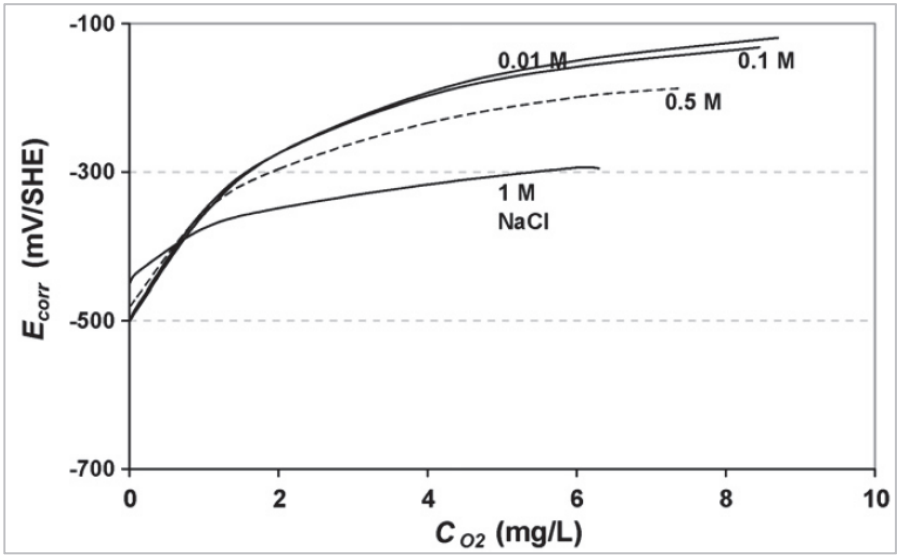

Figure 70: Free corrosion potential of carbon steel versus dissolved oxygen concentration at different NaCl levels[134]

C. Effect of nitrates

The addition of nitrates to bicarbonate / carbonate systems increases the free corrosion potential in comparison with pure bicarbonate / carbonate systems as illustrated in Figure 71 and Figure 72. At low temperatures (23°C), as the system reaches saturation at high nitrate concentrations (+20%wt $NaNO_3$), E_{corr} tends to a limit.

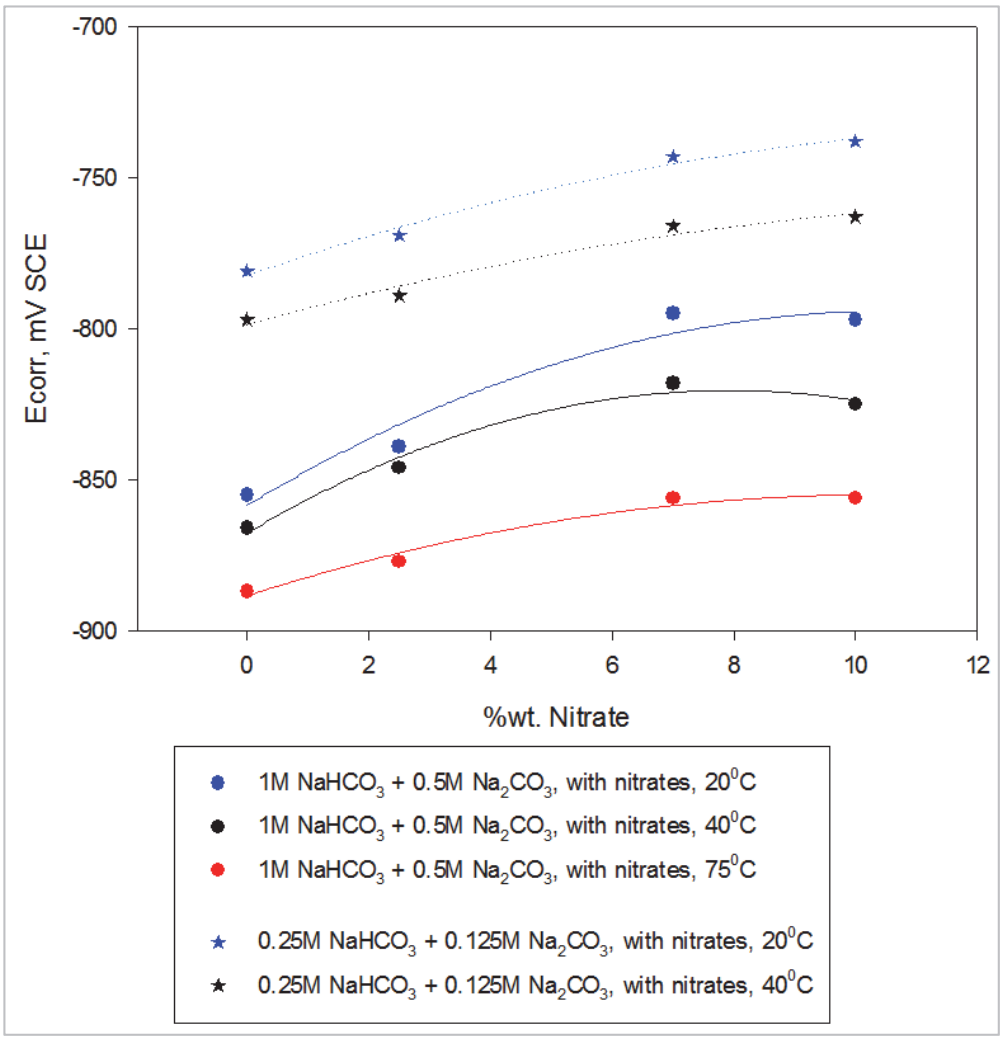

Figure 71: Effect of nitrates on E_{corr} in bicarbonate/ carbonate systems, CO_2-free environments

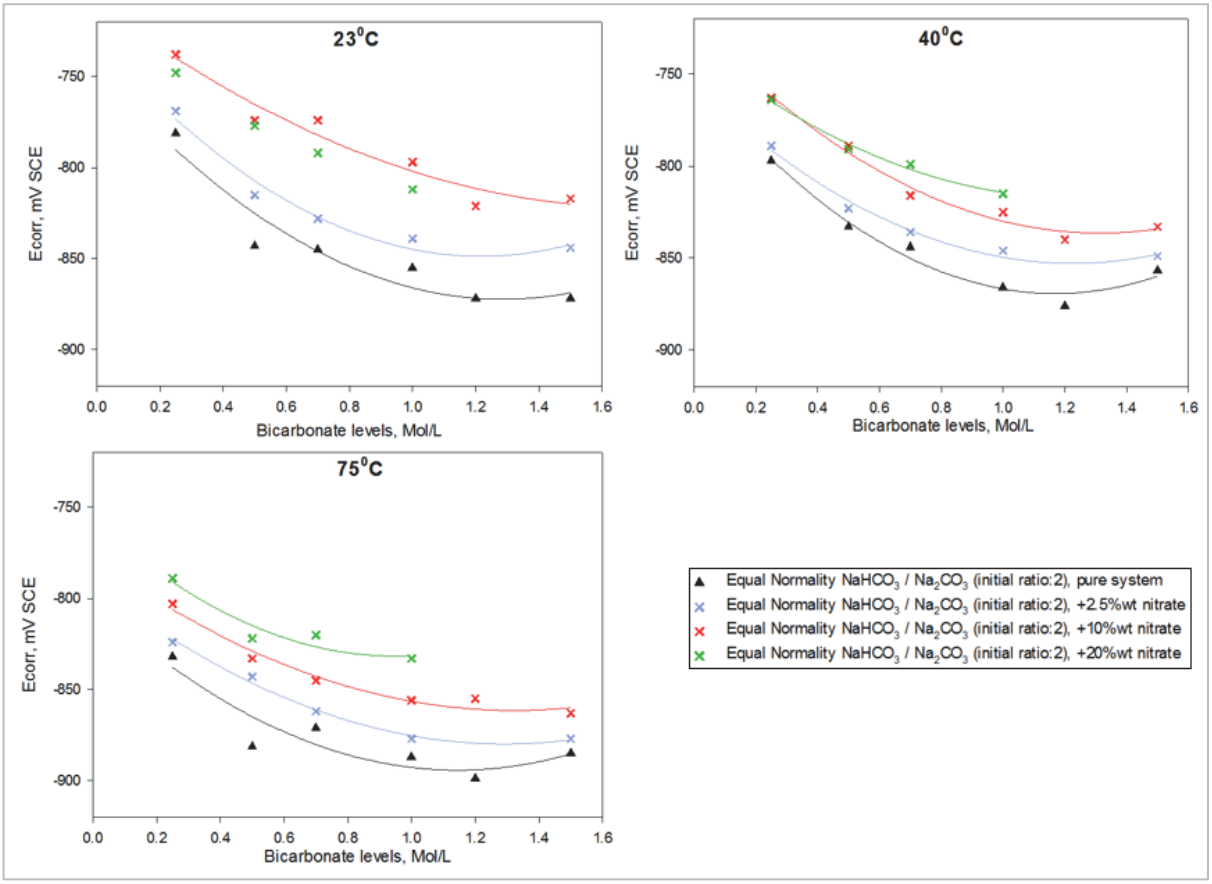

Figure 72: Effect of nitrates on E_{corr} in bicarbonate/ carbonate systems at various temperatures, CO_2-free environments

Mohammed[91] also reported the increase in E_{corr} with the concentration of nitrates in ammonium nitrate systems at 95°C. As discussed in previous sections, E_{corr} is a measure of the tendency of the alloy to be active; a lower free corrosion potential suggests that the materials is more susceptible to corrosion. Equally, higher E_{corr} suggests the materials become nobler and have a lesser tendency to anodic dissolution. The nobility of the materials could be favoured if conditions for surface passivation are present. Mohammed identified[91] that in more concentrated nitrate solutions the passivation of steels starts at lower anodic potentials and the domain of passivity is wider. This suggests that the tendency to form a passive film in nitrate solutions is increased with the nitrate concentration. The susceptibility to SCC in nitrate solutions has been associated with the formation of hematite and magnetite.[135,136] In which ways iron oxides and iron carbonate interact in bicarbonate / carbonate / nitrate systems is beyond the scope of this thesis; however it is plausible that the presence of nitrates augments the protectiveness of films formed on steel materials in bicarbonate / carbonate systems, especially at higher temperatures.

It is noted that nitrates are strong oxidants (e.g. E° NO_3^-/HNO_2= +0.94 V, E° NO_3^-/NH_4^+= +0.88 V) and, similarly to oxygen, could result in an increase in the mixed potential E_{corr}. This effect is probably dominant under conditions for which the metal is free from protective film.

D. Effect of sulphur compounds

The addition of sulphite compounds to bicarbonate / carbonate systems appears to move the free corrosion potential to more cathodic values in relation to pure bicarbonate / carbonate systems, as illustrated in Figure 73. In comparison, sulphates do not significantly influence E_{corr} relatively to pure bicarbonate / carbonate systems.

The shift of E_{corr} towards more negative potentials could be explained by:

1. The role of sulphur compounds in destabilising passive films, such as iron carbonate, has been discussed in section 2.7.2. In the first instance the decrease of E_{corr} when sulphites are added to bicarbonate / carbonate systems could be related to the system being more active. This is consistent with the measurement of the current density at the first oxidation peak under conditions (e.g. accelerated potential sweep rate) for which surface passivity is limited and anodic dissolution is favoured. This will be discussed further in section 4.2.4-C.

2. Sulphites also react with oxygen to form sulphates, and thus sulphite compounds have been widely used in industry as oxygen scavengers. The role of oxygen concentration on E_{corr} has been discussed in previous sections. It is plausible that the shift of E_{corr} to more negative potentials, when sulphites are added, is also related to oxygen scavenging. At higher bicarbonate/carbonate concentrations and at 75°C, the free corrosion potential in the presence of sulphite tends to that of the pure bicarbonate / carbonate system; at such temperatures and bicarbonate/ carbonate concentrations, the levels of oxygen in the pure bicarbonate / carbonate system are low, and the effect of sulphite on the oxygen present in solution is minimal.

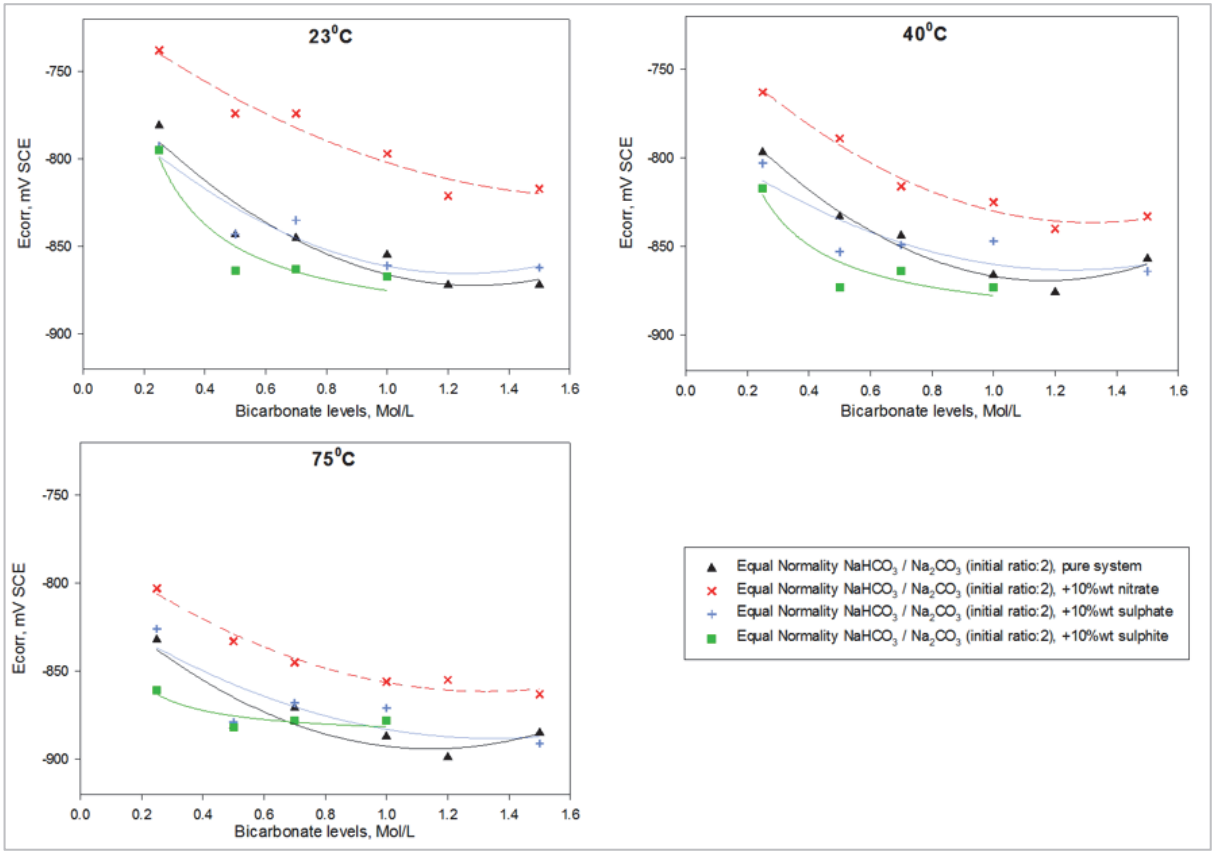

Figure 73: Effect of sulphur compounds on E_{corr} in bicarbonate/ carbonate systems at various temperatures, CO_2-free environments

E. Effect of carbon dioxide

Figure 74 and Figure 75 show that the addition of carbon dioxide in the different test bicarbonate / carbonate environments, independently of the presence of nitrates or sulphites, increases E_{corr} at 23 and 75°C:

- This shift is more important at 23°C (Figure 75), as the solubility of CO_2 in solution is higher than at 75°C.
- The most significant shift is also observed in the presence of sulphites. This is eventually related to the increased solubility of CO_2 in such systems, since the levels of oxygen present in these environments would have been low due to the scavenging action of the sulphites.

In the first instance, the trend of the E_{corr} shifting towards nobility would suggest surface passivation, e.g. due to iron carbonate precipitation. However, this statement will be in contradiction with the increasing trend observed for the anodic currents when CO_2 is added (see section 4.2.4-D). The increase in anodic currents with the presence of carbon dioxide suggests that the steel surface is

more active and more susceptible to anodic dissolution. The addition of carbon dioxide has two major effects:

- Destabilisation of protective film formation (e.g. iron carbonate) due to acidification of the solution associated with the presence of CO_2.
- Increase in the cathodic reduction rate (and therefore of the anodic dissolution process). The formation of carbonic acid in solution (due to the hydrolysis of CO_2) serves as an additional source of hydroniums H_3O^+, and at high pH can also be involved in an indirect reduction process through the formation of bicarbonates:

$$2H_3O^+ + 2e- \leftrightarrow 2H_2 + H_2O$$
$$2HCO_3^- + 2e- \leftrightarrow 2CO_3^{2-} + H_2$$

It has been suggested[137,138] that the direct reduction of bicarbonates into carbonates is particularly favoured at pH>5, since the concentrations of bicarbonates increase with pH and can become predominant over carbonic acid levels.

The shift of E_{corr} to more noble values is therefore considered to be related to an increase in the cathodic reduction processes which leads to some type of surface depolarisation.

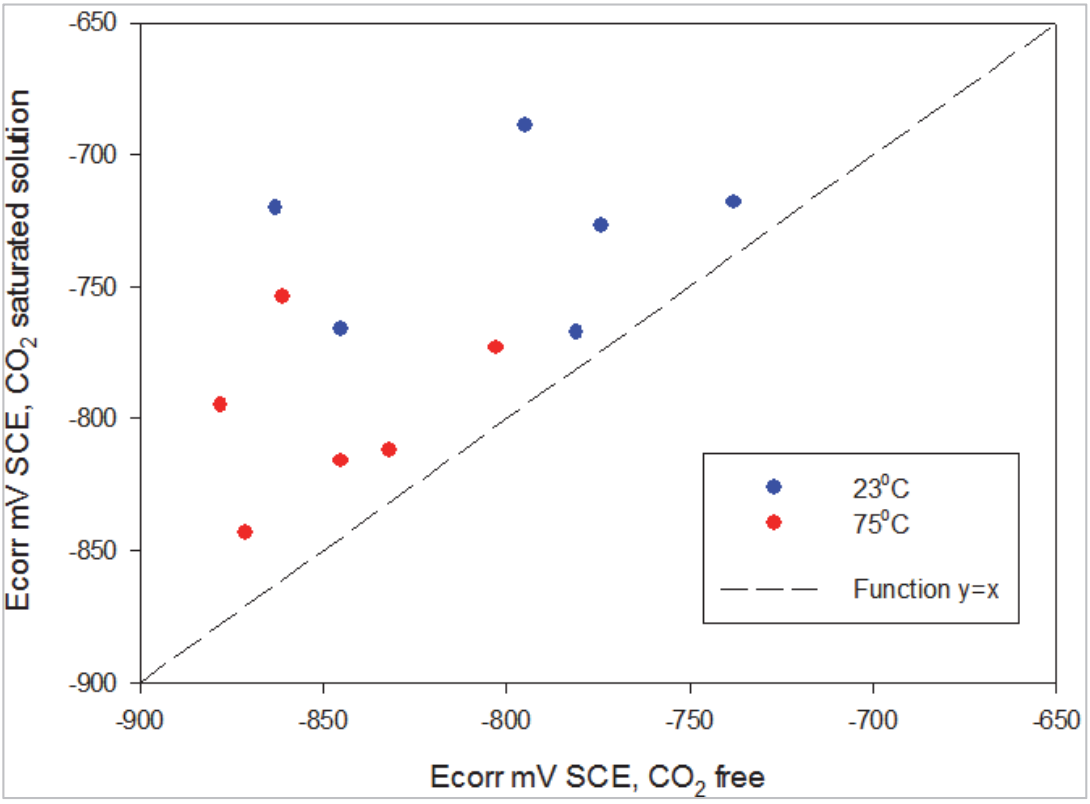

Figure 74: Free Corrosion potential of CO_2-saturated vs CO_2-free test environments

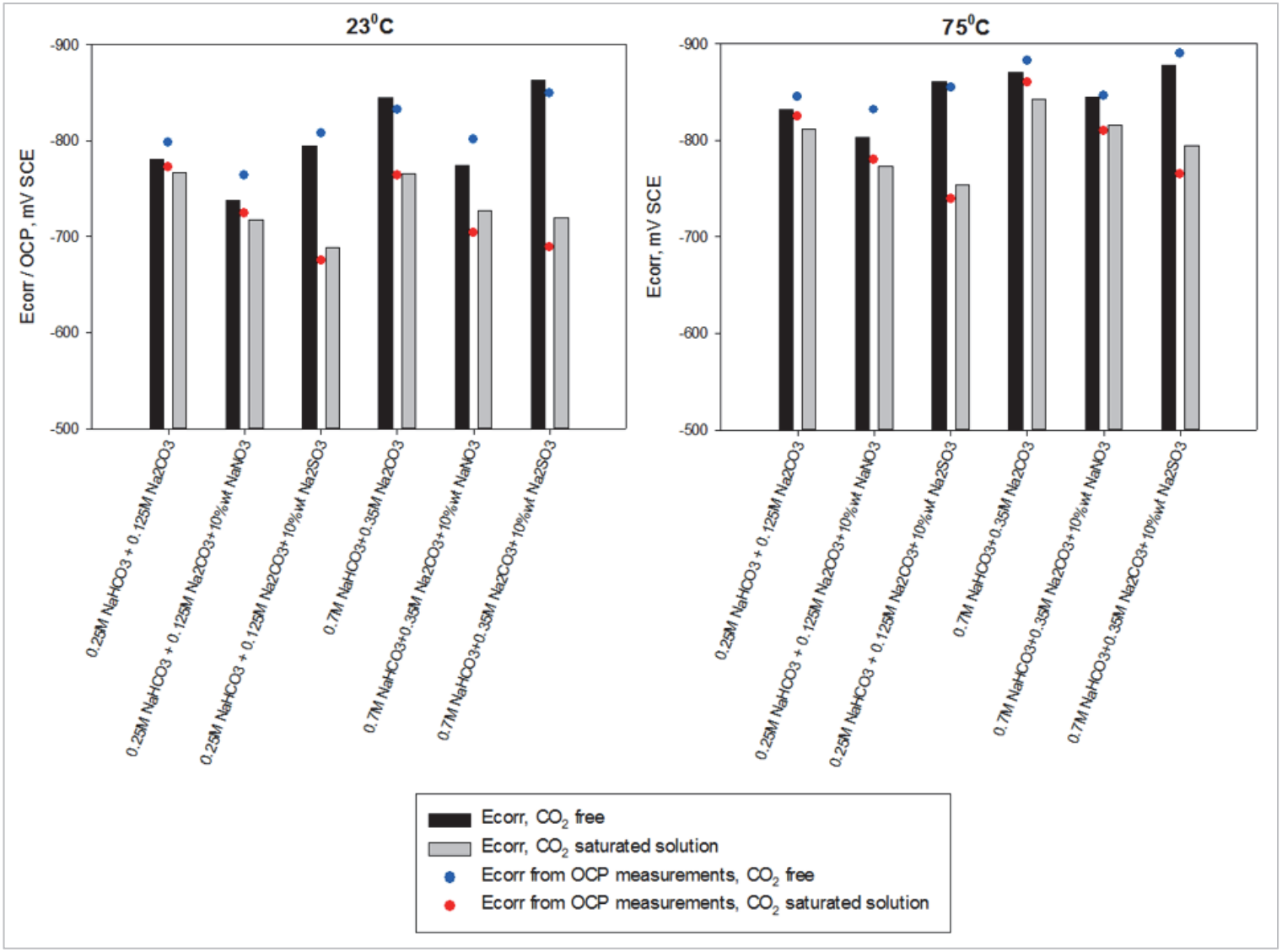

Figure 75: Effect of carbon dioxide on E_{corr} in bicarbonate/ carbonate systems and in the presence of nitrates and sulphites at various temperatures, CO_2-free environments

4.2.3. *First oxidation peak potential, E_p*

A. Effect of bicarbonate levels

In contrast to E_{corr}, E_p increases with the concentrations of bicarbonate / carbonates (Figure 76). This trend was also reported by Parkins[117,118]. Parkins discussed the fact that the peak potential shifts to more anodic values due to a decrease in pH as the levels of bicarbonates are increased.[117] The combination of bicarbonate levels and pH have a strong influence on the peak potential.

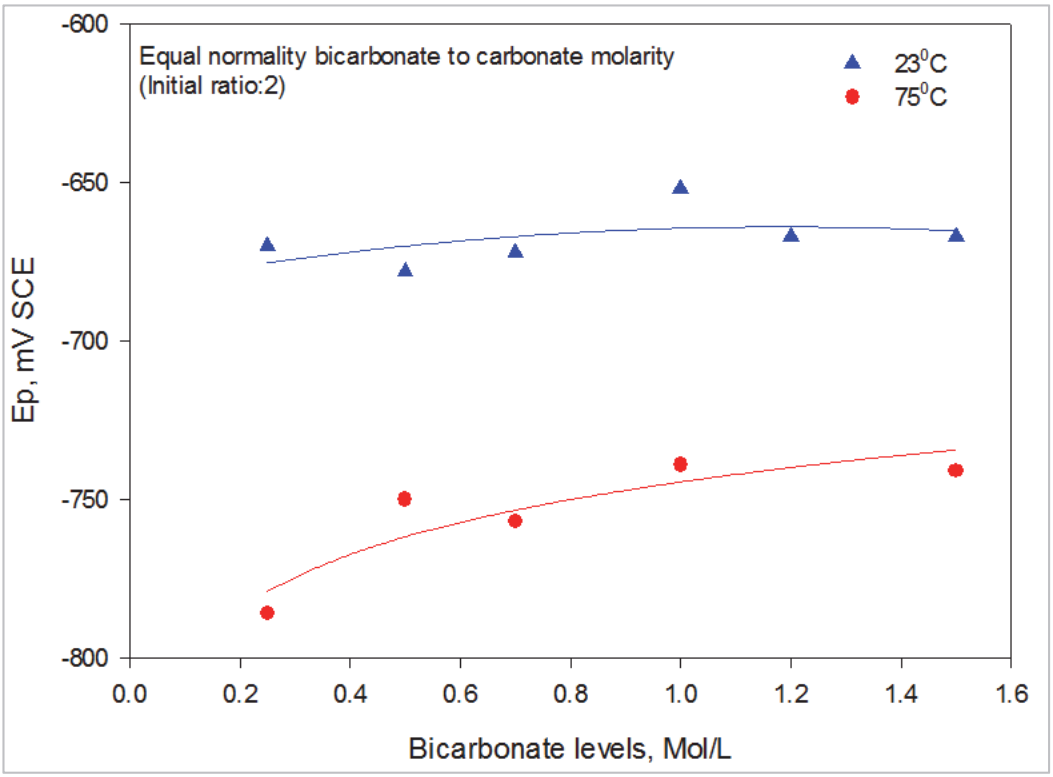

Figure 76: Effect of bicarbonate / carbonate concentrations on E_p, CO_2-free environments

B. Effect of temperature and impurities

The following trends previously discussed for E_{corr} also apply to E_p:

- E_p decreases with the temperature (Figure 77)
- In the presence of nitrates, E_p shifts towards more anodic potentials in relation to pure bicarbonate/carbonate systems (Figure 78)
- In the presence of sulphites, E_p shifts towards more cathodic potentials in relation to pure bicarbonate/carbonate systems (Figure 78)

It is plausible that the behaviour of E_p in regards to the temperature and the presence of nitrates and sulphites is strongly influenced by the shift in E_{corr} as a function of these parameters (see section 4.2.2).

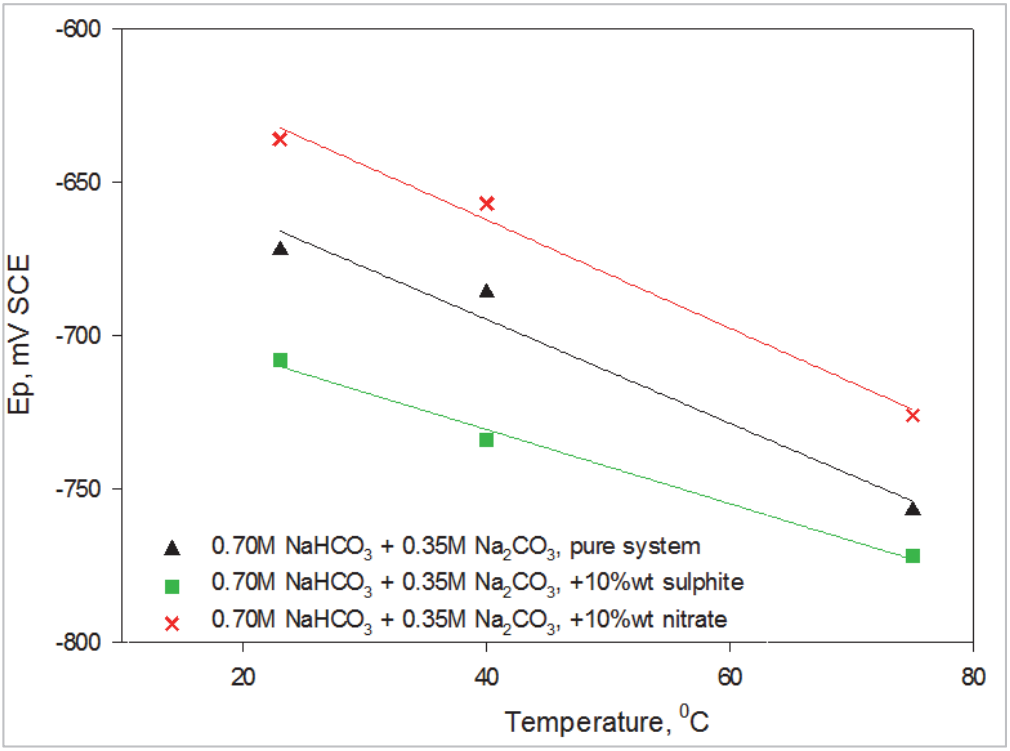

Figure 77: Effect of temperature on E_p, CO_2-free environments

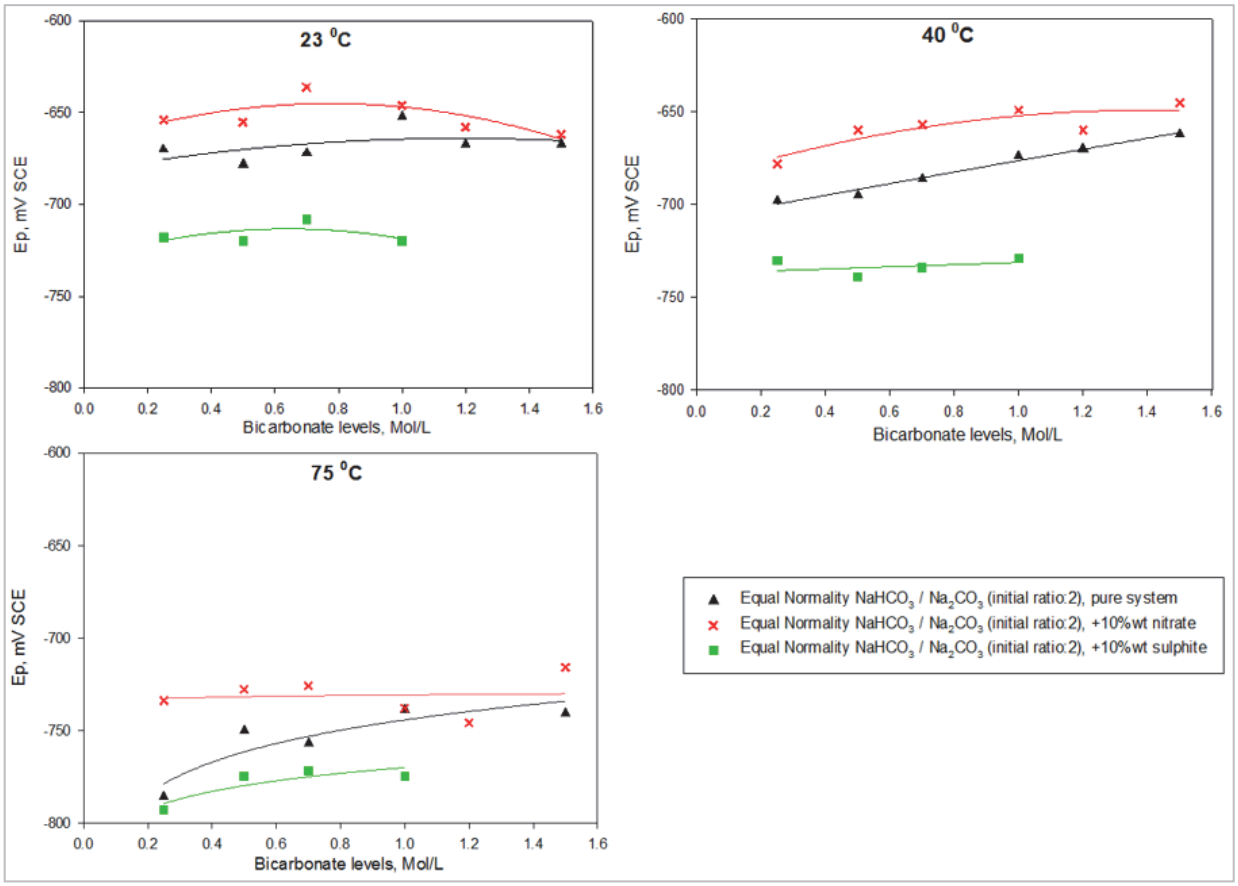

Figure 78: Effect of nitrates and sulphites on E_p in bicarbonate/ carbonate systems at various temperatures, CO_2-free environments

C. Effect of carbon dioxide

As for E_{corr}, the addition of carbon dioxide to the different test environments increases E_p (Figure 84). The effect is more marked at 23°C than at 75°C, due to the higher solubility of CO_2 in solution at 23°C than at 75°C (at constant pressure). It is plausible that the behaviour of E_p in regards to carbon dioxide addition is strongly influenced by the anodic shift in E_{corr} as discussed in section 4.2.2-E.

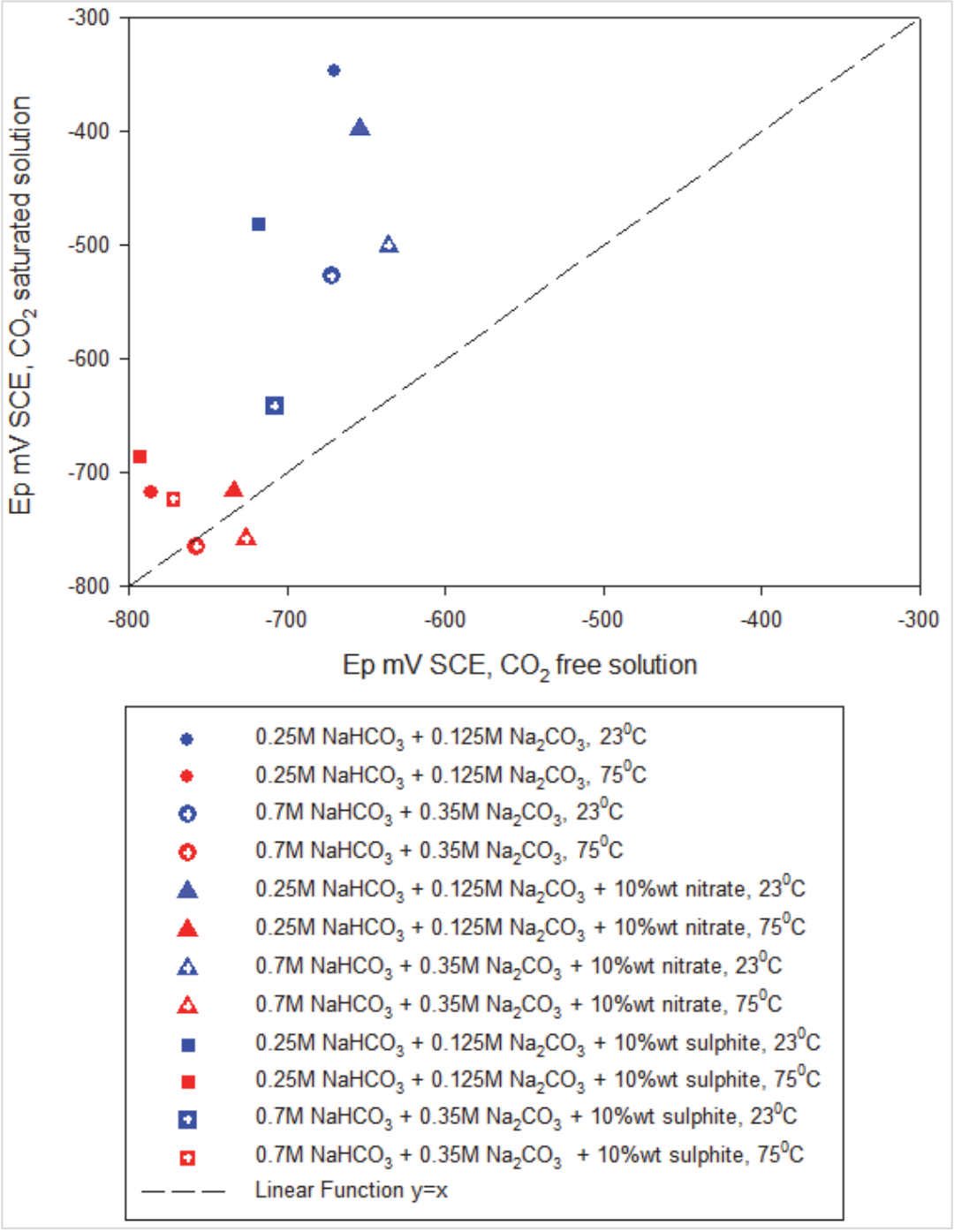

Figure 79: First oxidation peak potential of CO_2-saturated vs CO_2-free test environments

D. Peak potential vs. Stress Corrosion Cracking Potential

The first oxidation peak potential E_p is the potential at which the surface of the material enters a transitional region from being fully active (anodic dissolution) to becoming passive. As discussed in previous chapters, material passivity is an important criteria for a materials to be susceptible to SCC. Zhou and Parkins[118] have reported that the most critical potential for SCC of low alloy steels (i.e. where deepest cracking was identified), E_{SCC}, follows a positive linear relationship with E_p: $E_p = E_{SCC} + b$. This relationship is illustrated in Figure 80. Experimental data generated within this work for different test environments are shown alongside Zhou and Parkins data[118] obtained in pure $NaHCO_3$ / Na_2CO_3 systems. The linear relationship of E_{SCC} vs. E_p generally provides a fairly accurate prediction of E_{SCC} with a deviation within 0.05 V (generally less than 0.02 V).

Figure 80 also shows that the deepest cracking (see Chapter 4) was always produced at potentials more anodic than the first oxidation peak potential.

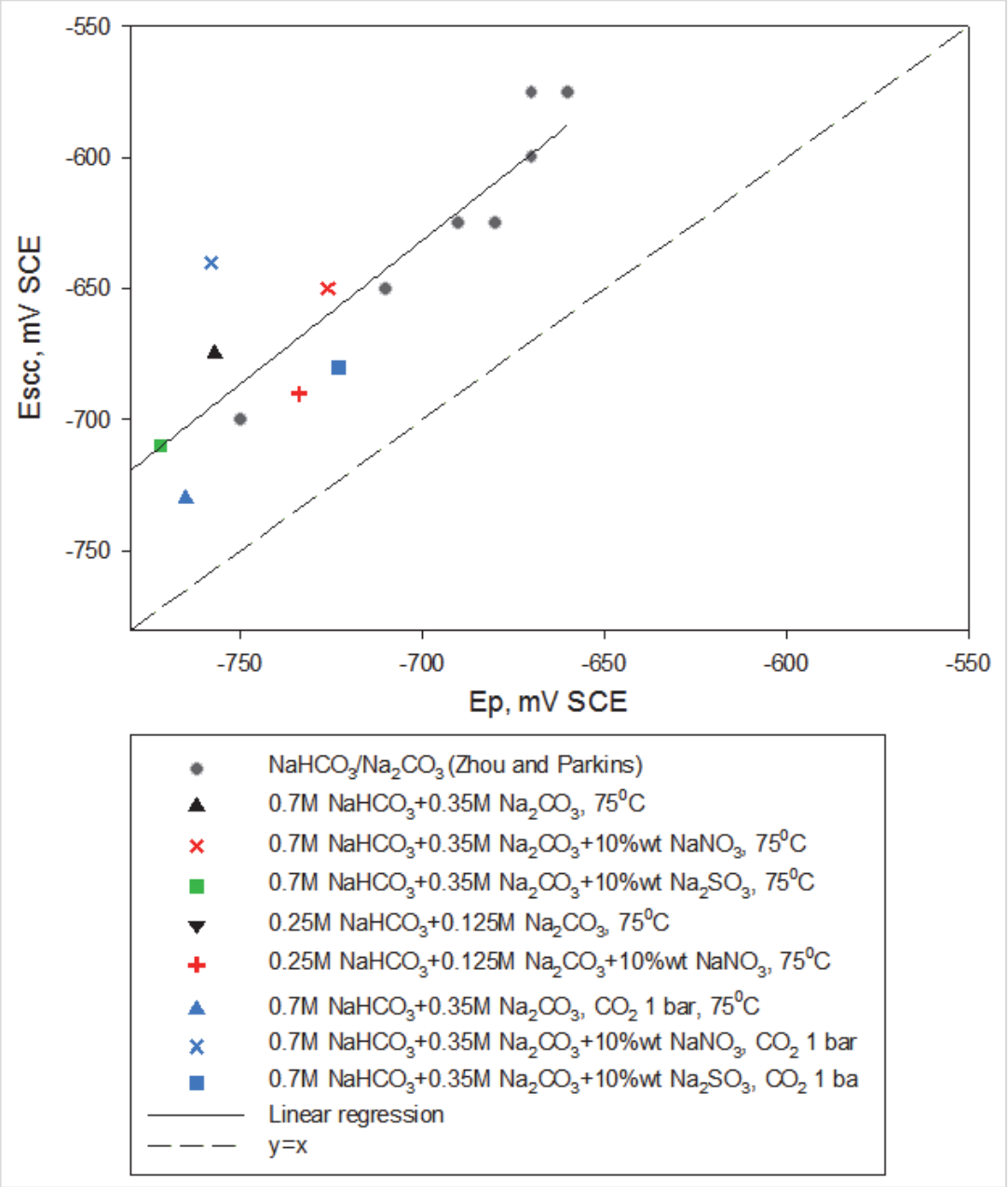

Figure 80: First oxidation peak potential vs. Critical Potential for SCC

4.2.4. First oxidation peak current density, I_p

At fast potential sweep rates (10mV/s), a fully protective film cannot be established on the material surface. The material virtually remains in a pseudo-active state, in which anodic dissolution dominates passive film formation. I_p is the current density at the first oxidation peak potential for a polarisation curve produced at fast sweep rates.

A. Effect of temperature

I_p increases with temperature as illustrated in Figure 81. By definition, the current density of an anodic oxidation or a cathodic reduction is the direct translation of the reaction rate, V. Re is given for an oxidation reaction $Red \leftrightarrow Ox + n.e -$ by:

$$V = k(T).[Red]^m$$

Where,

$k(T)$ *is the constant of reaction rate and is a function of temperature*

$[Red]$ *is the concentration of the reducing species*

m *is the order of reaction*

The dependence of k on temperature is given by the Arrhenius relationship:

$$k(T) = A.e^{-\frac{E_A}{R.T}}$$

With,

A *is a constant*

R *is the gas constant*

E_A *is the energy of activation*

T *is the temperature*

Then, it may be seen that the rate of the reaction and thus the equivalent reaction current density is increased with increase in temperature.

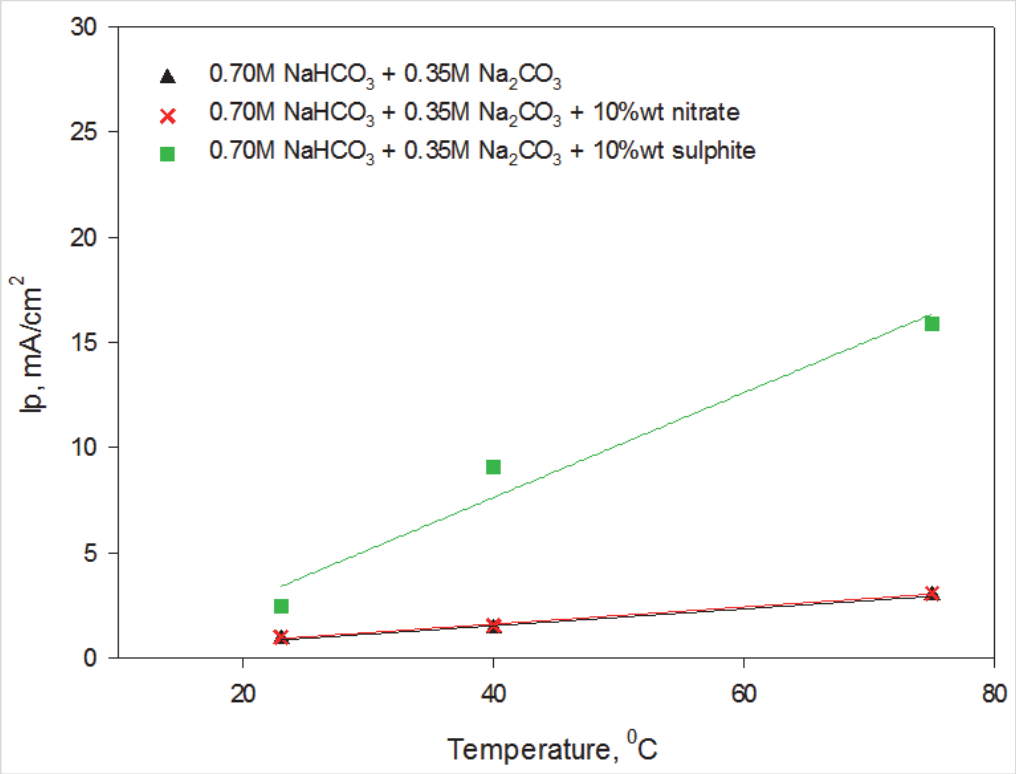

Figure 81: Effect of temperature on I_p, CO_2-free environments

B. Effect of bicarbonates / carbonates

I_p increases with the bicarbonate levels as illustrated in Figure 82.

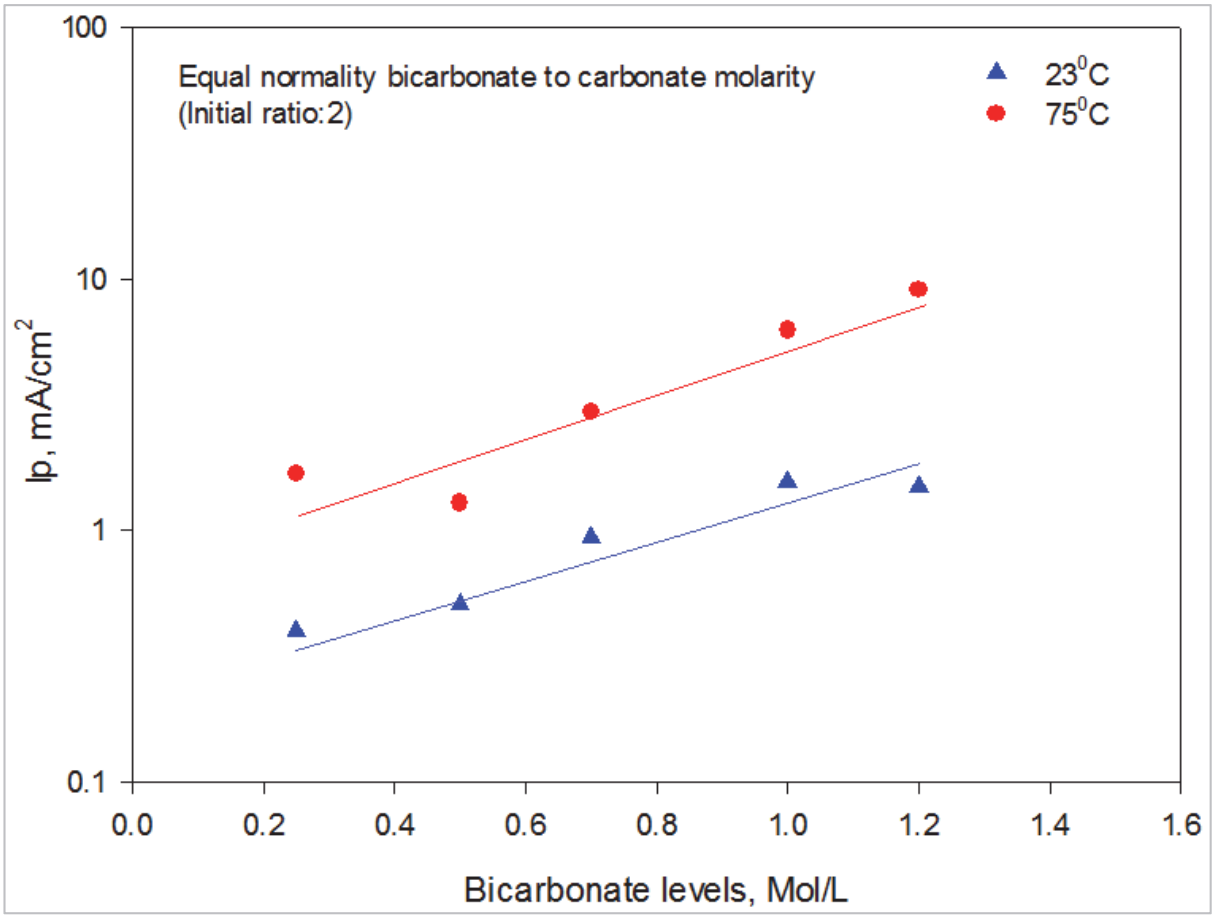

Figure 82: Effect of bicarbonate / carbonate concentrations on I_p, CO_2-free environments

The anodic behaviour of iron in its active domain in bicarbonate and carbonate aqueous systems has been discussed elsewhere. Armstrong and Coates[130] suggested that bicarbonates or carbonate species could behave as catalysts in the dissolution process of iron. Davies and Burstein[133] showed that the anodic current densities increase linearly with the bicarbonate levels. They proposed the following chemical reaction scheme to explain the anodic dissolution of iron within the active region in bicarbonate systems:

$$Fe + 2H_2O \rightarrow Fe(OH)_2(s) + 2H^+ + 2e-$$

$$Fe + HCO_3^- \rightarrow FeCO_3(s) + H^+ + 2e-$$

$$Fe(OH)_2(s) + HCO_3^- \rightarrow FeCO_3(s) + H_2O + OH^-$$

$$FeCO_3(s) + HCO_3^- \leftrightarrow Fe(CO_3)_2{}^{2-} + H^+$$

Within this process, Davies and Burstein suggested that the anodic dissolution rate is controlled by the formation of a soluble complex of carbonate $Fe(CO_3)_2{}^{2-}$and by its diffusion away from the iron surface:

- As the concentration of $Fe(CO_3)_2{}^{2-}$ increases, the anodic currents decrease.
- As the bicarbonate levels increase, the anodic current rise and this was associated with the solubility of the complex at higher bicarbonate concentrations.

Zhou and Parkins[118] however point out that, although this mechanism supports the proportionality between the anodic current and the bicarbonate concentrations, this scheme has weaknesses,

- The complex $Fe(CO_3)_2{}^{2-}$ has only been found as a solid as part of the salt $K_2Fe(CO_3)_2, 4H_2O$.
- The formation of the complex $Fe(CO_3)_2{}^{2-}$in the active domain is a pure chemical process which occurs under saturated conditions. The concentration of the complex ion and the anodic currents would therefore be independent of the electrode potential. This is in contradiction of the anodic currents increasing with potential at the approach of the oxidation peak potential.

They favoured the formation of a complex ion to explain the active dissolution of iron in bicarbonate-containing solutions:

$$Fe + HCO_3^- \leftrightarrow Fe(HCO_3)^+ + 2e -$$

This reaction is electrochemical, in contrast to the pure chemical nature involving the formation of $Fe(CO_3)_2{}^{2-}$.

Castro et al. [139] also supported that the anodic dissolution of iron in bicarbonate-carbonate systems is probably related to the formation of soluble compounds, such as $Fe(HCO_3)^+$(and $Fe(HCO_3)_2$).

C. Effect of impurities

The addition of nitrates or sulphates does not significantly affect I_p in relation to the pure bicarbonate/carbonate system (Figure 83). In contrast, the sulphites significantly increase I_p. This suggests that the presence of sulphites hinders (or retards) the formation of protective surface film (e.g. iron carbonate) allowing higher anodic dissolution rates to be reached. This is consistent with the measurement of E_{corr}, which suggested higher activity of the sulphite containing system in comparison with the pure bicarbonate/carbonate system.

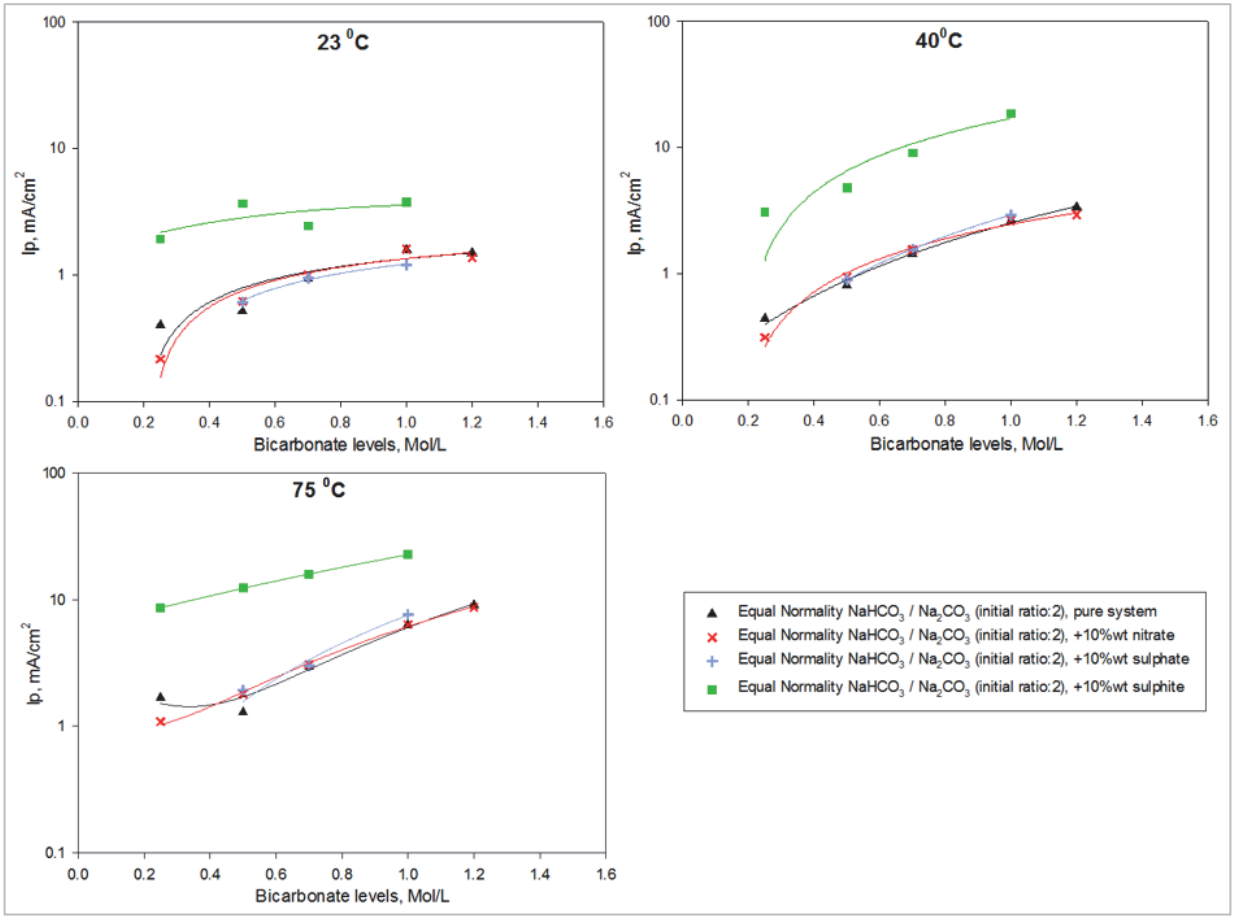

Figure 83: Effect of nitrates and sulphites on I_p in bicarbonate/ carbonate systems at various temperatures, CO_2-free environments

D. Effect of carbon dioxide

Figure 84 shows that the addition of carbon dioxide in the different test bicarbonate / carbonate environments, independently of the presence of nitrates or sulphites, increases I_p at 23 and 75°C. As discussed above (see section 4.2.2-E), it is considered that the addition of carbon dioxide has two major effects:

- Destabilisation of protective film formation e.g. iron carbonate
- Increase in the cathodic reduction rate (and therefore of the anodic dissolution process).

The combination of surface film destabilisation and increase in environment corrosivity could be translated into an increase in the anodic currents in the presence of carbon dioxide. The increase in anodic dissolution of the surface due to the presence of carbon dioxide contributes to some type of surface depolarisation which is associated with the increase in E_{corr} as discussed in section 4.2.2-E.

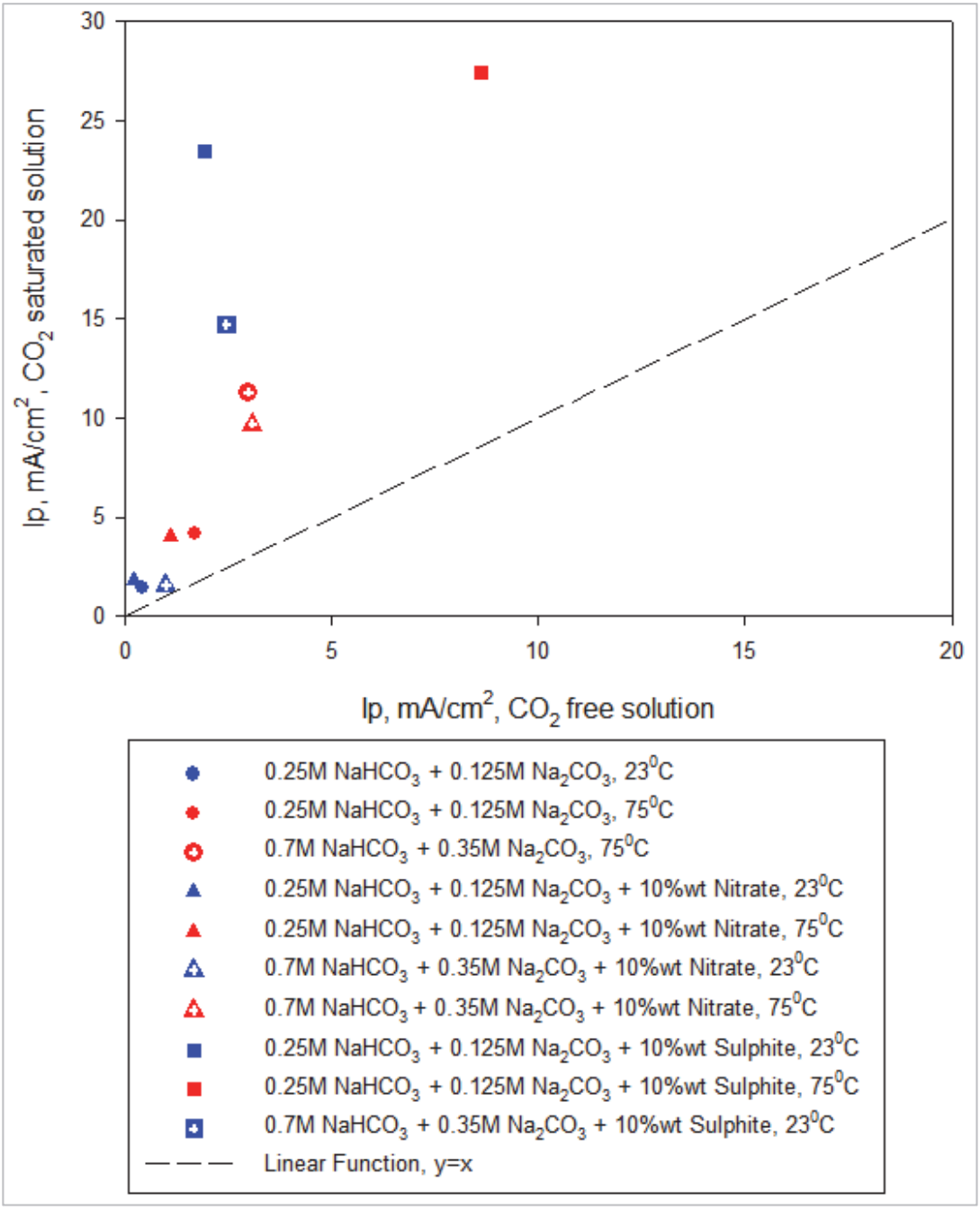

Figure 84: First oxidation peak current density of CO_2-saturated vs CO_2-free test environments

Chapter 5: Results from Slow Strain Rate Test

5.1. Qualitative assessment of SCC susceptibility and mode of cracking: SEM and optical microscopy

5.1.1. CO_2-free systems

A. Summary of findings: SCC susceptibility and mode of cracking

The susceptibility and the mode of cracking in the different test environments (in the absence of gaseous CO_2) is initially qualitatively presented following scanning electron and optical microscopy examination.

The results are qualitatively categorised in the following categories:

- Presence or absence of Stress Corrosion Cracking (Yes or No). The presence of pits is reported.
- Severity to cracking; three qualitative levels of stress corrosion susceptibility are defined:
  - ✓ 0: No indication of SCC susceptibility
  - ✓ 1: Pitting is mainly identified; their morphology however indicates that they may eventually turn into cracks over time
  - ✓ 2: Medium susceptibility to SCC; material is susceptible to SCC but cracks are short in size.
  - ✓ 3: Severe susceptibility to SCC; material is categorically susceptible to SCC with multiple deep cracks present.
- Mode of cracking: Intergranular (i.g.) or Transgranular (t.g.))

The results are summarised in Table 15 to Table 18. For each specific environment only the potential at which the "*maximum*" susceptibility to SCC was identified is presented in these tables, in order to facilitate comparison between environmental parameters:

- Table 15: Qualitative susceptibility of SCC in concentrated bicarbonate / carbonate systems (0.70M $NaHCO_3$ + 0.35M Na_2CO_3), with or without nitrates or sulphites, at 75°C and over the material active-passive transition domain (i.e. at potentials higher than E_p)
- Table 16: Qualitative susceptibility of SCC in less concentrated bicarbonate / carbonate systems (0.25M $NaHCO_3$ + 0.125M Na_2CO_3), with

or without nitrates or sulphites, at 75°C and over the material-active passive transition domain (i.e. at potentials higher than E_p)

- Table 17: Qualitative susceptibility of SCC in concentrated bicarbonate / carbonate systems (0.70M $NaHCO_3$ + 0.35M Na_2CO_3), with or without nitrates or sulphites, at 75°C and over the material active (dissolution) domain (i.e. at potentials between E_{corr} and E_p)
- Table 18: Qualitative susceptibility of SCC in concentrated bicarbonate / carbonate systems (0.70M $NaHCO_3$ + 0.35M Na_2CO_3), with or without nitrates or sulphites, at 23°C and over the material-active passive transition domain (i.e. at potentials higher than E_p)

The effects of environments including,

- Bicarbonate and carbonate concentrations
- Presence of impurities
- Electrochemical Potential
- Temperature,

on the susceptibility and mode of cracking are discussed in more detail in the subsequent sections.

Table 15: Qualitative susceptibility to SCC and mode of cracking- concentrated bicarbonate / carbonate levels, 75°C, material active-passive region

Environment	Cross-Section		SCC presence	SCC severity	SCC mode
0.70M $NaHCO_3$ + 0.35M Na_2CO_3 -675 mV SCE*	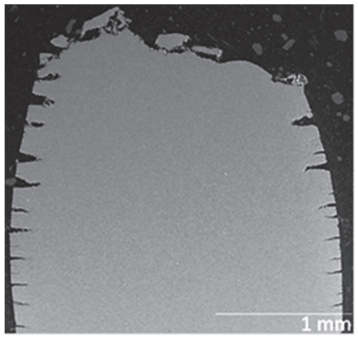	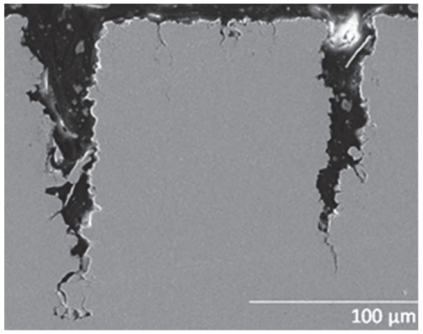	**Y**	3	i.g.
0.70M $NaHCO_3$ + 0.35M Na_2CO_3 + 10%wt $NaNO_3$ -650 mV SCE*	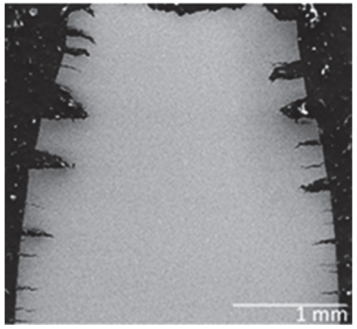	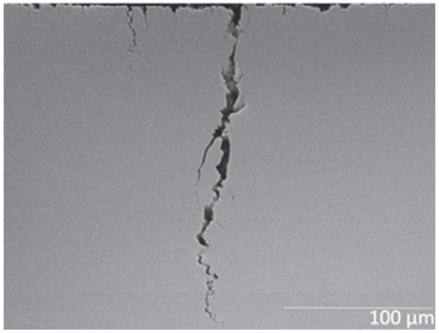	**Y**	3	i.g.
0.70M $NaHCO_3$ + 0.35M Na_2CO_3 + 10%wt Na_2SO_3 -710 mV SCE*	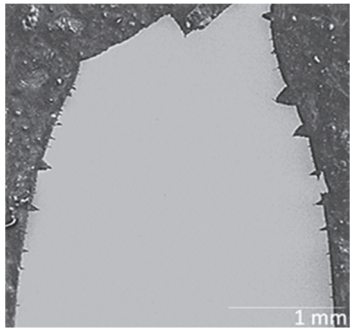	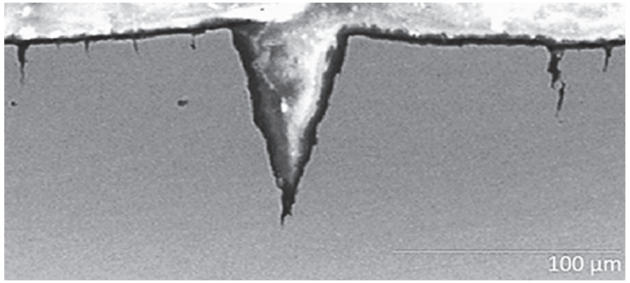	**Y**	2-3	t.g.

**Potential at which "maximum" susceptibility to SCC was identified for the specific environmental condition*

Table 16: Qualitative susceptibility to SCC and mode of cracking- lower bicarbonate / carbonate levels, 75°C, material active-passive region

Environment	Cross-Section		SCC presence	SCC severity	SCC mode
0.25M $NaHCO_3$ + 0.125M Na_2CO_3 -725 mV SCE*	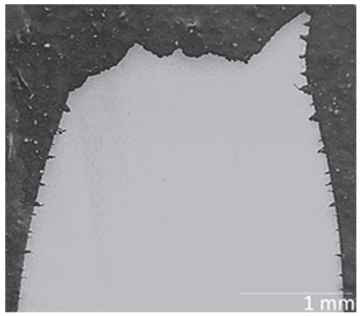	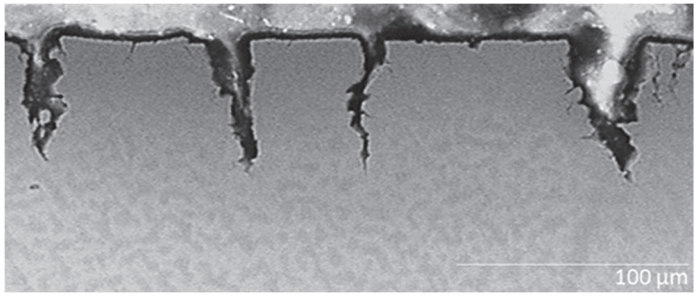	**Y**	2	i.g.
0.25M $NaHCO_3$ + 0.125M Na_2CO_3 + 10%wt $NaNO_3$ -690mV SCE*	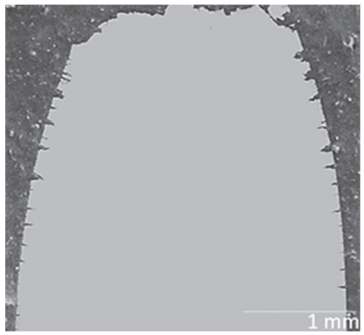	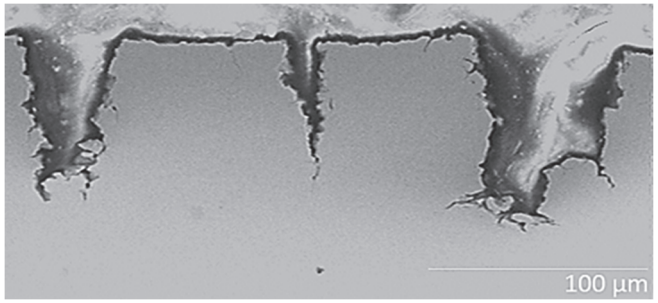	**Y**	2	i.g.
0.25M $NaHCO_3$ + 0.125M Na_2CO_3 + 10%wt Na_2SO_3 -770 mV SCE*	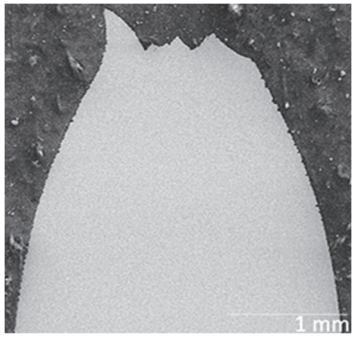	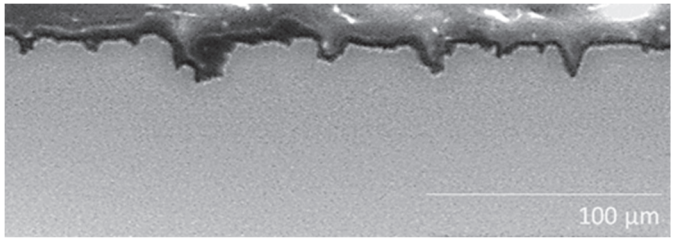	**N** Small surface pits	0	N/A

**Potential, at which "maximum" susceptibility to SCC was identified for the specific environmental condition*

Table 17: Qualitative susceptibility to SCC and mode of cracking- concentrated bicarbonate / carbonate levels, 75°C, material active region

Environment	Cross-Section	SCC presence	SCC severity	SCC mode
0.70M $NaHCO_3$ + 0.35M Na_2CO_3 -770 mV SCE*	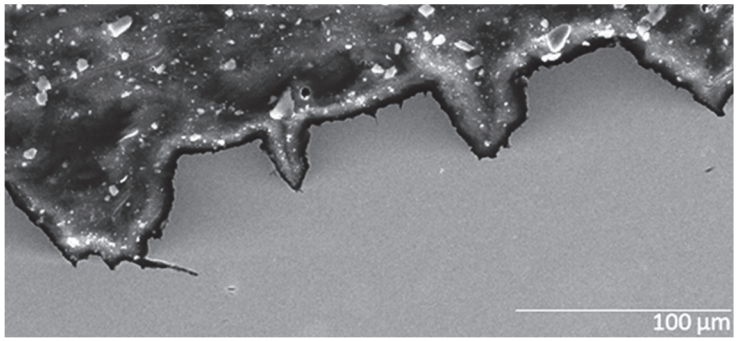	**Y**	2	t.g.
0.70M NaHCO3 + 0.35M Na_2CO_3 + 10%wt $NaNO_3$ -740 mV SCE*	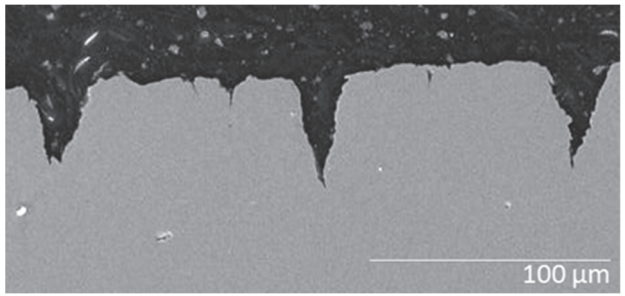	**Y**	2	t.g.
0.70M $NaHCO_3$ + 0.35M Na_2CO_3 + 10%wt Na_2SO_3 -790 mV SCE*	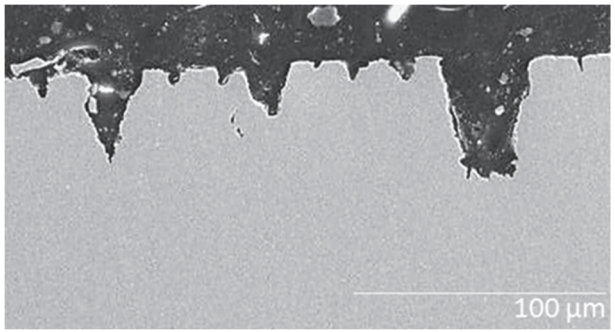	**Y**	2	t.g.

**Potential, at which "maximum" susceptibility to SCC was identified for the specific environmental condition*

Table 18: Qualitative susceptibility to SCC and mode of cracking- concentrated bicarbonate / carbonate levels, 23°C, material active-passive region

Environment	Cross-Section	SCC presence	SCC severity
0.70M $NaHCO_3$ + 0.35M Na_2CO_3 -600 mV SCE*	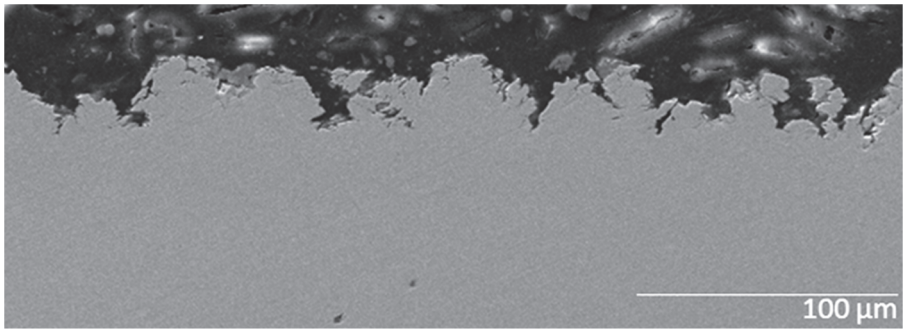	**Y/N** Small pits May turn into cracks at longer exposure	1
0.70M $NaHCO_3$ + 0.35M Na_2CO_3 + 10%wt $NaNO_3$ -590 mV SCE*	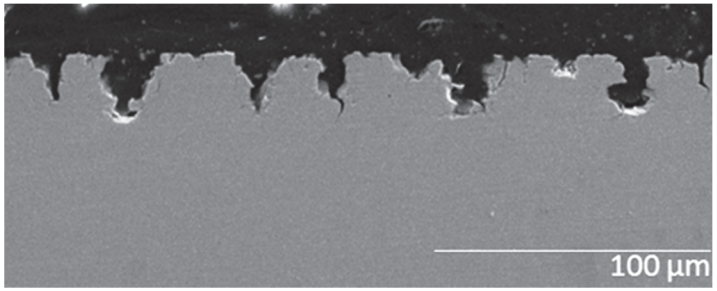	**Y/N** Small pits May turn into cracks at longer exposure	1
0.70M $NaHCO_3$ + 0.35M Na_2CO_3 + 10%wt Na_2SO_3. -670 mV SCE*	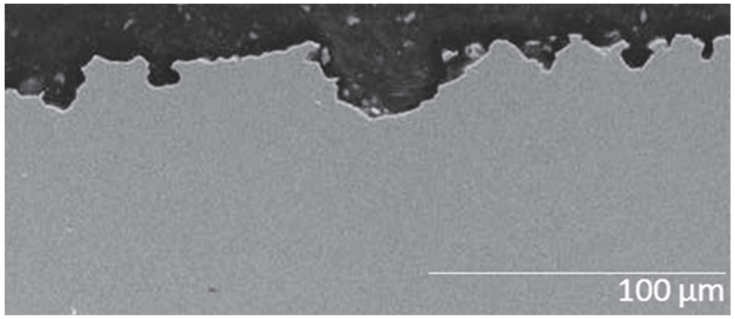	**N** Small surface pits	0

**Potential, at which "maximum" susceptibility to SCC was identified for the specific environmental condition*

B. Pure bicarbonate /carbonate system

Effect of bicarbonate / carbonate concentrations at 75°C

In the range of potentials associated with active-passive transition ($E>E_p$), the pipeline steel materials suffer from significant Stress Corrosion Cracking (SCC) in the concentrated bicarbonate / carbonate environments (0.7M $NaHCO_3$+0.35M Na_2CO_3) at 75°C. Multiple initiated cracks could be witnessed on the side surface of the SSRT specimen away from the necking as illustrated in Figure 85. The cracking initiates at the grain boundary (Figure 86), and grows as deep fine-branched SCC (see Figure 87 and Figure 88).

It is noted that the fracture surfaces of the test material throughout the SSRT testing programme have generally presented oval features. As discussed in Chapter 2, the cross-section of the specimen gauge is parallel to the plane of the pipeline steel wall thickness (short transverse direction). This ovality can be associated with the specific steel microstructure in the short transverse direction, which consists of elongated and banded pearlite in an elongated and lightly banded ferrite matrix. The effect of elongated and banded grains on the ovality of tensile test specimen fracture surfaces has been discussed by Mustapha.[140]

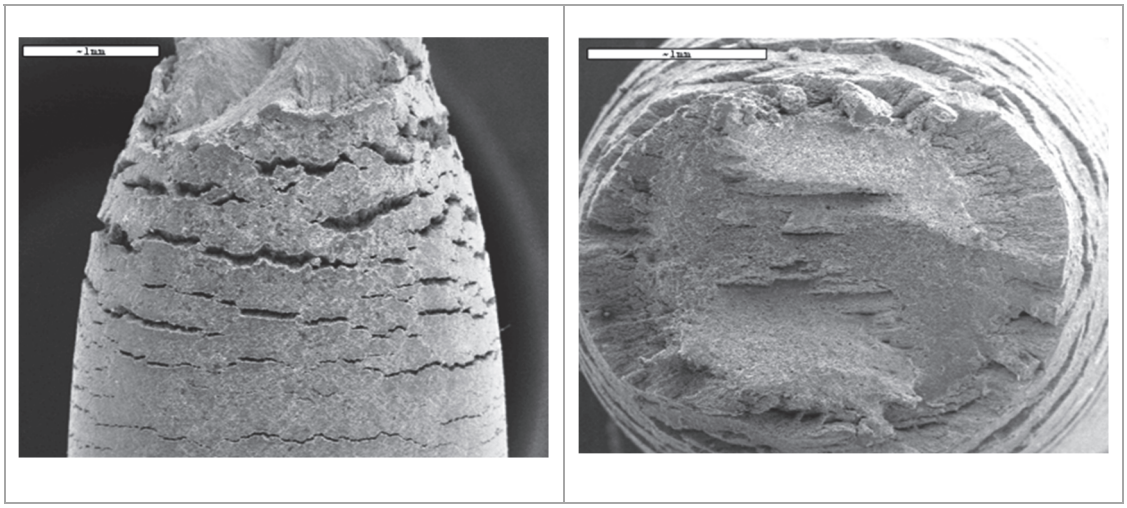

Figure 85: 0.70M $NaHCO_3$ + 0.35M Na_2CO_3, 75°C, -675 mV SCE, SSRT fractured specimen

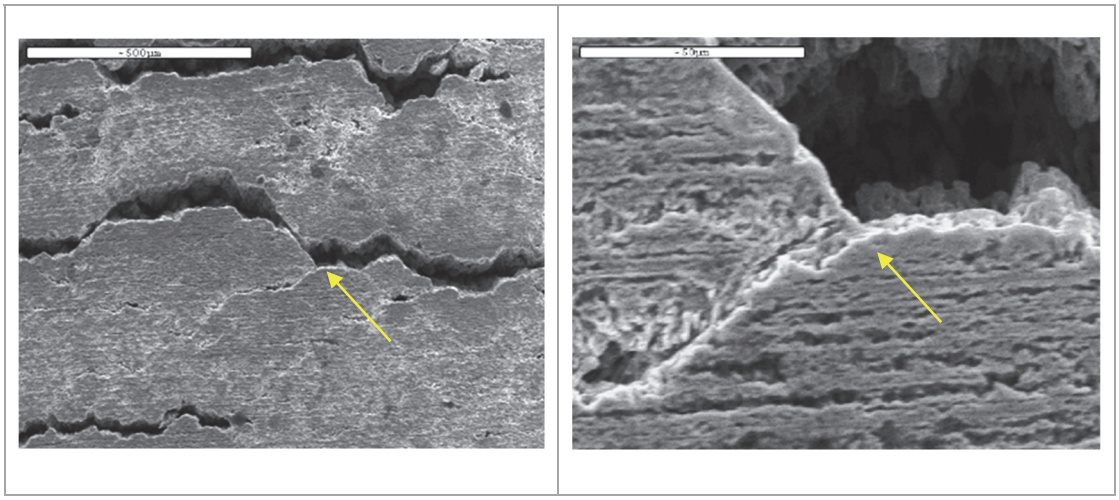

Figure 86: 0.70M $NaHCO_3$ + 0.35M Na_2CO_3, 75°C, -675 mV SCE, SCC initiating at grain boundary

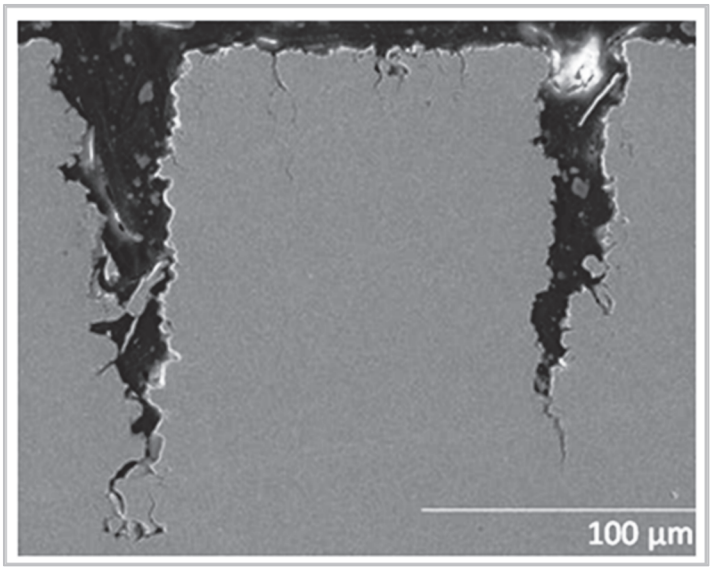

Figure 87: 0.70M NaHCO3 + 0.35M Na_2CO_3, 75°C , -675 mV SCE, cross-section showing SCC

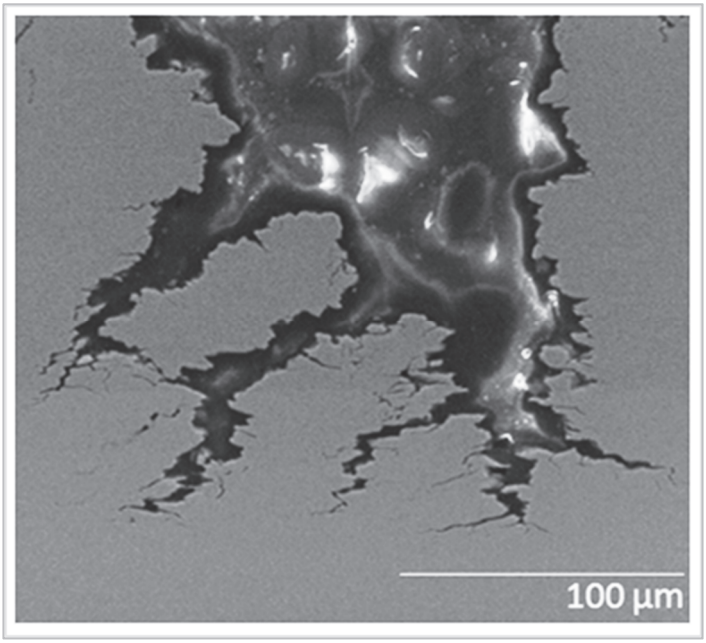

Figure 88: 0.70M NaHCO3 + 0.35M Na_2CO_3, 75°C , -675 mV SCE, branched SCC

At lower bicarbonate / carbonate concentrations (0.25M $NaHCO_3$+0.125M Na_2CO_3), the steel remains susceptible in the active-passive transition at 75°C (Figure 89 and Figure 90), but the severity of cracking is decreased with cracks being smaller and not as fine as at higher bicarbonate and carbonate concentrations (Figure 91) .

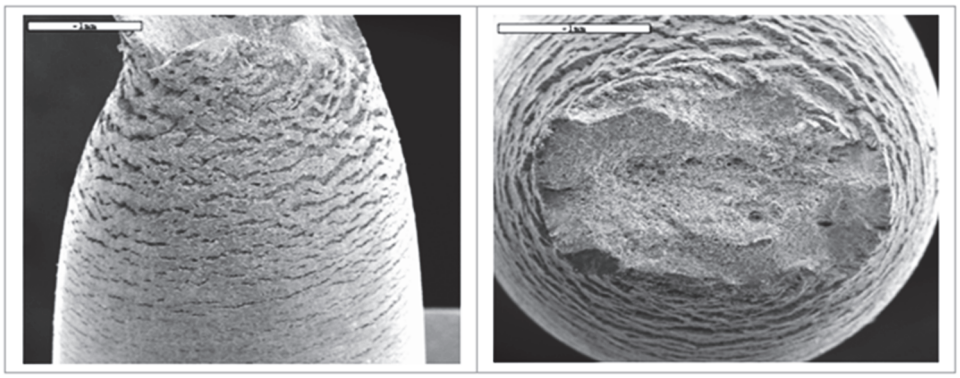

Figure 89: 0.25 M $NaHCO_3$ + 0.125 M Na_2CO_3, 75°C, -725 mV SCE, SSRT fractured specimen

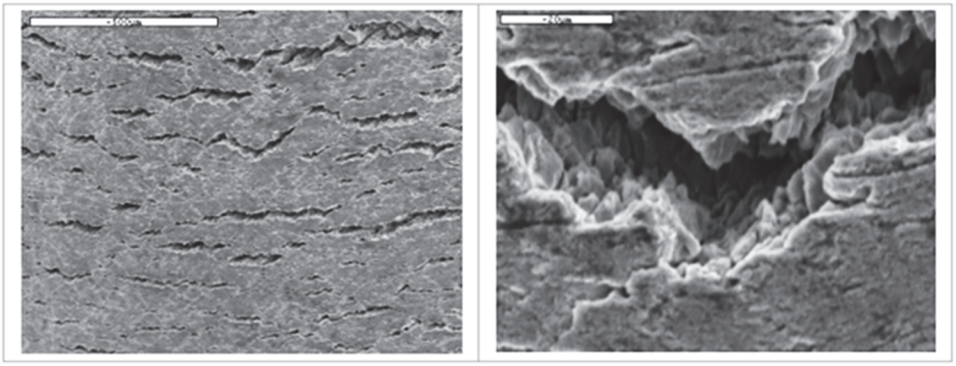

Figure 90: 0.25 M $NaHCO_3$ + 0.125 M Na_2CO_3, 75°C, -725 mV SCE, colony of i.g. SCC

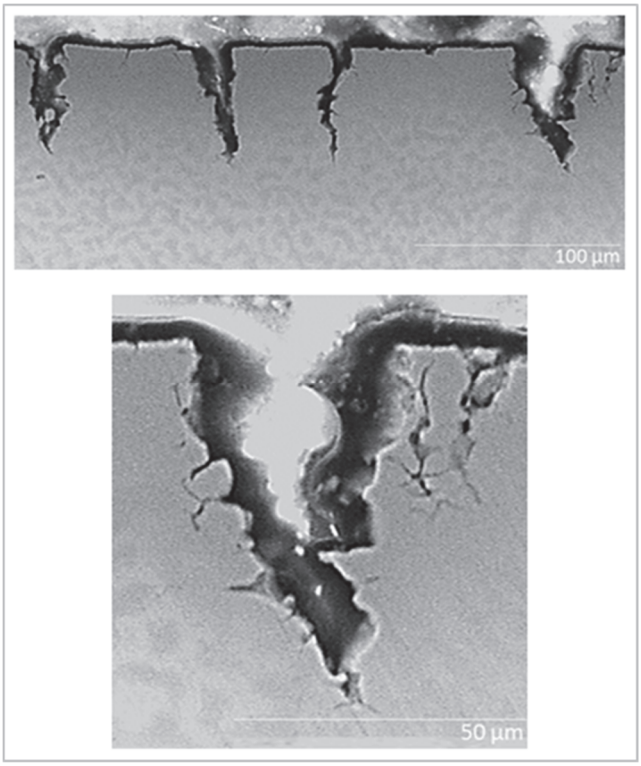

Figure 91: 0.25 M $NaHCO_3$ + 0.125 M Na_2CO_3, 75°C, -725 mV SCE, cross-section (1µm polish)

Effect of temperature

The susceptibility to SCC in the active-passive transition region appears to decrease with decreasing the temperature.

At 23°C, the materials suffer from significant plastic deformation as illustrated by the magnitude of necking on the fracture face (Figure 92). At low magnification, examination of the side surface of the fractured specimen indicates tiny localised corrosion features whose morphology and geometry could suggest stress corrosion cracks at the initiation stage (Figure 93). At higher magnification, some of the surface corrosion features show significant tearing due to mechanical plastic deformation suggesting that the corrosion growth has been significantly less than the strain rate (Figure 93).

The cross-section of the SSRT specimen indicates the presence of surface pits, whose morphology is similar to cracking (Figure 94). At 23°C, the anodic dissolution rates associated with the corrosion process are probably too low to sustain rapid crack growth within the time scale of the SSRT experiment. Under these conditions, the growth rate of any eventual initiated stress corrosion cracks will be so slow compared to the deformation of the specimen produced by the experimental strain rate and so the specimen finally fails due to plastic deformation.

It is plausible that for much longer exposure tests (i.e. at lower strain rate), the pits could turn into deeper stress corrosion cracks.

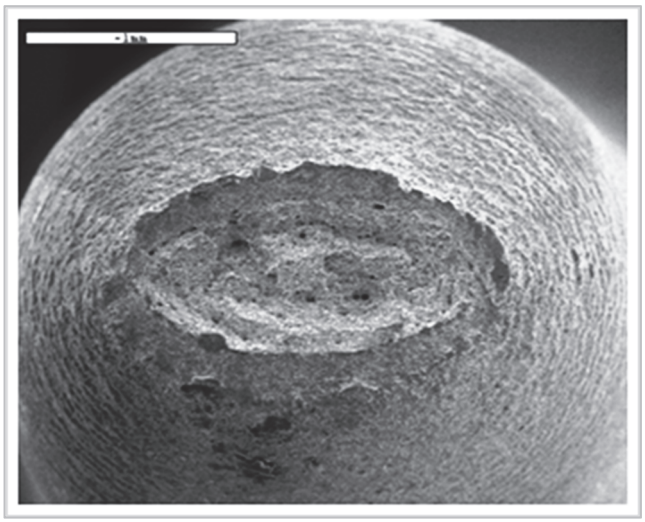

Figure 92: 0.70M $NaHCO_3$ + 0.35M Na_2CO_3, 23°C, -600 mV SCE, SSRT fractured specimen

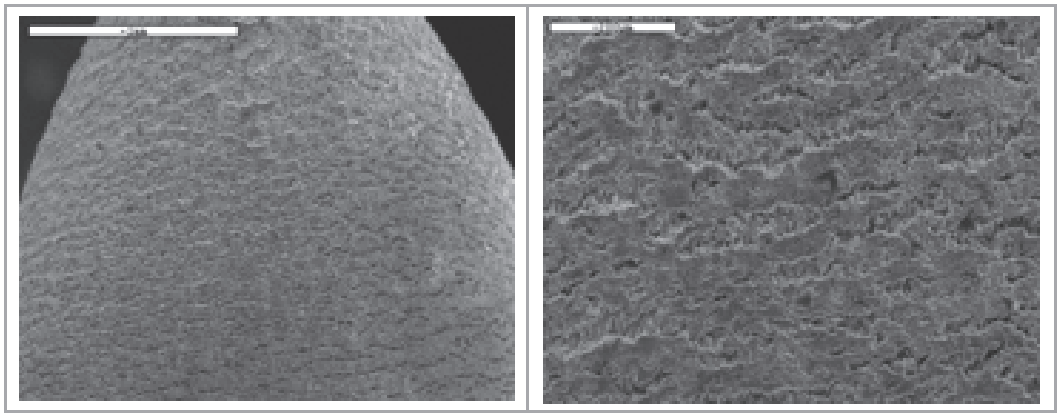

Figure 93: 0.70M $NaHCO_3$ + 0.35M Na_2CO_3, 23°C, -600 mV SCE

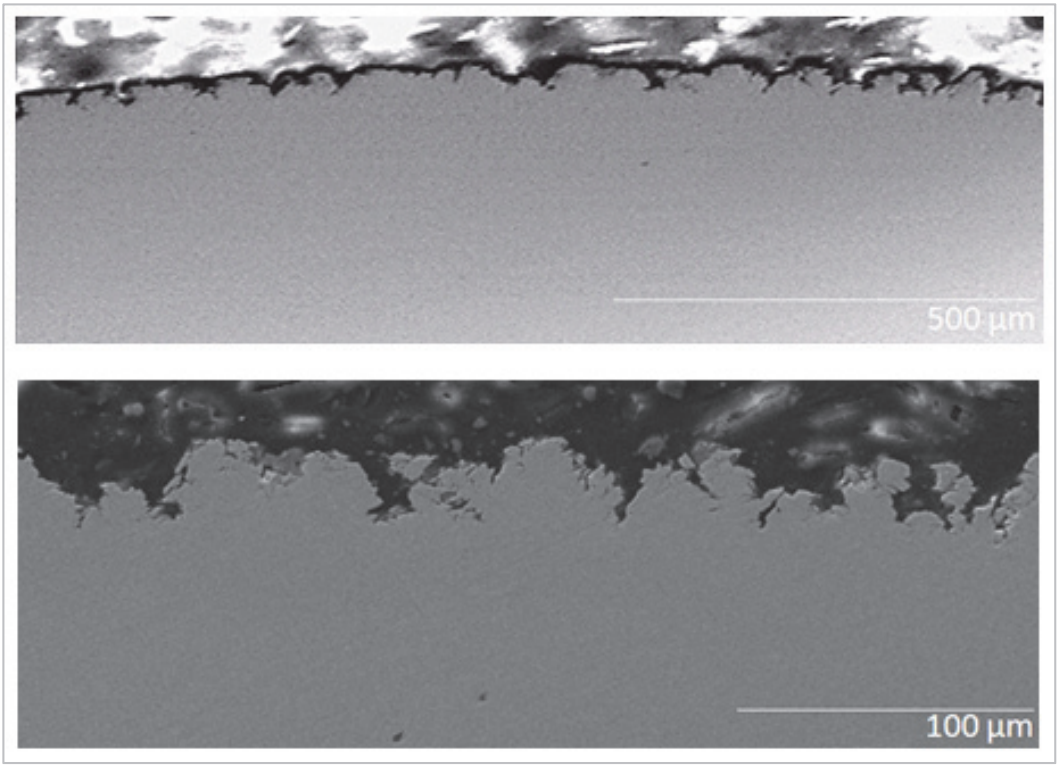

Figure 94: 0.70M $NaHCO_3$ + 0.35M Na_2CO_3, 23°C, -600 mV SCE, cross-section polished to 1µm

Effect of electrochemical potential at 75°C

As presented above, the steel can suffer from significant stress corrosion cracking in bicarbonate / carbonate environments at 75°C at potentials associated with the active-passive transition region ($E>E_p$). As shown in Figure 95 and Figure 96, the mode of cracking for this system in the active-passive transition region is intergranular.

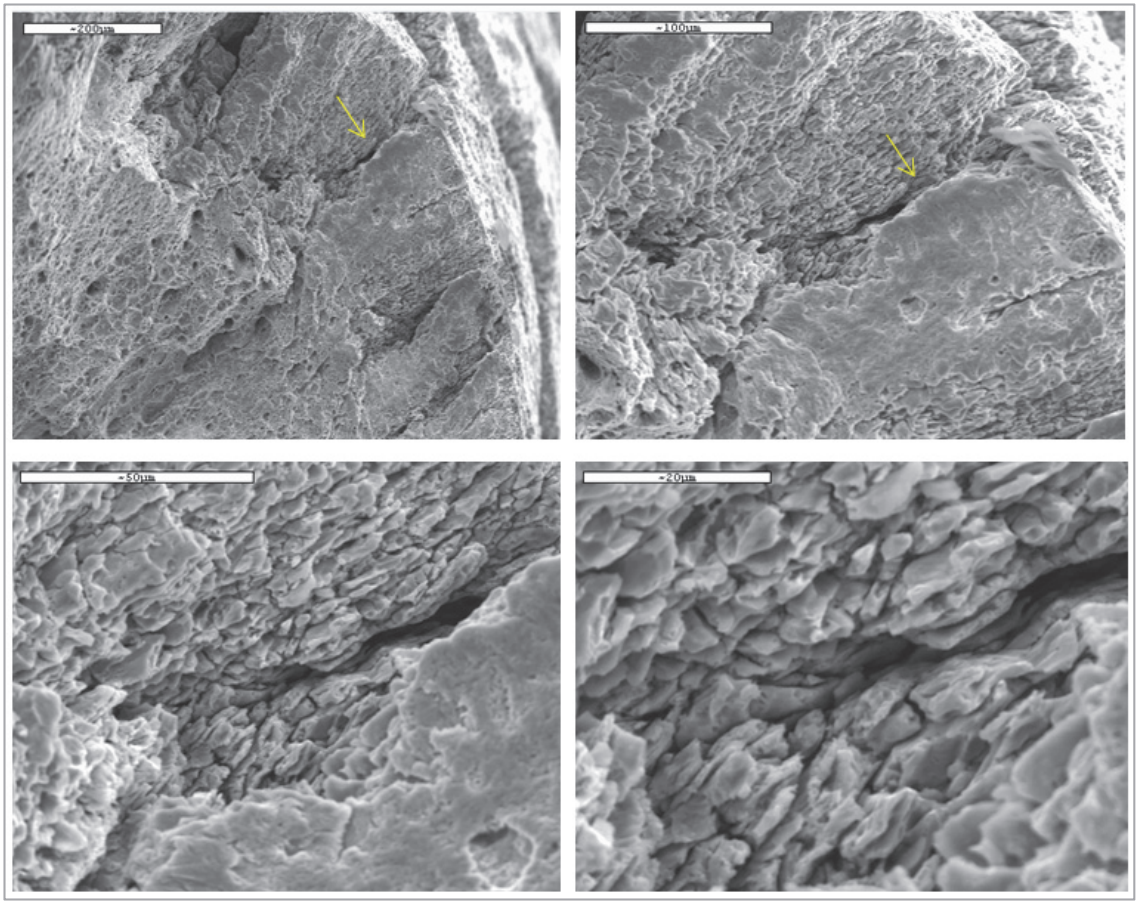

Figure 95: 0.70M $NaHCO_3$ + 0.35M Na_2CO_3, 75°C, -675 mV SCE, i.g. SCC on fracture surface

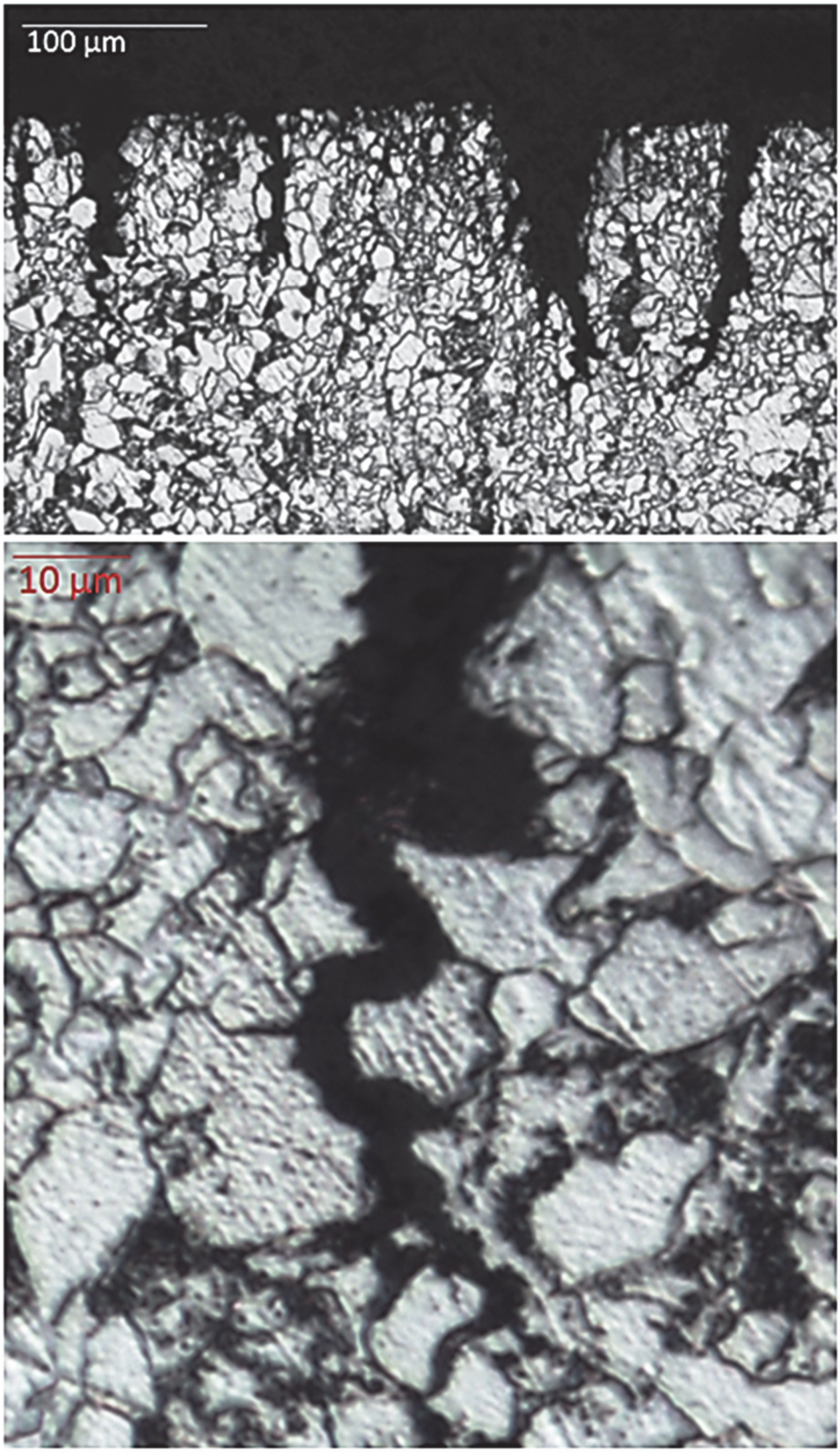

Figure 96: 0.70M $NaHCO_3$ + 0.35M Na_2CO_3, 75°C, -675 mV SCE, cross-section etched with Nital 2%vol., i.g. SCC

At potentials between E_{corr} and E_p, which is related to the material active region, stress corrosion cracking is still possible (Figure 97) but the mode of cracking shifts to transgranular as illustrated in Figure 98 to Figure 100. The susceptibility to cracking however appears to be decreased as the potential tends to the free corrosion potential E_{corr} (Figure 101).

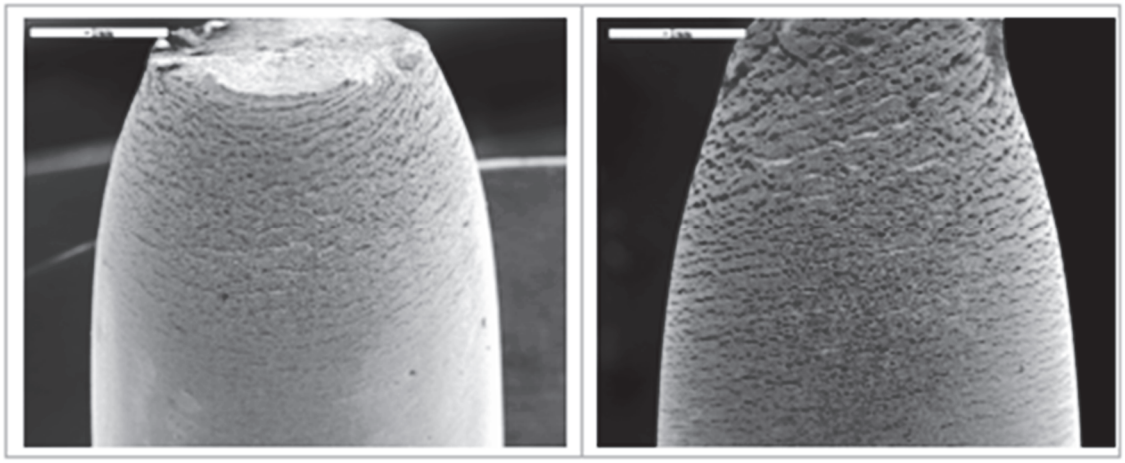

Figure 97: 0.70M $NaHCO_3$ + 0.35M Na_2CO_3, 75°C, (a) -820 mV SCE and (b) -770 mV SCE, SSRT fractured specimen

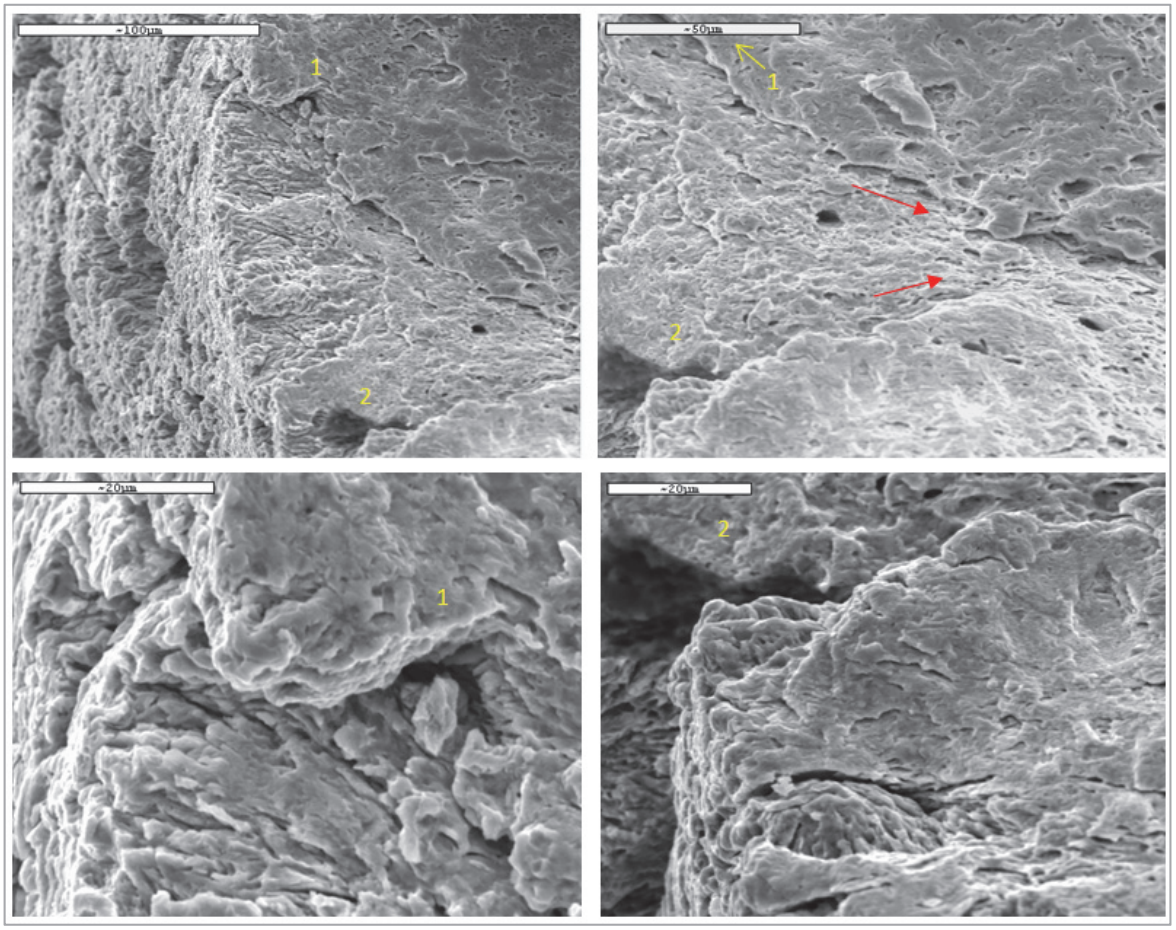

Figure 98: 0.70M $NaHCO_3$ + 0.35M Na_2CO_3, 75°C, -770 mV SCE, t.g. SCC converging on fracture surface

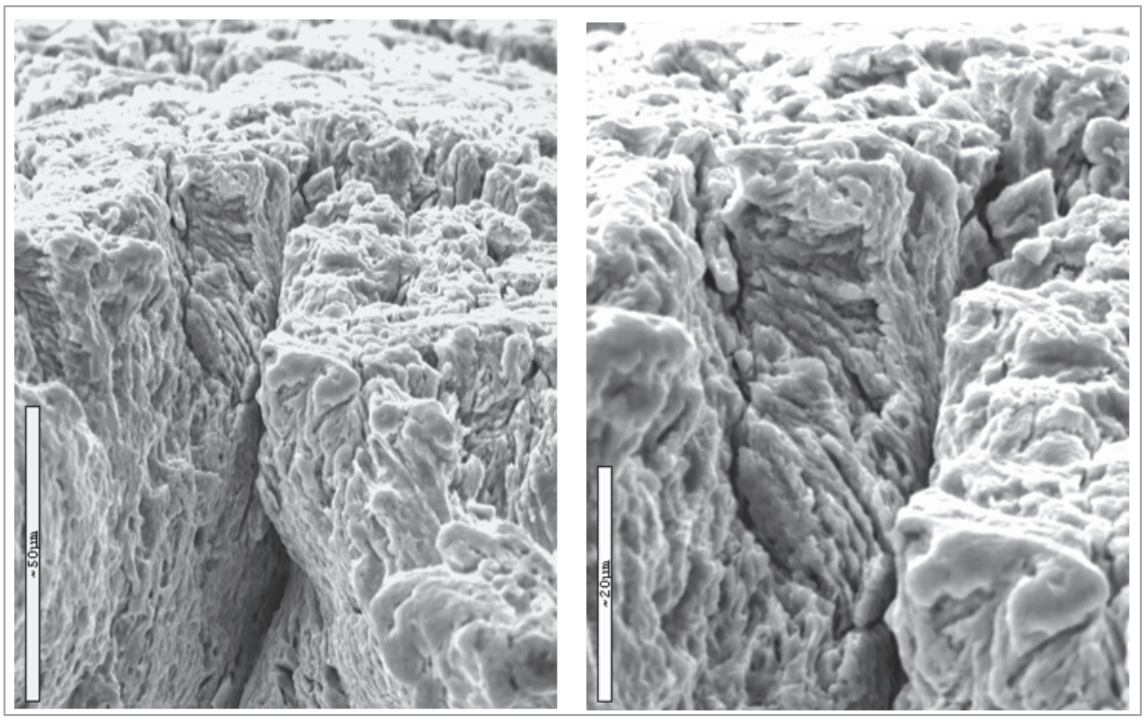

Figure 99: 0.70M $NaHCO_3$ + 0.35M Na_2CO_3, 75°C, -770 mV SCE, secondary t.g. SCC propagating perpendicularly from gauge surface

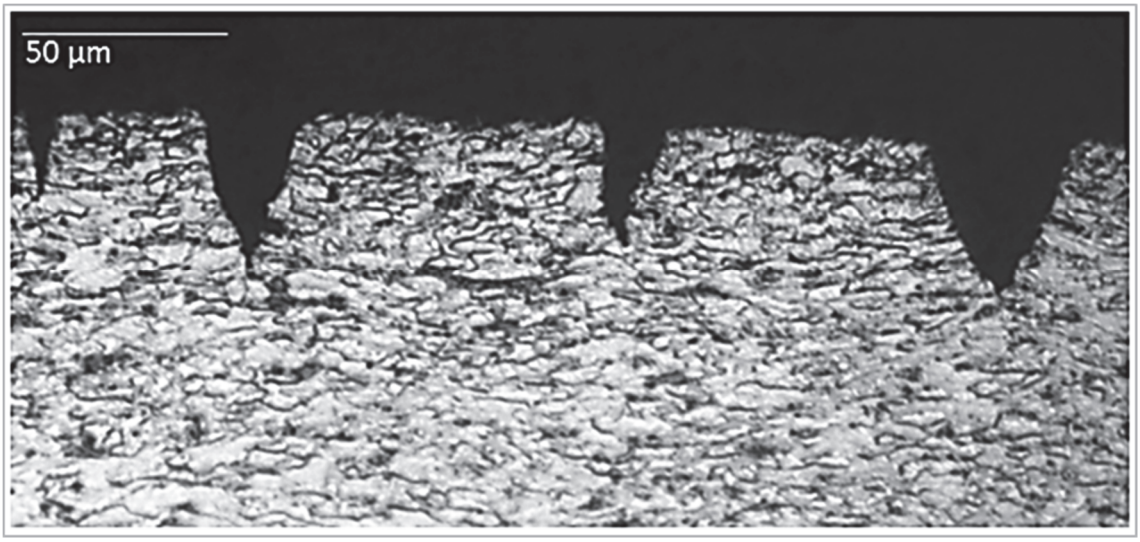

Figure 100: 0.70M $NaHCO_3$ + 0.35M Na_2CO_3, 75°C, -770 mV SCE, cross-section etched with Nital 2%vol., t.g. SCC

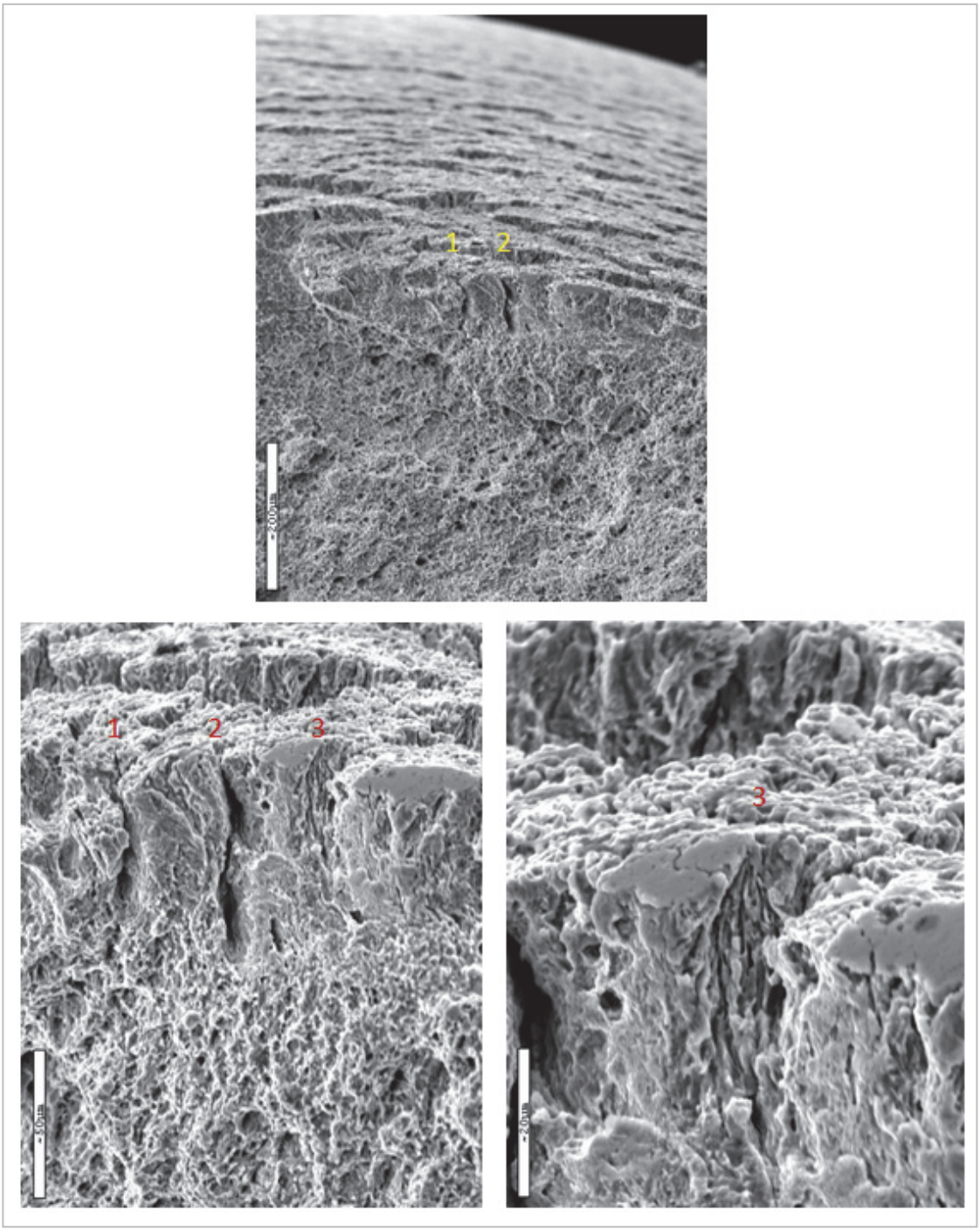

Figure 101: 0.70M $NaHCO_3$ + 0.35M Na_2CO_3, 75°C, -820 mV SCE, small t.g. SCC at potentials closer to free corrosion potential

C. Presence of nitrates in bicarbonate /carbonate systems

Effect of bicarbonate / carbonate concentrations at 75°C

As illustrated in Figure 102, Stress Corrosion Cracking is still possible when nitrate is present in concentrated bicarbonate / carbonate aqueous environments (0.7M $NaHCO_3$ / 0.35M Na_2CO_3) at 75°C at potentials associated with the active-passive transition ($E>E_p$). Multiple initiated cracks could be witnessed on the side surface of the SSRT specimen away from the neck as illustrated in Figure 102. The cracks grow as deep fine branched SCC (see Figure 103 and Figure 104).

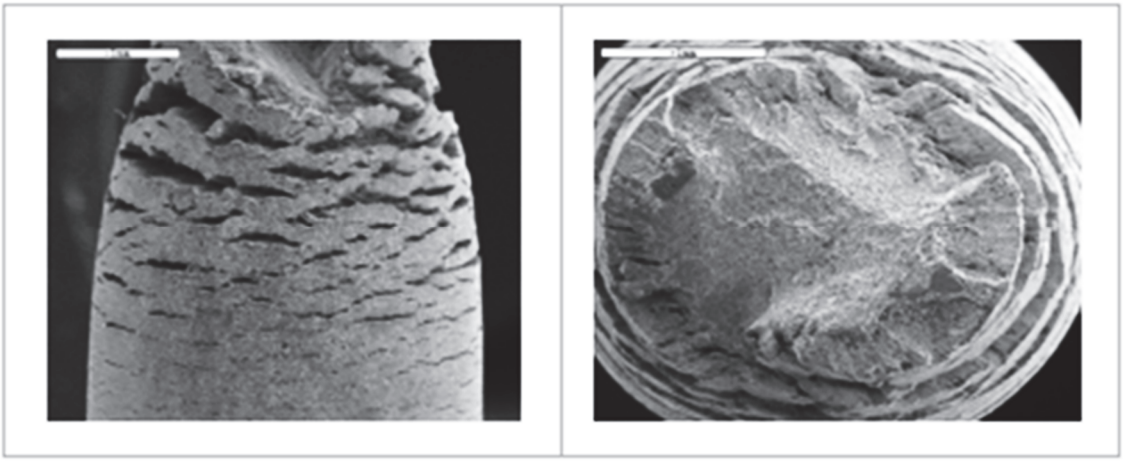

Figure 102: 0.70 M $NaHCO_3$ + 0.35 M Na_2CO_3 + 10%wt $NaNO_3$, 75°C, -650mV SCE, SSRT fractured specimen

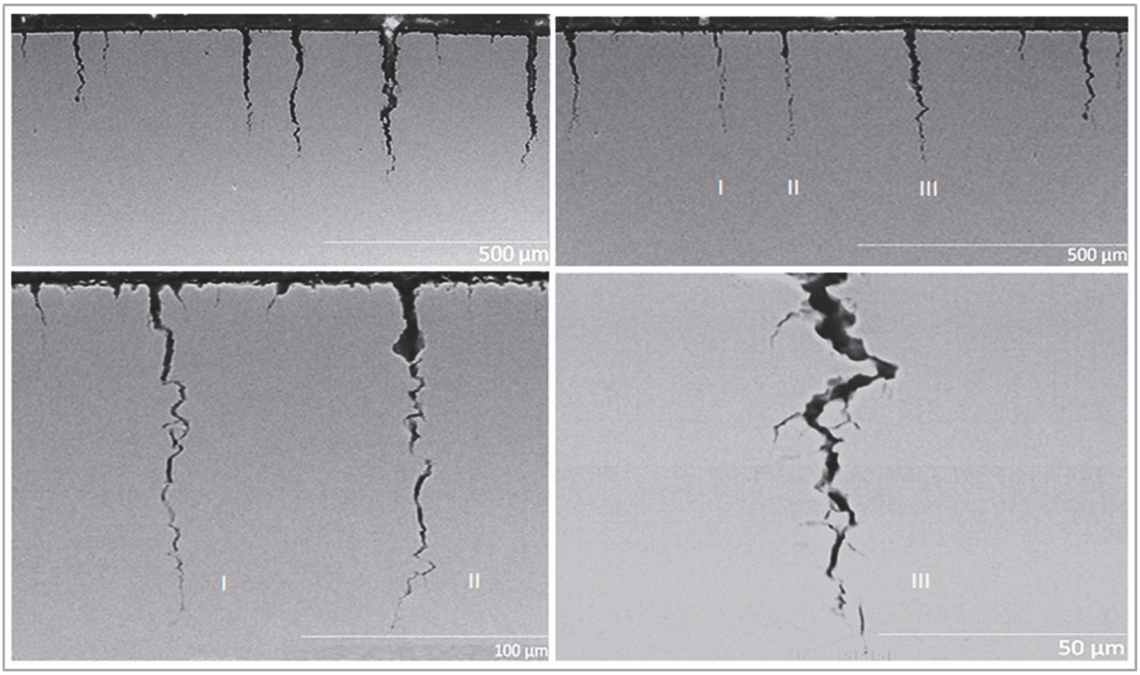

Figure 103: 0.70 M $NaHCO_3$ + 0.35 M Na_2CO_3 + 10%wt $NaNO_3$, 75°C, -650mV SCE, cross-section of SSRT specimen gauge, colony of fine i.g. SCC

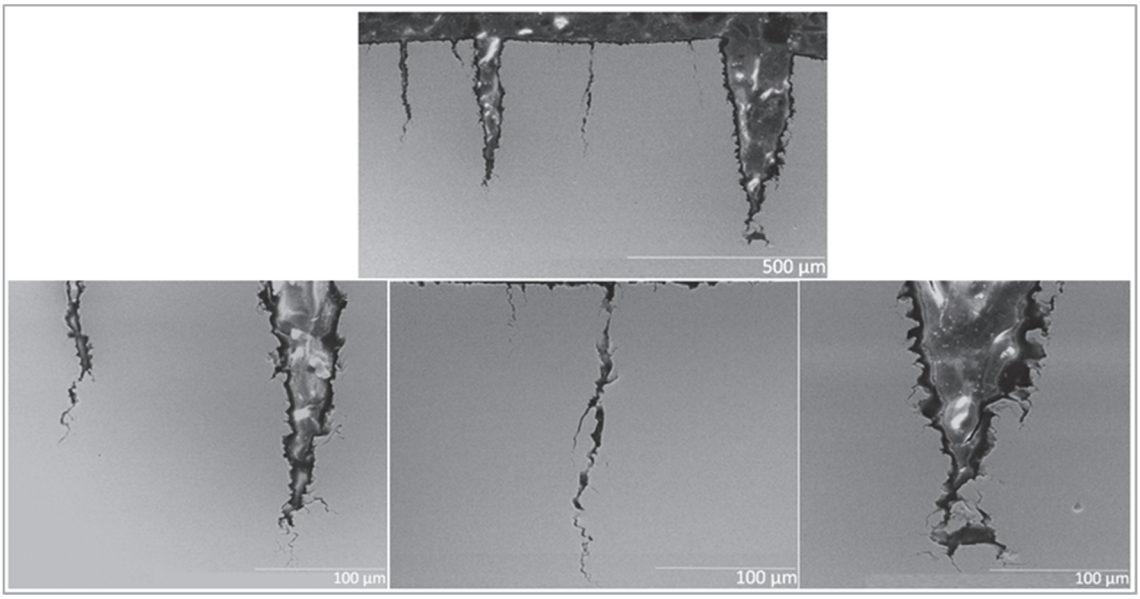

Figure 104: 0.70 M $NaHCO_3$ + 0.35 M Na_2CO_3 + 10%wt $NaNO_3$, 75°C, -650mV SCE, Cross-Section of SSRT specimen gauge showing i.g. SCC

Similarly to pure bicarbonate/carbonate systems, at lower bicarbonate / carbonate concentrations (0.25M $NaHCO_3$ / 0.125M Na_2CO_3), the steel remains susceptible in the active-passive transition at 75°C in the presence of nitrates (Figure 105), but the severity of cracking is decreased with cracks being smaller and less finer than at higher bicarbonate / carbonate concentrations .

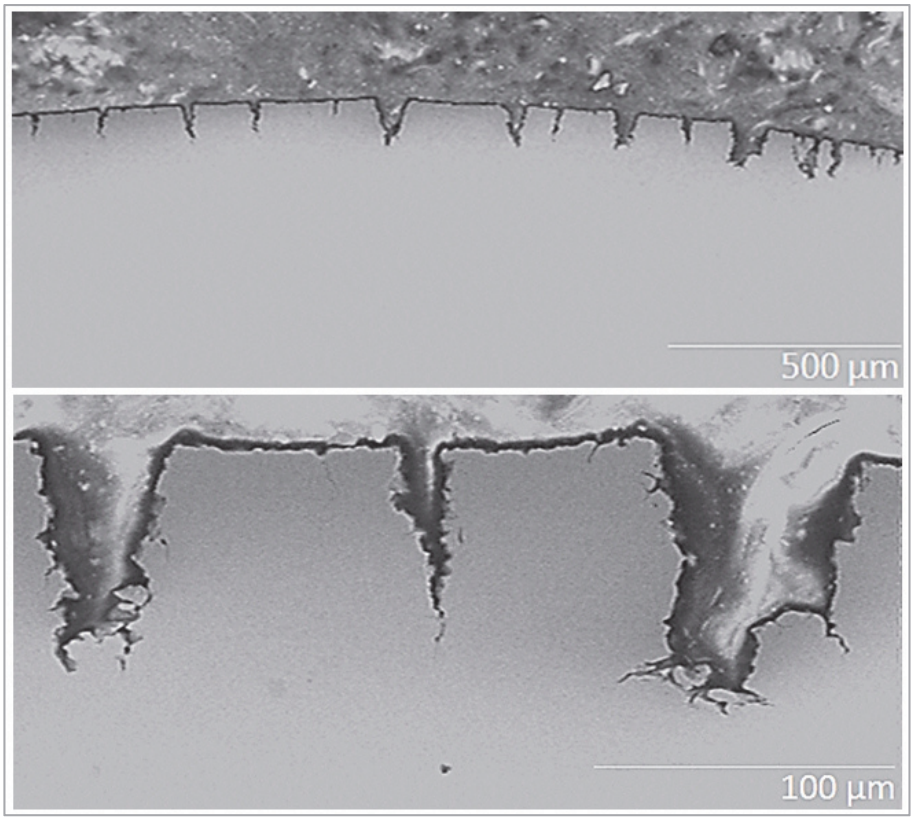

Figure 105: 0.25 M $NaHCO_3$ + 0.125 M Na_2CO_3 + 10%wt $NaNO_3$, 75°C, -690 SCE, cross-section polished to 1 µm

Effect of temperature

The susceptibility to SCC in the active-passive transition region appears to decrease with the temperature in the presence of nitrates.

At 23°C, in the range of potentials associated with active-passive transition, the materials exposed to 0.70 M $NaHCO_3$ + 0.35 M Na_2CO_3 + 10%wt $NaNO_3$ environments suffer from significant plastic deformation as illustrated by the magnitude of necking on the fracture face (Figure 106). The side surface of the specimen appears irregular, which indicates the material has suffered from some localised corrosion processes (Figure 106 and Figure 107).

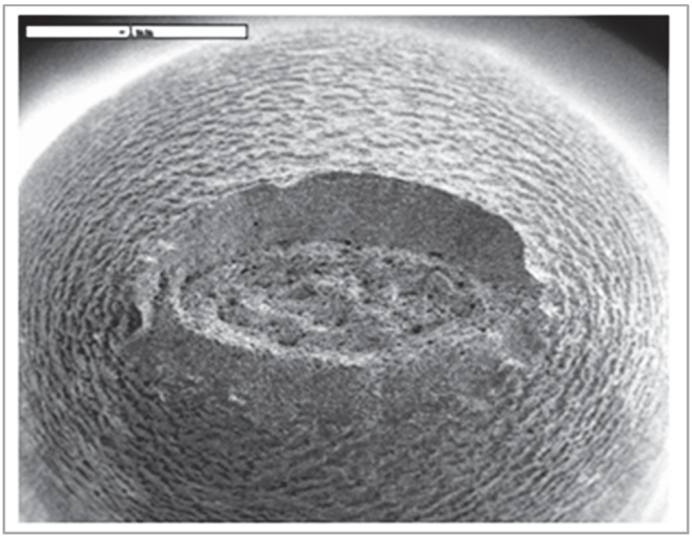

Figure 106: 0.70 M $NaHCO_3$ + 0.35 M Na_2CO_3 + 10%wt $NaNO_3$, 23°C, -590 mV SCE, SSRT fractured specimen

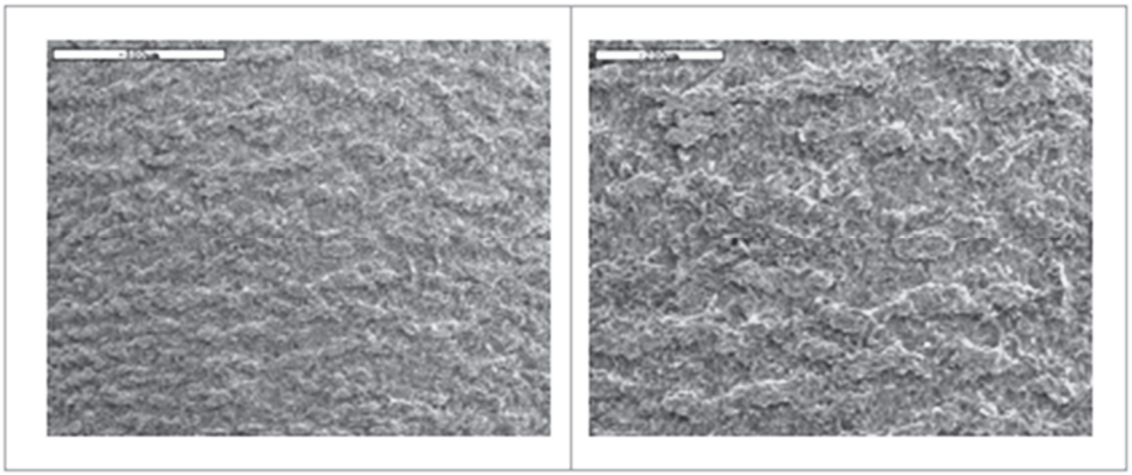

Figure 107: 0.70 M $NaHCO_3$ + 0.35 M Na_2CO_3 + 10%wt $NaNO_3$, 23°C, -590 mV SCE, SSRT fractured specimen

The cross-section of the SSRT specimen indicates the presence of surface pits, whose morphology resembles cracking (Figure 108). At 23°C, the anodic dissolution rates associated with the corrosion process are probably too low to sustain rapid crack growths within the time scale of the SSRT experiment conducted. Under these conditions, the growth rate of any eventual stress corrosion cracks will be so slow compared to the deformation of the specimen produced by the experimental strain rate, and so the specimen finally fails due to plastic deformation.

It is plausible that for much longer exposure tests (i.e. at lower strain rate), the pits could turn into deeper stress corrosion cracks.

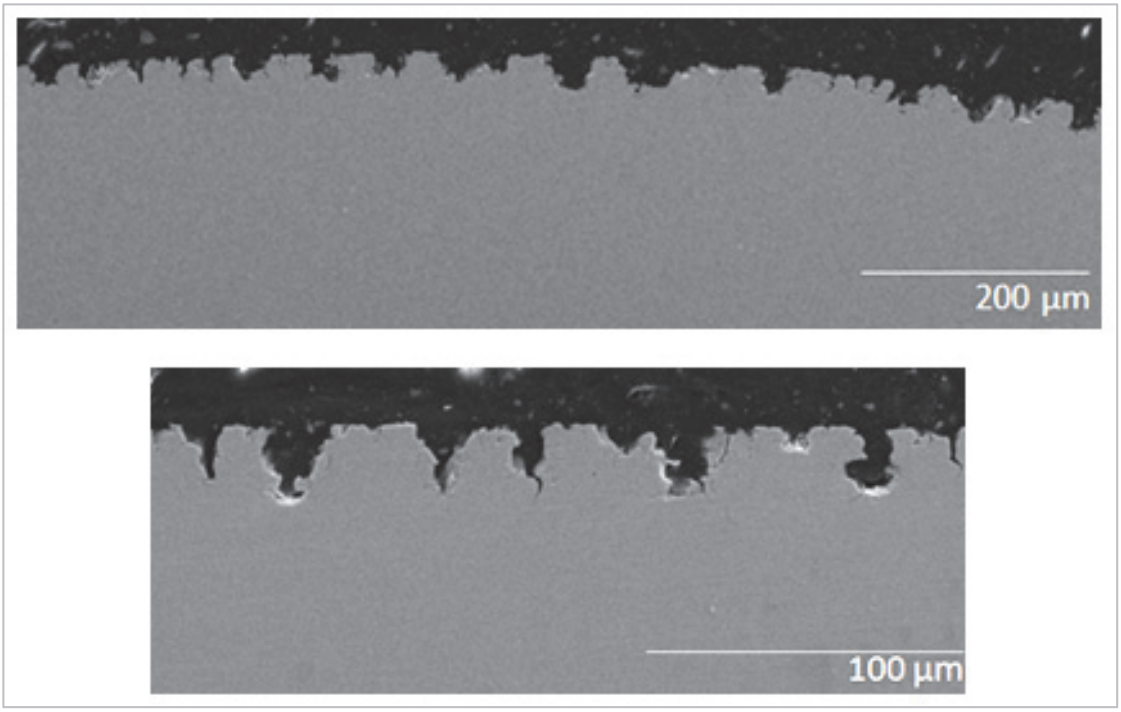

Figure 108: 0.70 M $NaHCO_3$ + 0.35 M Na_2CO_3 + 10%wt $NaNO_3$, 23°C, -590 mV SCE, cross-section polished to 1µm

It is noticed that, as the bicarbonate / carbonate concentrations are decreased (0.25M $NaHCO_3$ / 0.125M Na_2CO_3), the presence of nitrates induces severe pitting and intergranular attack of the materials at potentials associated with the active-passive transition region at 23°C. This phenomenon was not observed in pure 0.25M $NaHCO_3$ + 0.125M Na_2CO_3 systems at 23°C. Figure 109 shows the premature and rapid mechanical failure of the steel specimen in the 0.25M $NaHCO_3$ / 0.125M Na_2CO_3 system at 23°C (in comparison to 75°C) as a result of significant corrosion.

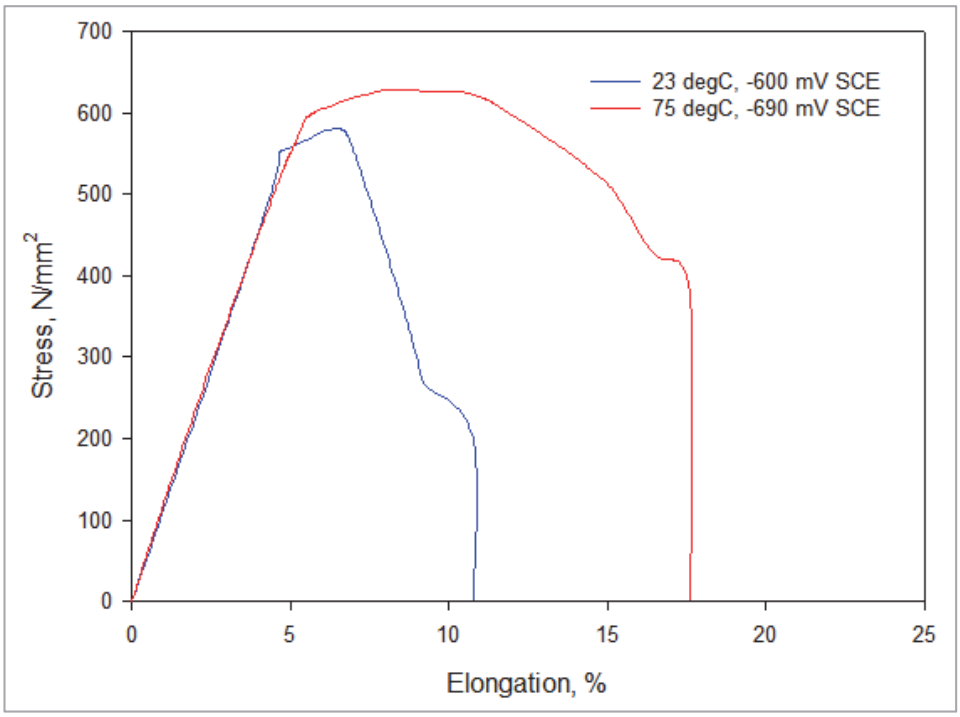

Figure 109: Typical stress vs deformation at 23°C and 75°C for : 0.25M $NaHCO_3$ + 0.125M Na_2CO_3 + 10%wt $NaNO_3$

A significant amount of dark green corrosion product is identified on the specimen (Figure 110) and at the bottom of the test cell. When stirred, the test solution is dark green. The greenish deposit on the SSRT fractured specimen is not adherent to the surface and can be easily stripped. The green nature of the deposit was probably related to the presence of iron hydroxides. The removal of the loose green deposits reveals a more compact and adherent film on the surface, probably magnetite (Figure 111).

The cleaning of the specimen under Clarke's solution for 2 seconds reveals the severe attack of the steel material in 0.25M $NaHCO_3$+0.125M Na_2CO_3 + 10%wt $NaNO_3$ at 23 °C (Figure 112 and Figure 113). After cleaning, the specimen was washed in a methanol bath with ultrasonic agitation, rinsed with distilled water and methanol and then dried. The roughness of the surface as illustrated in Figure 113 and Figure 114 suggests that the corrosion mechanism has been primarily of localised nature. The localised corrosion process generated clusters of pits which over time joined to leave a surface overall degraded; spalling of grains away from the bulk matrix (Figure 114) could also have been produced from intergranular localised corrosion.

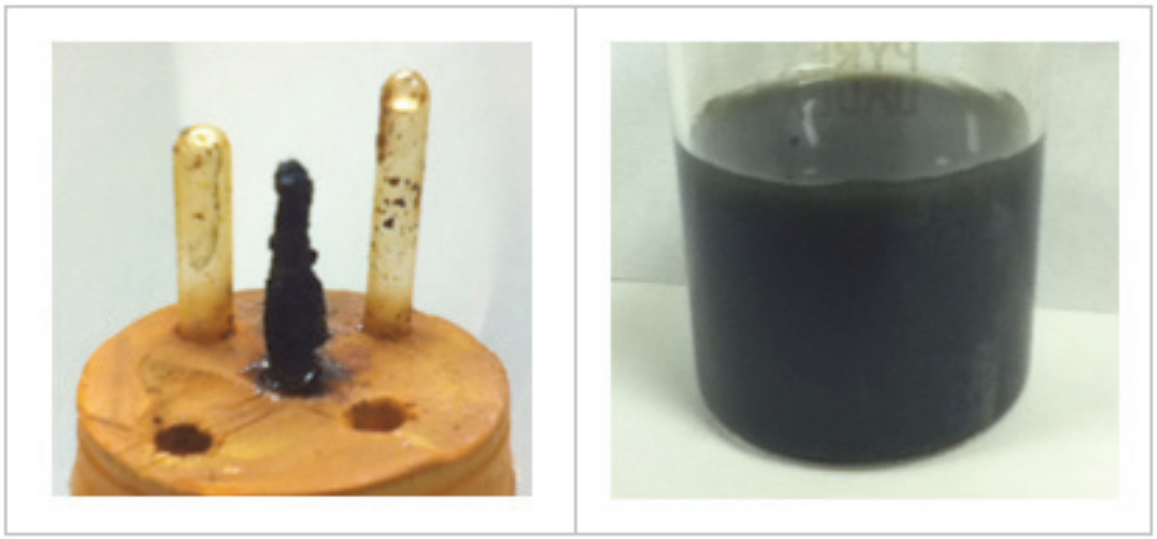

Figure 110: 0.25M $NaHCO_3$ + 0.125M Na_2CO_3 + 10%wt $NaNO_3$, 23°C, -600 mV SCE, SSRT fractured Specimen and solution after test

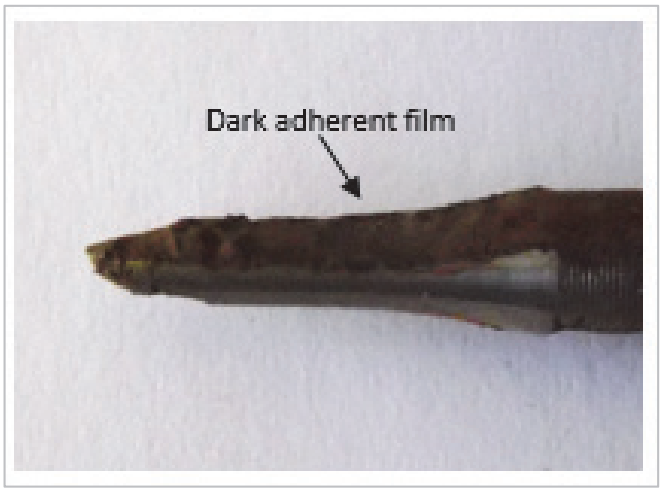

Figure 111: 0.25M $NaHCO_3$ + 0.125M Na_2CO_3 + 10%wt $NaNO_3$, 23°C, -600 mV SCE, Specimen after distilled water rinse

Figure 112: 0.25M $NaHCO_3$ + 0.125M Na_2CO_3 + 10%wt $NaNO_3$, 23°C, -600 mV SCE, SSRT Specimen after surface cleaning with Clarks Solution

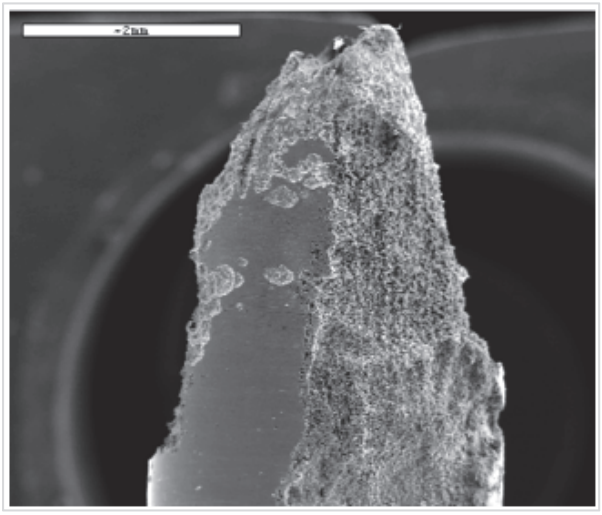

Figure 113: 0.25M $NaHCO_3$ + 0.125M Na_2CO_3 + 10%wt $NaNO_3$, 23°C, -600 mV SCE, severe corrosion attack

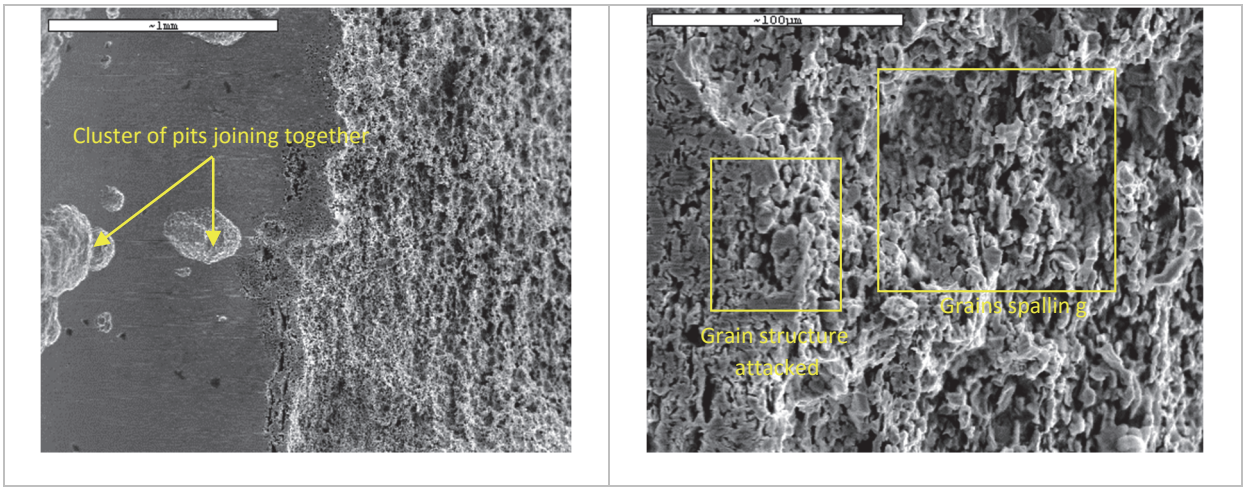

Figure 114: 0.25M $NaHCO_3$ + 0.125M Na_2CO_3 + 10%wt $NaNO_3$, 23°C, -600 mV SCE, severe corrosion attack

Effect of electrochemical potential at 75°C

As presented above, the steel can suffer from significant stress corrosion cracking in bicarbonate / carbonate environments in the presence of nitrates at 75°C at potentials associated with the active-passive transition region ($E>E_p$). Similarly to pure bicarbonate/carbonate systems, the mode of cracking for this system in the active-passive transition region is intergranular (see Figure 115 to Figure 117).

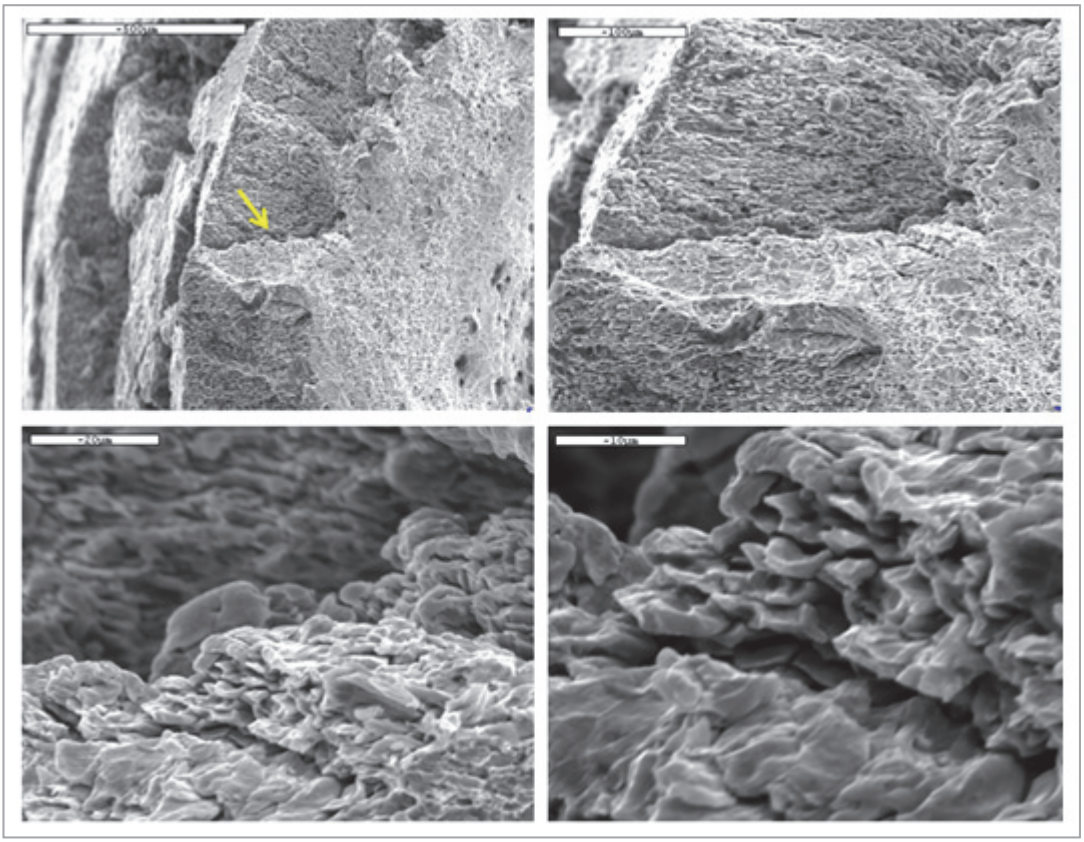

Figure 115: 0.70 M $NaHCO_3$ + 0.35 M Na_2CO_3 + 10%wt $NaNO_3$, 75°C, -650mV SCE, i.g. SCC on fracture surface

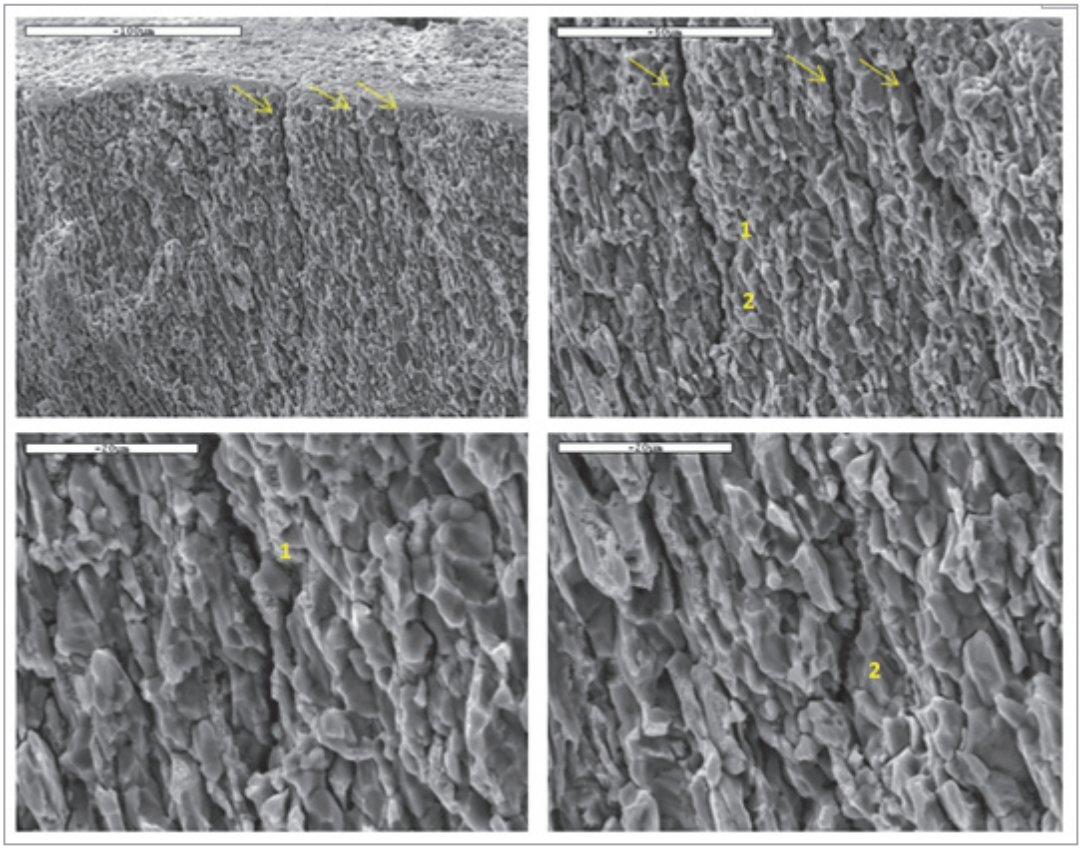

Figure 116: 0.70 M $NaHCO_3$ + 0.35 M Na_2CO_3 + 10%wt $NaNO_3$, 75°C, -650mV SCE, secondary i.g. cracks propagating perpendicularly from gauge surface

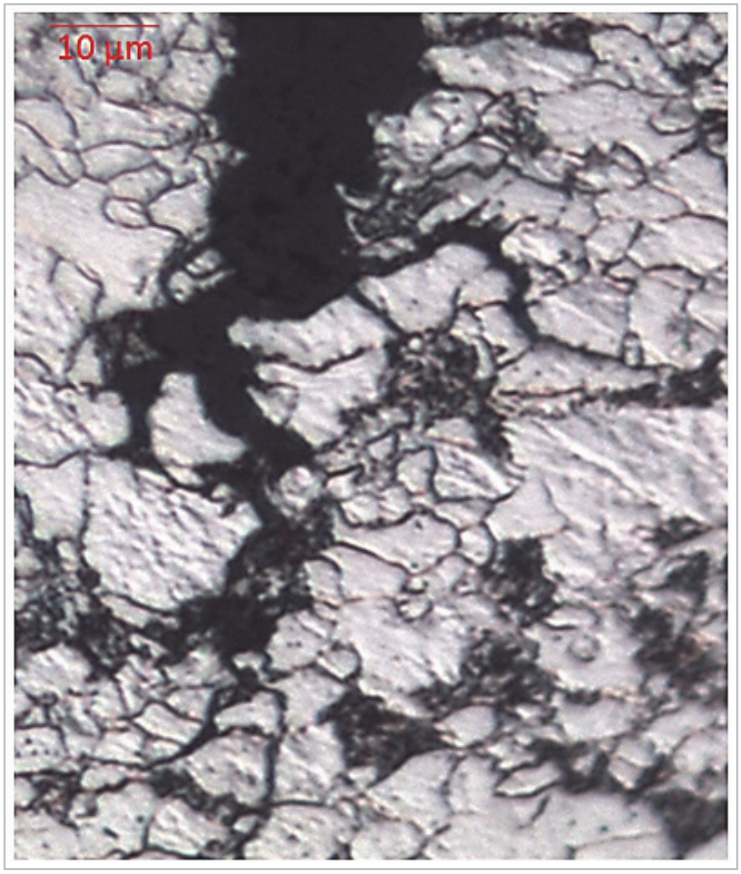

Figure 117: 0.70 M $NaHCO_3$ + 0.35 M Na_2CO_3 + 10%wt $NaNO_3$, 75°C, -650mV SCE, cross-section etched with Nital 2%vol., i.g. cracking

At potentials between E_{corr} and E_p, which is related to the material active region, stress corrosion cracking is still possible (Figure 118) but, similarly to pure bicarbonate/carbonate systems, the mode of cracking shifts to transgranular (see Figure 119 to Figure 121). The susceptibility to cracking appears to be, however, decreased as the potential approaches the free corrosion potential E_{corr} (Figure 122).

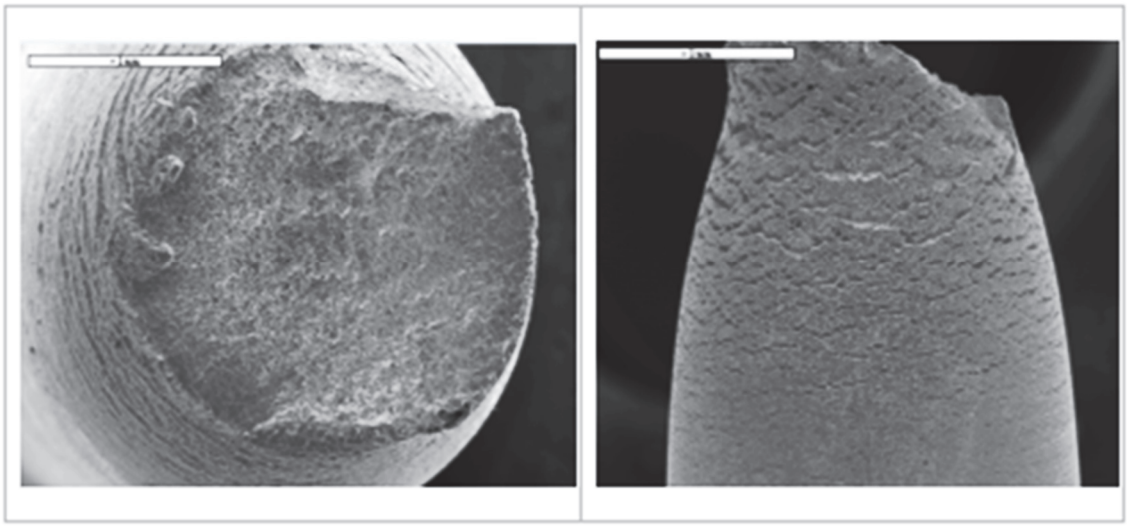

Figure 118: 0.70 M $NaHCO_3$ + 0.35 M Na_2CO_3 + 10%wt $NaNO_3$, 75°C, (a) -790 mV SCE and (b) -740 mV SCE, SSRT fractured specimen

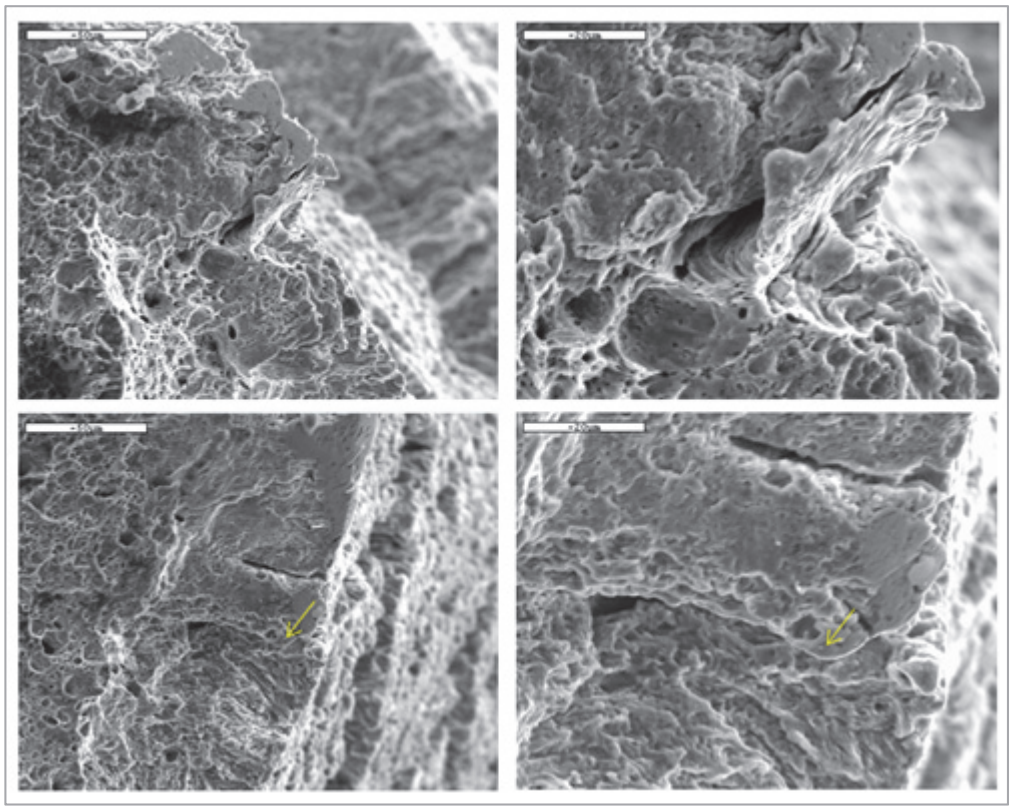

Figure 119: 0.70 M $NaHCO_3$ + 0.35 M Na_2CO_3 + 10%wt $NaNO_3$, 75°C, -740mV SCE, t.g. cracking on fracture surface

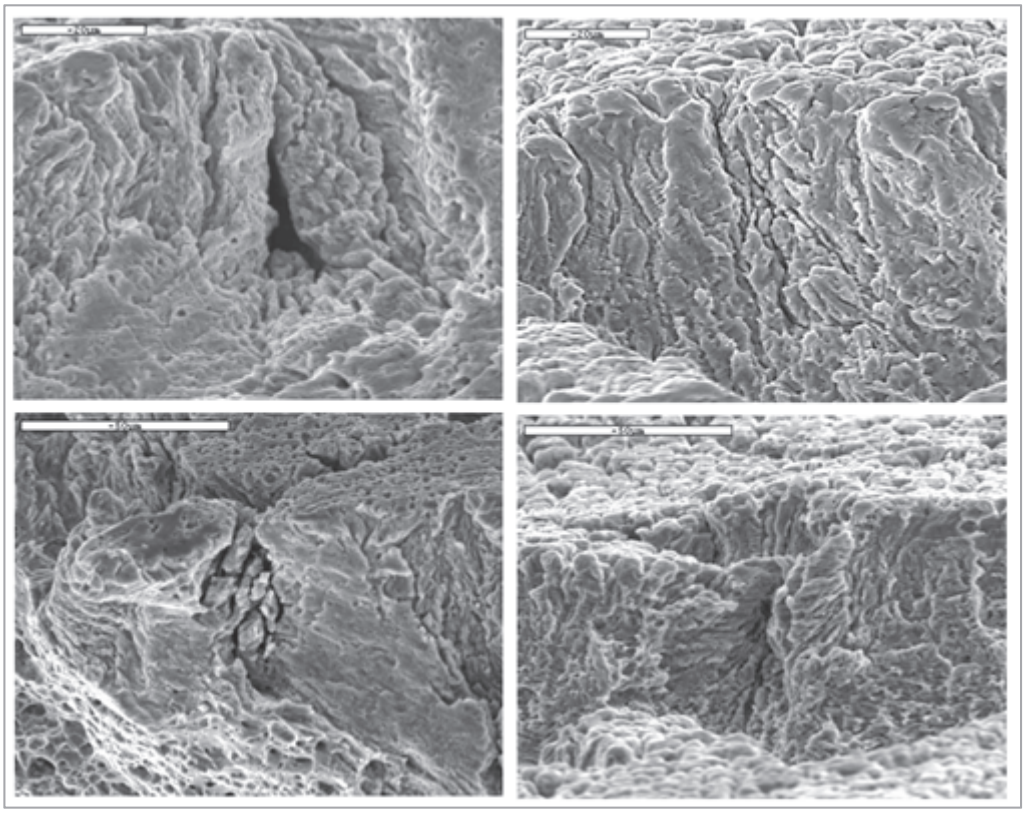

Figure 120: 0.70 M $NaHCO_3$ + 0.35 M Na_2CO_3 + 10%wt $NaNO_3$, 75°C, -740mV SCE, secondary t.g. cracking propagating perpendicularly from the gauge surface

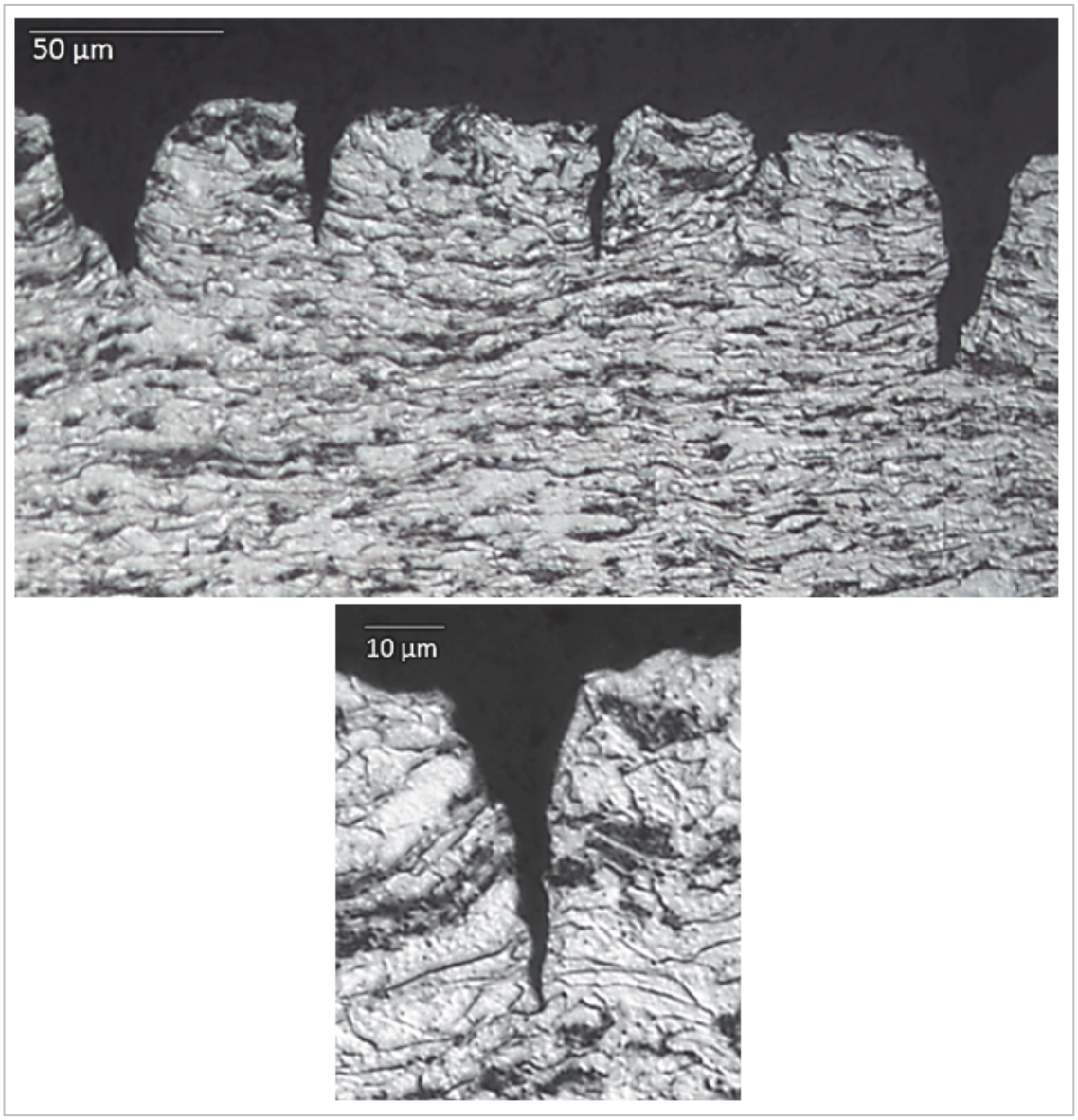

Figure 121: 0.70 M $NaHCO_3$ + 0.35 M Na_2CO_3 + 10%wt $NaNO_3$, 75°C, -740mV SCE, cross-section etched with Nital 2%vol., t.g. SCC

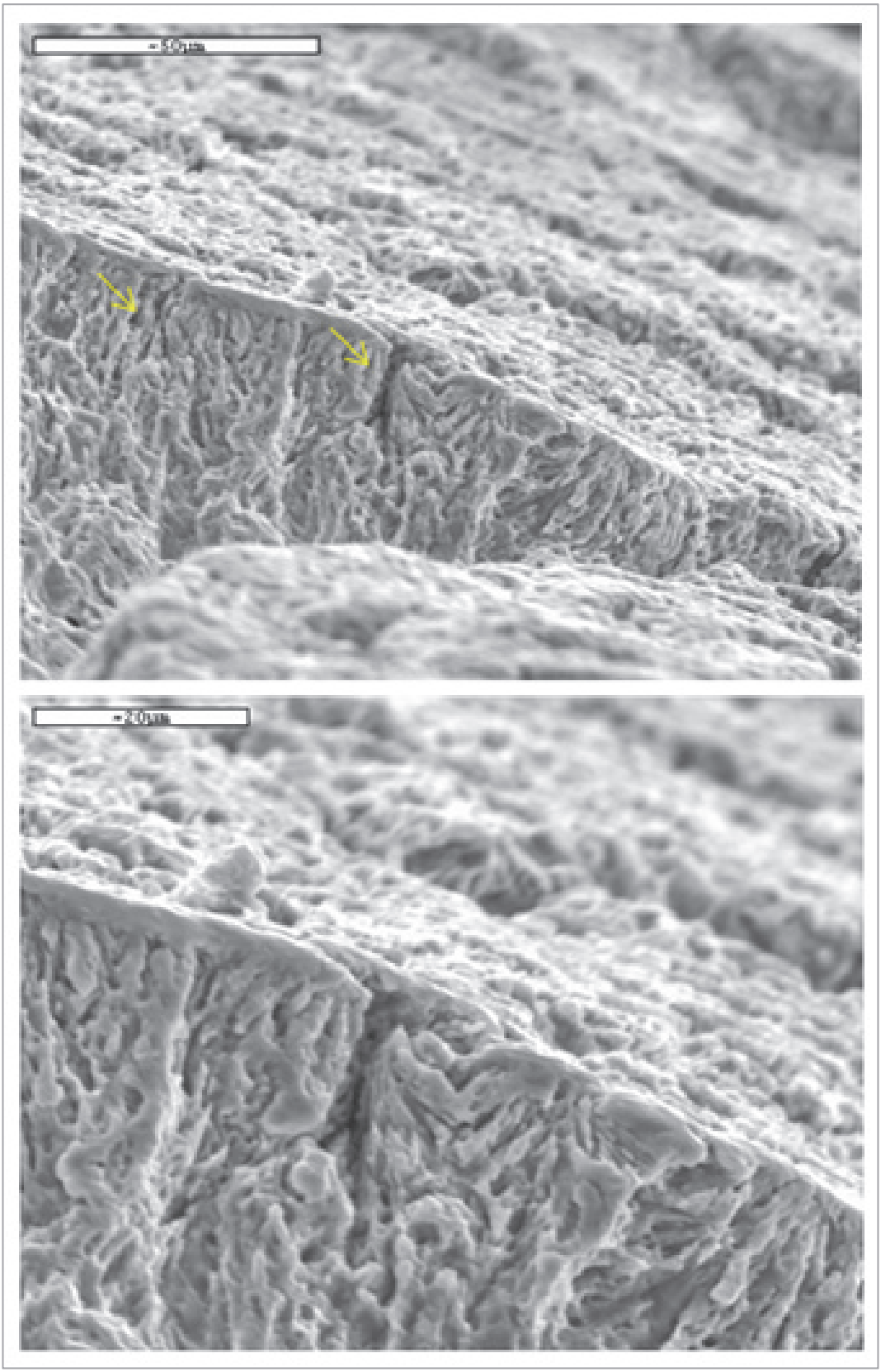

Figure 122: 0.70 M $NaHCO_3$ + 0.35 M Na_2CO_3 + 10%wt $NaNO_3$, 75°C, -790mV SCE, small t.g. cracking at potentials closer to free corrosion potentials

D. Presence of sulphites in bicarbonate /carbonate systems

Effect of bicarbonate / carbonate concentrations at 75°C

In the range of potentials associated with active-passive transition ($E>E_p$), the appearance of the fractured specimen side surface (Figure 123 and Figure 124) suggests that the steel has some degree of susceptibility in concentrated bicarbonate / carbonate aqueous environments (0.7M $NaHCO_3$ / 0.35M Na_2CO_3) with the additional presence of sulphites at 75°C. However, the susceptibility to Stress Corrosion Cracking in the presence of sulphite (Figure 125) appears to be less than in the pure concentrated bicarbonate / carbonate systems (0.70 M $NaHCO_3$ / 0.35 M Na_2CO_3) or in the presence of nitrates at 75°C.

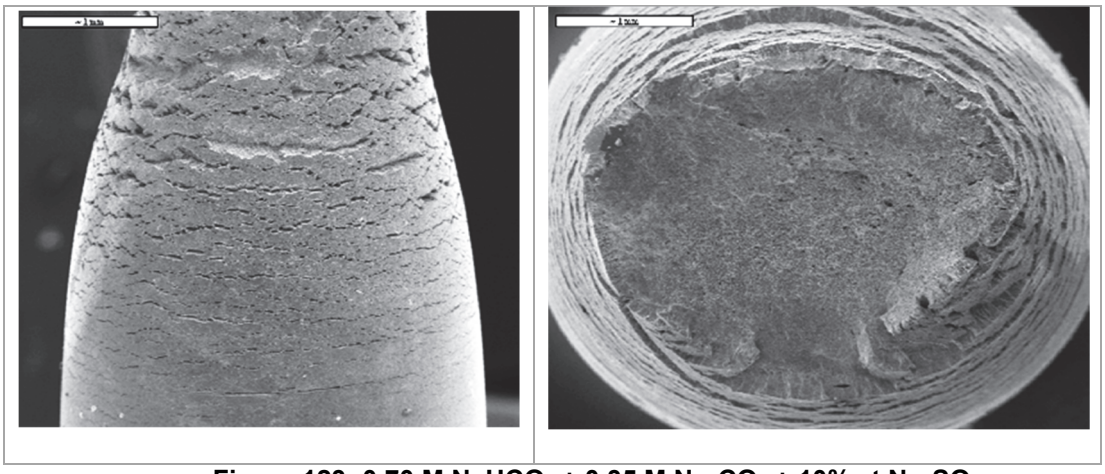

Figure 123: 0.70 M $NaHCO_3$ + 0.35 M Na_2CO_3 + 10%wt Na_2SO_3, 75°C, -710mVSCE, SSRT fractured specimen

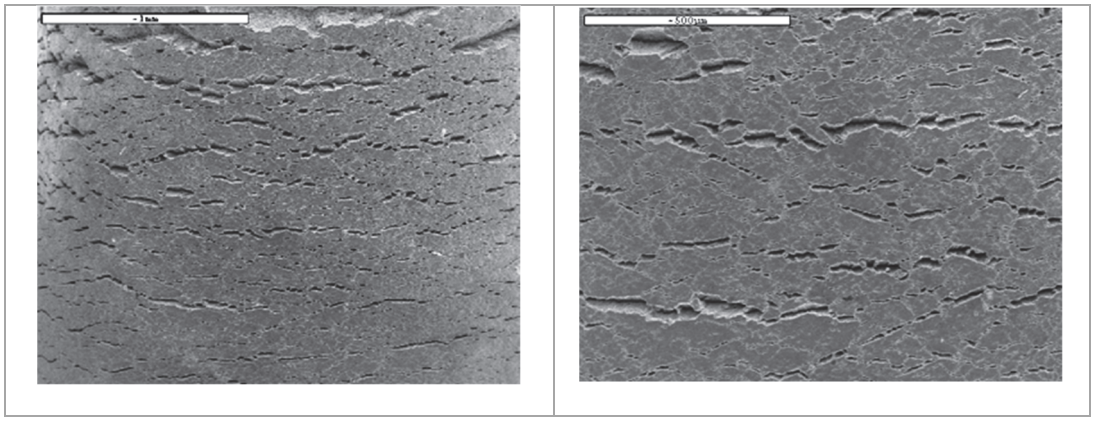

Figure 124: 0.70 M $NaHCO_3$ + 0.35 M Na_2CO_3 + 10%wt Na_2SO_3, 75°C, -710mVSCE, colony of tiny and shallow stress corrosion cracks

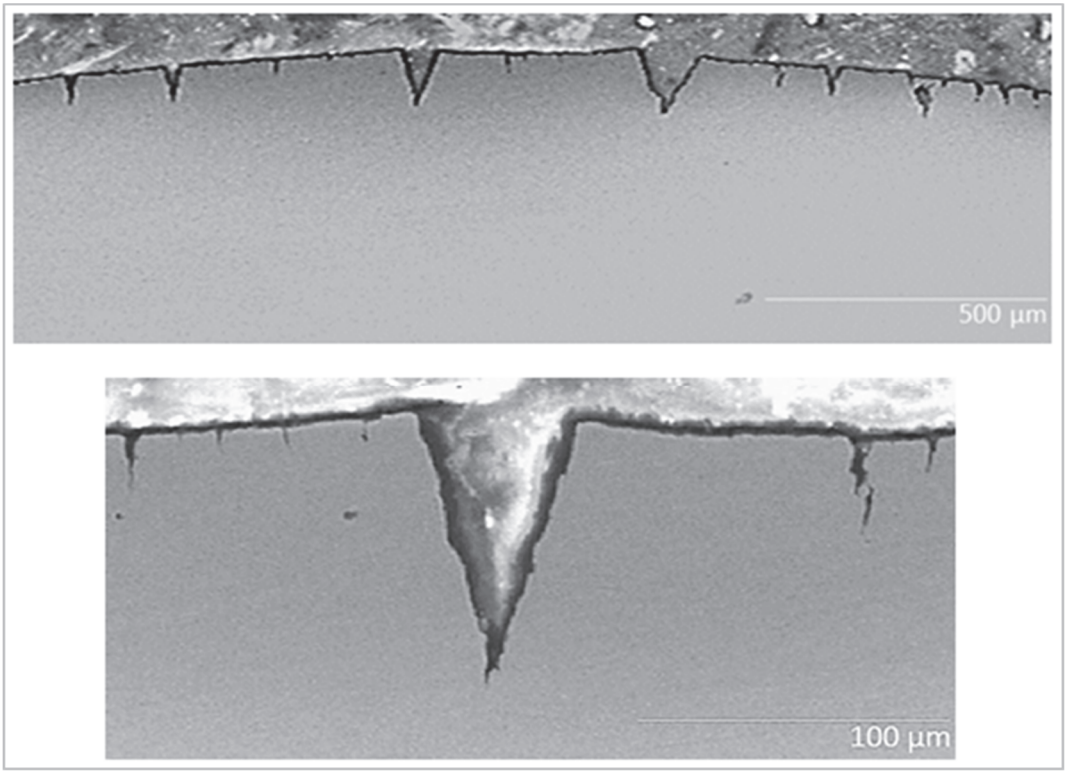

Figure 125: 0.70 M $NaHCO_3$ + 0.35 M Na_2CO_3 + 10%wt Na_2SO_3, 75°C, -710 mV SCE, cross-section polished to 1µm, stress corrosion cracks

Effect of temperature

Similarly to pure bicarbonate / carbonate systems or in the presence of nitrates, the susceptibility to SCC in the active-passive transition region appears to decrease with temperature in the presence of nitrates.

At 23°C, in the range of potentials associated with active-passive transition, the materials exposed to 0.70 M $NaHCO_3$ + 0.35 M Na_2CO_3 + 10%wt Na_2SO_3 environments suffer from significant plastic deformation as illustrated by the magnitude of necking on the fracture face. The side surface of the specimen appears irregular, which indicates the material has suffered from localised corrosion processes (Figure 126). The cross-section of the SSRT specimen (Figure 127) indicates the presence of tiny surface pits. The bottoms of the deeper pits are mostly rounded or blunt and do not necessarily indicate that they could develop into cracks over time.

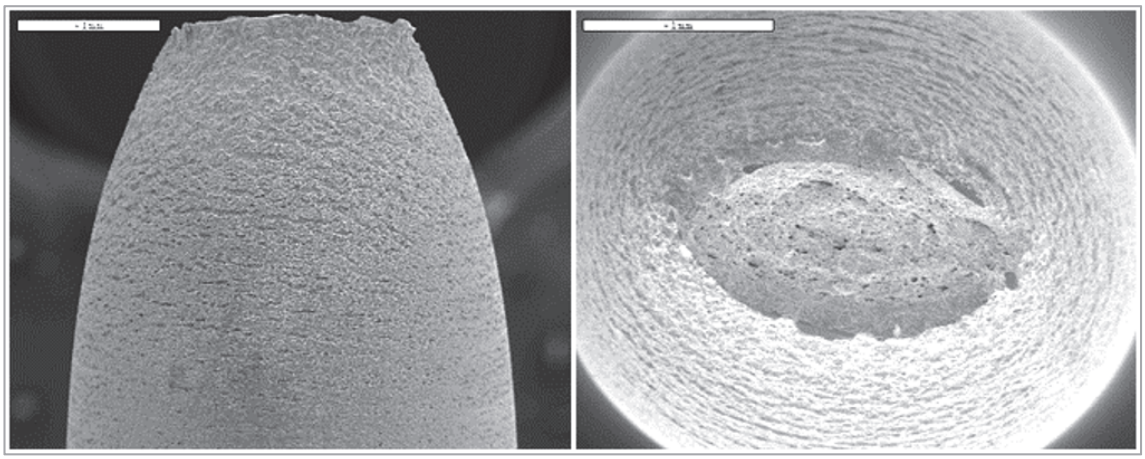

Figure 126: 0.70 M $NaHCO_3$ + 0.35 M Na_2CO_3 + 10%wt Na_2SO_3, 23°C, -670 mV SCE, SSRT fractured specimen

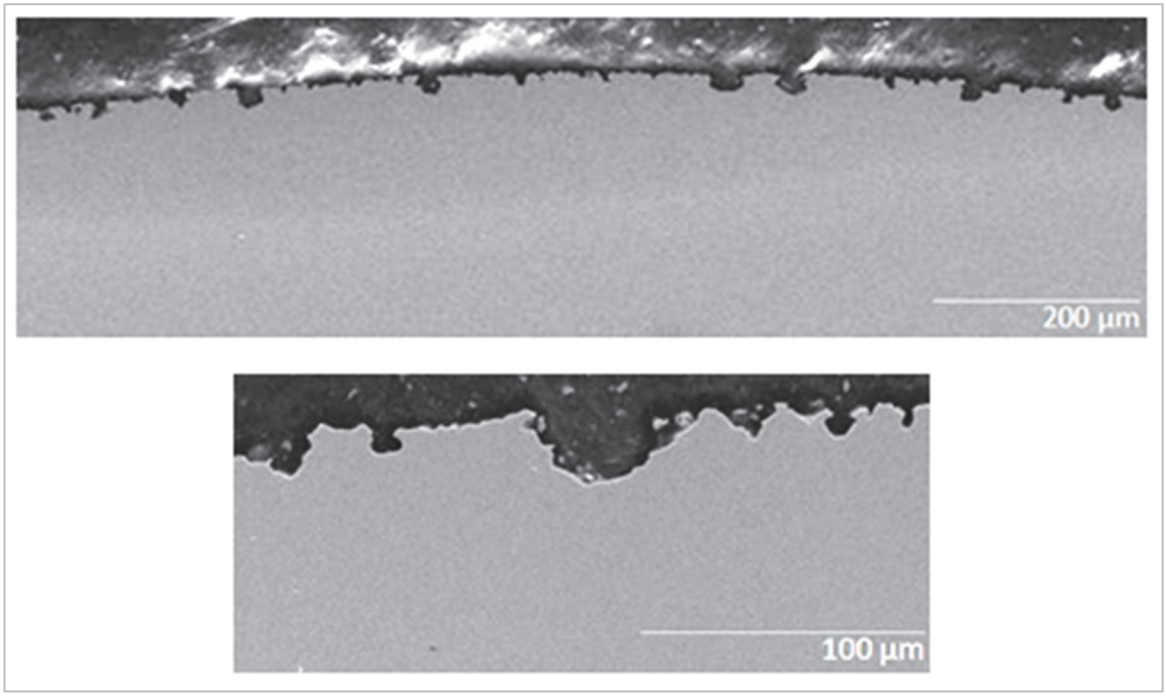

Figure 127: 0.70 M $NaHCO_3$ + 0.35 M Na_2CO_3 + 10%wt Na_2SO_3, 23°C, -670 mV SCE, cross-section

Effect of electrochemical potential at 75°C

In the active-passive transition region, the steel is susceptible to SCC. However, in contrast to pure bicarbonate/carbonate systems or in the presence of nitrates, the mode of cracking for the sulphite-containing system in the active-passive transition region is transgranular (see Figure 128).

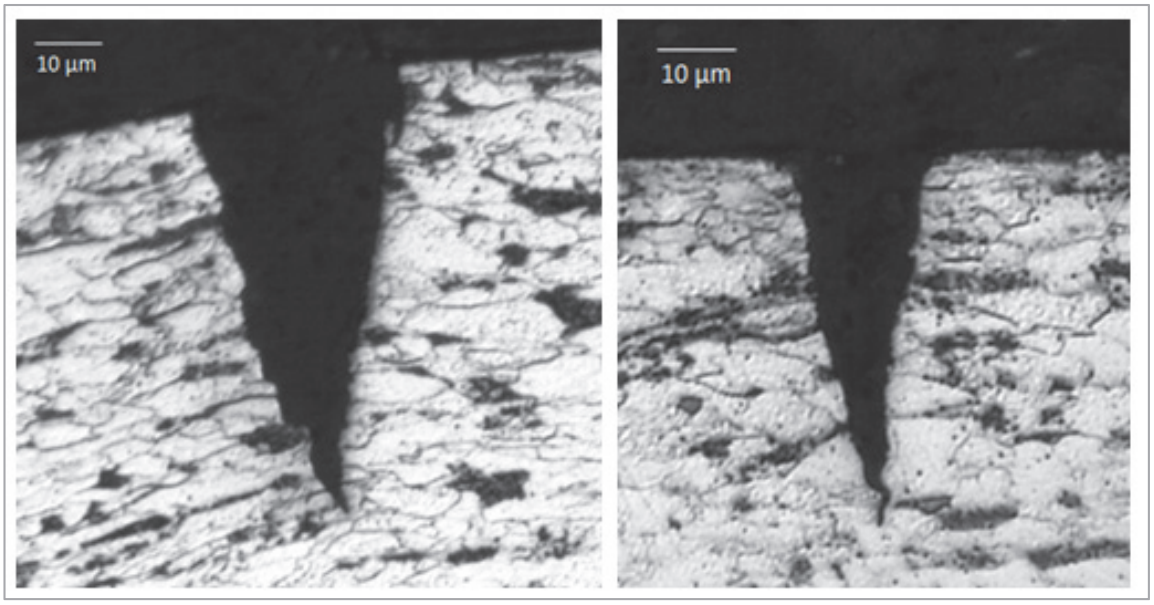

Figure 128: 0.70 M $NaHCO_3$ + 0.35 M Na_2CO_3 + 10%wt Na_2SO_3, 75°C, -710mV SCE, cross-section etched with Nital 2%vol., t.g. SCC

At potentials between E_{corr} and E_p, which is related to the material active region, stress corrosion cracking is still possible (Figure 129). Similarly to pure bicarbonate/carbonate systems or in the presence of nitrates, the mode of cracking in the active region is transgranular (see Figure 130, Figure 131, Figure 132, Figure 133). The susceptibility to cracking appears however to be decreased as the potential tends to the free corrosion potential E_{corr} (Figure 132).

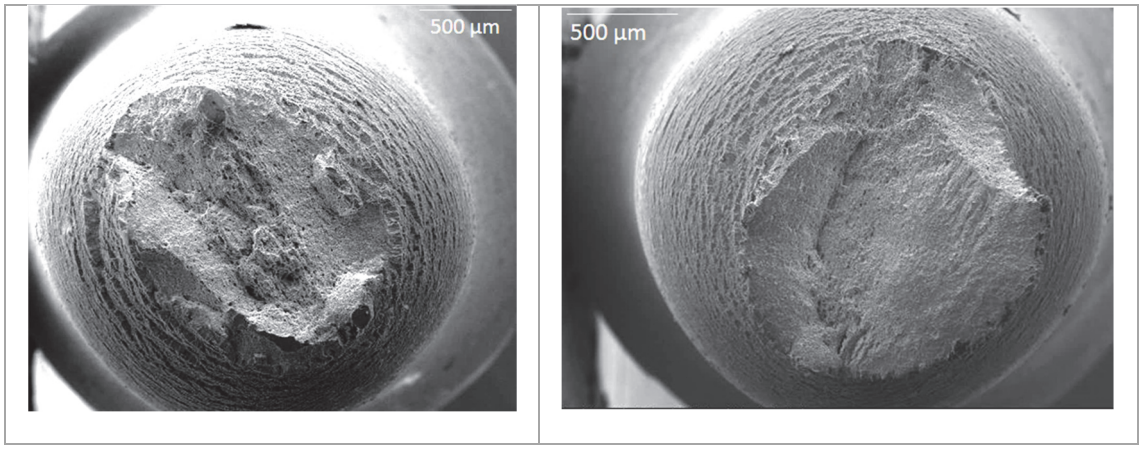

Figure 129: 0.70 M $NaHCO_3$ + 0.35 M Na_2CO_3 + 10%wt Na_2SO_3, 75°C, (a) -790 mV SCE and (b) -805 mV SCE, SSRT fractured specimen

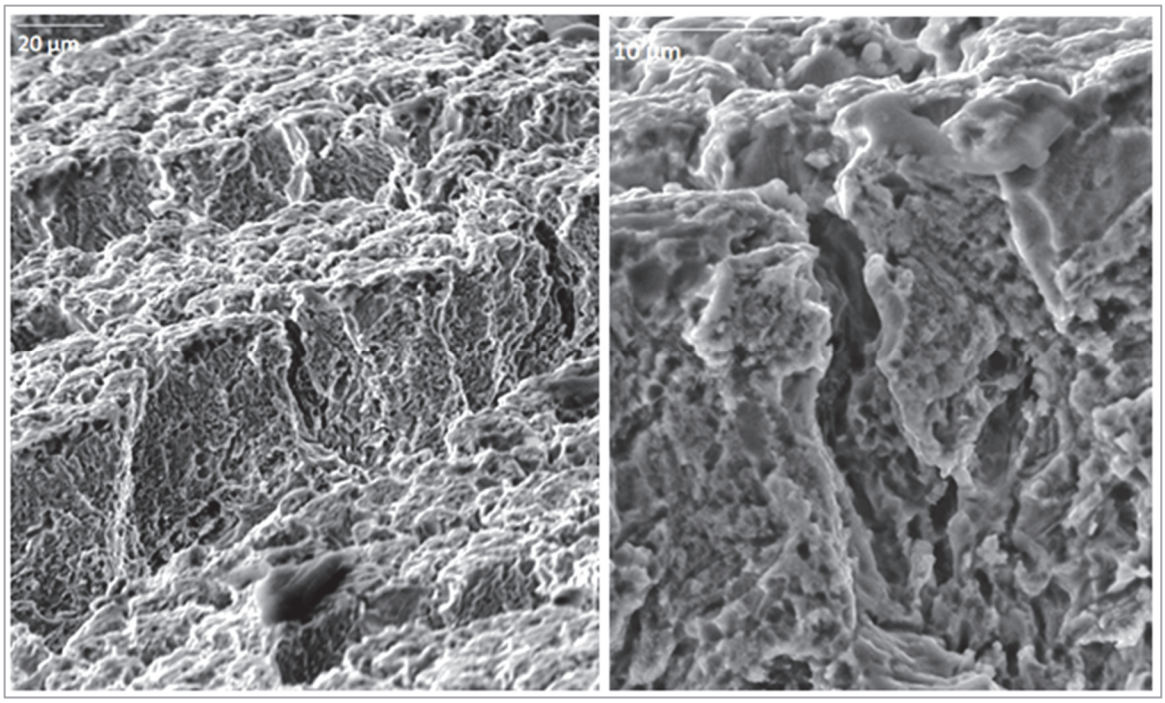

Figure 130: 0.70 M $NaHCO_3$ + 0.35 M Na_2CO_3 + 10%wt Na_2SO_3, 75°C, -790 mV SCE, t.g. SCC

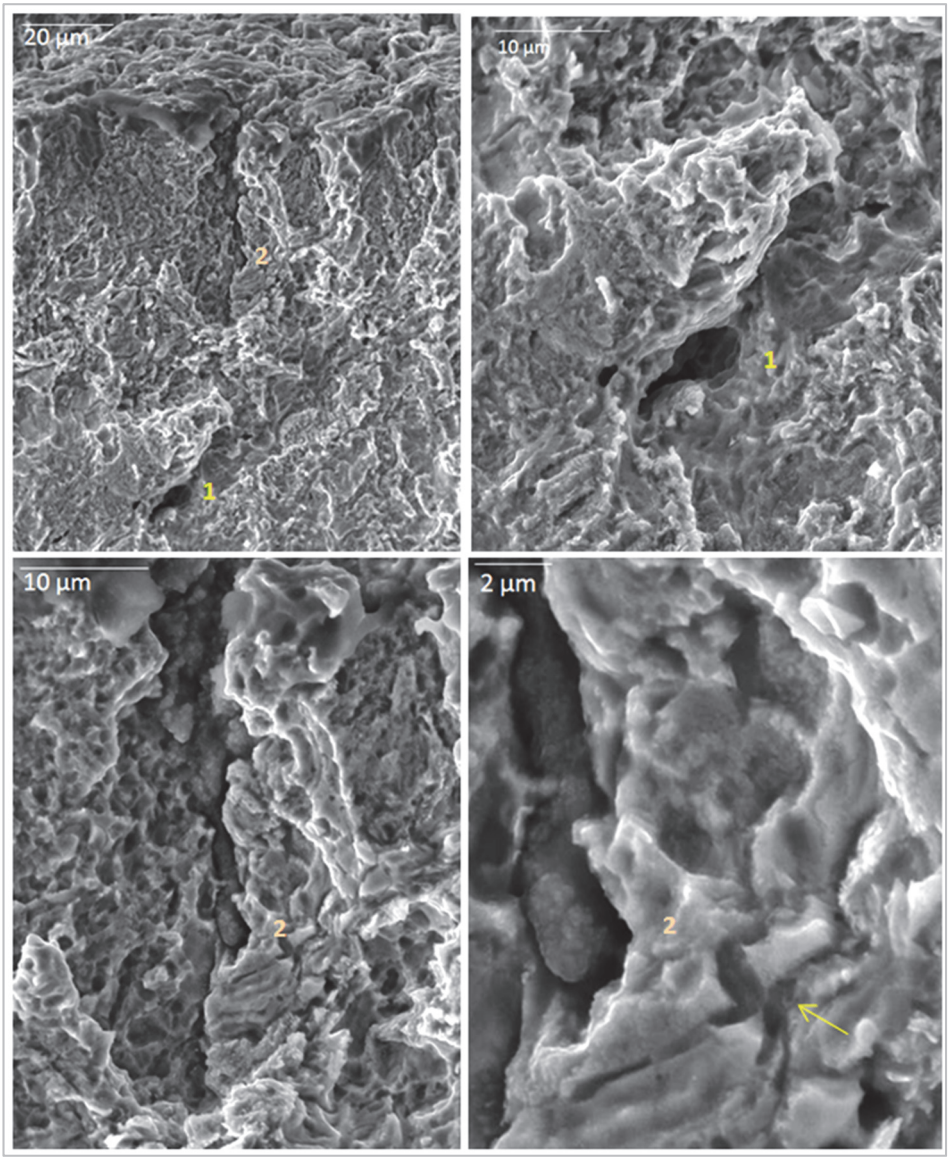

Figure 131: 0.70 M $NaHCO_3$ + 0.35 M Na_2CO_3 + 10%wt Na_2SO_3, 75°C, -790 mV SCE, t.g. SCC

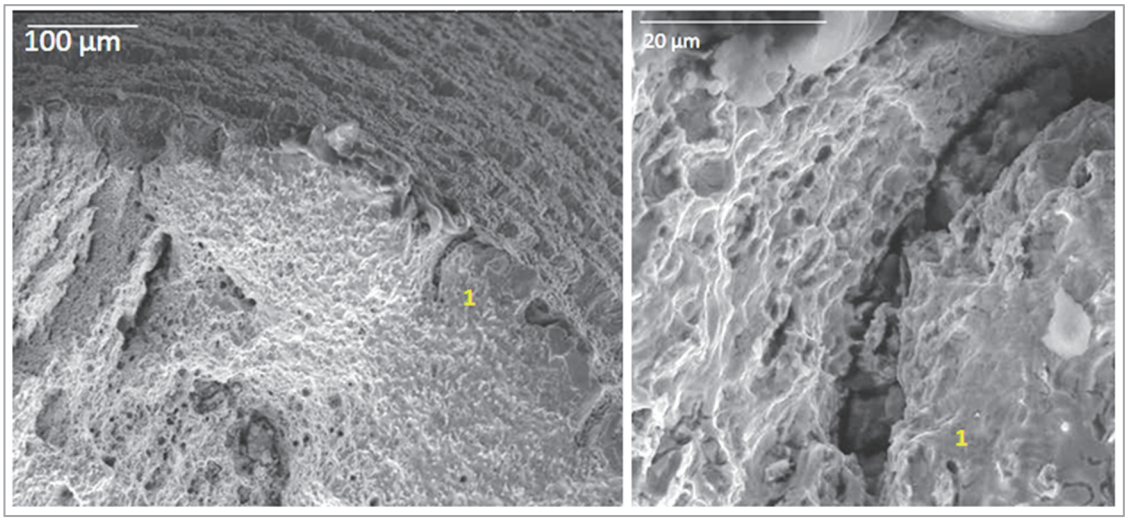

Figure 132: 0.70 M $NaHCO_3$ + 0.35 M Na_2CO_3 + 10%wt Na_2SO_3, 75°C, -840 mV SCE, t.g. SCC

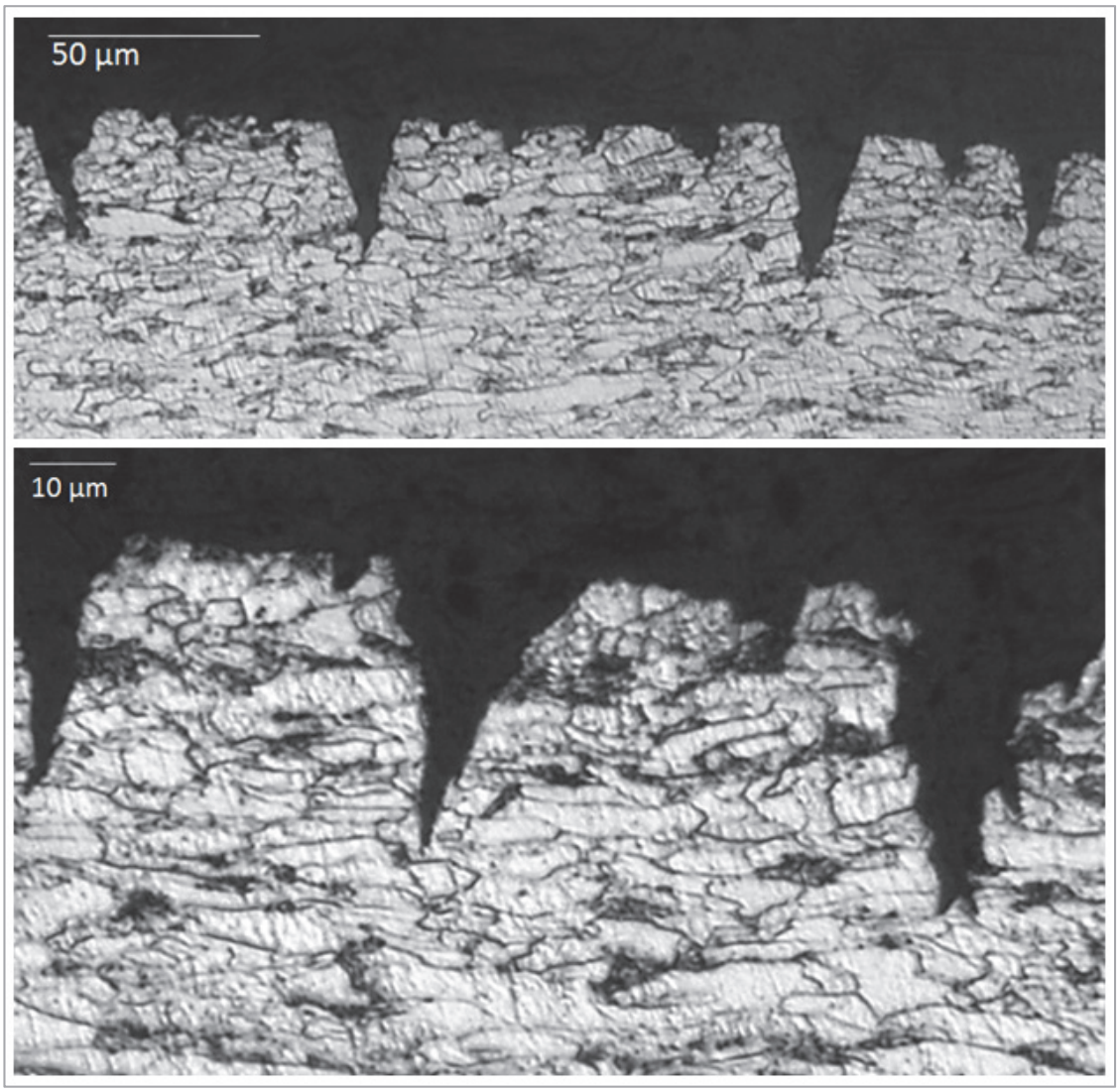

Figure 133: 0.70 M $NaHCO_3$ + 0.35 M Na_2CO_3 + 10%wt Na_2SO_3, 75°C, -790 mV SCE, cross-section etched with Nital 2%vol., t.g. SCC

5.1.2. CO_2-saturated systems

A. Summary of findings: SCC susceptibility and mode of cracking

The susceptibility and the mode of cracking in the different test environments in the presence of 1 bar gaseous CO_2 is initially qualitatively presented following scanning electron and optical microscopy examination. The same approach described for the CO_2-free systems, in section 5.1.1-A, is used.

The results are summarised in Table 19 and Table 20. For each specific environment only the potential, at which the "*maximum*" susceptibility to SCC was identified, is presented in these tables in order to facilitate comparison between environmental parameters:

- Table 19 Qualitative susceptibility of SCC in concentrated bicarbonate / carbonate systems (0.70M $NaHCO_3$ + 0.35M Na_2CO_3), saturated with 1 bar CO_2, with or without nitrates or sulphites, at 75°C. The susceptibility is assessed over the range of potentials associated with the material active-passive transition domain (i.e. at potentials higher than E_p).
- Table 20: Qualitative susceptibility of SCC in concentrated bicarbonate / carbonate systems (0.70M $NaHCO_3$ + 0.35M Na_2CO_3), saturated with 1 bar CO_2, with or without nitrates or sulphites, at 75°C. The susceptibility is assessed over the range of potentials associated with the material active (dissolution) domain (i.e. at potentials between E_{corr} and E_p).

Table 19: Qualitative susceptibility to SCC and mode of cracking- concentrated bicarbonate / carbonate levels with CO_2 (1 bar), 75 °C, material active-passive region

Environment	Cross-Section		SCC presence	SCC severity	SCC mode
0.70M $NaHCO_3$ + 0.35M Na_2CO_3 -730 mV SCE	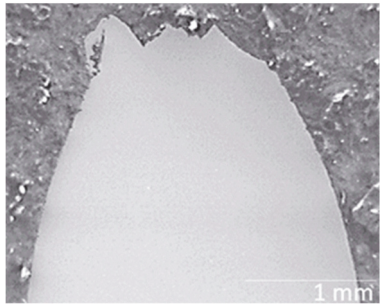	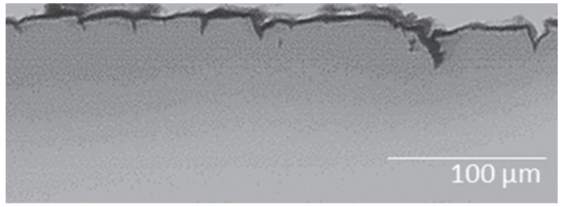	Y/N	0/1	t.g.
0.70M $NaHCO_3$ + 0.35M Na_2CO_3 + 10%wt $NaNO_3$ -640 mV SCE	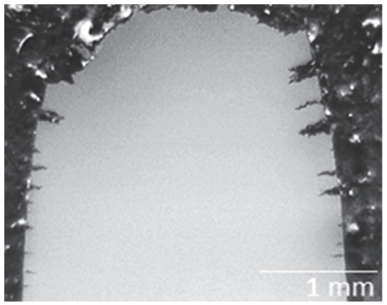	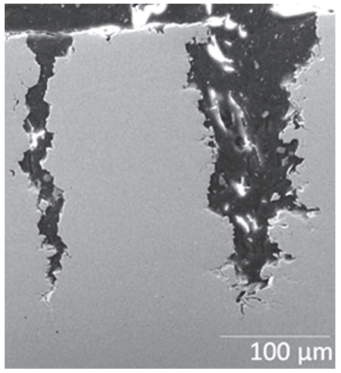	Y	3	i.g.
0.70M $NaHCO_3$ + 0.35M Na_2CO_3 + 10%wt Na_2SO_3 -680 mV SCE	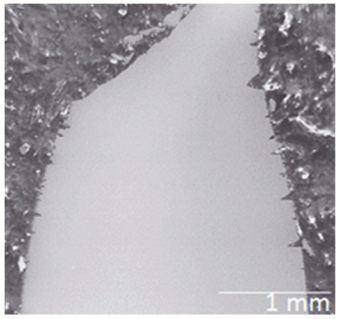	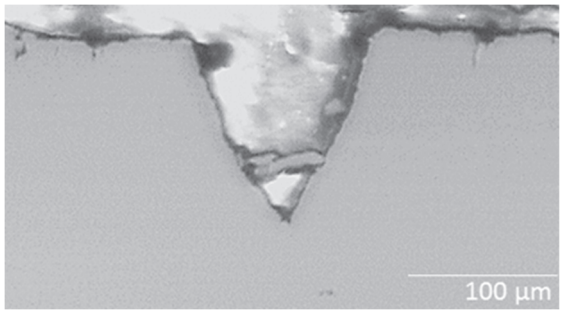	Y	2	t.g.

**Potential at which "maximum" susceptibility to SCC was identified for the specific environmental condition*

Table 20: Qualitative susceptibility to SCC and mode of cracking- concentrated bicarbonate / carbonate levels with CO_2 (1 bar), 75 °C, material active region

Environment	Cross-Section	SCC presence	SCC severity	SCC mode
0.70M $NaHCO_3$ + 0.35M Na_2CO_3 -800 mV SCE	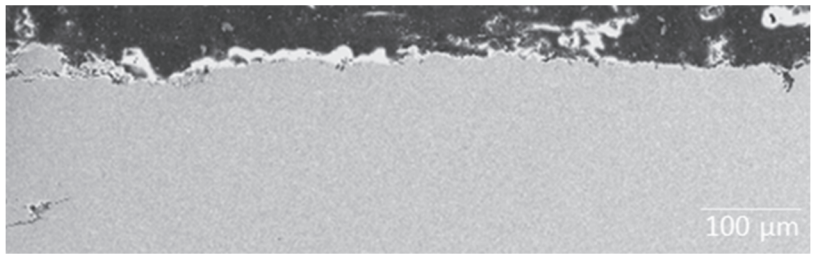	Y/N	0/1	t.g.
0.70M $NaHCO_3$ + 0.35M Na_2CO_3 + 10%wt $NaNO_3$ -800 mV SCE	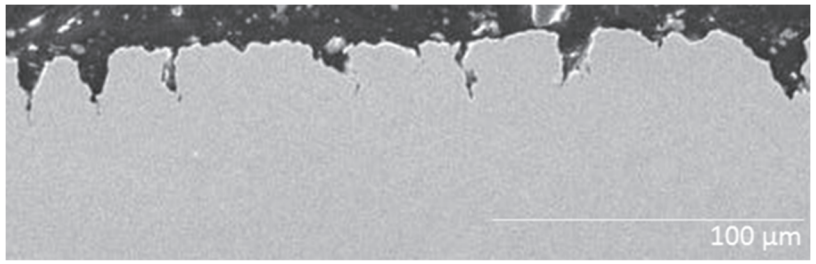	Y	1	t.g.
0.70M $NaHCO_3$ + 0.35M Na_2CO_3 + 10%wt Na_2SO_3 -750 mV SCE	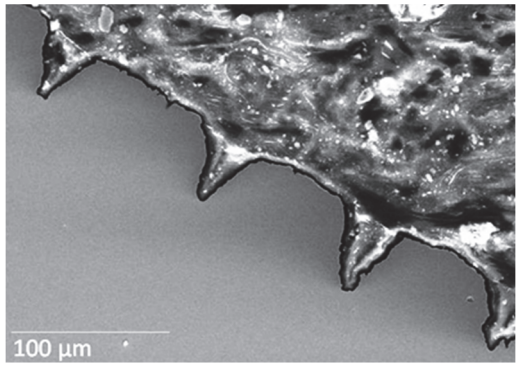	Y	2	t.g.

**Potential at which "maximum" susceptibility to SCC was identified for the specific environmental condition*

B. Pure bicarbonate /carbonate system, CO_2-saturated

SCC Susceptibility in Active-Passive transition region at 75°C

In the range of potentials associated with active-passive transition, the materials exposed to pure bicarbonate/carbonate environments saturated with CO_2 (1 bar) suffer from localised corrosion at 75°C (Figure 134). Visualisation of the SSRT specimen cross-section indicates the presence of surface pits, whose morphology resembles cracks at the initiation stage (Figure 135). The nature of the localised corrosion process is transgranular (Figure 136). Small transgranular cracks could be seen on the fracture surface (Figure 137).

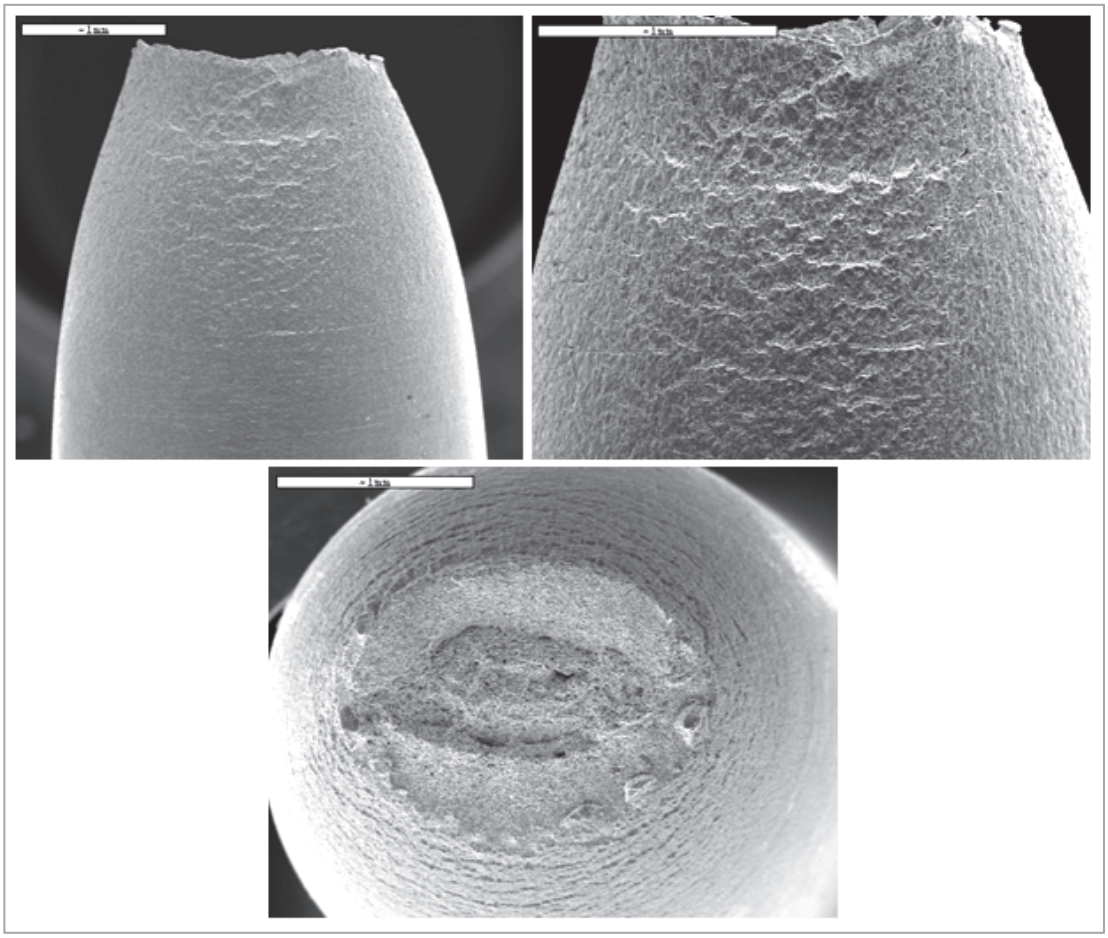

Figure 134: 0.70 M $NaHCO_3$ + 0.35 M Na_2CO_3, CO_2-saturated, 75°C, -730 mV SCE, SSRT fractured specimen

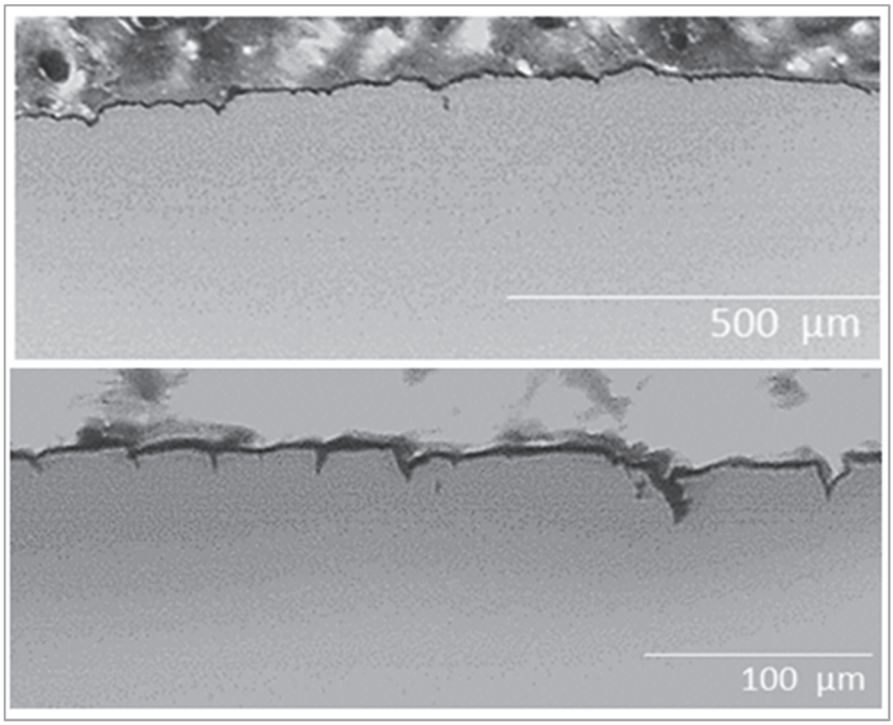

Figure 135: 0.70 M $NaHCO_3$ + 0.35 M Na_2CO_3, CO_2-saturated, 75°C, -730 mV SCE, cross - section polished to 1µm

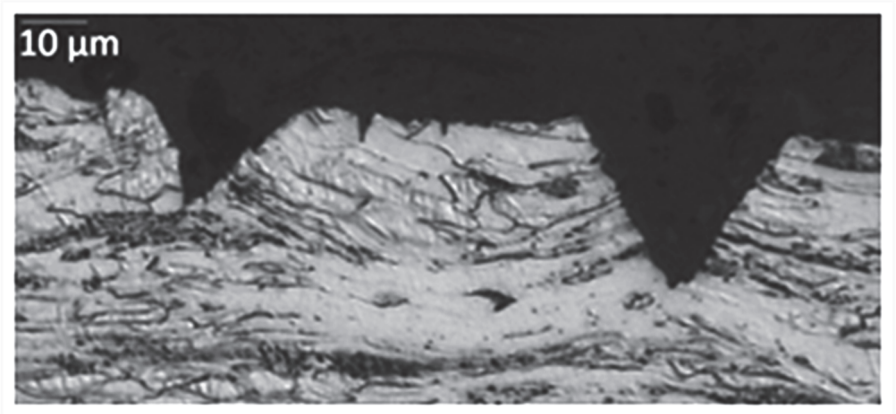

Figure 136: 0.70 M $NaHCO_3$ + 0.35 M Na_2CO_3, CO_2-saturated, 75°C, -730 mV SCE, cross - section etched to Nital 2%vol., transgranular localised corrosion process

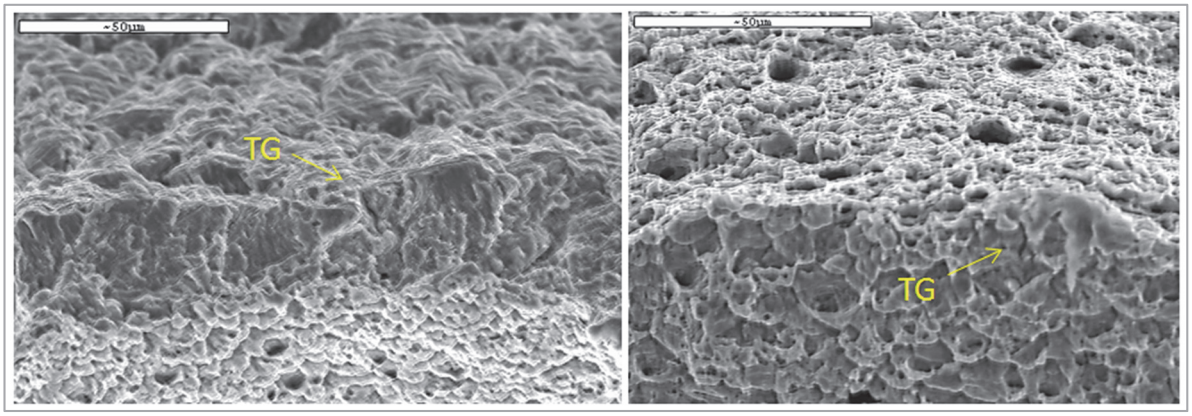

Figure 137: 0.70 M $NaHCO_3$ + 0.35 M Na_2CO_3, CO_2-saturated, 75°C, -730 mV SCE, minor t.g. **cracking on fracture surface**

SCC Susceptibility in active region at 75°C

In the range of potentials associated with active transition, the materials exposed to pure bicarbonate/carbonate environments saturated with CO_2 (1 bar) suffer some degree of localised corrosion at 75°C (Figure 138 and Figure 139). The nature of the localised corrosion process is transgranular (Figure 140). Secondary tiny transgranular cracks could be seen, Figure 141.

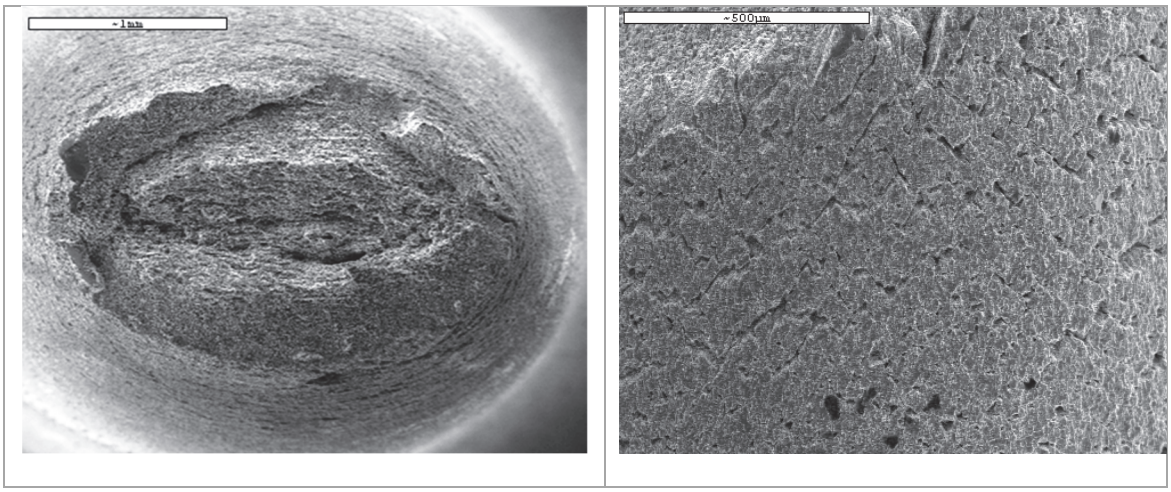

Figure 138: 0.70 M $NaHCO_3$ + 0.35 M Na_2CO_3, CO_2-saturated, 75°C, -800 mV SCE, SSRT fractured specimen

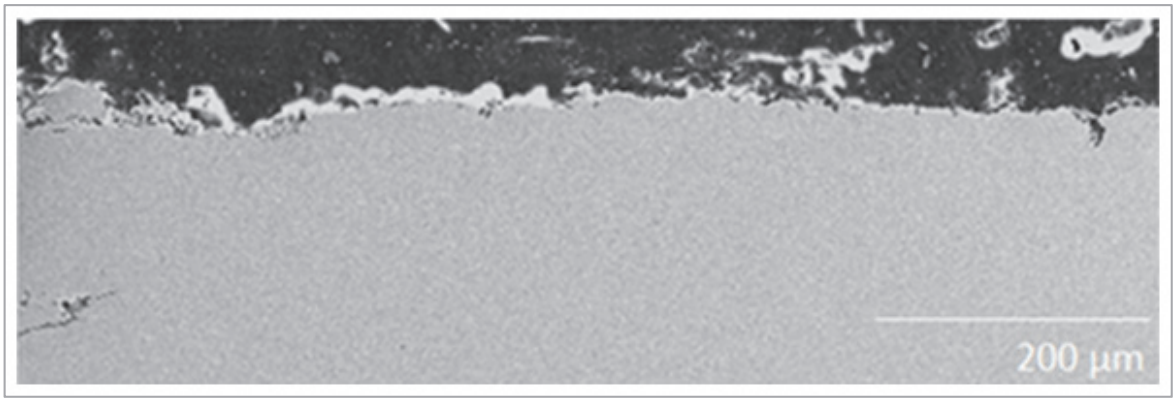

Figure 139: 0.70 M $NaHCO_3$ + 0.35 M Na_2CO_3, CO_2-saturated, 75°C, -800 mV SCE, cross-section (1 µm polished)

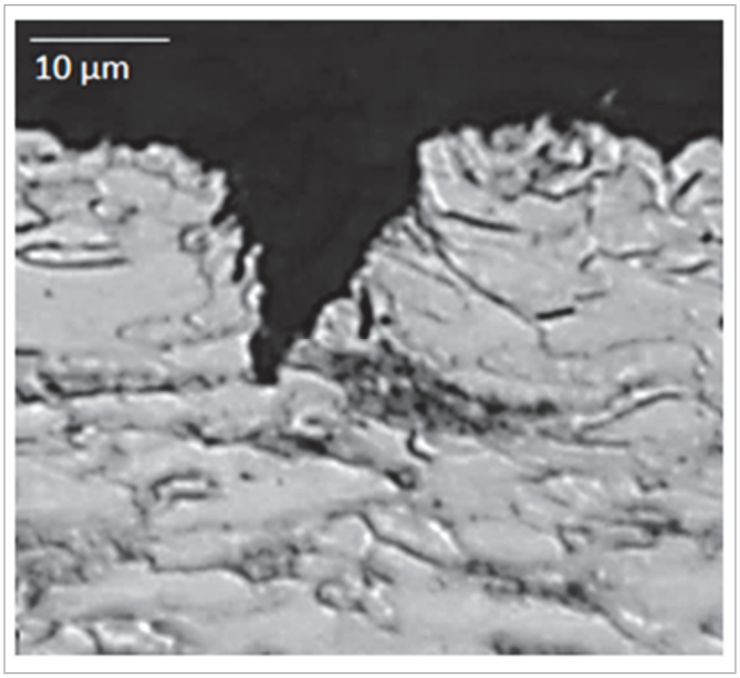

Figure 140: 0.70 M $NaHCO_3$ + 0.35 M Na_2CO_3, CO_2-saturated, 75°C, -800 mV SCE, cross-section etched with Nital 2%vol., transgranular localised corrosion process

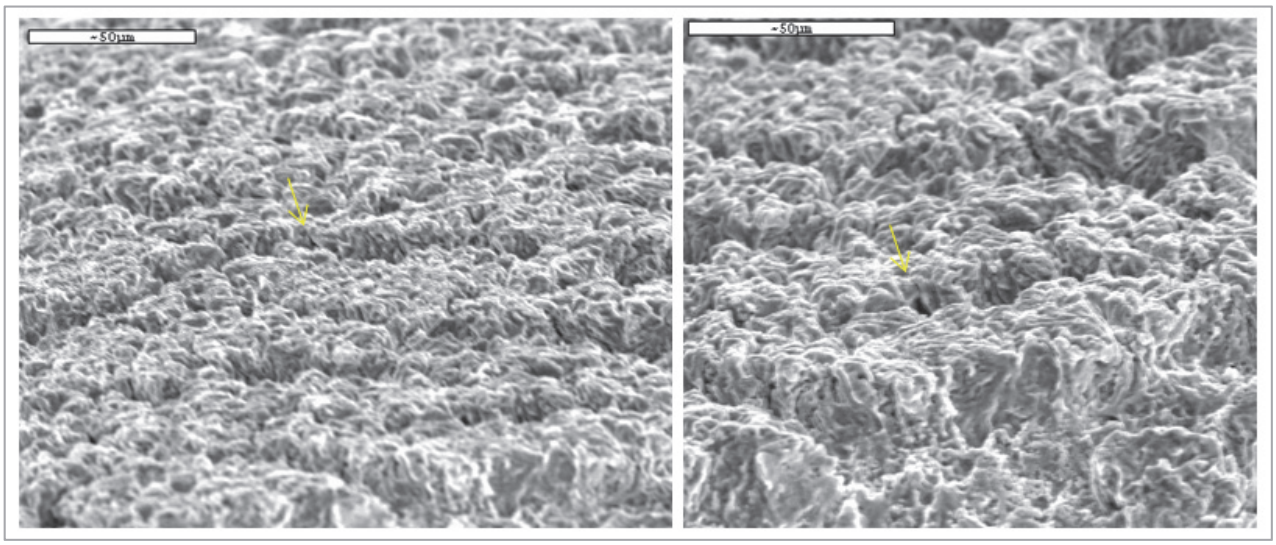

Figure 141: 0.70 M $NaHCO_3$ + 0.35 M Na_2CO_3, CO_2-saturated, 75°C, -800 mV SCE, very tiny secondary t.g. cracks

C. Presence of nitrates in bicarbonate /carbonate system, CO_2 saturated

SCC Susceptibility in active-passive transition region at 75°C

In the range of potentials associated with active-passive transition, the materials exposed to 0.70 M $NaHCO_3$ + 0.35 M Na_2CO_3 + 10%wt $NaNO_3$ environments saturated with CO_2 (1 bar) suffer from significant SCC at 75°C (Figure 142 and Figure 143). The nature of the SCC process is intergranular as illustrated by Figure 144 and Figure 145.

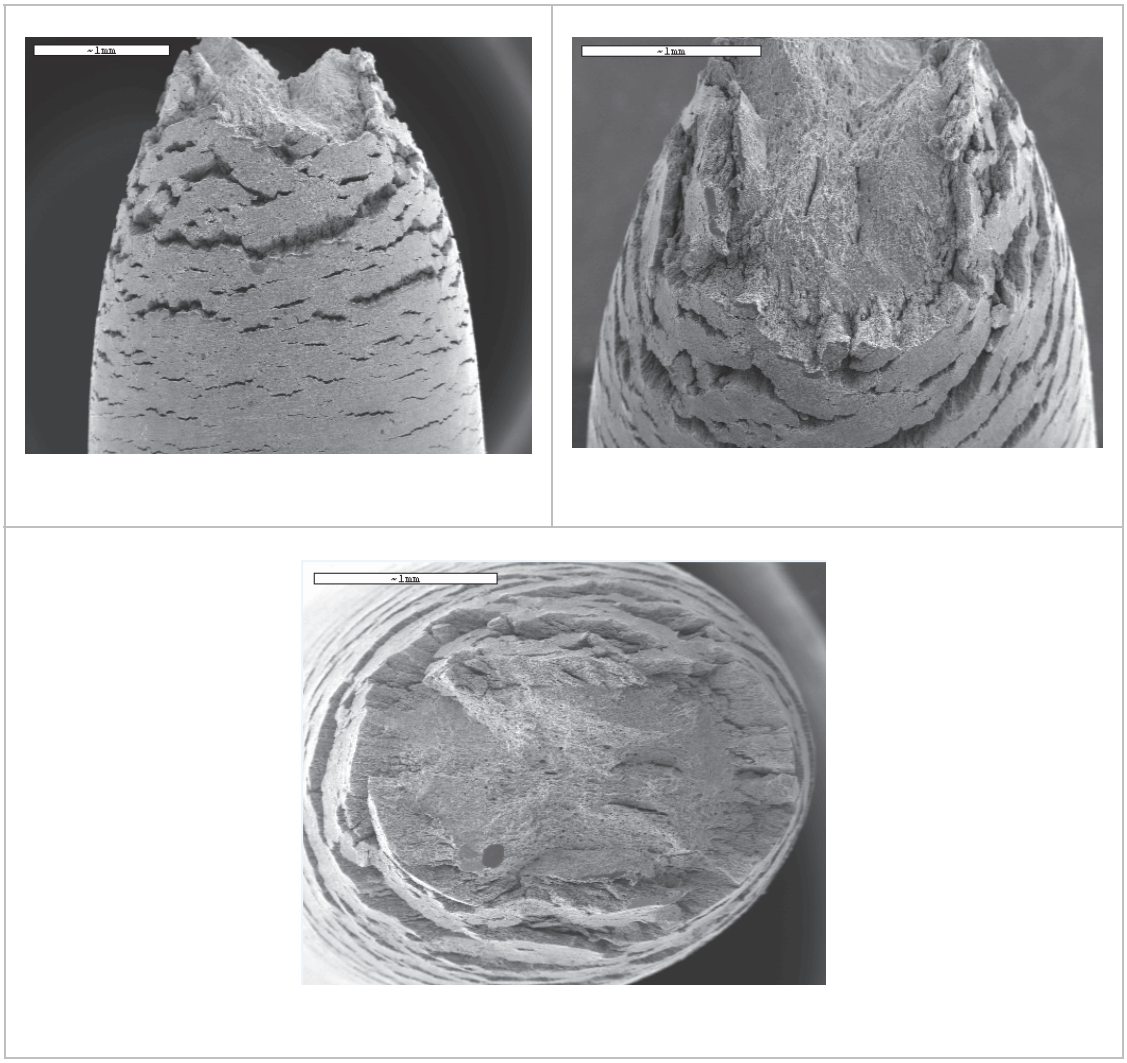

Figure 142: 0.70 M $NaHCO_3$ + 0.35 M Na_2CO_3 + 10%wt $NaNO_3$, CO_2-saturated, 75°C, -640 mV SCE, SSRT fractured specimen

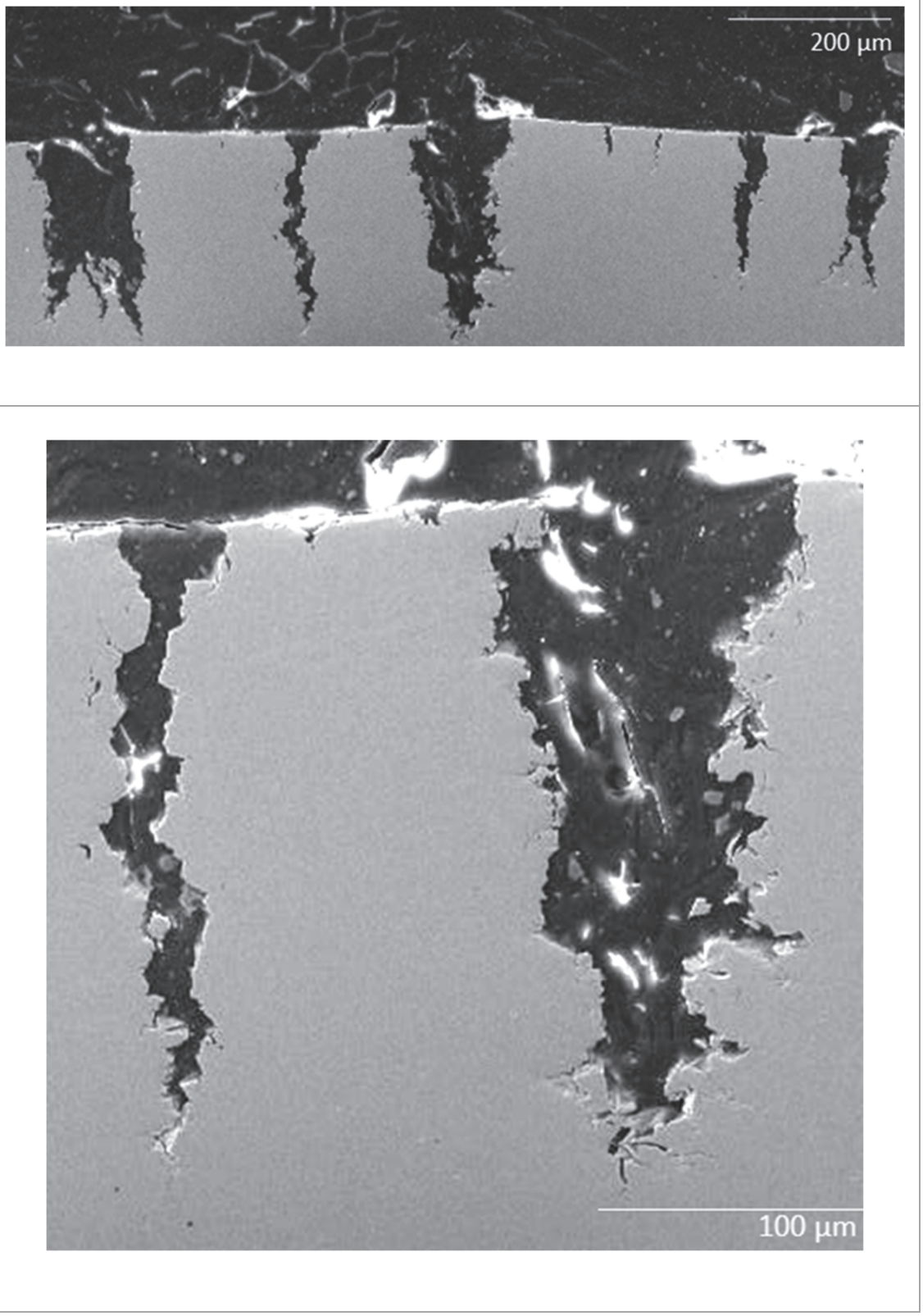

Figure 143: 0.70 M $NaHCO_3$ + 0.35 M Na_2CO_3 + 10%wt $NaNO_3$, CO_2-saturated, 75°C, -640 mV SCE, cross- section, significant stress corrosion cracking

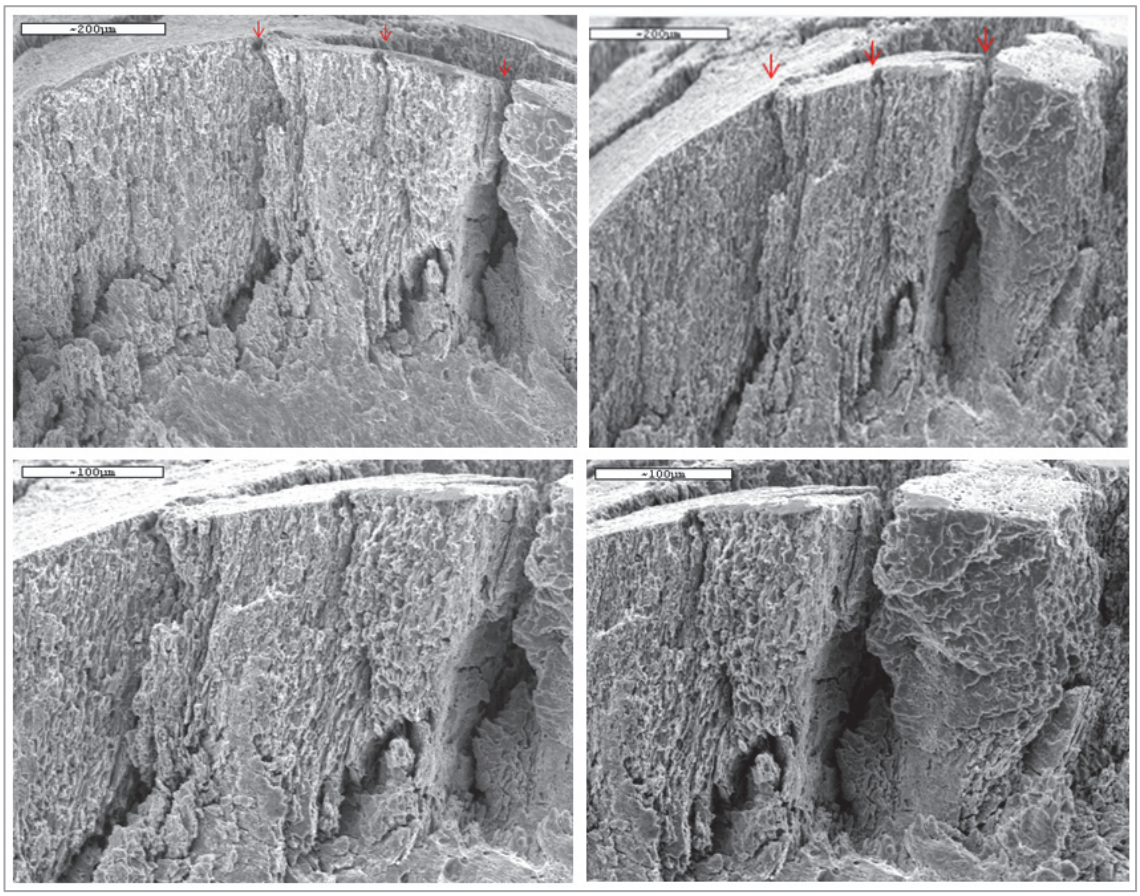

Figure 144: 0.70 M $NaHCO_3$ + 0.35 M Na_2CO_3 + 10%wt $NaNO_3$, CO_2-saturated, 75°C, -640 mV SCE, significant i.g. cracking on fracture surface

Figure 145: 0.70 M $NaHCO_3$ + 0.35 M Na_2CO_3 + 10%wt $NaNO_3$, CO_2-saturated, 75°C, -640 mV SCE, cross- section etched with Nital 2%vol., i.g. SCC

Susceptibility in Active- region at 75°C

In the range of potentials associated with active transition, the materials exposed to 0.70 M $NaHCO_3$ + 0.35 M Na_2CO_3 + 10%wt $NaNO_3$ environments saturated with CO_2 (1 bar) present some degree of susceptibility to SCC (Figure 146). The nature of the cracking is transgranular (Figure 147 and Figure 148).

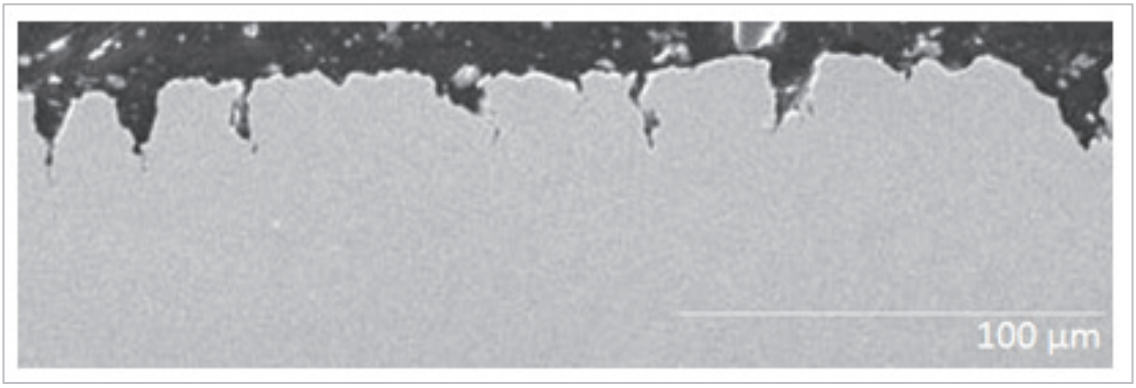

Figure 146: 0.70 M $NaHCO_3$ + 0.35 M Na_2CO_3 + 10%wt $NaNO_3$, 75°C, -640 mV SCE, cross- section (1 µm polish)

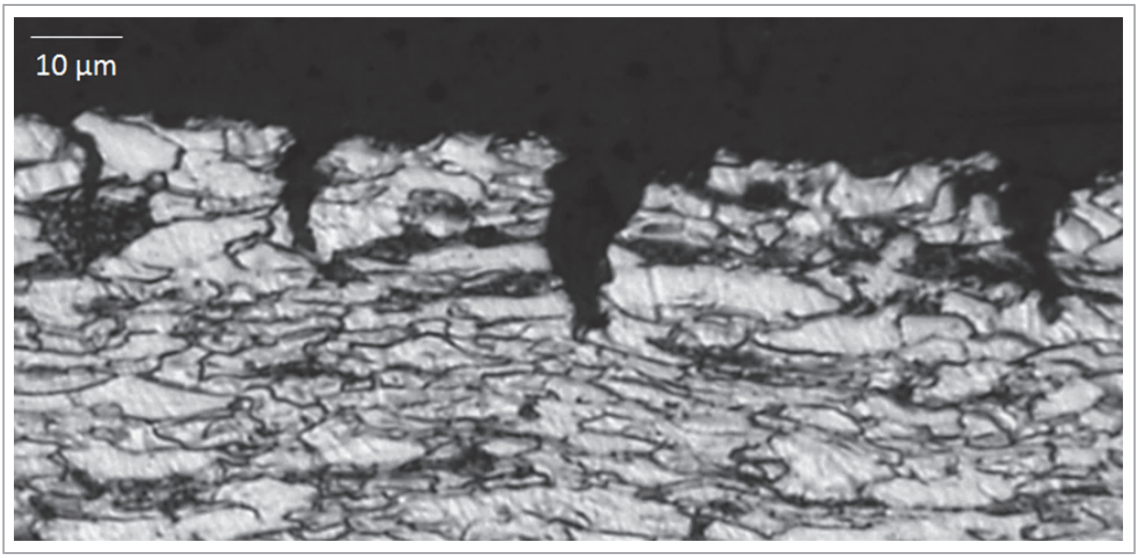

Figure 147: 0.70 M $NaHCO_3$ + 0.35 M Na_2CO_3 + 10%wt $NaNO_3$, 75°C, -640 mV SCE, cross- section etched with Nital 2%vol., t.g. cracking

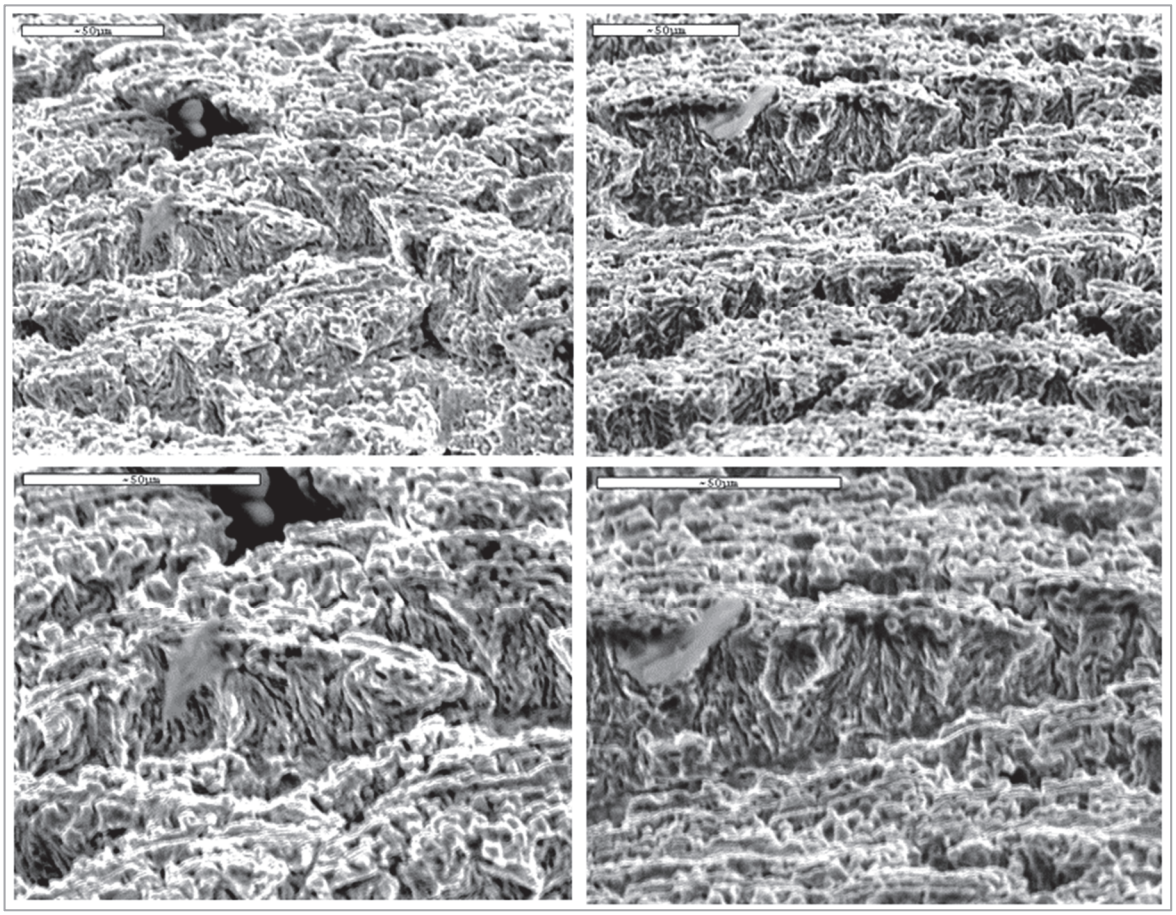

Figure 148: 0.70 M $NaHCO_3$ + 0.35 M Na_2CO_3 + 10%wt $NaNO_3$, 75°C, -640 mV SCE, secondary small t.g. cracking propagating perpendicularly from the gauge surface

D. Presence of sulphites in bicarbonate /carbonate system, CO_2-saturated

SCC Susceptibility in active-passive transition region at 75°C

In the range of potentials associated with active-passive transition, the material exposed to 0.70 M $NaHCO_3$ + 0.35 M Na_2CO_3 + 10%wt Na_2SO_3 environments saturated with CO_2 (1 bar) is susceptible to SCC (Figure 149 and Figure 150). In contrast to the nitrate-containing environment, the nature of the cracking is transgranular (Figure 151 and Figure 152).

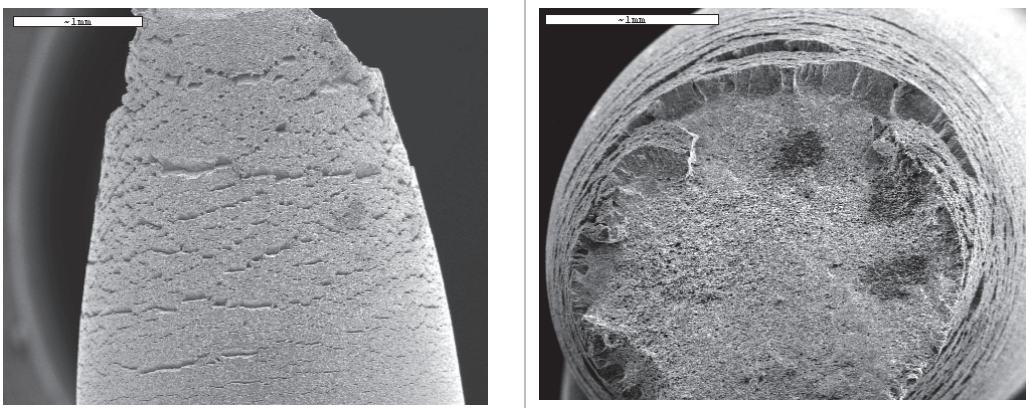

Figure 149: 0.70 M $NaHCO_3$ + 0.35 M Na_2CO_3 + 10%wt Na_2SO_3, CO_2-saturated, 75°C, -680 mV SCE, SSRT fractured specimen

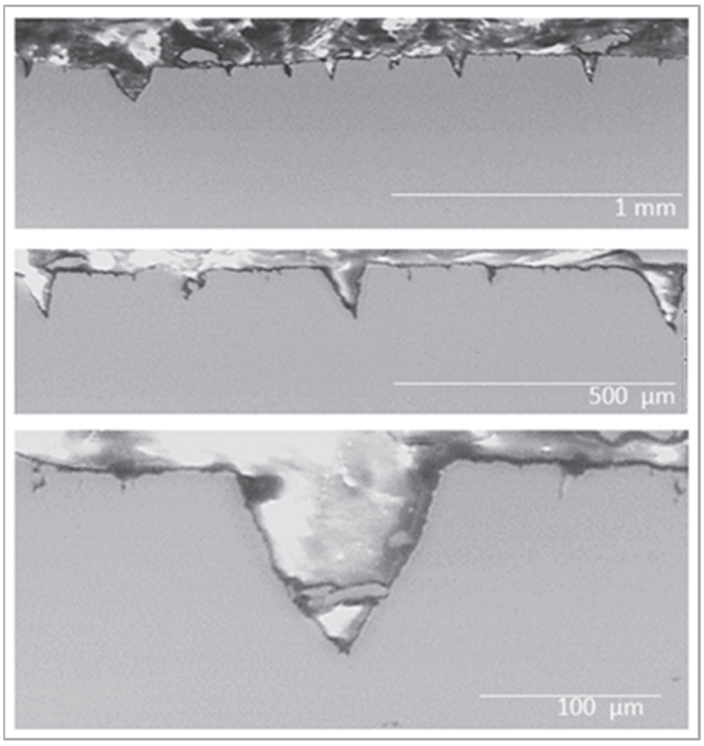

Figure 150: 0.70 M $NaHCO_3$ + 0.35 M Na_2CO_3 + 10%wt Na_2SO_3, CO_2-saturated, 75°C, -680 mV SCE, t.g. cracking

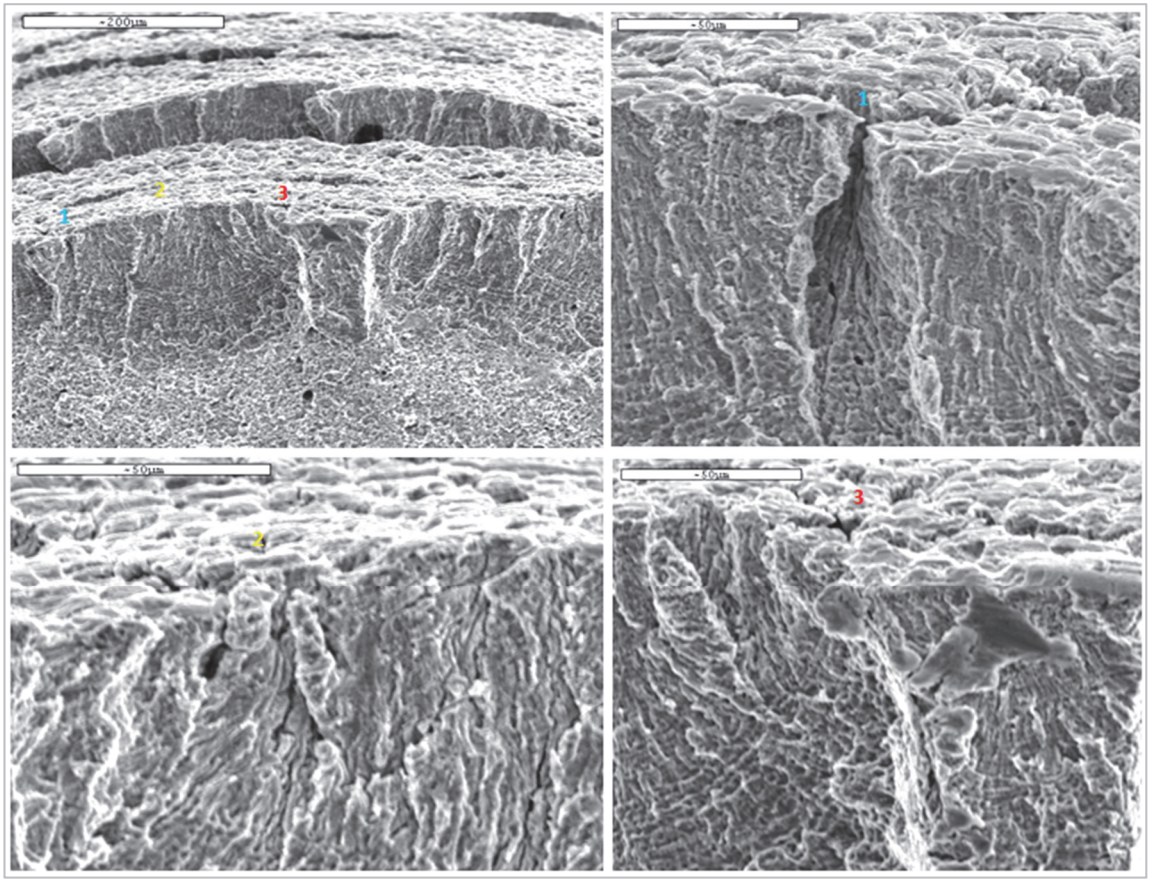

Figure 151: 0.70 M $NaHCO_3$ + 0.35 M Na_2CO_3 + 10%wt Na_2SO_3, CO_2-saturated, 75°C, -680 mV SCE, t.g. cracking on fracture surface

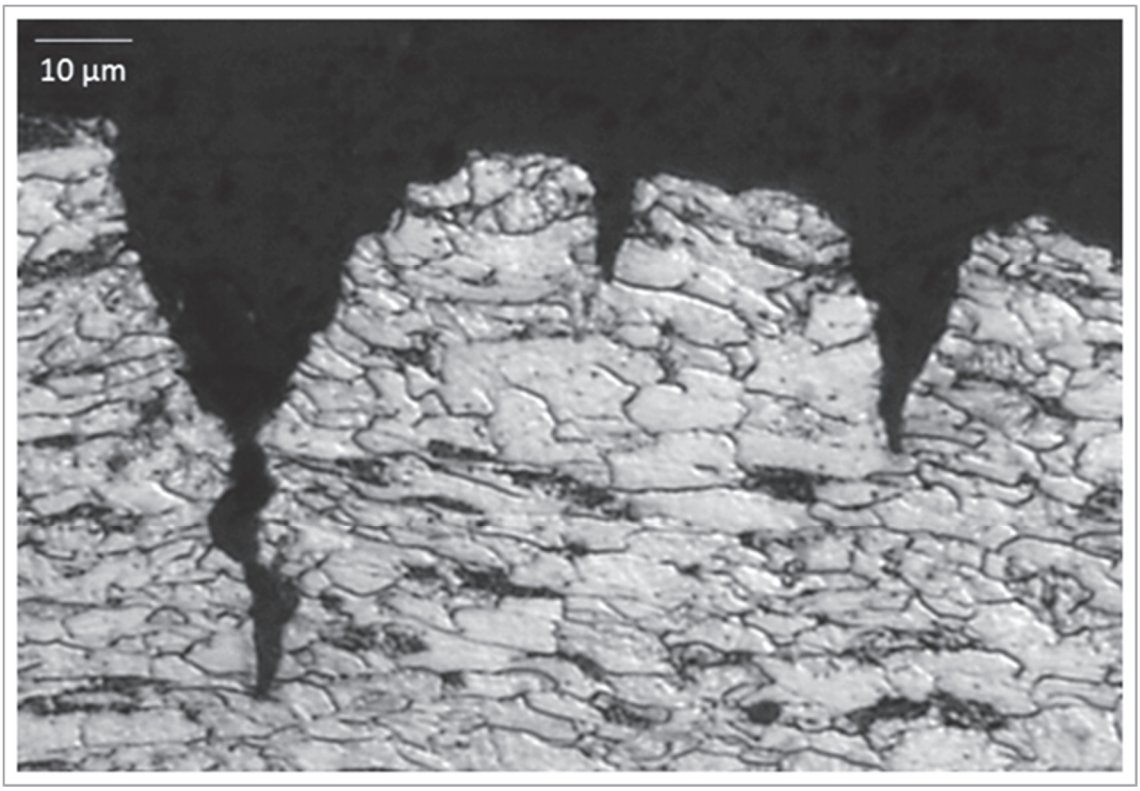

Figure 152: 0.70 M $NaHCO_3$ + 0.35 M Na_2CO_3 + 10%wt Na_2SO_3, CO_2-saturated, 75°C, -680 mV SCE, cross-section etched with Nital 2%vol., t.g. SCC

Susceptibility in active- region at 75°C

In the range of potentials associated with active transition, the material exposed to 0.70 M $NaHCO_3$ + 0.35 M Na_2CO_3 + 10%wt Na_2SO_3 environments saturated with CO_2 (1 bar) is susceptible to SCC (Figure 153). The nature of the cracking is transgranular (Figure 154 and Figure 155).

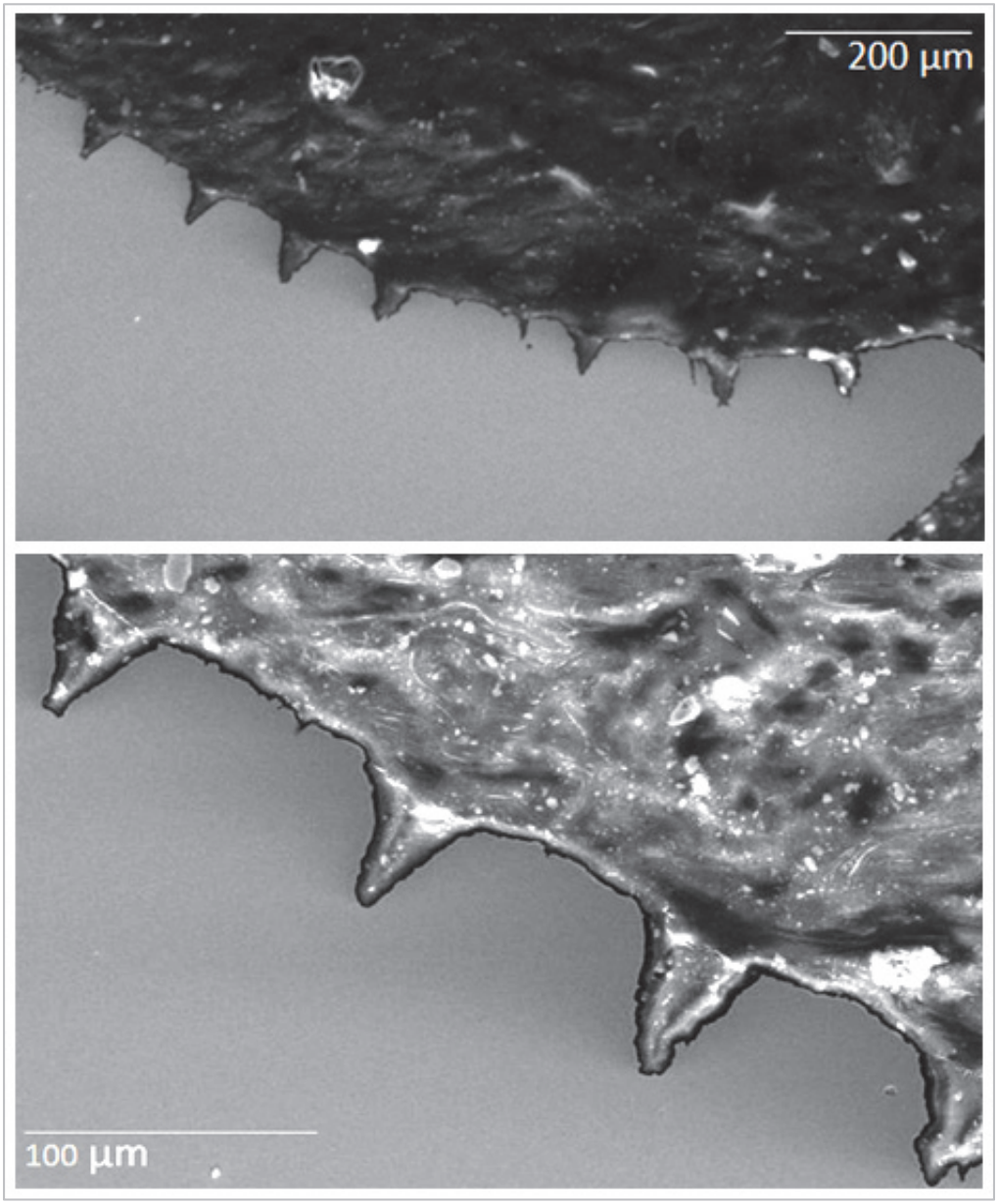

Figure 153: 0.70 M $NaHCO_3$ + 0.35 M Na_2CO_3 + 10%wt Na_2SO_3, CO_2-saturated, 75°C, -750 mV SCE, cross-section (1 µm polish)

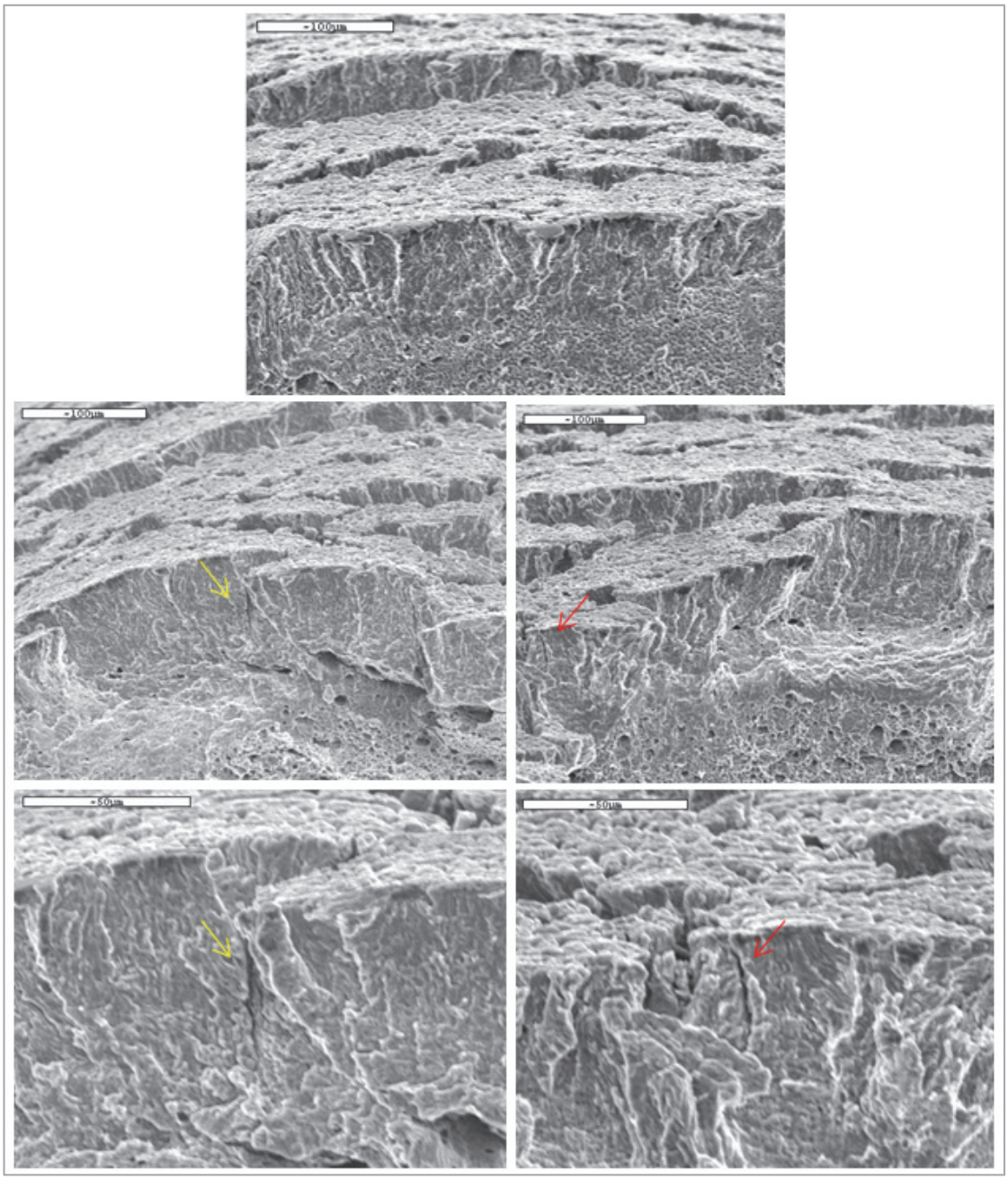

Figure 154: 0.70 M $NaHCO_3$ + 0.35 M Na_2CO_3 + 10%wt Na_2SO_3, CO_2-saturated, 75°C, -750 mV SCE, tiny transgranular cracks on fracture surface

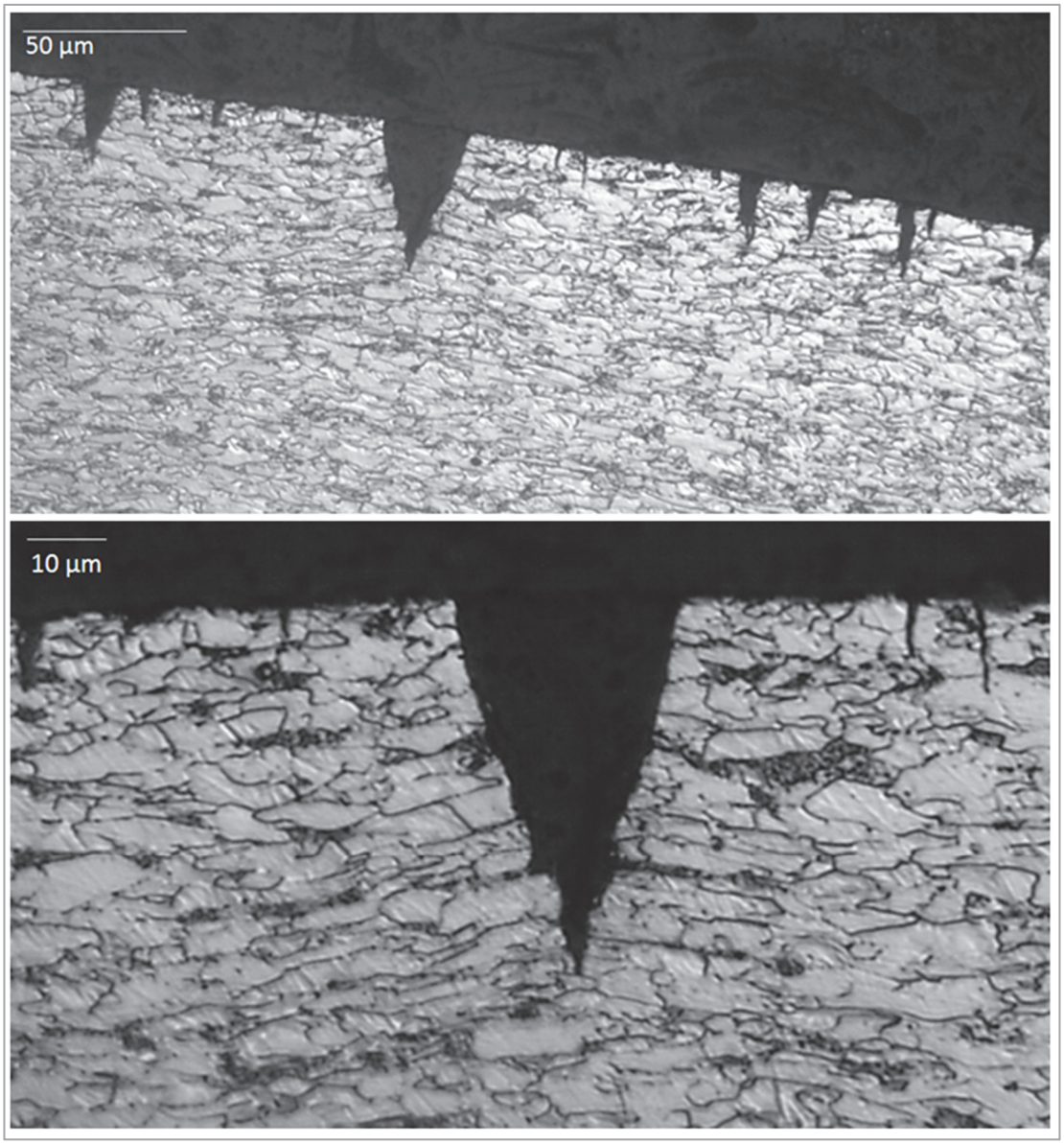

Figure 155: 0.70 M $NaHCO_3$ + 0.35 M Na_2CO_3 + 10%wt Na_2SO_3, CO_2-saturated, 75°C, -750 mV SCE, cross-section etched to Nital 2%vol., Transgranular cracking

5.2. Quantitative Assessment of SCC susceptibility: Reduction of Area and Crack Growth Rate

5.2.1. CO_2-free systems

The measurements of the cross-section reduction of area (Figure 156) and the crack velocity (Figure 157) suggest that in the region of potentials associated with the materials active-passive transition:

- Significant SCC could be generated at 75°C. Crack velocities (Figure 157) in the pure bicarbonate/carbonate systems, and in the presence of nitrates or sulphites have been found in excess of 10^{-6} mm/s.

- The susceptibility to cracking in the pure bicarbonate / carbonate system and in the presence of nitrates appears to be of the same order of magnitude. At 75°C, the reduction of area and the crack velocities have been of the order of 55%, and 3.10^{-6} $mm.s^{-1}$ respectively, in 0.7M $NaHCO_3$ / 0.35M Na_2CO_3 systems with or without 10%wt $NaNO_3$.

- The presence of sulphites appears to decrease the susceptibility to SCC in comparison with the pure bicarbonate / carbonate system and in the presence of nitrates. At 75°C, the crack velocities decrease from approximately 3.10^{-6} $mm.s^{-1}$ to 1.10^{-6} $mm.s^{-1}$ in 0.7M $NaHCO_3$ / 0.35M Na_2CO_3 systems when 10%wt. sulphites are added.

- The susceptibility to cracking decreases as the concentrations of bicarbonates/carbonates decrease. This trend remains valid when nitrates and sulphites are added to the $NaHCO_3$ / Na_2CO_3 system. At 75°C, the reduction of area increases from approximately 55% in 0.7M $NaHCO_3$ + 0.35M Na_2CO_3+10%wt $NaNO_3$ systems to 75% in 0.25M $NaHCO_3$ + 0.125M Na_2CO_3 +10%wt $NaNO_3$ systems.

- The susceptibility to cracking decreases as the temperature decreases. At 23°C, the measurement of the reduction of area suggests that the failure of the materials is mechanically driven in all test environments. At 23°C, the RA in the 0.7M $NaHCO_3$ / 0.35M Na_2CO_3 systems (with and without nitrates / sulphites) were found within 75%-80%, while the measurements in air were found of the order of 80%. The microscopic examination of the specimens in the concentrated bicarbonate/carbonate containing

environments however suggests the presence of pits whose morphology indicate eventually crack initiation at 23°C (see section 5.1). The measurement of the reduction of area is not significantly sensitive to the presence of minor localised corrosion processes.

As discussed in section 5.1, in the region of potentials associated with the materials active-passive transition ($E>E_p$), the mode of cracking in the pure bicarbonate/carbonate environments or in the presence of nitrates is intergranular, whilst in the presence of sulphites the mode of cracking is transgranular.

At potentials associated with the material active region ($E_{corr}<E<E_p$), the mode of cracking for the pure bicarbonate/carbonate environments or in the presence of nitrates shifts to transgranular.

Figure 158 and Figure 159 suggest that the mode of cracking dictates the material susceptibility to SCC. The material appears to be more sensitive to Intergranular cracking than to transgranular cracking. Although SCC is still possible in the material active region, the material is less vulnerable than in the active-passive transition. The cracking susceptibility decreases as the potential is shifted towards the free corrosion potential. Small transgranular cracks are still identified at +50 mV from E_{corr}.

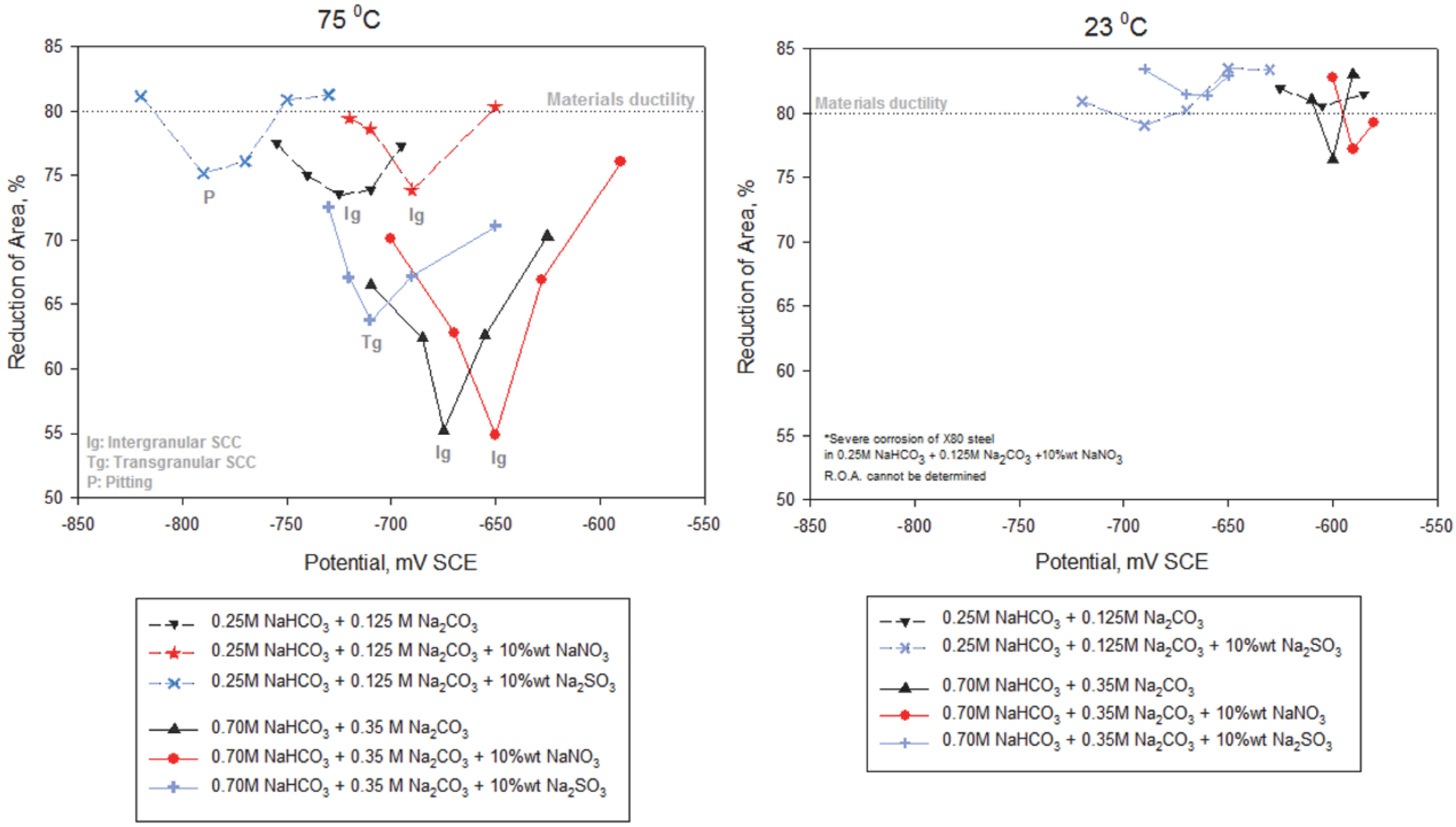

Figure 156: Reduction of area in the material active-passive transition region, effect of impurities in bicarbonate / carbonate environment (CO_2-free) at 75^{0}C and 23^{0}C

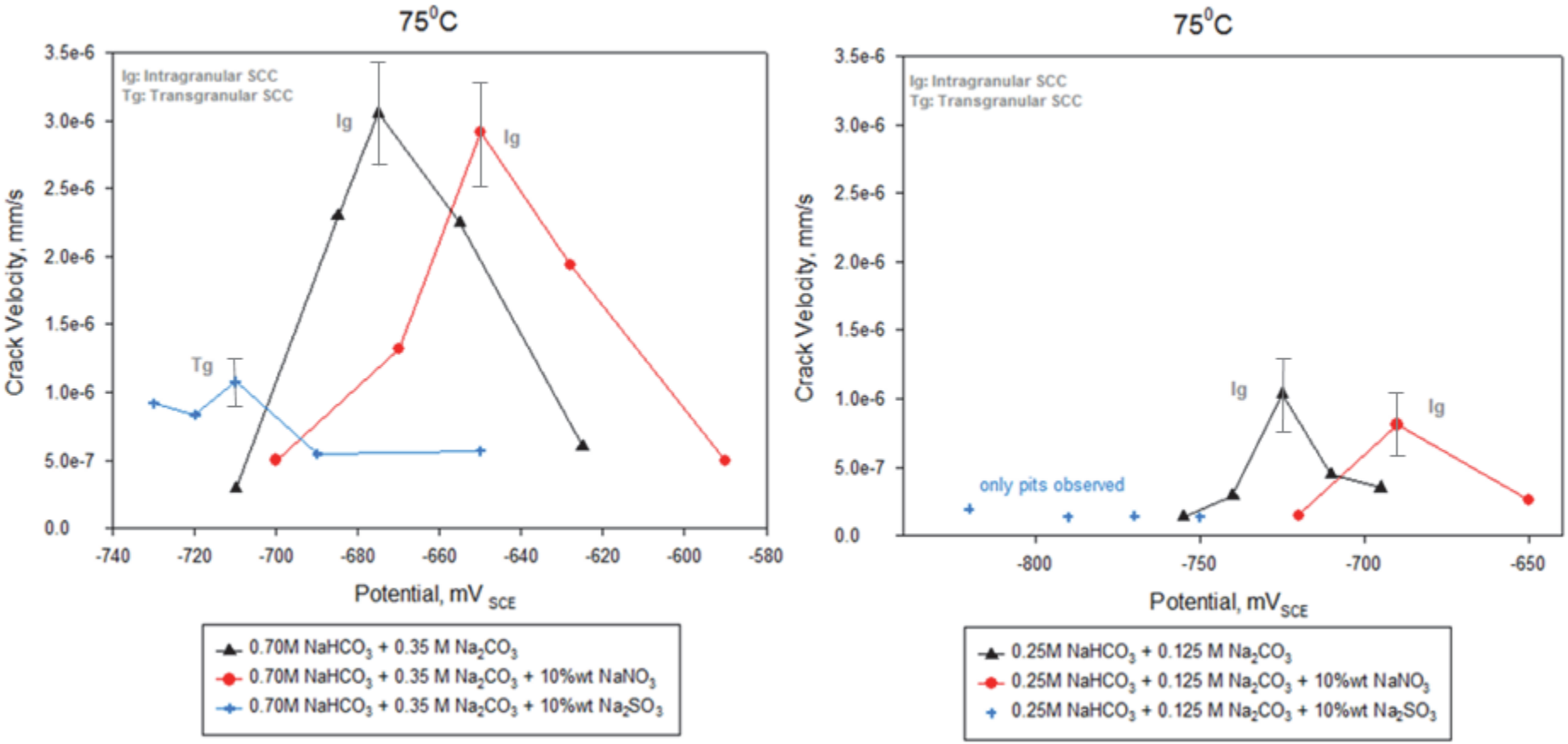

Figure 157: Crack velocity in the material active-passive transition region, effect of impurities in bicarbonate / carbonate environment (CO_2-free) at 75 ^{0}C

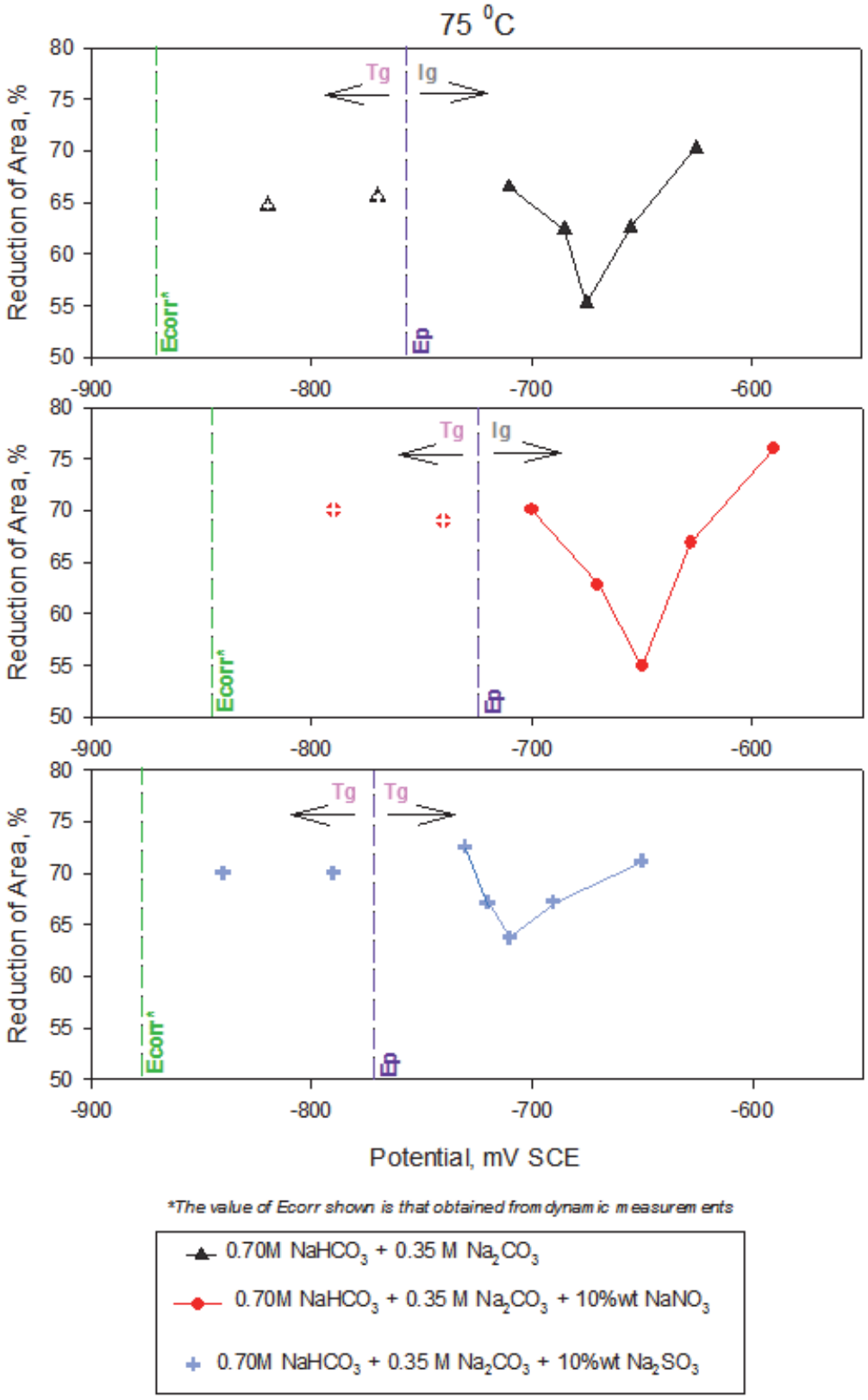

Figure 158: Reduction of area in pure bicarbonate / carbonate environments and in the presence of nitrates and sulphites at 75 ^{0}C and effect of potential on mode of cracking

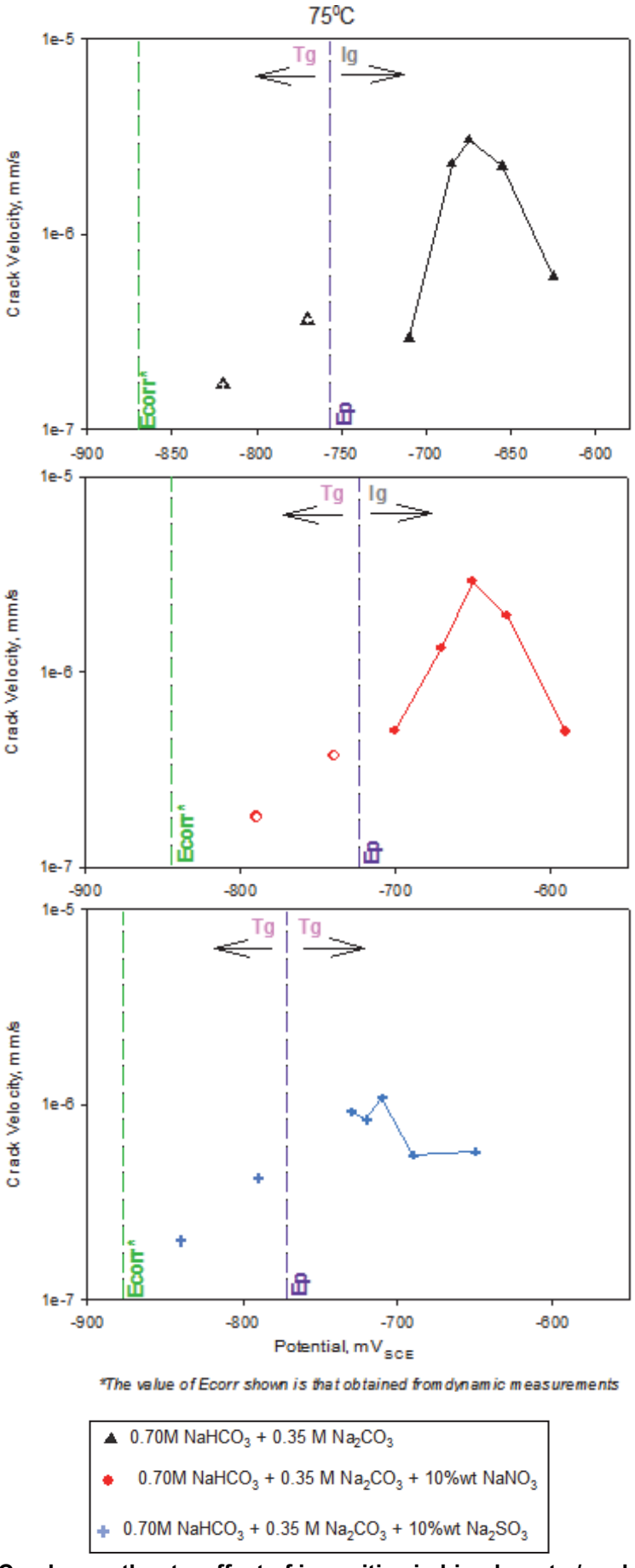

Figure 159: Crack growth rate, effect of impurities in bicarbonate / carbonate environment at 75 ^{0}C

The quantitative assessment is generally consistent with observations made during the qualitative assessment as discussed in section 5.1. In addition, Figure 160 shows that there is a satisfactory correlation between the Reduction of Area and the Crack Velocity measurements; this confirms the reliability / adequacy of these measurements in determining the susceptibility to SCC, especially in systems showing a significant predisposition to SCC: The systems featuring lower ductility behaviour (i.e. lower Reduction of Area) were associated with higher SCC Cracking velocities.

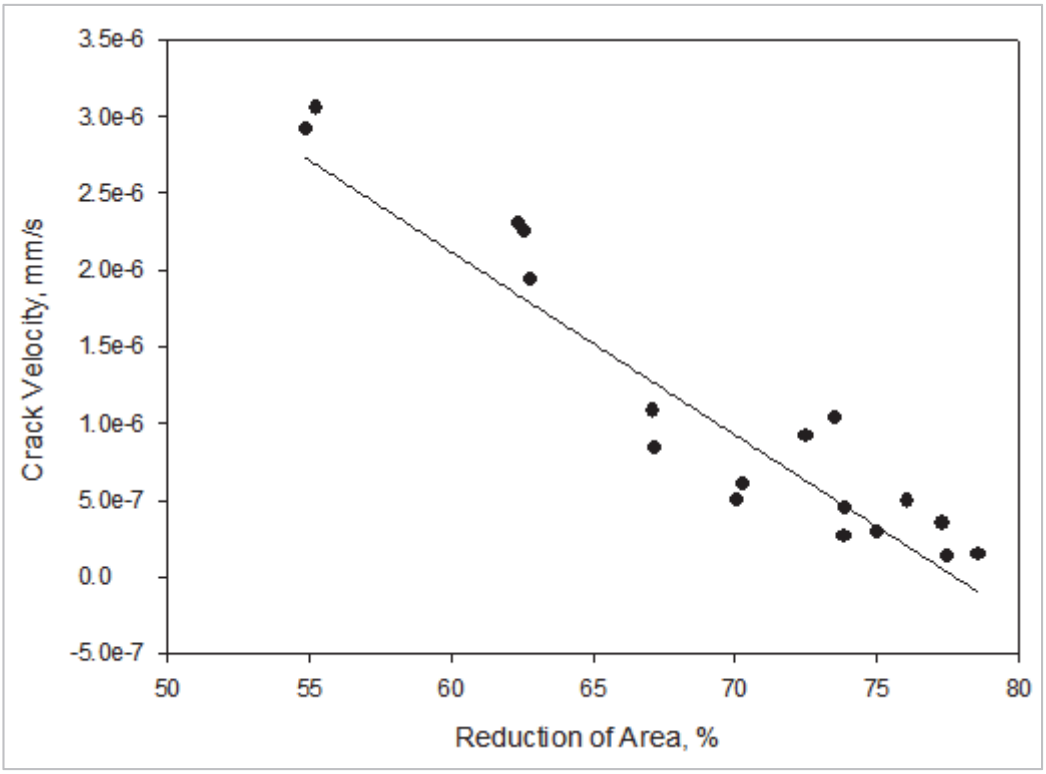

Figure 160: Correlation between Crack velocity and Reduction of area

5.2.2. CO_2-saturated system

Figure 161 describes the shift in cracking mode and susceptibility to SCC when CO_2 is added to the 0.70M $NaHCO_3$ + 0.35M Na_2CO_3 system with or without nitrates or sulphites. The main observations related to the addition of carbon dioxide in the various test environments are as followed:

- The addition of CO_2 (1 bar) decreases the magnitude of Stress Corrosion Cracking in all the test environments.
- At potentials associated with active-passive transition of the material:
    - The mode of cracking for the pure bicarbonate / carbonate system shifts to transgranular with the presence of CO_2, whilst the nitrate- and sulphite- containing test environments preserve their mode of cracking (respectively intergranular and transgranular).
    - There is a drop in SCC susceptibility which is particularly significant in the case of the pure bicarbonate/carbonate environment in comparison with the nitrate-, and sulphite- containing environments. This seems to be associated with the shift of cracking mode from intergranular to transgranular.
    - The highest susceptibility was identified in the presence of nitrates (and then sulphites). The susceptibility to SCC as a function of the bicarbonate/carbonate environment could be ranked as follows: *nitrate-containing > sulphite-containing > Pure bicarbonate/carbonate system.*
- At potentials associated with the materials active region,
    - Stress Corrosion Cracking is still possible
    - The mode of cracking in this region remains transgranular.
    - Sulphite-containing environments appear to produce the highest susceptibility to cracking.

In freely corroding conditions, the materials does not seem to exhibit SCC susceptibility. The cross-section reduction of area were found between 75 and 80%.

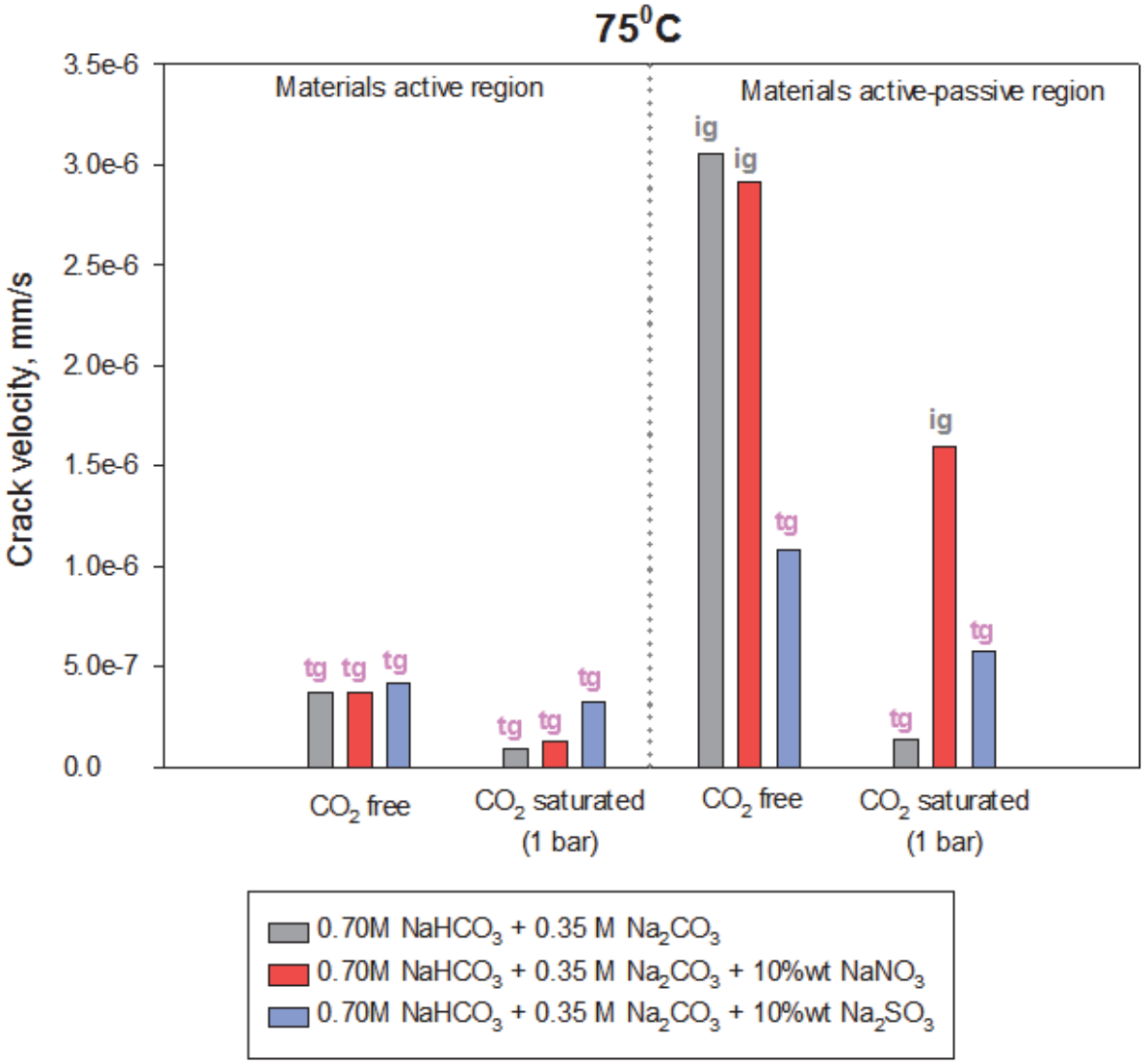

Figure 161: Maximum cracking susceptibility and mode of cracking, effect of CO_2

Chapter 6. Summary and further discussion

The following sections discuss whether the system CO_2-HCO_3^--CO_3^{2-}-H_2O and in the presence of nitrates and / or sulphites could produce Stress Corrosion Cracking.

6.1. Effect of bicarbonate/carbonate concentrations

The susceptibility to cracking in the HCO_3^--CO_3^{2-}-H_2O system in the steel active-passive transition domain decreases with diminishing bicarbonate / carbonate levels at high pH (>9) (see Figure 156 and Figure 157). This trend has also been reported by Parkins.[84,118] The density and depth of cracks become lower, and the crack morphology becomes less fine. The change in SCC susceptibly with the bicarbonate levels can be associated with two major processes:

- Destabilisation of the iron carbonate film protectiveness as the concentrations of bicarbonate and carbonate decline. As has been discussed before, an essential requirement for the realisation of SCC is the existence of passivating conditions at the crack walls whilst corrosion activity at the crack tip is being maintained.[68,141] Since the formation of a protective film is hindered at lower bicarbonate and carbonate levels,[60,93,142,143] uniform or general corrosion will be favoured over localised corrosion processes. If a crack however develops at lower bicarbonate/carbonate levels, the anodic dissolution rates could be significant at the crack walls and blunt cracks have a tendency to form.
- Under film-free conditions, the iron anodic dissolution rates are increased at higher bicarbonate levels, as was shown by Davies and Burstein[133]. The nature of the dissolution processes in bicarbonate-containing environments is complex and remains open to debate. However, most authors[118,133,139,142] agree that the anodic dissolution of iron in its active domain is controlled by the formation of soluble complex compounds. Parkins and Castro[118,139] supported the idea that the anodic dissolution of iron in bicarbonate-carbonate systems is probably controlled by the formation of soluble compounds, such as $Fe(HCO_3)^+$. Increased crack velocities and fine cracks are generated at higher bicarbonate levels since the active crack tips (directly exposed to environment) see higher

dissolution rates under these conditions, whilst the crack walls are protected by the iron carbonate film.

The effect of pH in the HCO_3^--CO_3^{2-} system will be discussed in section 6.3.

6.2. Effect of impurities (nitrates, sulphites)

Stress Corrosion Cracking can still be generated in the presence of nitrates or sulphites (produced as by-products of the reaction of nitrogen oxides or sulphur oxides with water) in the HCO_3^--CO_3^{2-}-H_2O system.

The discussion in this section is limited to the steel active passive transition domain at high pH (>9) and at 75°C.

6.2.1. Effect of nitrates

In the presence of nitrates, the morphology and severity of cracking in the active-passive transition is similar to that of pure bicarbonates / carbonates at high pH (>9) (see Figure 159).

The addition of nitrates to bicarbonate / carbonate systems increases the free corrosion potential in comparison to pure bicarbonate / carbonate systems (see Figure 71 and Figure 72). This is considered to be related to a change in surface film properties and to the formation of a more protective film. In nitrate-containing systems, SCC has been associated with the formation of iron oxides:[87,90,109] hematite α-Fe_2O_3 and magnetite Fe_3O_4. Humphries and Parkins[109] showed that cracking is produced in the presence of both type of films, but the susceptibility is highest with α-Fe_2O_3. Flis[90] confirmed that shorter times of failure are observed in the presence of α-Fe_2O_3 rather than that of Fe_3O_4. Perdieus et al.[144] defined the most susceptible regions for nitrate SCC over the iron Pourbaix diagram, but the diagram they used is that of 25°C. Beverskog and Puigdomenech[145] developed more recently a revision of the iron Pourbaix diagram for higher temperatures which will probably provide a better visualisation of the domain of nitrate SCC as a function of potential, pH, and iron compounds stability. Further work is however needed to determine in which way the nitrate affects surface films in a HCO_3^--CO_3^{2-}-H_2O system over a wide pH spectrum and temperatures.

The maximum anodic currents in pseudo-active conditions (fast potentiodynamic sweep rates) were however similar in both the pure bicarbonate / carbonate

system and in the presence of nitrates (Figure 83). Figure 162 suggests that crack growth rates within the HCO_3^--CO_3^{2-}-H_2O and $NaNO_3$-HCO_3^--CO_3^{2-}-H_2O systems are both controlled by dissolution processes at the crack tip, since there is a reasonable correlation between the crack growth rate and the anodic current density. The crack velocity in both systems is expected to be associated with the bare metal dissolution rate. Figure 162 also shows that the crack velocities and dissolution current densities are in a similar order of magnitude for HCO_3^--CO_3^{2-}-H_2O and $NaNO_3$-HCO_3^--CO_3^{2-}-H_2O systems. This strongly suggests that, although nitrates may interfere with the nature of the surface films, the overall cracking mechanism in the steel active-passive transition domain remains dominated by the HCO_3^--CO_3^{2-}-H_2O system at high pH (>9) even in the presence of nitrates. This hypothesis is further validated by previous work[88], which suggests that the SCC susceptibility of steels in aqueous nitrate environments is significantly lessened in alkaline environments i.e. at pH above 7. In a more recent study, Mohammed[91] also suggested that although nitrate SCC can be produced in alkaline environments e.g. at pH 9.6, nitrate SCC velocity is very slow compared with that in more acidic media.

As for the HCO_3^--CO_3^{2-}-H_2O system, the crack morphology in the steel active-passive transition domain at high pH (>9) is intergranular in the $NaNO_3$-HCO_3^--CO_3^{2-}-H_2O system.

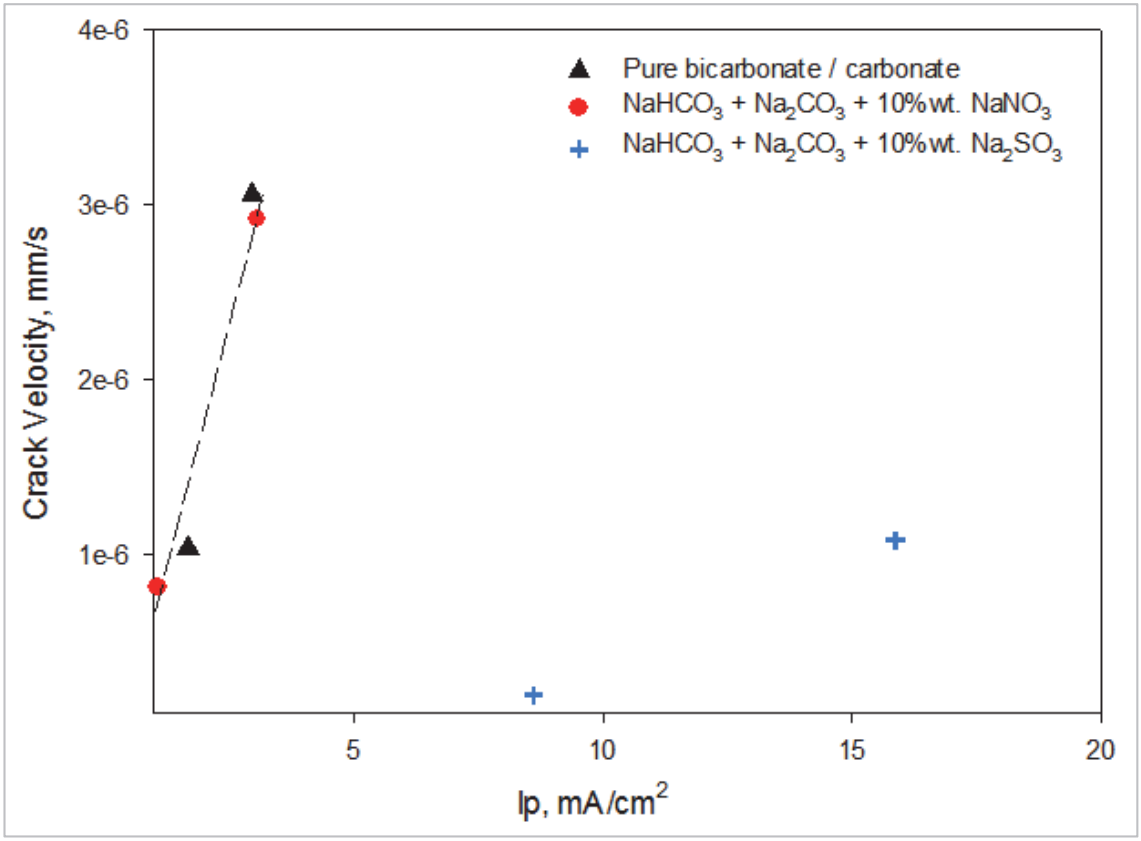

Figure 162: Crack velocity vs. first oxidation peak anodic current

6.2.2. Effect of sulphites

In the presence of sulphites, the severity of cracking in the active-passive transition is lower than that of pure bicarbonates / carbonates or in the presence of nitrates at high pH (pH>9) (Figure 159). The addition of sulphites to bicarbonate / carbonate systems decreases the free corrosion potential in comparison to pure bicarbonate / carbonate systems (Figure 73). In addition, a significant increase in maximum anodic currents in pseudo-active conditions (fast potentiodynamic sweeping) in comparison to the HCO_3^--CO_3^{2-}-H_2O system (and in presence of nitrates) is observed (Figure 83). The electrochemical measurements suggest an increased activity of the material surface at high pH.

Sulphites favour the destabilisation of surface protective films such as iron carbonate and rather promote anodic dissolution, whose combined effects deter the growth of stress corrosion cracks (see Figure 162). The impact of sulphur species in destabilising passive films and contributing in localised corrosion has been discussed elsewhere. For example, Haleem et al.[107] indicated that sulphates can lead to the instability of steel passivation in alkaline environments.

The establishment of a porous and non-passivating film condition mechanism in the presence of sulphates was also associated with a negative shift of the free corrosion potential to lower potentials with time. Premlall et al.[108] indicated that the sole presence of sulphate anions in alkaline solution (pH 9-12) can induce noticeable attack of mild steels. At pH 12, pitting corrosion was observed, whilst uniform corrosion was reported at pH 9. The oxygen scavenging property of sulphite compounds will contribute further in hindering the formation of protective oxides on the surface of the steel.

At high pH (pH>9) and in the presence of sulphites, the decline in crack growth in the material active-passive region is also associated with a change in cracking morphology (see Figure 159). The mode of cracking is transgranular in the presence of sulphites, in contrast to the intergranular cracking morphology observed in the pure bicarbonate/carbonate system or in the presence of nitrates. The additional presence of sulphites in the HCO_3^--CO_3^{2-}-H_2O system appears to change the cracking mechanism; the transgranular mode can be associated with the increased deterioration of surface passivity when sulphites are in solution. The role of sulphites in interfering with protective films in the HCO_3^--CO_3^{2-}-H_2O system should be further investigated over a wide range of pHs and temperatures.

6.3. Effect of pH

6.3.1. HCO_3^--CO_3^{2-}-H_2O system

At high pH (>9), significant intergranular cracking (>10^{-6} mm/s) was produced in the pure bicarbonate/carbonate system in the X80 steel active-passive domain (Figure 159). Cracking of pipeline steels in such an environment has been referred to “high pH SCC” and has been largely documented in literature and by Parkins[84,117,118]. High pH SCC has commonly been found to occur in highly concentrated bicarbonate-carbonate environments with high pH typically between 9 and 11. In the material active-passive transition domain, the mode of cracking is of intergranular nature. One of the key aspects in the realisation of SCC in bicarbonate-carbonate environments is the formation of a protective iron carbonate, the crack growth being controlled by anodic dissolution at the crack tip while the crack walls remain passive. The driving force for iron carbonate precipitation is associated with the supersaturation of $FeCO_3$, which is a function of the concentrations of dissolved (ferrous) iron and the carbonate species and

the solubility limit of iron carbonate as expressed in section 2.7.1. The solubility limit is itself a function of pH (and temperature). The formation of protective iron carbonate is favoured at more alkaline pH. A high pH typically above 9 is therefore an important environmental condition to produce intergranular SCC in the HCO_3^--CO_3^{2-}-H_2O system.[60,93]

Parkins[84] indicated that there is a correlation between the pH of the bicarbonate/carbonate solutions and the susceptibility to cracking. He suggested[84] that higher crack growth rates were associated with bicarbonate-carbonate solutions of lower pH. However, this statement does not consider the close relationship between the bicarbonate / carbonate levels and the solution pH. The solutions with higher bicarbonate and carbonate levels have a lower pH. (Figure 54); as discussed in section 6.1, the higher severity to cracking has been identified in the more concentrated bicarbonate-carbonate systems (Figure 156). Parkins did not look precisely at the effect of carbon dioxide on the concentrated HCO_3^--CO_3^{2-}-H_2O systems.

In the presence of CO_2, as the pH moves towards acidity, it will be anticipated that the precipitation of iron carbonate is hindered, and therefore the SCC susceptibility in the active-passive domain is decreased. The SSRT experiments in bicarbonate-carbonate solutions in the presence of CO_2 confirm this. As the pH drops due to the presence of carbon dioxide, the severity of cracking decreases (Figure 163). This study particularly shows that the acidification of the bicarbonate / carbonate environment as a result of CO_2 addition shifts the mode of cracking from intergranular to transgranular in the active-passive domain (Figure 163).

As the acidity of the solution increases, as a result of an increase in CO_2 partial pressure, it is envisaged that a pH threshold will be reached for which anodic dissolution dominates iron carbonate precipitation, and thus SCC susceptibility in the HCO_3^--CO_3^{2-}-H_2O system will become low.

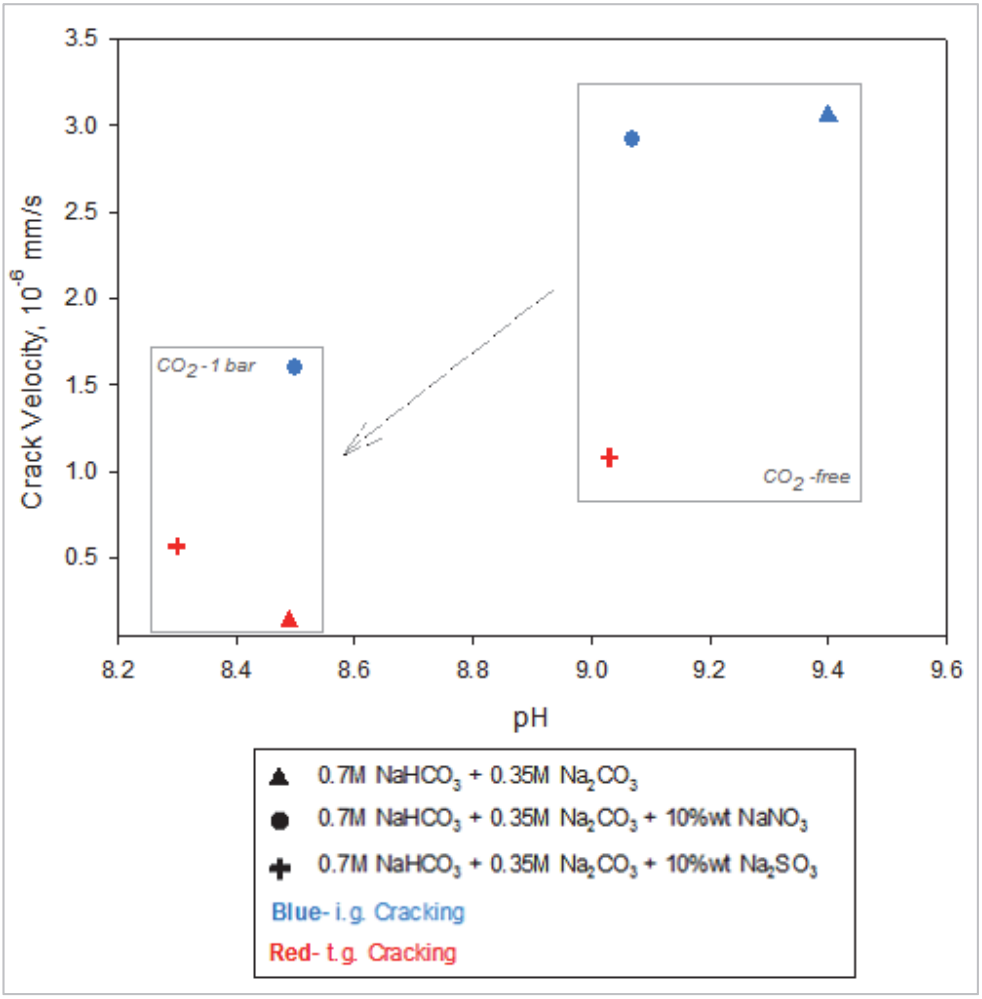

Figure 163: Crack mode and velocity as a function of pH

6.3.2. Addition of nitrates to the HCO_3^--CO_3^{2-}-H_2O system

At high pH (pH>9), the morphology of cracking in the presence of nitrates is intergranular in the material's active-passive transition as for the pure bicarbonate/carbonate system. As discussed in section 6.2.1, it is considered that the overall cracking mechanism in the steel active-passive transition domain remains dominated by the HCO_3^--CO_3^{2-}-H_2O system even in the presence of nitrates.

It was observed that the morphology of the cracking does not change with an increased acidification of the environment due to the presence of carbon dioxide, and remains intergranular in contrast to the HCO_3^--CO_3^{2-}-H_2O system, for which transgranular SCC was observed (Figure 163). As the solution becomes more acidic, the cracking severity is higher in the presence of nitrates than that observed in pure bicarbonate / carbonate environments (Figure 163) and it remains significant (>10^{-6} mm/s). Perdieus[144] and Szklarska Smialowska[88]

reported that the SCC susceptibility of steels in aqueous nitrate environments is significantly increased as the environment becomes more acid, typically for pH less than 7. Mohammed[91] indicated more recently that the critical range for nitrate cracking is between pH 3.0 and pH 7.5. As the mode of cracking in aqueous nitrate environments is intergranular and the susceptibility to cracking within the HCO_3^--CO_3^{2-}-H_2O system significantly decreases with pH drop, this suggests that as the pH of the environment tends towards acidity, the contribution of nitrate SCC will dominate the overall cracking mechanism when nitrates are present in the HCO_3^--CO_3^{2-}-H_2O system.

As the drop in pH is sustained by the increase in carbon dioxide partial pressure, nitrate Stress Corrosion Cracking becomes the dominant mechanism when nitrates are present in the HCO_3^--CO_3^{2-}-H_2O system. This is further favoured in the case of low bicarbonate / carbonate concentrations and at high temperatures (typically above 70°C).

6.3.3. Addition of sulphites to the HCO_3^--CO_3^{2-}-H_2O system

As the pH of the solution tends towards more acidic levels due to the presence of carbon dioxide, the crack growth rate associated with the SO_3^{2-}- HCO_3^--CO_3^{2-}-H_2O system in the materials active-passive domain decreases. Higher severity of cracking is however observed in the presence of sulphites in comparison with the HCO_3^--CO_3^{2-}-H_2O system (but lower than the NO_3^-- HCO_3^--CO_3^{2-}-H_2O system). The cracking mode remains transgranular.

6.4. Effect of electrochemical potential

Two domains of potential are identified in the three systems HCO_3^--CO_3^{2-}-H_2O, NO_3^-- HCO_3^--CO_3^{2-}-H_2O, and SO_3^{2-}- HCO_3^--CO_3^{2-}-H_2O in the absence or presence of CO_2:

- An active domain, at potentials between E_{corr} and E_p
- An active-passive transition domain, at potentials more anodic than E_p (until potentials for which surface passivation is reached)

Stress Corrosion Cracking has been found in both potential domains for all test environments. However, the severity of cracking is more significant in the active-passive transition domain than in the active domain, whichever test system is considered (see Figure 161). This is in agreement with findings from Zhou and

Parkins.[118] The change in severity is associated with a shift in cracking morphology: In the materials active region, the cracks are systematically transgranular irrespectively of the test environment, whilst in the active-passive transition domain, cracking is intergranular in the case of the HCO_3^--CO_3^{2-}-H_2O (at pH>9) and NO_3^-- HCO_3^--CO_3^{2-}-H_2O systems. Intergranular cracking has generated the highest crack growths (see Figure 163). There appears to be a relationship between the crack severity and the crack morphology, the steel being more susceptible to intergranular cracking than to transgranular cracking.

At high pH (pH>9), the HCO_3^--CO_3^{2-}-H_2O, NO_3^-- HCO_3^--CO_3^{2-}-H_2O, and SO_3^{2-}-HCO_3^--CO_3^{2-}-H_2O systems produce significant crack growth of the order of 10^{-6} mm/s in the materials active-passive region. As the potential shifts within the materials active region the crack velocities are only of the order of 10^{-7} mm/s (Figure 161). Although SCC declines as the potential shifts towards E_{corr}, tiny transgranular cracks are still observed at relatively small anodic polarisations of +50 mV. Acidification of the environments due to the presence of carbon dioxide was found to decrease crack growth rates in both the materials active region and the active-passive transition region. However as the CO_2 partial pressure increases and the pH is further shifted to lower values, the shift in SCC mechanism (from a dominating bicarbonate/carbonate mechanism) due to the presence of impurities at low pH should be considered especially at higher temperatures e.g. nitrate SCC above 70°C.

Under the current experimental program, no SCC was found at Open Circuit Potential conditions in the HCO_3^--CO_3^{2-}-H_2O, NO_3^-- HCO_3^--CO_3^{2-}-H_2O, and SO_3^{2-}- HCO_3^--CO_3^{2-}-H_2O systems in the presence of 1 bar carbon dioxide.

6.5. Effect of temperature

In the all the test environments (HCO_3^--CO_3^{2-}-H_2O, NO_3^-- HCO_3^--CO_3^{2-}-H_2O and SO_3^{2-}- HCO_3^--CO_3^{2-}-H_2O) the susceptibility to cracking in the materials active-passive transition region is higher as the temperature increases (see Figure 156). There is a close relationship between the cracking susceptibility and the formation of surface protective films as a function of temperature.

At 23°C, in the HCO_3^--CO_3^{2-}-H_2O and NO_3^-- HCO_3^--CO_3^{2-}-H_2O systems, tiny localised corrosion features whose morphology and geometry could suggest

stress corrosion cracks at the initiation stage are observed (see Figure 94 and Figure 108), indicating SCC is still possible in the material active-passive transition domain. At 23°C, the anodic dissolution associated with the corrosion process is probably too low to generate deeper corrosion features within the time scale of the SSRT experiment conducted. It is plausible that for much longer exposure tests, i.e. at lower strain rate, the pits could turn into deeper stress corrosion cracks in these environments. The presence of sulphites in the HCO_3^--CO_3^{2-}-H_2O system appears however to inhibit the initiation of cracks at 23°C.

At 75°C, the severity to cracking is significant (>10^{-6} mm/s) in the three systems HCO_3^--CO_3^{2-}-H_2O, NO_3^-- HCO_3^--CO_3^{2-}-H_2O, and SO_3^{2-}- HCO_3^--CO_3^{2-}-H_2O (see Figure 159). As discussed before, a key requirement for the realisation of SCC is the formation of a passive film on the surface of the steel. In these systems, passivation of the steel becomes more likely as the temperature is increased: In bicarbonate / carbonate environments, precipitation of protective iron carbonate is favoured at higher temperatures as has been discussed by Dugstad[93] and Sun[60]. In aqueous nitrate solutions, the occurrence of SCC is correlated with the formation of protective hematite and magnetite at temperatures above 70°C.[90,91,109]

6.6. CCS operational scenarios and SCC

Let us consider a low alloy steel pipeline transporting anthropogenic CO_2 from a carbon capture plant. As discussed in section 2.1.3, two extreme operational scenarios may be envisaged during the life cycle of such pipeline:[8,20]

1. The CO_2 is dehydrated to specification and the impurity levels are identified as negligible, (according to the CO_2 plant conditioning specification).
2. Upset in dehydration occurs such that a free liquid water phase is present at the 6-o-clock position of the pipeline transportation system. Upset in the CO_2 conditioning plant has also occurred with levels of impurities above the specified levels.

Scenario 1 represents the best case operation to which the duty holder would like to continuously comply, so that the risks related to internal corrosion are minimised and the pipeline remains fit for service for its entire operational life. Under Scenario A, SCC is not a risk since a water phase is not present.

Industrial experience in the oil and gas industry indicates that operational anomalies regularly occur. Therefore there is a certain probability that the worst case scenario (2), will be realised. The question is to determine whether the pipeline could suffer from internal SCC in a CO_2-HCO_3^--CO_3^{2-}-H_2O system and in the presence of the likely impurities, nitrates and/or sulphites.

When liquid water is present in the transport pipeline, the chemistry of the water pools will be initially driven by the partial pressure of CO_2, types and partial pressures of impurities present in the CO_2 stream and temperature. It is expected that at the high partial pressures of CO_2 typical of an operational carbon transport pipeline that:

- The concentration of bicarbonates and carbonates in solution will be initially low (less than 0.001M of bicarbonates for CO_2 partial pressures below 10 MPa).
- The pH of the solution will be initially typically below 4.

Under such environmental conditions, the probability of cracking within the HCO_3^--CO_3^{2-}-H_2O, and SO_3^{2-}- HCO_3^--CO_3^{2-}-H_2O systems is low as a result of the diluted levels of bicarbonates / carbonates and acid pH.

However, the presence of nitrates in diluted bicarbonate / carbonate solutions at low pH could enhance the possibility of nitrate intergranular SCC: as the drop in pH is sustained by the increase in carbon dioxide partial pressure, nitrate SCC becomes the dominant mechanism when nitrates are present in the HCO_3^--CO_3^{2-}-H_2O system. However this mechanism is favoured at high temperatures (typically above 70°C). As the temperature downstream of the CO_2 compression after-cooler stage is expected to be below 40°C (typical export gas temperature in North Sea assets e.g. Piper Bravo), this minimises the risk of nitrate SCC, unless an anomaly in the cooling stage occurs. Offshore anomalies at cooling stages are not uncommon, and would allow temperatures higher than 140°C at the pipeline inlet.

Another limiting parameter in the occurrence of nitrate SCC in anthropogenic CO_2 transport pipelines is the level of nitrate impurities expected in the CO_2 stream. Volumetric concentrations of the order of parts per million will be present in the CO_2 stream (unless upsets in the conditioning plant occur), whilst concentrated solutions of nitrates are generally required to produce SCC.

Operational circumstances may provide more favourable environmental conditions to develop SCC within the HCO_3^--CO_3^{2-}-H_2O, NO_3^-- HCO_3^--CO_3^{2-}-H_2O, and SO_3^{2-}- HCO_3^--CO_3^{2-}-H_2O systems, for example:

- ✓ The re-establishment of dry gas operations would lead to concentrating the levels of bicarbonates/carbonates in existing water pools, resulting in an increase in alkalinity. The time for which water pools will remain in the pipeline is dependent on the volume of water present, dryness and flow rate of the CO_2 stream, operational temperature pressure profile along the line, and the pipeline bathymetry. The pH of the water is a function of the partial pressure of CO_2, bicarbonate / carbonate concentrations, type and concentration of impurities and temperature.

- ✓ The re-establishment of dry gas operations will also lead to concentrating the levels of impurities (e.g. nitrates, sulphites) in water pools. This will especially contribute to increase the risk of nitrate SCC at low pH and high temperature.

- ✓ The carry-over of chemicals (e.g. amine) and by-products (e.g. ammonia) from the capture / conditioning process into the pipeline could also promote the establishment of highly alkaline conditions in aqueous phases present in a CO_2 pipeline.

Nevertheless, one of the major limits in developing SCC within the HCO_3^--CO_3^{2-}-H_2O, NO_3^-- HCO_3^--CO_3^{2-}-H_2O, and SO_3^{2-}- HCO_3^--CO_3^{2-}-H_2O systems is the requirement of electrochemical polarisation. The internal surface of the pipeline does not see any electrochemical polarisation driven from peripheral structures, in contrast to the external pipeline surface which could see polarisation from a cathodic protection system.

Although for the different HCO_3^--CO_3^{2-}-H_2O, NO_3^-- HCO_3^--CO_3^{2-}-H_2O, and SO_3^{2-}-HCO_3^--CO_3^{2-}-H_2O systems, transgranular cracking is possible in the active domain and is observed at polarisations as low as +50 mV from the E_{corr}, the cracking susceptibility does significantly decline when the potential tends towards E_{corr}. No Stress corrosion Cracking was found at Open Circuit Potential conditions in the HCO_3^--CO_3^{2-}-H_2O, NO_3^-- HCO_3^--CO_3^{2-}-H_2O, and SO_3^{2-}- HCO_3^--CO_3^{2-}-H_2O systems in the presence of 1 bar carbon dioxide. Circumstances may be present

inside a pipeline, which provide sufficient anodic polarisations to the steel to shift the potential with the cracking susceptibility domain. For example:

- ✓ Filler metals are usually used in welding. The metals used for welding could be of different composition and electrochemically nobler than the steel parent (base) material. This will generate a galvanic couple.
- ✓ An internal surface partially coated with oxide from the rolling process.
- ✓ The eventual presence of surface films (such as iron sulphides), cathodic to the steel.

The effect of welding materials and iron sulphide films in displacing the free corrosion potential of the steel in the different systems HCO_3^--CO_3^{2-}-H_2O, NO_3^--HCO_3^--CO_3^{2-}-H_2O, and SO_3^{2-}- HCO_3^--CO_3^{2-}-H_2O systems as a function of temperature and pH should be further investigated. If the polarisations are sufficient enough, transgranular cracks with low crack growth rates of the order of 10^{-7} mm/s are envisaged.

The possibility of generating other SCC mechanisms in an anthropogenic carbon dioxide pipeline is discussed in section 2.6. For example, should a water phase be present in the transport pipeline, it is expected that impurities such as hydrogen sulphide or carbon monoxide could generate SCC. Such mechanisms could evolve at the free corrosion potential. Further experimental work needs to be conducted to determine the operational envelope (e.g. concentration levels / partial pressure) for which H_2S and CO could produce SCC at high partial pressures of CO_2 typical of a carbon transport pipeline system.

Additionally, it is recommended that the threshold of nitrate concentration in generating SCC as a function of carbon dioxide pressures is investigated.

Chapter 7. Conclusions and further work

7.1. Conclusions

- The electrochemical measurements show that the X80 pipeline steel present an active-passive transition in the HCO_3^--CO_3^{2-}-H_2O, NO_3^-- HCO_3^--CO_3^{2-}-H_2O, and SO_3^{2-}- HCO_3^--CO_3^{2-}-H_2O systems, with or without CO_2 (1 bar), at 23 and 75°C. This suggests that the pipeline steel is susceptible to SCC in all these test environments.

- Stress Corrosion Cracking is produced on the X80 pipeline steel in pure aqueous bicarbonate / carbonate solutions, and in the presence of nitrates and sulphites at 75°C. SCC is identified both in the CO_2-free environments and CO_2- saturated environments (1 bar CO_2) at 75°C.

- Stress Corrosion Cracking is identified both in the steel active and active-passive transition domain for all test environments at 75°C:

    - The severity of cracking is however more significant in the active-passive transition domain than in the active domain, whichever test system considered. The linear relationship of E_{SCC} vs. E_p provides a fairly accurate prediction of E_{SCC} with a deviation within 0.05 V (generally less than 0.02 V).

    - SCC declines as the potential shifts towards the Free Corrosion Potential and no cracking is observed at E_{corr}. However cracking is still observed at relatively small anodic polarisations of +50 mV.

    - The mode of cracking in the active domain is transgranular for all the systems, while it is dependent on the nature of the environment in the active-passive domain.

- In CO_2-free systems at high pH (>9) and in the steel active-passive transition at 75°C:

    - The susceptibility to cracking in the HCO_3^--CO_3^{2-}-H_2O system decreases with diminishing bicarbonate / carbonate levels.

- Crack velocities of the order of 10^{-6} mm.s^{-1} are produced in pure concentrated bicarbonate / carbonate solutions and in the presence of nitrates and sulphites.

- The severity and the morphology of cracking in the HCO_3^--CO_3^{2-}-H_2O and $NaNO_3$-HCO_3^--CO_3^{2-}-H_2O systems is similar. The crack velocities are of the order of 3.10^{-6} mm.s^{-1} in concentrated bicarbonate / carbonate solutions and the mode of cracking is intergranular.

- Crack growth in the HCO_3^--CO_3^{2-}-H_2O and $NaNO_3$-HCO_3^--CO_3^{2-}-H_2O systems is controlled by anodic dissolution processes. In the presence of nitrates, the overall cracking mechanism in the steel active-passive transition domain is discussed to remain dominated by the HCO_3^--CO_3^{2-}-H_2O system.

- The addition of sulphites to the pure bicarbonate / carbonate system decreases the severity of cracking, and shifts the cracking mode to transgranular. Sulphites favour the destabilisation of surface protective films such as iron carbonate, and promote rather anodic dissolution, whose combined effects decrease the susceptibility to Stress Corrosion Cracking in the the HCO_3^--CO_3^{2-}-H_2O system.

- In CO_2-saturated systems, and in the steel active-passive transition at 75°C:

  - As the pH moves towards acidity, the SCC susceptibility in pure bicarbonate / carbonate system and in the presence of nitrates or sulphites is decreased. At lower pH, the highest susceptibility to SCC is identified in the presence of nitrates with crack velocities of the order of $1.5.10^{-6}$ mm.s^{-1}, and then in the presence of sulphites with crack growths of the order of $5.5.10^{-7}$ mm.s^{-1}. Crack velocities in the pure bicarbonate / carbonate system are of the order of $1.5.10^{-7}$ mm.s^{-1}.

- The drop in pH as a result of CO_2 addition shifts the mode of cracking from intergranular to transgranular in the pure bicarbonate / carbonate system, while it remains intergranular in the presence of nitrates. The cracking mode remains transgranular in the presence of sulphites.

- As the acidity of the solution increases, as a result of an increase in CO_2 partial pressure, it is expected that a pH threshold is reached for which anodic dissolution dominates iron carbonate precipitation, and thus SCC susceptibility in the HCO_3^--CO_3^{2-}-H_2O system becomes low.

- As the drop in pH is sustained by the increase in carbon dioxide partial pressure, it is expected that nitrate SCC becomes the dominant mechanism when nitrates are present in the HCO_3^--CO_3^{2-}-H_2O system. This is further favoured in the case of low bicarbonate / carbonate concentrations and at high temperatures (typically above 70°C).

- The severity of cracking increases with the temperature. At lower temperatures e.g. 23°C, the anodic dissolution associated with the corrosion process is too low to generate deeper corrosion features within the time scale of the SSRT experiment conducted. However, it is plausible that for much longer exposure tests (i.e. at lower strain rate), the pits could turn into deeper stress corrosion cracks in the pure bicarbonate / carbonate system, and in the presence of nitrates in CO_2-free environments. The presence of sulphites in the HCO_3^--CO_3^{2-}-H_2O system appear however to inhibit the initiation of cracks at 23°C.

7.2. Further work

- The role of nitrates and sulphites in interfering with protective films in the HCO_3^--CO_3^{2-}-H_2O system should be further investigated over a wide range of pH and temperatures.

- The effect of nitrates and sulphites in producing SCC in the HCO_3^--CO_3^{2-}-H_2O system under Open Circuit Potential Conditions shall be further investigated over a wide range of pH and temperatures by using Constant Stress or Strain methods (e.g. U-bends) over long period testing times.

- The effect of welding materials and iron sulphide films in displacing the free corrosion potential of the steel in the different systems HCO_3^--CO_3^{2-}-H_2O, NO_3^-- HCO_3^--CO_3^{2-}-H_2O, and SO_3^{2-}- HCO_3^--CO_3^{2-}-H_2O as a function of temperature and pH should be further investigated to further assess the risk of SCC under freely corroding conditions .

- The threshold of nitrate concentration in generating SCC as a function of carbon dioxide pressures should be investigated.

- The effect of steel microstructures and pipeline steel grades on the occurrence of SCC in NO_3^-- HCO_3^--CO_3^{2-}-H_2O, and SO_3^{2-}- HCO_3^--CO_3^{2-}-H_2O systems should be instigated.

- Although the standard ISO 15156 / MR0175 is a starting point, it is critical to obtain data at the high partial pressures of CO_2 in presence of H_2S to understand in which conditions of H_2S partial pressure, pH, temperature SSCC or HIC can be realised in CO_2 pipelines.

- It is critical to obtain data at the high partial pressures of CO_2 in presence of CO to understand in which conditions of CO partial pressure, pH, temperature CO_2-CO-H_2O SCC can be realised in CO_2 pipelines.

References

1. IPCC (2007) *Climate change 2007: Synthesis report*.
2. Seiersten, M. (2001) 'Materials Selection for Separation, Transportation and Disposal of CO_2', *Corrosion 2001*. NACE International.
3. Ayello, F., Evans, K., Thodla, R. and Sridhar, N. (2010) 'Effect of Impurities on corrosion of steel in supercritical CO_2', *Corrosion 2010*. NACE International.
4. Choi, Y.-S. and Nešić, S. (2011) 'Determining the corrosive potential of CO_2 transport pipeline in high pCO_2–water environments', *International Journal of Greenhouse Gas Control*, 5(4), 788-797.
5. Dugstad, A., Morland, B. and Clausen, S. (2011) 'Corrosion of transport pipelines for CO_2–Effect of water ingress', *Energy Procedia*, 4, 3063-3070.
6. Zhang, Y., Kewei, G. and Guenter, S. (2011) 'Water Effect on Steel Under Supercritical CO_2 Condition', *Corrosion 2011*. NACE International.
7. Dugstad, A. and Halseid, M. (2012) 'Internal Corrosion In Dense Phase CO_2 Transport Pipelines - State of the Art And the Need For Further R&D', *Corrosion 2012*. NACE International.
8. Sandana, D., Hadden, M., Race, J. and Charles, A. (2012) 'Transport of gaseous and dense carbon dioxide in pipelines : is there an internal corrosion risk ?', *Journal of Pipeline Engineering*, 11(3), 229-238.
9. Hua, Y., Barker, R. and Neville, A. (2015) 'Understanding the Influence of SO_2 and O_2 on the Corrosion of Carbon Steel in Water-Saturated Supercritical CO_2', *Corrosion*, 71(5), 667-683.
10. Seevam, P.N., Race, J., Downie, M.J. and Hopkins, P. (2008) 'Transporting the Next Generation of CO_2 for Carbon, Capture and Storage: The Impact of Impurities on Supercritical CO_2 Pipelines ', *7th International Pipeline Conference*.
11. IPCC (2005) *Carbon Dioxide Capture and Storage*.
12. Race, J. (2012) 'Towards a CO_2 pipeline specification: defining tolerance limits for impurities', *Journal of Pipeline Engineering*, 11(3), 173-190.
13. Seevam, P.N., Race, J., Downie, M.J., Barnett, J. and Cooper, R. (2010) 'Capturing carbon dioxide : the feasibility of re-using existing pipeline infrastructure to transport anthropogenic CO_2 ', *8th International Pipeline Conference*.
14. Mohitpour, M., Golshan, H. and Murray, M.A. (2007) *Pipeline Design & Construction, A practical approach*. ASME Press.
15. Spycher, N., Pruess, K. and Ennis-King, J. (2003) 'CO_2-H_2O mixtures in the geological sequestration of CO_2. I. Assessment and calculation of mutual solubilities from 12 to 100°C and up to 600 bar', *Geochimica et Cosmochimica Acta*, 67(16), 3015-3031.
16. Austegard, A., Solbraa, E., De Koeijer, G. and Mølnvik, M.J. (2006) 'Thermodynamic Models for Calculating Mutual Solubilities in H_2O–CO_2–CH_4 Mixtures', *Chemical Engineering Research and Design*, 84(9), 781-794.
17. de Visser, E., Hendriks, C., Barrio, M., Mølnvik, M.J., de Koeijer, G., Liljemark, S. and Le Gallo, Y. (2008) 'Dynamis CO_2 quality recommendations', *International Journal of Greenhouse Gas Control*, 2(4), 478-484.
18. Kear, R.W. (1956) 'Low-Temperature Corrosion: by flue-gas condensates Part 1', *Anti-Corrosion Methods and Materials*, 3(2), 59-64.
19. Huijbregts, W.M.M. and Leferink, R.G.I. (2004) 'Latest advances in the understanding of acid dewpoint corrosion: corrosion and stress corrosion cracking in combustion gas condensates', *Anti-Corrosion Methods and Materials*, 51(3), 173-188.
20. Dugstad, A., Halseid, M. and Morland, B. (2013) 'Corrosion in dense phase CO_2 pipelines - consequences of upset conditions, ' *3rd International Forum on the Transportation of CO_2 by Pipeline*.

21. Dugstad, A., Halseid, M. and Morland, B. (2013) 'Effect of SO_2 and NO_2 on Corrosion and Solid Formation in Dense Phase CO_2 Pipelines', *Energy Procedia*, 37, 2877-2887.
22. Arroyave, C. and Morcillo, M. (1995) 'The effect of nitrogen oxides in atmospheric corrosion of metals', *Corrosion Science*, 37(2), 293-305.
23. Schwartz, S.E. and White, W.H. (1981) 'Solubility equilibria of the nitrogen oxides and oxyacids in dilute aqueous solution', *Advances in Environmental sciences and technology*, 4.
24. Suchak, N.J. and Joshi, J.B. (1994) 'Simulation and optimization of NO_x absorption system in nitric acid manufacture', *AIChE Journal*, 40(6), 944-956.
25. Cape, J.N. (1984) 'The importance of solution equilibria in studying the effects of sulphite on plants', *Environmental Pollution Series A, Ecological and Biological*, 34(3), 259-274.
26. Maahs, H.G. (1982) 'Sulfur-Dioxide/Water Equilibria Between 0° and 50°C. An Examination of Data at Low Concentrations', in *Heterogeneous Atmospheric Chemistry*. American Geophysical Union, 187-195.
27. Hales, J.M. and Slitter, S.L. (1973) 'Solubility of sulfur dioxide in water at low concentrations', *Atmospheric Environment (1967)*, 7(10), 997-1001.
28. Huss, A. and Eckert, C.A. (1977) 'Equilibria and ion activities in aqueous sulfur dioxide solutions', *The Journal of Physical Chemistry*, 81(24), 2268-2270.
29. Liss, P.S. (1971) 'Exchange of SO_2 between the Atmosphere and Natural Waters', *Nature*, 233(5318), 327-329.
30. Garsed, S.G. (1981) 'The use of sulphite solutions for studying the effects of SO_2 on higher plants', *Environmental Pollution Series A, Ecological and Biological*, 24(4), 303-311.
31. Obinata, T. (1981) 'An introductory review of the effects of steelmaking practice on the development of high strength steels for pipeline', in *Steels for line pipe and pipeline fittings (Conference proceedings)*. London: The Metals Society, 185-191.
32. Sage, A.M. (1981) 'A review of the physical metallurgy of high strength, low alloy line pipe and pipe fitting steels', in *Steels for line pipe and pipeline fittings (Conference proceedings)*. London: The Metals Society, 39-50.
33. ASTM (2008) *E436-Standard Test Method for Drop-Weight Tear Tests of Ferritic Steels*.
34. Irvine, K. (1970) 'Controlled Rolling of structural steels', *Jounal of the Iron Steel Institute*, 208, 717.
35. Tamura, I., Ouchi, C., Tanaka, T. and Sekine, H. (1988) *Thermomechanical Processing of High-Strength Low-Alloy Steels*. Butterworth & co.
36. Roberts, W. (1983) 'Recent innovations in alloy design and processing of microalloyed steels', in Korchynsky, M. (ed.) *HSLA Steels Technology & Application (Conference proceedings)*. ASM.
37. Zheng, Y., Fitzsimons, G. and Deardo, A.J. (1983) 'Achieving grain refinement through recrystallisation controlled rolling and controlled rolling in V-Ti-N microalloyed steels', in Korchynsky, M. (ed.) *HSLA Steels Technology & Application (Conference proceedings)*. ASM.
38. Tamehiro, I.H. and Chino , H. (1991) *The progress in pipeline material properties*. Nippon Steel Corporation
39. Yurioka, N. (1995) 'TMCP steels and their welding', *Welding in the World*, 35(6), 375-390.
40. Hillenbrand, H.G., Niederhoff, K., Amoris, E., Perdix, C., Streisselberger, A. and Zeislmair, U. (1999) *Development of linepipe in grades up to X100*.
41. Hillenbrand, H., Heckmann, C.J. and Niederhoff, K.A. (2002) 'X80 linepipe for large-diameter high strength pipelines', *APIA 2002 conference*. Australia.
42. Spinelli, C.M. and Prandi, L. (2012) 'High Grade Steel Pipeline for Long Distance Projects at Intermediate Pressure ', *7th Pipeline Technology Conference*. Germany.
43. Billingham, J., Sharp, J.V., Spurrier, J. and Kilgallon, P.J. (2003) *Review of the performance of high strength steels used offshore*.

44. Gräf, M.K., Hillenbrand, H., Heckmann, C.J. and Niederhoff, K. (2003) 'High-strength large-diameter pipe for long-distance high pressure gas pipelines', *ISOPE 2003*. Hawaii, U.S.A.
45. Althouse, J., Dorling, D., Ferguson, J. and TAylor, D. (2013) 'TransCanada's State of the Art Development and Utilization of High Strength Materials, Fully Automated Welding and Automated Ultrasonic NDE Testing', *The NDT in Canada 2013 Conference in conjunction with the International Workshop on Smart Materials & Structures, SHM and NDT for the Energy Industry*. Alberta, Canada.
46. Cheng, Y.F. (2013) *Stress Corrosion Cracking of Pipelines*. John Wiley & Sons.
47. Uhlig, H.H. (1948) *Uhlig's Corrosion Handbook*. John Wiley.
48. Uhlig, H.H. (1971) *Corrosion and Corrosion Control: An Introduction to Corrosion Science and Engineering* John Wiley & Sons
49. *Corrosion- Volume 1: Metal / Environment Reactions (Shreir, 2nd edition)* (1976). Newnes-Butterworth.
50. Evans, J. (1968) 'Verification of the form of the Nernst equation: An experiment for introductory chemistry', *Journal of Chemical Education*, 45(8), 532.
51. Rochaix, C. (2000) *Thermodynamique-Cinétique*. Nathan
52. Burstein, G.T. (2009) 'Passivity and localised corrosion', in Richardson, T. (ed.) *Shreir's Corrosion (4th edition)*. Elsevier Science, 731-752.
53. Kermani, M.B. and Smith, L.M. (1997) *CO_2 corrosion control in oil and gas production* (23). Corrosion, E.F.o.
54. Kermani, M.B. and Morshed, A. (2003) 'Carbon Dioxide Corrosion in Oil and Gas Production—A Compendium', *Corrosion*, 59(8), 659-683.
55. Dugstad, A. (2006) 'Fundamental Aspects of CO_2 Metal Loss Corrosion - Part 1: Mechanism', *Corrosion 2006*. NACE International.
56. Fyfe, D. (1976) 'The Atmosphere', in Shreir, L.L. (ed.) *Corrosion- Volume 1: Metal / Environment Reactions (Shreir, 2nd edition)*. Newnes-Butterworth, 2:29-2:37.
57. Rosenfeld, I.L. (1962) *First International congress on metallic corrosion*. London, U.K. Butterworth.
58. Justo, M.J. and Ferreira, M.G.S. (1989) 'The corrosion of mild steel in simulated SO_2 containing atmospheres', *Corrosion Science*, 29(11–12), 1353-1369.
59. Cox, A. and Lyon, S.B. (1994) 'An electrochemical study of the atmospheric corrosion of mild steel—III. The effect of sulphur dioxide', *Corrosion Science*, 36(7), 1193-1199.
60. Sun, W., Nešić, S. and Woollam, R.C. (2009) 'The effect of temperature and ionic strength on iron carbonate ($FeCO_3$) solubility limit', *Corrosion Science*, 51(6), 1273-1276.
61. Xiang, Y., Wang, Z., Xu, C., Zhou, C., Li, Z. and Ni, W. (2011) 'Impact of SO_2 concentration on the corrosion rate of X70 steel and iron in water-saturated supercritical CO_2 mixed with SO_2', *The Journal of Supercritical Fluids*, 58(2), 286-294.
62. Choi, Y.-S., Nesic, S. and Young, D. (2010) 'Effect of Impurities on the Corrosion Behavior of CO_2 Transmission Pipeline Steel in Supercritical CO_2−Water Environments', *Environmental Science & Technology*, 44(23), 9233-9238.
63. Farelas, F., Choi, Y.S. and Nesic, S. (2012) 'Effects of CO_2 Phase Change, SO_2 Content And Flow On the Corrosion of CO_2 Transmission Pipeline Steel', *Corrosion 2012*. NACE International.
64. Arroyave, C., Lopez, F.A. and Morcillo, M. (1995) 'The early atmospheric corrosion stages of carbon steel in acidic fogs', *Corrosion Science*, 37(11), 1751-1761.
65. Hoar, T.P. (1971) 'The theory of SCC in alloys', in Scully, J.C. (ed.) *NATO Science Commitee Research Evaluation Conference (Conference proceedings)*. Brussels, Belgium: NATO, 105.
66. Jones, R.J. (1992) *Stress-Corrosion Cracking: Materials Performance and Evaluation*. ASM International.
67. *NACE Corrosion Engineer's Reference Book (3rd Edition)* (2002). NACE international.

68. Parkins, R.N. (1980) 'Predictive approaches to stress corrosion cracking failure', *Corrosion Science*, 20(2), 147-166.
69. Newman, R.C. (2002) 'Stress corrosion cracking mechanisms', in Marcus, P. and Oudar, J. (eds.) *Corrosion mechanisms in theory and practice (2nd edition)*. Marcel Decker.
70. Staehle, R.W., Royuela, J.J., Raredon, T.L., Serrate, E., Morin, C.R. and Farrar, R.V. (1970) 'Effect of Alloy Composition on Stress Corrosion Cracking of Fe-Cr-Ni Base Alloys', *Corrosion*, 26(11), 451-486.
71. Engell, H.J. (1971) 'The theory of SCC in alloys', in Scully, J.C. (ed.) *NATO Science Commitee Research Evaluation Conference (Conference proceedings)*. Brussels, Belgium: NATO, 86.
72. Diegle, R.B. and Boyd, W.K. (1977) 'The role of film rupture during Slow strain rate SCC testing', in *Stress Corrosion Cracking-The slow Strain Rate Technique Symposium (Conference proceedings)*. Toronto, Canada: ASTM, 26-46.
73. Parkins, R.N. (1964) 'Stress Corrosion Cracking', *Metallurgical Reviews*, 9(1), 201-260.
74. Scully, J.C. (1975) 'Stress corrosion crack propagation: A constant charge criterion', *Corrosion Science*, 15(4), 207-224.
75. Parkins, R.N. (1976) 'Mechanism of SCC', in *Corrosion- Volume 1: Metal / Environment Reactions (Shreir, 2nd edition)*. Newnes-Butterworth, 10.
76. Staehle, R.W. (1969) 'Stress Corrosion Cracking of Iron Nickel Chromium Alloys', in Staehle, R.W. (ed.) *NACE 1-Fundamental aspects of stress corrosion cracking (Proceedings of conference)*. NACE International, 3.
77. Parkins, R.N. (1972) 'Stress Corrosion Spectrum', *British Corrosion Journal*, 7(1), 15-28.
78. Newman, R.C. (2009) 'Stress Corrosion Cracking', in Richardson, T. (ed.) *Shreir's corrosion (4th Edition)*. Elsevier, 864-901.
79. Hudgins, C.M., McGlasson, R.L., MehdlZadeh, P. and Rosborough, W.M. (1966) 'Hydrogen Sulfide Cracking of Carbon and Alloy Steels', *Corrosion*, 22(8), 238-251.
80. Sandana, D., Dale, M., Charles, A. and Race, J. (2013) 'Internal stress corrosion cracking in anthropogenic CO_2 pipelines : is it possible? ', *Journal of Pipeline Engineering*, 12(4), 321-334.
81. Brown, Harrison and Wilkins (1973) *Electrochemical investigation of SCC of plain carbon steel in carbon dioxide-carbon monoxide-water system*. NACE international.
82. Kowaka, M. and Nagata, S. (1976) 'Stress Corrosion Cracking of Mild and Low Alloy Steels in CO-CO_2-H_2O Environments', *Corrosion*, 32(10), 395-401.
83. NACE (2009) *NACE MR0175/ISO 15156, Petroleum and Natural Gas Industries- Materials for use in H_2S environments in Oil and Gas production*. NACE International.
84. Parkins, R.N. and Zhou, S. (1997) 'The stress corrosion cracking of C-Mn steel in CO_2-HCO_3^- -CO_3^{2-} – solutions. I: Stress corrosion data', *Corrosion Science*, 39(1), 159-173.
85. Parkins, R.N. and Usher, R. (1961) *The 1st International Congress on Metallic Corrosion*. London, U.K.
86. Leferink, R.G.I. and Huijbregts, W.M.M. (2002) 'Nitrate stress corrosion cracking in waste heat recovery boilers', *Anti-Corrosion Methods and Materials*, 49(2), 118-126.
87. Hoar, T.P. and Galvele, J.R. (1970) 'Anodic behaviour of mild steel during yielding in nitrate solutions', *Corrosion Science*, 10(4), 211-224.
88. Szklarska-Smialowska, Z. (1964) 'Effect of Potential of Mild Steel On Stress Corrosion Cracking In Ammonium Nitrate Solutions', *Corrosion*, 20(6), 198-202.
89. Mazille, H. and Uhlig, H.H. (1972) 'Effect of Temperature and Some Inhibitors on Stress Corrosion Cracking of Carbon Steels in Nitrate and Alkaline Solutions', *Corrosion*, 28(11), 427-434.
90. Flis, J. (1975) 'Role of oxide films in stress corrosion cracking of mild steel in nitrate solutions', *Corrosion Science*, 15(6–12), 553-564.
91. Mohammed, F., Yahya, S. and Elramady, A. (2010) 'Effect of Temperature and Concentration of Ammonium Nitrate Solution on the Succeptibility of Mild Steel to

Stress Corrosion Cracking', *Journal of Electromagnetic Analysis and Applications*, 2(2), 91-97.
92. Nyborg, R. and Dugstad, A. (2003) 'Understanding and Prediction of Mesa Corrosion Attack', *Corrosion 2003*. NACE International.
93. Dugstad, A. (1992) 'The Importance of $FeCO_3$ Super-saturation on CO_2 Corrosion of Carbon Steels', *Corrosion 1992*. Houston, U.S.A. NACE International.
94. Lopez, D.A. (2003) 'The influence of microstructure and chemical composition of carbon and low alloy steels in CO2 corrosion. A state-of-the-art appraisal, Materials and Design ', *Materials and Design*, 24(8), 561-575.
95. Crolet, J.L. (1998) 'Role of Conductive Corrosion Products on the Protectiveness of Corrosion Layers', *Corrosion 1998*. Houston, U.S.A. NACE International.
96. Dugstad, A. (1998) 'Mechanism of Protective Layer Formation During CO2 Corrosion of Mild steel', *Corrosion 1998*. Houston, U.S.A. NACE International.
97. Farelas, F. (2013) 'Iron Carbide and its Influence on the Formation of Protective Iron Carbonate in CO2 Corrosion of Mild Steel', *Corrosion 2013*. Orlando, Florida, U.S.A. NACE Internaltional.
98. Marcus, P. and Talah, H. (1989) 'The sulphur-induced breakdown of the passive film and pitting studied on nickel and nickel alloys', *Corrosion Science*, 29(4), 455-459.
99. Sun, W. (2006) *Kinetics of iron carbonate and iron sulfide scale formation in CO_2/H_2S corrosion*. Ohio University.
100. Crolet, J.L. and Bonis, M. (2010) 'Algorithm of the Protectiveness of Corrosion Layers-Mechanisms and H_2S Corrosion Prediction ', *Corrosion 2010*. NACE international.
101. Sun, W. (2007) ' A Mechanistic Model of H_2S Corrosion of Mild Steel', *Corrosion 2007*. NACE International.
102. Sun, W., Nešić, S. and Papavinasam, S. (2008) 'Kinetics of Corrosion Layer Formation. Part 2—Iron Sulfide and Mixed Iron Sulfide/Carbonate Layers in Carbon Dioxide/Hydrogen Sulfide Corrosion', *Corrosion*, 64(7), 586-599.
103. Pourbaix, M. (1974) *Atlas of Electrochemical Equilibria in Aqueous Solutions*. NACE International.
104. Broomfield, J. (2006) *Corrosion of steel in concrete (2nd edition)*. CRC press.
105. Khan, M. and Al ‐ Tayyib, A. (1992) 'Rebar Corrosion in $MgSO_4$ Solution', *Journal of Materials in Civil Engineering*, 4(3), 292-299.
106. M.A., A. and M.A., M. (1983) *Corrosion of Reinforcement in Concrete Construction*. London, U.K.
107. Abd El Haleem, S.M., Abd El Wanees, S. and Bahgat, A. (2013) 'Environmental factors affecting the corrosion behaviour of reinforcing steel. V. Role of chloride and sulphate ions in the corrosion of reinforcing steel in saturated Ca(OH)2 solutions', *Corrosion Science*, 75, 1-15.
108. Kasturie, P., Potgieter, J.H. and Potgieter ‐ Vermaak, S. (2011) 'Laser surface treatment to inhibit observed corrosion of reinforcing steel in sulphate: alkaline media', *Anti-Corrosion Methods and Materials*, 58(5), 267-284.
109. Humphries, M.J. and Parkins, R.N. (1969) *Fundamental aspects of Stress Corrosion Cracking*. Houston, U.S.A.
110. Lees, D.J. and Lockington, N.A. (1970) 'Influence of the Cation on the Mode of Stress-Corrosion Failure of Iron In Nitrate Solutions', *British Corrosion Journal*, 5(4), 167-171.
111. Smialowski, M. (1961) *The 1st International Congress on Metallic Corrosion*. London, U.K.
112. Bhat, P.C., Sathyavathiamma, M.P., Puttaswamy, N.G. and Mallya, R.M. (1983) 'Mössbauer studies of the corrosion products of iron formed in aqueous ammonium nitrate solution', *Corrosion Science*, 23(7), 733-752.
113. Sedriks, A.J. (1990) *Corrosion Testing Made Easy, Stress Corrosion Cracking Test Methods*. NACE International.
114. API (2010) *API 5L-Specification for linepipe (44th Edition)*.

115. ASTM (2007) *E1268 - 01:Standard Practice for Assessing the Degree of Banding or Orientation of Microstructures*.
116. NPL 'Guides to good practice in corrosion control: Stress Corrosion Cracking'.
117. Parkins, R.N. and Zhou, S. (1997) 'The stress corrosion cracking of C-Mn steel in CO_2-HCO_3^- -CO_3^{2-} solutions. II: Electrochemical and other data', *Corrosion Science*, 39(1), 175-191.
118. Zhou, S. (1991) *Environment sensitive fracture of ferritic steels in aqueous $CO_2/HCO_3^-/CO_3^{2-}$ solutions*. Newcastle University.
119. Payer, J.H., Berry, W.E. and Boyd, W.K. (1977) 'Evaluation of Slow Strain-Rate stress Corrosion Tests results', in *Stress Corrosion Cracking-The slow Strain Rate Technique Symposium (Conference proceedings)*. Toronto, Canada: ASTM, 26-46.
120. Kim, C.D. and Wilde, B.E. (1977) 'A review of the constant strain rate stress corrosion cracking test', in *Stress Corrosion Cracking-The slow Strain Rate Technique Symposium (Conference proceedings)*. Toronto, Canada: ASTM.
121. Henthorne, M. (1965). Newcastle University.
122. Henthorne, M. and Parkins, R.N. (1966) 'Some aspects of stress-corrosion crack propagation in mild steel', *Corrosion Science*, 6(8), 357-369.
123. Parkins, R.N. (1977) 'Development of Strain-Rate Testing and its implications', in *Stress Corrosion Cracking-The slow Strain Rate Technique Symposium (Conference proceedings)*. Toronto, Canada: ASTM.
124. Goldstein (2003) *Scanning electron microscopy and X-ray microanalysis*. Plenum Press.
125. Stockes, D. (2008) *Principles and practices of variable pressure/environmental scanning electron microscopy (VP-ESEM)*. Wiley.
126. Poulsen, B. *Courtesy of Brian Poulsen*.
127. Garrels, R.M. and Christ, C.L. (1965) *Solutions, Minerals and Equilibria*. Harper & Row.
128. Green, J. (1949) 'Effect of Temperature on pH of Alkaline Waters - Waters Containing Carbonate, Bicarbonate, and Hydroxide Alkalinity', *Industrial & Engineering Chemistry*, 41(8), 1795-1797.
129. Stefánsson, A., Bénézeth, P. and Schott, J. (2013) 'Carbonic acid ionization and the stability of sodium bicarbonate and carbonate ion pairs to 200 °C – A potentiometric and spectrophotometric study', *Geochimica et Cosmochimica Acta*, 120, 600-611.
130. Armstrong, R.D. and Coates, A.C. (1974) 'The passivation of iron in carbonate/bicarbonate solutions', *Journal of Electroanalytical Chemistry and Interfacial Electrochemistry*, 50(3), 303-313.
131. Indig, M.E., Weber, J.E. and Weinstein, D. (1982) in *Reviews on Coatings and Corrosion (Volume 5)*. Scientific Publications Division, Freund Publishing House, 173-225.
132. Sridhar, N., Dunn, D.S., Anderko, A.M., Lencka, M.M. and Schutt, H.U. (2001) 'Effects of Water and Gas Compositions on the Internal Corrosion of Gas Pipelines—Modeling and Experimental Studies', *Corrosion*, 57(3), 221-235.
133. Davies, D.H. and Burstein, G.T. (1980) 'The Effects of Bicarbonate on the Corrosion and Passivation of Iron', *Corrosion*, 36(8), 416-422.
134. Cáceres, L., Vargas, T. and Parra, M. (2009) 'Study of the variational patterns for corrosion kinetics of carbon steel as a function of dissolved oxygen and NaCl concentration', *Electrochimica Acta*, 54(28), 7435-7443.
135. Evans, U.R. (1960) *The corrosion and oxidation of metal*. Edward Arnold Ltd.
136. Subramanian, K. and Mickalonis, J. (2005) 'Anodic polarization behavior of low-carbon steel in concentrated sodium hydroxide and sodium nitrate solutions', *Electrochimica Acta*, 50(13), 2685-2691.
137. Nordsveen, M., Nešić, S., Nyborg, R. and Stangeland, A. (2003) 'A Mechanistic Model for Carbon Dioxide Corrosion of Mild Steel in the Presence of Protective Iron Carbonate Films—Part 1: Theory and Verification', *Corrosion*, 59(5), 443-456.

138. Gray, L.G.S., Anderson, B.G., Danysh, M.J. and Tremaine, P.R. 'Effect of pH and Temperature on the Mechanism of Carbon Steel Corrosion by Aqueous Carbon Dioxide', *Corrosion 1990*. Nace International.
139. Castro, E.B., Vilche, J.R. and Arvia, A.J. (1991) 'Iron dissolution and passivation in K_2CO_3-$KHCO_3$ solutions. rotating ring disc electrode and XPS studies', *Corrosion Science*, 32(1), 37-50.
140. Mustapha, A. (2010) *The effect of microstructure on the susceptibility of pipeline steels to environment-assisted cracking*. Newcastle University.
141. Staehle, R.W. (1971) 'The theory of SCC in alloys', in Scully, J.C. (ed.) *NATO Science Commitee Research Evaluation Conference (Conference proceedings)*. Brussels, Belgium: NATO, 223.
142. Eliyan, F.F. and Alfantazi, A. (2014) 'Mechanisms of Corrosion and Electrochemical Significance of Metallurgy and Environment with Corrosion of Iron and Steel in Bicarbonate and Carbonate Solutions—A Review', *Corrosion*, 70(9), 880-898.
143. Eliyan, F.F. and Alfantazi, A. (2014) 'Effect of bicarbonate concentration on corrosion of high strength steel', *Corrosion Engineering, Science and Technology*, 50(3), 178-185.
144. Perdieus, E., Brabers, M. and Van Haute, C. (1977) 'A mechanism of stress corrosion cracking of carbon steels in hot carbonate, hydroxide and nitrate solutions', *Mechanism of environmental cracking of materials*. London, U.K. Metals society, 53-65.
145. Beverskog, B. and Puigdomenech, I. (1996) 'Revised pourbaix diagrams for iron at 25–300 °C', *Corrosion Science*, 38(12), 2121-2135.